

THE UNIVERSITY OF EDINBURGH

SCHOOL OF GEOSCIENCES

**THE CONTRIBUTION OF PHOTOSYNTHESIS
AND RESPIRATION TO THE NET ECOSYSTEM
EXCHANGE AND ECOSYSTEM ^{13}C
DISCRIMINATION OF A SITKA SPRUCE
PLANTATION**

Lisa Wingate

BSc (Hons), Edinburgh

A thesis submitted for the degree of Doctor of Philosophy

March 2003

*Dedicated to Amber
Geoff
Mum
Dad*

and the memory of Natasha

Acknowledgements

First of all I would like to thank my supervisors John Moncrieff and Paul Jarvis who have provided encouragement and assistance during this study. I would like to thank Paul for sowing the seeds of scientific curiosity (or distraction as Paul prefers to describe it!) and John for allowing me the freedom to develop and explore that curiosity. I would also like to thank Paul for his tower construction skills, providing tractors to pull trucks out of ditches and thermos flasks of coffee during field work.

Many thanks are due to Robert Clement, Veronica Finlayson, Franz Conen and Kate Heal for their company, advice and technical assistance in the field. This is especially the case for Rob who has politely listened to me chattering about anything and everything whilst in the truck and lab for the past four years. I am very grateful you didn't leave me behind in the forest on occasions.

I would also like to thank Eric and Margaret Jarvis for their hospitality and generosity over the past 6 years at Durieskin, especially Eric who always kept an eye out for our safe return from the field.

I would also like to thank Francesco Ripullone, Argyro Zerva, Sandra Patino, Daniel Gorman and John Finnegan, who have all assisted me in the field during this study.

Special thanks are due to Mark Rayment, Jon Massheder and Keith McNaughton who have provided advice and guidance on everything from how to walk gracefully, write SAS code and survive the PhD process. I am very grateful for their patience answering my endless questions over and over and over.....

I would especially like to thank John Grace who has provided me with encouraging words throughout this study, they have been greatly appreciated. I would especially like to acknowledge his instrumental role in the collaboration with Jon Lloyd during this study.

I would also like to thank Caroline Nichol, Johanna Pulli, Naomi Towers, Ana Rey and Maree Lucas for their words of comfort and friendship through some difficult times over the past four years.

Thanks to Maurizio Mencuccini, Patrick Meir, Bart Kruijt, Peter Levy, Belinda Medlyn, Guy Woodward, Alasdair Hardie, Mat Williams, Colin Legg, Jill Lancaster and Richard Ennos for general assistance, discussion and laughter and, Shiela Wilson, Derek Scott and Malcolm Ritchie for their help printing material, arranging laptops and field equipment generally on short notice.

Many thanks are also due to Davy, Graeme, George and Peter in the workshop with their technical assistance, supply of materials and good advice.

This work was made possible through the award of a NERC studentship and funding provided through the EU-CARBOEUROFLUX programme.

I have had the great pleasure of meeting some of the most friendly, helpful and enthusiastic researchers from the Max Planck Institute for Biogeochemistry in Jena, the University of Cambridge and the University of Utah. Attending a course on stable isotopes in Utah I had the pleasure of meeting Thure Cerling, Jim Ehleringer and Larry Flanagan. I'd like to thank them for running a fun and interesting course that changed the way I look at plants and hair growth forever. This course was also special because Ulli Seibt and I met for the first time.

On return from Utah, I contacted Howard Griffiths and Jon Lloyd who were all too keen to jump on motorbikes and planes and help me get started. I am very grateful to Jon for his relaxed (literally horizontal) field manner and helping me develop the sampling protocol used in this study along with Jens Schmerler. I also thank Howard for welcoming me into his lab and showing me there are always many more uses for picnic cups, baked bean tins and plant pots than you could ever imagine. I would also like to thank Kate Maxwell, Nick Betson and Gary Lanigan for their hospitality, generosity and Gin & Tonic whilst visiting Cambridge.

Many thanks go to Willi Brand, Armin Jordan, Michael Rothe and Heike Geilmann for carrying out the analysis on flask air and organic samples in Jena. I'd especially like to thank Willi Brand for making me laugh till I cried whilst debating water vapour problems in branch chambers. With serious conviction he advised the solution was to heat the chambers including branch to one hundred degrees and do the measurements, simple! Many thanks also to Almut Arneth, Lina Mercado, Jed Kaplan, Alexander Knohl and Nina Buchmann for their discussions and hospitality whilst visiting Jena. I would also like to thank Suan Chin Wong at the Australian National University for his technical assistance with the provision of useful equipment for the field.

For the past 3 years, Ulli Seibt has provided me with energy, excitement, encouragement and companionship through a process that at times was quite lonely and frustrating. I'd like to thank her for being at the end of the phone, for sharing her tent, building watertight shelters in the field and for flamboyant and robust discussions on any topic you care to mention.

I would like to thank my family and close friend Ruth, for their continued support, which made fieldwork possible and kept Amber in clothes that fit.

Thank you, Amber and Geoff for constant love, patience, flexibility and support throughout this study. This has been important in the completion of this thesis and maintaining perspective.

ABSTRACT

Quantification of foliage and canopy photosynthesis can be difficult because of respiratory counter fluxes, from foliage, wood and soils. De-convoluting this net exchange of CO₂ into component processes is commonly tackled using chamber or eddy covariance measurements of nocturnal net CO₂ exchange and its relationship with temperature. These different methods become comparable when chamber measurements are scaled using inventories of biomass within a defined area. More recently, methods are being developed which utilise the natural differences in ¹³C/¹²C ratios ($\delta^{13}\text{C}$) between plant carbon and atmospheric CO₂ to partition the net ecosystem CO₂ exchange during the day into the component processes of canopy photosynthesis (F_A) and ecosystem respiration (F_R). However, validating assumptions underlying all these methods is necessary with appropriate datasets where possible. This thesis presents data collected using all of the above approaches from a Sitka spruce plantation in Scotland, UK during May and July 2001. Data are presented that quantify the daily pattern of environmental variables and their effect on rates of key physiological processes monitored from branches, soils and entire canopies using each method.

A method was also developed to measure the carbon isotope composition of CO₂ in air exchanged directly with branches. Daily patterns in instantaneous ¹³C discrimination (Δ_{obs}) and the $\delta^{13}\text{C}$ of respired CO₂ were combined with continuous environmental and gas exchange data to explore theoretical models describing photosynthetic discrimination, Δ . This study demonstrated fractionation factors associated with respiratory processes and mesophyll conductance (g_w) were important for explaining daily patterns in Δ_{obs} . Models were also developed and parameterised to predict daily cycles of instantaneous ¹³C discrimination and $\delta^{13}\text{C}$ of recently assimilated needle carbohydrates at the branch and canopy scale. This dynamically simulated the links between environmental conditions, canopy discrimination and the $\delta^{13}\text{C}$ of branch respired CO₂. Providing both a method and

model to directly test hypotheses concerning the environmental regulation of autotrophic respiration measured aboveground and from soil surfaces, potentially leading to a clearer understanding of temporal variability in observed ecosystem Δ and $\delta^{13}\text{C}$ of ecosystem respired CO_2 . Furthermore, these bottom-up estimates of canopy ^{13}C discrimination provided a means of comparison with top-down estimates calculated from a recently developed method incorporating the eddy covariance method and profiles of $\delta^{13}\text{C}$ and CO_2 mole fraction.

At the forest scale daily patterns and estimates of F_A and F_R were determined using the three approaches described above. Daily patterns of F_A were comparable in magnitude and timing between methods and tightly coupled to environmental variables. Daily maximum uptake for F_A ranged from -20 to $-30 \mu\text{mol m}^{-2} \text{s}^{-1}$ and were similar to other published studies for Sitka spruce plantations. The present study highlighted several gaps in present knowledge that could constrain estimates of F_A and F_R using the above methods. The first concerns the quantification of daytime dark respiration fluxes. When this was explored at the canopy scale estimates of F_R were $\approx 50 \%$ lower than commonly used relationships describing F_R . The second related to the $^{13}\text{CO}_2$ partitioning approach and its reliability. Estimates for F_A and Δ_C using this method were questionable primarily because of uncertainties in canopy transpiration (E_T) and g_w estimates. This study concluded that this method is best suited to dry observation periods. Furthermore, that by using branch chambers it was possible to constrain estimates of E_T during all weather conditions and develop parameterised models of g_s that could be used to fill gaps in data when canopies are wet. Lastly, g_w appeared to play an important role in the calculation of F_A using the $^{13}\text{CO}_2$ partitioning approach. Data presented in this study showed that neglecting this extra resistance led to a substantial overestimation of F_A and underestimation of Δ_C . Therefore, field quantification of g_w would also be desirable to constrain estimates of F_A and Δ_{obs} as demonstrated at both the branch and canopy scale.

TABLE OF CONTENTS

Title Pagei
Declarationii
Dedicationiii
Acknowledgementsiv
Abstractvi
Table of contentsviii
List of symbols and abbreviationsxiii

1. INTRODUCTION

1.1 CONTEXT1
 The Global Greenhouse Problem1
 The 'missing sink' for CO₂.....2
1.2 BACKGROUND2
 1.2.1 *Estimating the carbon balance of forests*.....2
 Measuring CO₂ exchange between forests and the atmosphere3
 Ecosystem scale measurements.....3
 Component scale measurements5
 Are rates of daytime dark respiration currently overestimated?7
 1.2.2 *Fractionation of CO₂ by the terrestrial biosphere*.....8
 Can stable isotope methods constrain estimates of canopy photosynthesis?.....9
 Can stable isotopes reveal the dynamic links between weather, canopy photosynthesis and autotrophic respiration.....11
1.3 THESIS AIMS AND STRUCTURE12

2. STRUCTURE OF GRIFFIN FOREST: BIOMASS, LEAF AREA AND SOIL CHARACTERISTICS

2.1 INTRODUCTION15
 The need for biomass, leaf area and soil characterisation15
2.2 CHAPTER AIMS16
2.3 METHODS17
 2.3.1 *Study site*17
 2.3.2 *Forest structure*18
 Leaf area determination.....18
 Above-ground biomass distribution20

	<i>Soil structure</i>	20
2.4	RESULTS	23
2.4.1	Crown structure	23
	<i>Leaf area determination</i>	23
	<i>Above-ground biomass distribution</i>	25
2.4.2	<i>Soil structure</i>	28
2.5	DISCUSSION	29
3.	DAILY VARIATION OF GAS EXCHANGE AND ¹³C DISCRIMINATION BY SITKA SPRUCE BRANCHES UNDER FIELD CONDITIONS – THEORY AND METHOD	
3.1	INTRODUCTION	32
	<i>Photosynthesis, stomatal conductance and ¹³C discrimination</i>	32
	<i>Photorespiration and daytime dark respiration</i>	34
	<i>Applications of integrated ¹³C discrimination</i>	35
	<i>Applications of instantaneous ¹³C discrimination</i>	35
3.2	CHAPTER AIMS	36
3.3	METHOD	37
3.3.1	Gas exchange measurements	37
	<i>Sources of errors during gas exchange</i>	40
3.3.2	Sample collections	42
	<i>Needle area and biomass</i>	42
	<i>Needle, stem and soil collection for $\delta^{13}\text{C}$ analysis</i>	43
	<i>Air collection for CO₂ and $\delta^{13}\text{CO}_2$ analysis</i>	43
3.3.3	Stable isotope analysis	45
	<i>Needle, stem and soil $\delta^{13}\text{C}$ analysis</i>	45
	<i>Air sample CO₂ and $\delta^{13}\text{CO}_2$ analysis</i>	46
	<i>Sources of error during isotopic sampling and analysis</i>	47
3.4	CALCULATIONS	50
3.4.1	Relating to gas exchange	50
3.4.2	Relating to net observed discrimination and $\delta^{13}\text{C}$ of respired CO₂	55
	<i>Net observed photosynthetic discrimination</i>	55
	<i>$\delta^{13}\text{C}$ of respired CO₂</i>	56
3.4.3	Relating to modelled photosynthetic ¹³C discrimination	57
	<i>Simple model, Δ_s</i>	57
	<i>Respiration corrected model, Δ_{Rd}</i>	58
	<i>Full model, Δ_F</i>	60
	<i>$\delta^{13}\text{C}$ of recently assimilated carbohydrates</i>	62

4. DAILY VARIATION OF GAS EXCHANGE AND ^{13}C DISCRIMINATION BY SITKA SPRUCE BRANCHES UNDER FIELD CONDITIONS – RESULTS AND DISCUSSION	
4.1 RESULTS	64
4.1.1 <i>Branch micro-climate</i>	64
4.1.2 <i>Branch gas exchange</i>	67
<i>Field observed assimilation, stomatal conductance and C_i/C_a</i>	67
<i>Modelled Component Fluxes</i>	73
4.1.3 <i>Flask method for stable isotope collection</i>	75
4.1.4 <i>Field observed instantaneous net discrimination against $^{13}\text{CO}_2$</i>	76
4.1.5 <i>Modelling the diurnal variation of discrimination against $^{13}\text{CO}_2$</i>	79
<i>Stable isotope composition of canopy CO_2</i>	79
<i>Apparent fractionation during daytime dark respiration</i>	80
<i>Mesophyll conductance</i>	83
<i>Predicting the diurnal variation of discrimination against $^{13}\text{CO}_2$</i>	84
<i>Validating theoretical models of discrimination against $^{13}\text{CO}_2$</i>	87
4.1.6 <i>Modelling the diurnal variation of $\delta^{13}\text{C}$ composition in needle substrate pools</i>	89
4.2 DISCUSSION	94
4.2.1 <i>Branch gas exchange</i>	94
<i>Assimilation, stomatal conductance and C_i/C_a</i>	94
<i>Modelled Component Fluxes</i>	96
4.2.2 <i>Flask method for stable isotope collection</i>	101
4.2.3 <i>Field observed instantaneous net discrimination against $^{13}\text{CO}_2$</i>	102
4.2.4 <i>Diurnal variation of needle substrate pool $\delta^{13}\text{C}$ composition</i>	105
4.3 CONCLUSIONS	107
5. DAILY VARIATION OF GAS EXCHANGE AND ^{13}C DISCRIMINATION BY A SITKA SPRUCE PLANTATION – THEORY AND METHODS	
5.1 INTRODUCTION	111
5.2 CHAPTER AIMS	112
5.3 THEORY	114
5.3.1 <i>Forest CO_2 exchange</i>	114

	<i>Net ecosystem exchange</i>	114
	<i>Canopy assimilation and respiration</i>	115
	<i>Application of nocturnal models of respiration to</i> <i>predict daytime gross fluxes</i>	117
	<i>Uncertainties estimating nocturnal respiration rates</i>	118
5.3.2	Evaluating stable isotope methods to partition net ecosystem exchange	121
	<i>Ecosystem respired $^{13}\text{CO}_2$</i>	121
	<i>Ecosystem discrimination against ^{13}C</i>	123
	<i>Estimating F_A, F_R and canopy ^{13}C discrimination</i> <i>using the partitioning approach</i>	124
5.4	METHOD	126
5.4.1	Net ecosystem exchange	126
	<i>Eddy covariance system</i>	126
	<i>Climatological data</i>	127
	<i>Processing of eddy flux data - obtaining isofluxes</i>	128
5.4.2	Chamber measurements	129
	<i>Canopy assimilation, respiration and transpiration</i> <i>from branch chambers</i>	129
	<i>Soil CO_2 efflux and $\delta^{13}\text{C}$ of soil respired CO_2</i>	132
5.5	CALCULATIONS	134
5.5.1	Relating to canopy assimilation	134
	<i>Estimating F_A from $F_{E,N}$</i>	134
	<i>Estimating F_A from combined eddy covariance and</i> <i>$^{13}\text{C}/^{12}\text{C}$ ratios</i>	135
	<i>Constraining estimates of F_A from combined eddy</i> <i>covariance and $^{13}\text{C}/^{12}\text{C}$ ratios</i>	137
6.	DAILY VARIATION OF GAS EXCHANGE AND ^{13}C DISCRIMINATION BY A SITKA SPRUCE PLANTATION – RESULTS AND DISCUSSION	
6.1	RESULTS	140
6.1.1	<i>Driving environmental variables</i>	140
6.1.2	<i>Ecosystem water vapour exchange</i>	143
6.1.3	<i>Canopy conductance</i>	146
	<i>Modelling branch conductance</i>	146
	<i>Eddy flux and chamber estimates</i>	150
6.1.4	<i>Ecosystem respiration</i>	152
	<i>Soil respiration</i>	152
	<i>Modelling soil, branch and ecosystem respiration</i>	156
6.1.5	<i>Canopy photosynthesis</i>	164
	<i>Modelling branch photosynthesis</i>	164

	<i>Eddy covariance and chamber-based estimates of Canopy photosynthesis.....</i>	166
6.1.6	<i>Application of stable isotopes</i>	173
	<i>Isotopic composition of ecosystem respired CO₂.....</i>	173
	<i>Isotopic composition of component respired CO₂</i>	174
	<i>Canopy and ecosystem ¹³C discrimination</i>	176
	<i>Canopy photosynthesis obtained from δ³CO₂.....</i>	180
6.1.7	<i>Daily carbon balance</i>	185
6.2	DISCUSSION	188
6.2.1	<i>Ecosystem water vapour exchange</i>	188
	<i>Ecosystem evaporation.....</i>	188
	<i>Canopy transpiration</i>	189
6.2.2	<i>Canopy conductance to water vapour.....</i>	190
6.2.3	<i>Ecosystem respiration</i>	196
	<i>Soil respiration.....</i>	196
	<i>Spatial variability.....</i>	196
	<i>Temporal variability.....</i>	199
	<i>Soil system differences</i>	201
	<i>Ecosystem respiration</i>	204
	<i>Comparing eddy covariance and chamber-scaled methods</i>	204
6.2.4	<i>Canopy photosynthesis.....</i>	211
6.2.5	<i>Integration of flux and stable isotope methods at the canopy and ecosystem scale</i>	214
	<i>δ³C of respired CO₂.....</i>	214
	<i>δ³C of ecosystem respiration and ¹³C discrimination... </i>	219
6.2.6	<i>Ecosystem carbon balance.....</i>	226
	<i>Daily ecosystem carbon balance.....</i>	226
	<i>Annual carbon balance</i>	227
6.3	CONCLUSIONS.....	229
7.	CONCLUDING REMARKS	231
	REFERENCES.....	235
APPENDIX I	<i>Stable isotope measurement and units</i>	263
APPENDIX II	<i>Estimating C_i/C_a corrected for respiratory processes from net observed discrimination Δ.....</i>	266
APPENDIX III	<i>Solution to the stable isotope partitioning equations as described in the Appendix of Bowling et al., 2001</i>	268

LIST OF SYMBOLS AND ABBREVIATIONS

a	fractionation resulting from diffusion of CO ₂ in air = 4.4	‰
a_b	fractionation during diffusion through a laminar boundary layer = 2.9	‰
a_d	fractionation factor during diffusion of CO ₂ in water = 0.7	‰
a_l	Empirical coefficient for the L-BWB stomatal conductance model	dimensionless
a_m	Sum of fractionation factors during internal CO ₂ transfer = 1.8	‰
A	net assimilation rate per unit projected leaf area	$\mu\text{mol m}^{-2} \text{s}^{-1}$
A_{max}	Q saturated rate of assimilation	$\mu\text{mol m}^{-2} \text{s}^{-1}$
A_{pred}	Predicted net assimilation rate per unit projected leaf area	$\mu\text{mol m}^{-2} \text{s}^{-1}$
A_{PT}	Liquid phase transport of carbohydrates in phloem	$\text{Mg C ha}^{-1} \text{y}^{-1}$
b	net fractionation factor during carboxylation by Rubisco and PEPC = 30	‰
B_A	Over-bark basal area	cm^2
C_a	carbon dioxide mole fraction in the surrounding atmosphere	$\mu\text{mol mol}^{-1}$
C_a'	fluctuations of instantaneous ambient CO ₂ mole fraction from the mean C_a	$\mu\text{mol mol}^{-1}$
\bar{C}_a	mean ambient CO ₂ mole fraction	$\mu\text{mol mol}^{-1}$
C_c	carbon dioxide mole fraction at the sites of carboxylation	$\mu\text{mol mol}^{-1}$
C_i	carbon dioxide mole fraction in the intercellular air spaces	$\mu\text{mol mol}^{-1}$
C_R	carbon dioxide mole fraction added to a background gas	$\mu\text{mol mol}^{-1}$
C_s	carbon dioxide mole fraction at the leaf surface	$\mu\text{mol mol}^{-1}$
C_T	carbon dioxide mole fraction of the background troposphere	$\mu\text{mol mol}^{-1}$
c_p	Specific heat of dry air	$\text{J kg}^{-1} \text{K}^{-1}$
D	discrimination factor against CO ₂ in a closed chamber	‰
D_a	atmospheric mole fraction humidity deficit	mmol mol^{-1}
D_{AG}	Litter transfers from above-ground components	$\text{Mg C ha}^{-1} \text{y}^{-1}$
D_{BG}	Litter transfers from below-ground components	$\text{Mg C ha}^{-1} \text{y}^{-1}$
D_{BH}	Diameter at breast height (1.3 m)	cm
D_{EX}	Liquid phase transport of carbohydrates in root exudates	$\text{Mg C ha}^{-1} \text{y}^{-1}$
D_l	needle-to-atmosphere mole fraction humidity deficit	mmol mol^{-1}
D_s	mole fraction humidity deficit at the leaf surface	mmol mol^{-1}

D_0	Empirical coefficient for the L-BWB stomatal conductance model	mmol mol^{-1}
e_s	Equilibrium fractionation factor of CO_2 entering solution = 1.1	‰
e	fractionation factor during dark respiration = 0	‰
e^*	apparent fractionation factor expressing the difference between the isotopic signal of day respiration and photosynthesis at each time step	‰
e^*_{obs}	apparent fractionation factor expressing the difference between the isotopic signal of day respiration and photosynthesis predicted for each flask pair from Δ_{obs}	‰
e^*_{pred}	apparent fractionation factor expressing the difference between the isotopic signal of day respiration and photosynthesis predicted from Δ_s for each 30 min	‰
E	rate of evapotranspiration per unit ground area	$\text{mmol m}^{-2} \text{s}^{-1}$ or mm h^{-1}
E_i	rate of evaporation for intercepted water per unit ground area	$\text{mmol m}^{-2} \text{s}^{-1}$ or mm h^{-1}
E_L	rate of transpiration per unit projected leaf area	$\text{mmol m}^{-2} \text{s}^{-1}$
E_P	Potential rate of evaporation per unit ground area	$\text{mmol m}^{-2} \text{s}^{-1}$
E_T	rate of transpiration per unit ground area	$\text{mmol m}^{-2} \text{s}^{-1}$ or mm h^{-1}
E_0	the activation energy assumed to = 56, 734	$\text{J mol}^{-1} \text{K}^{-1}$
f	fractionation factor during photorespiration = 8	‰
F_A	Canopy assimilation expressed on a ground area basis	$\mu\text{mol CO}_2 \text{m}^{-2} \text{s}^{-1}$
$F_A (Rd)$	Canopy photosynthesis predicted from scaled chamber relationships including partial inhibition of daytime dark respiration by Q	$\mu\text{mol CO}_2 \text{m}^{-2} \text{s}^{-1}$
$F_A (Rn)$	Canopy photosynthesis predicted from scaled chamber relationships excluding partial inhibition of daytime dark respiration by Q	$\mu\text{mol CO}_2 \text{m}^{-2} \text{s}^{-1}$
$F_A (\text{Eddy } G_c)$	Canopy photosynthesis predicted from stable isotope partitioning and eddy covariance derived G_C	$\mu\text{mol CO}_2 \text{m}^{-2} \text{s}^{-1}$
$F_A (\text{Eddy } G_c \text{ and } G_w)$	Canopy photosynthesis predicted from stable isotope partitioning, eddy covariance derived G_C and G_w	$\mu\text{mol CO}_2 \text{m}^{-2} \text{s}^{-1}$
$F_A (\text{Branch } G_c \text{ and } G_w)$	Canopy photosynthesis predicted from stable isotope partitioning, branch scaled G_C and G_w	$\mu\text{mol CO}_2 \text{m}^{-2} \text{s}^{-1}$
$F_A (\text{L-BWB } G_c \text{ and } G_w)$	Canopy photosynthesis predicted from stable isotope partitioning, and L-BWB derived G_C and G_w	$\mu\text{mol CO}_2 \text{m}^{-2} \text{s}^{-1}$
$F_A (T_a)$	Canopy photosynthesis predicted from $F_{E,N}$ and T_a including all U^* data	$\mu\text{mol CO}_2 \text{m}^{-2} \text{s}^{-1}$
$F_A (T_s)$	Canopy photosynthesis predicted from $F_{E,N}$ and T_s	$\mu\text{mol CO}_2 \text{m}^{-2} \text{s}^{-1}$

	including all U^* data	
F_A (T_a and U^*)	Canopy photosynthesis predicted from $F_{E,N}$ and T_a excluding low U^* data	$\mu\text{mol CO}_2 \text{ m}^{-2} \text{ s}^{-1}$
F_A (T_s and U^*)	Canopy photosynthesis predicted from $F_{E,N}$ and T_s excluding low U^* data	$\mu\text{mol CO}_2 \text{ m}^{-2} \text{ s}^{-1}$
F_E	Net ecosystem exchange expressed on a ground area basis	$\mu\text{mol CO}_2 \text{ m}^{-2} \text{ s}^{-1}$
$F_{E,N}$	Net ecosystem exchange during the night expressed on a ground area basis	$\mu\text{mol CO}_2 \text{ m}^{-2} \text{ s}^{-1}$
$F_{E,D}$	Net ecosystem exchange during the day expressed on a ground area basis	$\mu\text{mol CO}_2 \text{ m}^{-2} \text{ s}^{-1}$
F_I	net isoflux of $^{13}\text{CO}_2$	$\mu\text{mol CO}_2 \text{ m}^{-2} \text{ s}^{-1}$ ‰
F_R	Ecosystem respiration expressed on a ground area basis	$\mu\text{mol CO}_2 \text{ m}^{-2} \text{ s}^{-1}$
F_R (T_a)	Ecosystem respiration predicted from $F_{E,N}$ and T_a including all U^* data	$\mu\text{mol CO}_2 \text{ m}^{-2} \text{ s}^{-1}$
F_R (T_s)	Ecosystem respiration predicted from $F_{E,N}$ and T_s including all U^* data	$\mu\text{mol CO}_2 \text{ m}^{-2} \text{ s}^{-1}$
F_R (T_a and U^*)	Ecosystem respiration predicted from $F_{E,N}$ and T_a excluding low U^* data	$\mu\text{mol CO}_2 \text{ m}^{-2} \text{ s}^{-1}$
F_R (T_s and U^*)	Ecosystem respiration predicted from $F_{E,N}$ and T_s excluding low U^* data	$\mu\text{mol CO}_2 \text{ m}^{-2} \text{ s}^{-1}$
F_R (R_d)	Ecosystem respiration predicted from scaled chamber relationships including partial inhibition of daytime dark respiration by Q	$\mu\text{mol CO}_2 \text{ m}^{-2} \text{ s}^{-1}$
F_R (R_n)	Ecosystem respiration predicted from scaled chamber relationships excluding partial inhibition of daytime dark respiration by Q	$\mu\text{mol CO}_2 \text{ m}^{-2} \text{ s}^{-1}$
F_R (Eddy G_c)	Ecosystem respiration predicted from stable isotope partitioning and eddy covariance derived G_c	$\mu\text{mol CO}_2 \text{ m}^{-2} \text{ s}^{-1}$
F_R (Eddy G_c and G_w)	Ecosystem respiration predicted from stable isotope partitioning, eddy covariance derived G_c and G_w	$\mu\text{mol CO}_2 \text{ m}^{-2} \text{ s}^{-1}$
F_R (Branch G_c and G_w)	Ecosystem respiration predicted from stable isotope partitioning, branch scaled G_c and G_w	$\mu\text{mol CO}_2 \text{ m}^{-2} \text{ s}^{-1}$
F_R (L-BWB G_c and G_w)	Ecosystem respiration predicted from stable isotope partitioning, and L-BWB derived G_c and G_w	$\mu\text{mol CO}_2 \text{ m}^{-2} \text{ s}^{-1}$
g_b	boundary layer conductance to water vapour per unit projected leaf area	$\text{mmol m}^{-2} \text{ s}^{-1}$
g_c	stomatal conductance to carbon dioxide per unit projected leaf area	$\mu\text{mol m}^{-2} \text{ s}^{-1}$
g_s	stomatal conductance to water vapour per unit projected leaf area	$\text{mmol m}^{-2} \text{ s}^{-1}$
g_s pred	predicted stomatal conductance to water vapour using fitted L-BWB function per unit projected leaf	$\text{mmol m}^{-2} \text{ s}^{-1}$

	area	
g_w	mesophyll conductance to carbon dioxide per unit projected leaf area	$\mu\text{mol m}^{-2} \text{s}^{-1}$
g_0	lowest stomatal conductance derived from L-BWB curve fitting	$\mu\text{mol m}^{-2} \text{s}^{-1}$
G_a	aerodynamic conductance expressed on a ground area basis	$\text{mol m}^{-2} \text{s}^{-1}$
G_c	canopy conductance to CO_2 expressed on a ground area basis	$\text{mol m}^{-2} \text{s}^{-1}$
G_s	canopy conductance to H_2O expressed on a ground area basis	$\text{mol m}^{-2} \text{s}^{-1}$
G_T	total canopy conductance to CO_2 expressed on a ground area basis	$\text{mol m}^{-2} \text{s}^{-1}$
G_w	canopy mesophyll conductance to CO_2 expressed on a ground area basis	$\text{mol m}^{-2} \text{s}^{-1}$
h	Relative humidity	%
ha	hectare	10^4 m^2
H	live crown depth normalised to the maximum live crown depth	$0 < H < 1$
H_c	Maximum live crown depth	1
k	Carboxylation efficiency = v_c/C_i	$\mu\text{mol m}^{-2} \text{s}^{-1}$
K	temperature in kelvins	K
L	needle area index	$\text{m}^2 \text{ projected leaf area m}^{-2} \text{ ground area}$
L_A	Projected needle area	cm^2
M	moles of air per unit ground area in a closed system	mol m^{-2}
M_c	Total carbon content of branch foliage inside chamber	$\mu\text{mol C m}^{-2}$
P_{atm}	atmospheric pressure at 340 m elevation	hPa
P_{sat}	saturated vapour pressure	hPa
Q	photosynthetic photon flux density	$\mu\text{mol m}^{-2} \text{s}^{-1}$
Q_k	an extinction coefficient describing the relationship between Q and crown depth = 4.08	dimensionless
r	absolute molar abundance ratio	‰
r_a	absolute molar abundance ratio of ambient CO_2	‰
r_p	absolute molar abundance ratio of a product	‰
r_r	absolute molar abundance ratio of a reactant	‰
r_R	absolute molar abundance ratio of respired CO_2	‰
r_w	mesophyll resistance to internal CO_2 transfer to the sites of carboxylation	$\text{mol m}^{-2} \text{s}^{-1}$
\mathcal{R}	gas constant = 8.314	$\text{J mol}^{-1} \text{K}^{-1}$
R_B	efflux of carbon dioxide from branches	$\mu\text{mol m}^{-2} \text{s}^{-1}$
R_d	rate of daytime dark respiration	$\mu\text{mol m}^{-2} \text{s}^{-1}$
R_n	rate of dark respiration	$\mu\text{mol m}^{-2} \text{s}^{-1}$

R_S	efflux of carbon dioxide from respiring roots and microbes in the soil	$\mu\text{mol m}^{-2} \text{s}^{-1}$
R_W	efflux of carbon dioxide from stems	$\mu\text{mol m}^{-2} \text{s}^{-1}$
R_{10}	R at 10 °C	$\mu\text{mol m}^{-2} \text{s}^{-1}$
R_{20}	R_n at 20 °C	$\mu\text{mol m}^{-2} \text{s}^{-1}$
R_{net}	net radiation	W m^{-2}
s	Slope of the saturation vapour pressure vs temperature curve for water	Pa K^{-1}
S_A	Sapwood area	cm^2
T	Global temperature	$^{\circ}\text{C}$
T_a	Air temperature	$^{\circ}\text{C}$
T_l	Leaf temperature	$^{\circ}\text{C}$
T_s	Soil temperature at a depth of 5cm from the soil surface	$^{\circ}\text{C}$
U	horizontal wind velocity	m s^{-1}
U^*	friction velocity	m s^{-1}
v_c	rate of carboxylation	$\mu\text{mol m}^{-2} \text{s}^{-1}$
v_o	rate of oxygenation per unit projected leaf area	$\mu\text{mol m}^{-2} \text{s}^{-1}$
$0.5v_o$	rate of photorespiration per unit projected leaf area	$\mu\text{mol m}^{-2} \text{s}^{-1}$
V	temperature dependent molar volume	$\text{dm}^3 \text{mol}^{-1}$
w	instantaneous vertical wind velocity normal to the mean wind	m s^{-1}
w'	fluctuations of instantaneous vertical wind velocity from the mean w	m s^{-1}
\overline{w}	mean vertical wind velocity	m s^{-1}
W_A	Above-ground biomass	Mg ha^{-1}
z_c	Normalised whorl height on tree	$0 < z_c < 1$
z_m	height of measurement	m
z_t	Normalised top height of trees	1
α	fractionation factor also referred to as isotope effects	‰
λE	the latent heat flux of transpired water vapour	W m^{-2}
γ	psychrometric constant	Pa K^{-1}
ζ	Surface-layer scaling parameter	dimensionless
ϕ	Initial slope of A/Q response curve	$\text{mol CO}_2 \text{mol}^{-1} Q$
Θ	convexity of A/PPFD response curve	dimensionless
Γ^*	CO_2 mole fraction where $v_c = 0.5v_o$	$\mu\text{mol mol}^{-1}$
Γ	CO_2 compensation mole fraction	$\mu\text{mol mol}^{-1}$
θ	volumetric water content of soil	$\text{m}^3 \text{m}^{-3}$
ρ	density of dry air	kg m^{-3}
‰	parts per mille (1000)	
δ	Absolute molar abundance ratio expressed with respect to the standard PDB	‰
$\delta^{13}\text{C}$	carbon isotope ratio with respect to PDB	‰
$\delta^{13}\text{C}^{18}\text{O}^{16}\text{O}$	$\delta^{18}\text{O}$ of ambient CO_2 (with respect to PDB- CO_2)	‰

$\delta\text{H}_2^{18}\text{O}$	$\delta^{18}\text{O}$ of ambient water vapour (with respect to SMOW)	‰
δ_{T}	carbon isotope ratio of background tropospheric CO_2	‰
δ_{a}	carbon isotope ratio of atmospheric CO_2	‰
δ_{B}	carbon isotope ratio of branch respired CO_2	‰
δ_{D}	carbon isotope ratio of flux weighted assimilated material	‰
δ_{e}	carbon isotope ratio of daytime dark respired CO_2 with respect to canopy air	‰
δ_{FC}	carbon isotope ratio of net turbulent exchange	‰
δ_{R}	carbon isotope ratio of ecosystem respired CO_2	‰
δ_{S}	carbon isotope ratio of soil respired CO_2	‰
δ_{W}	carbon isotope ratio of stem respired CO_2	‰
δ_{plant}	carbon isotope ratio of the substrate pool of recently assimilated needle carbohydrates $\approx \delta_{\text{B}}$	‰
δ_{needle}	carbon isotope ratio of needle bulk material	‰
δ_{wood}	carbon isotope ratio of wood bulk material	‰
δ_{soil}	carbon isotope ratio of soil bulk material	‰
Δ_{AG}	changes in above-ground biomass storage	$\text{Mg C ha}^{-1} \text{ y}^{-1}$
Δ_{BG}	changes in below-ground biomass storage	$\text{Mg C ha}^{-1} \text{ y}^{-1}$
Δ	Photosynthetic ^{13}C discrimination by the plant	‰
Δ_{C}	Predicted instantaneous canopy ^{13}C discrimination	‰
Δ_{C} (Branch G_{c} and G_{w})	instantaneous canopy ^{13}C discrimination predicted from the stable isotope partitioning approach, constrained with branch scaled G_{c} and G_{w}	‰
Δ_{C} (Branch G_{c} and G_{w})	instantaneous canopy ^{13}C discrimination predicted from the stable isotope partitioning approach, constrained with branch scaled G_{c} and G_{w}	‰
Δ_{C} (Eddy G_{c})	instantaneous canopy ^{13}C discrimination predicted from the stable isotope partitioning approach and eddy covariance derived G_{c}	‰
Δ_{C} (Eddy G_{c} and G_{w})	instantaneous canopy ^{13}C discrimination predicted from the stable isotope partitioning approach, eddy covariance derived G_{c} and canopy estimates of G_{w}	‰
Δ_{CF}	instantaneous canopy ^{13}C discrimination predicted from a model correcting for photorespiration, daytime dark respiration and mesophyll conductance	‰
Δ_{C} (L-BWB G_{c} and G_{w})	instantaneous canopy ^{13}C discrimination predicted from the stable isotope partitioning approach, constrained with L-BWB estimates of G_{c} and G_{w}	‰
Δ_{CS}	instantaneous canopy ^{13}C discrimination predicted from the simple model using C_i/C_{a}	‰
Δ_{E}	Predicted instantaneous ecosystem ^{13}C discrimination	‰

Δ_F	Photosynthetic ^{13}C discrimination corrected for mesophyll conductance, dark daytime respiration and photorespiration	‰
Δ_{gw}	Photosynthetic ^{13}C discrimination corrected for mesophyll conductance	‰
Δ_{KEELING}	Predicted integrated ecosystem ^{13}C discrimination relative to δ_T	‰
Δ_{LF}	Predicted integrated canopy ^{13}C discrimination, equal to $\delta_a - \delta_R$	‰
Δ_{obs}	Net observed instantaneous ^{13}C discrimination	‰
Δ_R	Photosynthetic ^{13}C discrimination corrected for dark daytime respiration and photorespiration	‰
Δ_{Rd}	Photosynthetic ^{13}C discrimination corrected for dark daytime respiration	‰
Δ_S	Photosynthetic ^{13}C discrimination predicted from C_i/C_a	‰
$\Delta_{0.5v_o}$	Photosynthetic ^{13}C discrimination corrected for photorespiration	‰

ABBREVIATIONS

ATP	Adenosine triphosphate	
CAM	crassulacean acid metabolism	
CDM	clean development mechanism	
C3	Photosynthetic pathway in which Rubisco is the primary carboxylation enzyme	
C4	Photosynthetic pathway in which the first stable products of CO_2 assimilation are 4-carbon anions	
ECD	Electron capture detector	
FACE	Free Air CO_2 Enrichment	
FID	Flame ionization detector	
GC	Gas Chromatograph	
GPP	Gross Primary Production expressed on a ground area basis	$\text{t C ha}^{-1} \text{ y}^{-1}$
IAEA	International Atomic Energy Agency	
L-BWB	Leunings modified Ball, Woodrow & Berry Model	
ME	Malic enzyme	
NAD+	Nicotinamide adenine dinucleotide	
NBS	United States Bureau of Standards	
NEE	net ecosystem exchange expressed on a ground area basis	$\mu\text{mol m}^{-2} \text{ s}^{-1}$
NEP	net ecosystem productivity expressed on a ground area basis	$\text{Mg C ha}^{-1} \text{ y}^{-1}$
P	probability critical threshold	
PDB	Pee Dee Belemnite (^{13}C standard)	‰

PDC	Pyruvate dehydrogenase complex	
PEPC	Phospho-enol-pyruvate carboxylase	
PGA	3-phosphoglycerate	
PGly	phosphoglycolate	
PPFD	photosynthetic photon flux density	$\mu\text{mol m}^{-2} \text{s}^{-1}$
RUBISCO	Ribulose-1,5-bisphosphate carboxylase-oxygenase	
RuBP	Ribulose-1,5-bisphosphate	
SMOW	Standard Mean Ocean Water (^{18}O standard)	‰
SNA	specific needle area	$\text{cm}^2 \text{g}^{-1}$
TCA	tricarboxylic acid	
V-PDB	Vienna Pee Dee Belemnite (^{13}C standard)	‰
V-SMOW	Vienna Standard Mean Ocean Water (^{18}O standard)	‰

1. Introduction

1.1 CONTEXT

The Global Greenhouse Problem

One of the primary scientific observations of the 20th century has been the rise in atmospheric carbon dioxide mole fraction (C_a) from 280 to 360 $\mu\text{mol mol}^{-1}$, over the past 120 years (Keeling *et al.*, 1995). The main causes for this rise have been attributed to the burning of fossil fuels and the clearing of forests, which have released CO_2 into the atmosphere. CO_2 is one of a collection of trace gases that absorb infra-red radiation. These trace gases, more commonly referred to as, radiatively active gases or 'greenhouse gases' reduce heat loss from the planet, through the 'greenhouse effect', and consequently maintain global temperatures, within a range that can support life. The relationship between the atmospheric CO_2 mole fraction and global temperature (T) was postulated over a century ago, and is now widely accepted (Arrhenius, 1896; IPCC, 1996). The observed rise in CO_2 emission rates motivated international agreement to limit the production of greenhouse gases, in an attempt to stabilise C_a and reduce the rate of global warming. The Kyoto Protocol of the UN Framework Convention on Climate Change provided further that, within prescribed rules, countries could remove CO_2 from the atmosphere into living plants, sequester the carbon in the terrestrial biosphere, and use the sequestered carbon to offset some of their greenhouse gas emissions from other sources. Identifying the terrestrial carbon sink as a Clean Development Mechanism (CDM), led to countries with large forested areas, e.g., Russia, United States and Canada, negotiating for an increased ceiling in the amount of CO_2 that could be offset against forest management activities, thereby effectively relaxing the parties emission targets (Conference of the Parties (COP) Meeting 7, Marrakech,

2002). This established a pressing need for the reduction in uncertainties in the science of global and regional carbon source and sink determination.

The ‘missing sink’ for CO₂

On the basis of estimated rates for anthropogenic emissions (including land use change) and simulations of oceanic carbon uptake, the accumulation of CO₂ in the atmosphere is less than expected. This incomplete closure of the carbon mass balance highlighted the existence of a so-called “missing sink” for CO₂ (Broecker *et al.*, 1979; Keeling *et al.*, 1995). Presently, the terrestrial biosphere is recognised to be the likely net sink for atmospheric CO₂, thus accounting to some extent for this disparity. The seasonal and spatial influence exerted by the terrestrial biosphere on the global distribution of CO₂, is now firmly established (Keeling, 1979; Tans *et al.*, 1993; Francey *et al.*, 1995).

1.2 BACKGROUND

1.2.1 *Estimating the carbon balance of forests*

Several studies at the global scale indicate a large terrestrial biosphere sink and this has focused research attention on the fluxes of CO₂ above and within terrestrial ecosystems (Keeling *et al.*, 1979; Tans *et al.*, 1993; Francey *et al.*, 1995; Ciais *et al.*, 1995a; Ciais *et al.*, 1995b; Trolier *et al.*, 1996; Fung *et al.*, 1997; Bakwin *et al.*, 1998; Bousquet *et al.*, 1999; Battle *et al.*, 2000). Measurement of the net ecosystem exchange (F_E) of CO₂ and methods for partitioning the F_E into the main component fluxes of net photosynthetic assimilation (F_A) and ecosystem respiration (F_R), assumed both scientific and political importance after the Kyoto Protocol (IGBP Terrestrial Carbon Working Group, 1998). Strategies implemented to quantify these

component fluxes vary (see Lloyd *et al.*, 1996; Ryan *et al.*, 1997; Goulden *et al.*, 1996; Rayment, 1998; Mahli *et al.*, 1998).

Measuring CO₂ exchange between forests and the atmosphere

Ecosystem scale measurements

At most sites the F_E of CO₂ and water vapour between the ecosystem and the atmosphere is measured using the eddy covariance method (Baldocchi *et al.*, 1988; Moncrieff *et al.*, 1996; Aubinet *et al.*, 2000). Incorporation of this technique in large-scale ecosystem studies formed an ideal intermediate scaling platform between global, regional and local scales of interest (Sellers *et al.*, 1997; Jarvis, 1995). Furthermore, it provided a powerful and reliable means of partially explaining interactions at the landscape and biome scale through the measurement and subsequent modelling of diurnal, seasonal and inter-annual changes in the carbon exchange of ecosystems. The technique yields the net flux, representative of the balance between the opposing fluxes of turbulent exchange, photosynthetic CO₂ uptake and respiratory release, in the case of CO₂. To understand the net flux it is necessary to separate these processes, quantify their magnitude and contribution to the net flux. The main processes responsible for the net ecosystem exchange of a forest are shown in Figure 1.1.

Furthermore, characterisation of how each process responds to particular environmental variables, especially temperature and precipitation inputs, are regarded as essential, as variability in both are likely in the event of climate change. However, the differential responses of F_A and F_R to environmental stimulation can be marked, and it is not always possible to attribute a response of F_E solely to any one process.

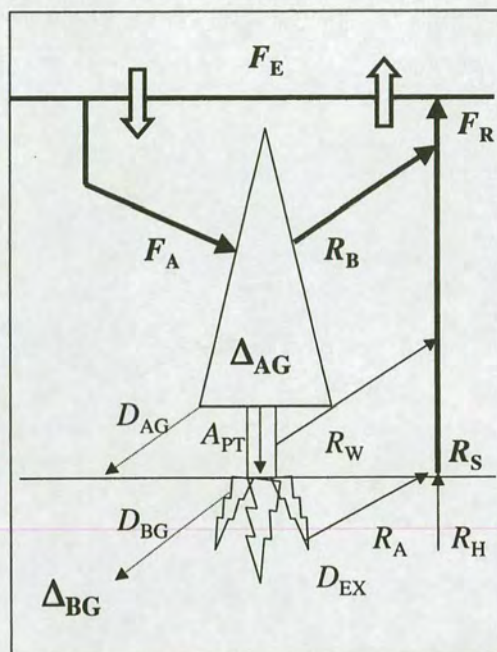


Figure 1.1 A simplified diagram showing the fluxes and reservoirs of CO_2 in a forest stand. F_A is the flux of CO_2 from the atmosphere into foliage *via* canopy assimilation. F_R is the flux of CO_2 from the forest to the atmosphere, which represents the sum of foliage (R_B), wood (R_W) and soil respiration (R_S) composed of both root (R_A) and microbial respiration (R_H). Dashed lines indicate litter transfers from above-ground (D_{AG}) and belowground (D_{BG}) components. A_{PT} represents the liquid phase transport of carbohydrates in the phloem and in root exudates D_{EX} . Changes in above-ground carbon storage Δ_{AG} and below-ground carbon storage Δ_{BG} are also represented. Arrows and symbols in bold represent fluxes and biomass stocks measured within the present study in units of $\text{Mg C ha}^{-1} \text{ yr}^{-1}$.

For instance, large estimates of F_E measured in the Sitka spruce plantation, used in the present PhD research programme, show that presently it is a substantial sink for about $6 \text{ tonnes of C ha}^{-1} \text{ yr}^{-1}$ (Valentini *et al.*, 2000). This sink could be the result of high rates of F_A , facilitated through favourable photon flux density (Q), temperature, humidity and soil moisture availability over a long growing season. Alternatively, it could be the result of low respiratory fluxes, as a consequence of low temperatures, poor substrate quality, efficient scavenging of respired CO_2 (Ludlow and Jarvis, 1972; Broadmeadow & Griffiths, 1993; Cernusak *et al.*, 2001) or soil moisture constraints on soil CO_2 efflux.

Measurements at the scale of the ecosystem and region cannot directly resolve these differences, but they can reveal substantial intra- and inter-annual variation in F_E . This information at best, provides an empirical means for evaluating the carbon transfer. However, understanding the processes at a mechanistic level remains largely conjectural without concurrent supplementary measurements.

Component scale measurements

Nearly all attempts to explain the observed variation of net CO_2 exchange at the stand-scale, have used relationships obtained from chamber studies (Levy, 1995; Meir, 1996; Goulden *et al.*, 1996; Lavigne *et al.*, 1997; Rayment, 1998; Moren, 1999). Usually the scale of observation is reduced to the leaf, branch, stem or soil surface, thereby isolating particular components and processes that contribute to F_E (Figure 1.1). For example, in order to separate out the CO_2 exchanged by the vegetation canopy from the CO_2 exchanged by the whole ecosystem, chamber measurements of the soil CO_2 efflux can be subtracted from the F_E , leaving the canopy contribution as the residual (Rayment, 1998) (Figure 1.1). However, scaling relationships measured in chambers relies on additional measurements that describe the amount and distribution of biomass within the area sampled by the eddy covariance method. This is labour intensive but necessary if chambers are to provide valuable constraints on the magnitudes of F_A and F_R estimated by eddy covariance.

Are nocturnal models of respiration suitable for daytime estimates of canopy photosynthesis and ecosystem respiration?

An alternative practice at the ecosystem scale to establish the magnitude in F_A and F_R involves fitting an Arrhenius function to the relationship between net CO_2 flux during the night ($F_{E,N}$) with changes in air (T_a) or soil temperature (T_s) (Greco & Baldocchi, 1996; Goulden *et al.*, 1997; Aubinet *et al.*, 2000. Differences in the

parameters obtained from fitting this relationship with different reference temperature locations to long-term datasets are typically negligible. However, subsequent prediction of F_R using the different reference locations will simulate fluxes of different magnitude, and the timing of maximum and minimum F_R will not occur at the same time during the day. For example, T_a is usually highest around midday, whereas T_s lags T_a and maximum T_s usually occurs in the early evening.

Furthermore, the distribution and differing contributions of respiring biomass in an ecosystem may indicate the appropriate temperature reference location for forcing this relationship. In open canopies with low leaf area index (L) and above ground biomass (W_A), or in ecosystems with very large contributions from soil CO_2 efflux (R_s), utilising T_s is likely to account for most of the variation in F_R , but if canopies are dense with high L and have relatively low contributions from R_s then employing T_s may not be entirely appropriate. Consequently, this could introduce uncertainties in the calculation of F_A , as this is calculated as the residual of the CO_2 mass balance (i.e., $F_A = F_E - F_R$, adopting the micrometeorological sign convention. See Chapter 5, section 5.3.1 for further details).

Presently, eddy covariance sites covering large regions adopt similar methodology thereby harmonising results and facilitating ecosystem comparisons across large regions. For instance the present study site, Griffin Forest represents one site in a group originally containing 16 other measurement sites across Europe (Aubinet et al., 2000; Valentini et al., 2000). However, harmonising temperature reference locations, to T_s for instance may cause F_A to be over- or underestimated during the day, making it difficult to establish both qualitative and quantitative relationships between F_A and environmental variables. Hence one of the objectives in the present study will be to explore the effects of reference temperature on the magnitude and timing of F_R and F_A and to establish which reference temperature best describes the relationships observed in independent chamber methods.

A further complication when fitting the relationship between net CO₂ flux during the night ($F_{E,N}$) is whether to include or exclude $F_{E,N}$ measured during unfavourable turbulence conditions; when wind speeds (U) are low and the friction velocity, (U^*) below 0.2 m s⁻¹ (Greco & Baldocchi, 1996; Goulden *et al.*, 1997; Rayment & Jarvis, 2000). Excluding low U^* data tends to increase estimates of F_R substantially, and can have a significant impact on annual estimates of forest carbon sequestration (Goulden *et al.*, 1996). Hence, another objective in the present study will be to explore the effects of U^* on the magnitude of F_R and F_A against relationships observed in independent chamber methods quantifying F_R and F_A .

Are rates of daytime dark respiration currently overestimated?

Fitting relationships to data only collected at night requires the assumption that metabolic activity during the daytime continues at the same rate as measured at night for the same temperature. Evidence from the literature has shown that partial inhibition of foliage and stem respiration occurs during the day and is responsive to changing environmental variables, e.g., irradiance and temperature (Atkin *et al.*, 2000; Cernusak & Marshall, 2000; Cernusak *et al.*, 2001). For example, *Picea sitchensis*, the species observed in the present study, has exhibited cortical re-fixation of CO₂ and partial inhibition of daytime dark respiration (Ludlow & Jarvis, 1971; Cornic & Jarvis, 1972). However, there are very few studies that consider the impact of such inhibition at the scale of a canopy. This is primarily because daytime dark respiration (R_d) is a challenging process to quantify, especially in the field. If substantial inhibition occurs during the day then present estimates of F_R during the day may be over-estimated. Hence, a further objective within the present study will explore the impact of partial inhibition on daytime dark respiration using the best available datasets describing the interaction of R_d with Q and T .

1.2.2 Fractionation of CO₂ by the terrestrial biosphere

The biosphere not only influences the amount and timing of CO₂ exchanged with the atmosphere, but also alters the ¹³C/¹²C ratio of CO₂ in the atmosphere (δ_a). An explanation of stable isotope methodology, theory and units is provided in Appendix I of this thesis.

During photosynthesis plants preferentially assimilate ¹²CO₂, resulting in an increase of the δ_a remaining. The annual average of δ_a is approximately -8 ‰ (Mook, 1986). A decrease in the ¹³C/¹²C ratio of photosynthetic assimilates constructed by the plant (δ_{plant}), relative to the atmosphere occurs, reflecting discrimination during uptake. For plants with the C3 photosynthetic pathway, the discrimination has been related primarily to differential diffusivities of ¹³CO₂ and ¹²CO₂ in air, as well as an intrinsically lower reactivity of ¹³C during initial fixation by photosynthetic enzymes (O'Leary, 1981; Farquhar *et al.*, 1982, 1989). Globally, photosynthesis discriminates against ¹³C by about 17 to 18 ‰ (Kaplan, 2001). The above fractionation processes are sensitive to environmental variables such as atmospheric mole fraction humidity deficit (D_a), Q , T_a and C_a . Thus fluctuations in environmental conditions can create transient isotopic disequilibrium, when fluxes of photosynthesis affect δ_a in a way different from fluxes of respiration, providing a natural tracer for component processes and their regulation by environmental conditions.

The process of respiration causes the release of these ¹³C-depleted products with δ_{plant} typically between -25 to -32‰ for C3 plants. Consequently, during the night, vertical gradients in δ_a are commonly observed within the plant canopy, reflecting respiratory processes (Keeling 1961; Lancaster, 1990; Buchmann *et al.*, 1998). Thus differential timing and isotopic composition of carbon uptake and release during photosynthesis and respiration can cause significant spatial and temporal variation in

the observed isotopic signal of the atmosphere surrounding a leaf and in an ecosystem. Furthermore, the spatial and seasonal variation of this signal from the biosphere is transferred to the globe. (Francey *et al.*, 1995; Flanagan *et al.*, 1996; Lloyd *et al.*, 1996; Gillon & Griffiths, 1997; Buchmann *et al.*, 1997).

The use of δ_a as a tracer for anthropogenic and biological activity, has enabled the partitioning of sources and sinks of atmospheric CO₂ between oceanic and terrestrial processes (Keeling *et al.*, 1979; Tans *et al.*, 1993; Francey *et al.*, 1995; Ciais *et al.*, 1995a; Ciais *et al.*, 1995b; Trolier *et al.*, 1996; Fung *et al.*, 1997; Bakwin *et al.*, 1998; Bousquet *et al.*, 1999a, 1999b; Battle *et al.*, 2000). Recently, Francey *et al.*, (1995) have shown a persistent flattening of the temporal trend in δ_a , observed globally since 1988. This flattening implies a significant change in the partitioning between oceanic and biospheric CO₂ uptake, with more carbon entering the biosphere since 1988 (Francey *et al.*, 1995). The partitioning calculations, however, are extremely sensitive to small changes in the carbon isotopic composition assumed for the terrestrial biosphere and a 1-2 ‰ error (~10% inaccuracy) can produce a change in the inferred terrestrial carbon sink equal to the entire magnitude of the sink (Fung *et al.*, 1997; Kaplan, 2001).

Can stable isotope methods constrain estimates of canopy photosynthesis?

The coupling of stable isotope sampling with flux measurements of CO₂ can reveal additional information regarding the underlying physiological processes involved in the net exchange of CO₂ between the biosphere and atmosphere, best demonstrated with a simple example. Lloyd *et al.*, (1996) demonstrated with mass balance equations how the relative contribution of F_A and F_R could be constrained using stable isotopes as follows:

$$M \frac{dC_a}{dt} = F_R - F_A. \quad (\text{Eq 1.1})$$

Within a closed system of arbitrary height (containing moles of air per unit ground area, M , mol m^{-2}), the component processes of F_A and F_R act in opposite directions during the day: the influx of CO_2 via F_A ($\mu\text{mol m}^{-2} \text{ s}^{-1}$) and the efflux of CO_2 via F_R ($\mu\text{mol m}^{-2} \text{ s}^{-1}$). During the day if both processes are occurring simultaneously the relative contributions of each flux cannot be determined from the observed dC_a/dt . However, an equivalent isotopic mass balance can be constructed as follows:

$$MC_a \frac{d\delta_a}{dt} = F_R (\delta_R - \delta_a) + F_A \Delta, \quad (\text{Eq 1.2})$$

where δ_a and δ_R are the isotopic compositions of atmospheric and ecosystem respired CO_2 , respectively and Δ the discrimination against $^{13}\text{CO}_2$, during F_A . With the two equations, the contributions of F_A and F_R can be determined from observations of $d\delta_a/dt$ and dC_a/dt . This requires that the isotopic signatures of the separate processes have been established and are detectably different. Thus combining isotopic gradients and the isotopic composition of component fluxes will constrain estimates of F_A and F_R at the ecosystem scale. In principle, the same two equations can be used to construct global mass balances for C_a and δ_a , distinguishing the relative contributions from different ecosystems with distinctive isotopic compositions of CO_2 exchange (e.g., the relative contributions of C3 and C4 ecosystems).

Methods developed to measure δ_a and δ_R in the field are relatively simple and consequently attempts to merge isotope ratio analysis with flux measurements have recently been made. Bowling *et al.*, (2001) demonstrated theory similar to the above mass balance could be applied to partition F_E into F_A and F_R . However, this approach relies on accurate estimates of canopy conductance (G_S) to determine

canopy photosynthetic discrimination and F_A . Canopy conductance estimates from eddy covariance can be extremely noisy because of contributions from additional sources of water. Thus if canopy conductance estimates cannot be attributed to transpiration solely, then it is likely over-estimates of F_A will be made and Δ underestimated. Hence, within the present study attempts were made to constrain estimates of canopy conductance using independent methods and partition F_E by combining eddy covariance measurements and sampling of δ_a and C_a . The estimates of F_A can then be compared to other methods described above.

Can stable isotopes reveal the dynamic links between weather, canopy photosynthesis and autotrophic respiration?

Another current research enquiry is the short-term variation in photosynthetic discrimination caused by changes in meteorological conditions. As environmental variables such as Q and D_a fluctuate over various time-scales instantaneous Δ should correspondingly follow these fluctuations through changes in F_A and G_s . As Δ and δ_a change over time, changes in the isotopic composition of needle carbohydrates (δ_{plant}) result and are subsequently used as the substrate for plant respiration or exported to alternative carbohydrate sinks. These changes in δ_{plant} caused by changes in weather could theoretically set up transient changes in the isotopic composition of respired CO_2 . These fluctuations would not only be observed in the foliage but if phloem transport of assimilates to belowground biomass is substantial, transient changes in the isotopic composition of soil respired CO_2 (δ_s) would also result (Ekblad & Högberg, 2001; Bowling et al., 2002).

Studies so far have observed a correlation between environmental variables, especially D_a and measured soil and ecosystem scale measurements of δ_s and δ_R (Ekblad & Högberg, 2001; Bowling et al., 2002). However, the direct link between

environmental variables and day to day variation of Δ and δ_{plant} have yet to be measured. Thus the last objective of the present study was to develop a method that could characterise instantaneous photosynthetic discrimination by branches measured in the field with the aim of modelling fluctuations in Δ and δ_{plant} in response to changes in assimilation and stomatal conductance, caused by fluctuations in environmental variables.

1.3 THESIS AIMS AND STRUCTURE

This aim of this present study will be to estimate the contribution of photosynthesis and respiration to the net ecosystem exchange and ecosystem ^{13}C discrimination in a Sitka spruce plantation by quantifying the following component processes, using a combination of measurement and modelling techniques:

- branch-scale photosynthetic fluxes and ^{13}C discrimination;
- respiratory $^{13}\text{CO}_2$ fluxes from soil and branches and;
- forest $^{13}\text{CO}_2$ fluxes and ^{13}C discrimination.

Specific objectives within this thesis will be to:

- explore the effects of reference temperature on the magnitude and timing of F_R and F_A and to establish which reference temperature best describes the relationships observed in independent chamber methods;
- explore the effects of U^* on the magnitude of F_R and F_A against relationships observed in independent chamber methods quantifying F_R and F_A ;
- explore the impact of partial inhibition on daytime dark respiration using the best available datasets describing the interaction of R_d with Q and T ;

- constrain estimates of canopy conductance using independent methods and partition F_E by combining eddy covariance measurements and sampling of δ_a and C_a . These estimates of F_A can then be compared to the eddy covariance and chamber-based estimates of F_A ;
- develop a method capable of measuring instantaneous photosynthetic discrimination by branches in the field and;
- model fluctuations in Δ and δ_{plant} in response to changes in assimilation and stomatal conductance, caused by fluctuations in environmental variables.

There are seven chapters. Chapter 2 describes the distribution and amount of biomass and carbon within the flux footprint of an eddy covariance tower at Griffin Forest.

Chapter 3 describes in detail the uncertainties and theory of photosynthesis, stomatal conductance and photosynthetic discrimination. A description of methods used in this study to measure the daily variation in photosynthesis, respiration and photosynthetic ^{13}C discrimination then follows.

Chapter 4 describes the diurnal variation of gas exchange from branches during photosynthesis and respiration *in situ* in response to observed variations in photosynthetic photon flux density (Q), temperature (T_a) and air vapour pressure deficit (D_a). These data are then used for estimating the contribution of photosynthetic CO_2 uptake, photorespiration and daytime dark respiration to the net CO_2 exchange over a diurnal time course. I then describe how additional sampling of δ_a exchanged during these processes was made using a novel field method. These data are then used in conjunction with gas exchange data to estimate the contributions of photosynthetic CO_2 uptake, photorespiration and day respiration to the net observed discrimination against $^{13}\text{CO}_2$ over a daily time course. The results

are critically compared against other frequently used methods and models that quantitatively estimate photosynthetic discrimination and gas exchange, in order to describe integrated observations at the leaf and ecosystem scales.

Chapter 5 describes the uncertainties and theory relating to the net ecosystem exchange of CO_2 and methods used to quantify the component processes of F_A and F_R . A description of methods used in this study to compare the daily variation in canopy photosynthesis, ecosystem respiration and canopy photosynthetic ^{13}C discrimination using different approaches then follows.

Chapter 6 describes the daily variation of *in situ* soil CO_2 efflux and $\delta^{13}\text{C}$ of soil respired CO_2 using chamber methods in response to environmental variables. Estimates of F_A and F_R were made by scaling component chamber results reported in Chapter 4. These results were subsequently compared with eddy covariance estimates of F_A and F_R .

Estimates of F_A and F_R were then estimated for the forest using an alternative partitioning approach, that combines F_E estimates from eddy covariance data with canopy scale stable isotope information. These results are then critically compared between methods and estimates of the contribution of photosynthesis and respiration to the net exchange of CO_2 with the atmosphere are made.

Estimates of canopy and ecosystem ^{13}C discrimination are also made using the eddy covariance approach and scaled chamber-based relationships. Estimates from these two methods are compared and the influence of canopy photosynthesis and respiration on ecosystem discrimination is explored.

Chapter 7 describes the conclusions of this study and highlights gaps in current knowledge.

2. Structure of Griffin Forest: biomass, leaf area and soil characteristics

2.1 INTRODUCTION

The need for biomass, leaf area and soil characterisation

The net carbon budget of a forest is a fine balance between processes of carbon acquisition (photosynthesis, tree growth, forest ageing, carbon accumulation in soils), and processes of carbon release (respiration of biomass, tree mortality, microbial decomposition of litter, oxidation of soil carbon, degradation and disturbance). The net ecosystem exchange (F_E), or carbon balance, between a forest and the atmosphere can be measured using micrometeorological techniques, e.g., the eddy covariance method.

Net ecosystem exchange can be partitioned to estimate the two component fluxes, canopy photosynthesis (F_A) and ecosystem respiration (F_R), by measuring temperature and nocturnal net CO_2 exchange ($F_{E,N}$) providing a method for calculating F_A through the mass balance calculation for CO_2 . However, uncertainties regarding the accuracy of $F_{E,N}$ measurement and application of a nocturnal model in a daylight situation are growing (see Chapters 1, 5 and 6). These two component fluxes can be quantified using two different strategies; by scaling small-scale chamber measurements of CO_2 exchange using information on stand biomass, leaf area and soil structure or, measuring the change in biomass and dead plant mass over longer timescales (i.e., litterfall, soil C accumulation, leaf area and girth increment). By using scaled chamber measurements, estimates of daily and annual CO_2 exchange can be assessed and directly compared with daily and annual estimates of F_E

provided by eddy covariance methods. However, it is also important that the amount and heterogeneity of biomass within the footprint of the eddy covariance tower are characterised well to reduce some of the uncertainties in the scaling process. Furthermore, by monitoring changes in biomass stocks a further constraint is provided for annual estimates of carbon balance, referred to as net ecosystem productivity (NEP) obtained from the eddy covariance method.

2.2 CHAPTER AIMS

The aims for this chapter are:

- (i) to characterise the total leaf area on Sitka spruce trees in relation to over-bark basal area;
 - (ii) to characterise the distribution of stem density and above ground basal area within the flux footprint;
 - (iii) to estimate indirectly the needle area index within the flux footprint using the basal area distribution;
 - (iv) to establish the annual above-ground increment in basal area and identify when the majority of this increment occurs during the growing season;
 - (v) to characterise the soil surface, structure and carbon content within the flux footprint and;
 - (vi) to estimate the annual below-ground increment in soil organic matter using site micro-topography as a proxy for C accumulation during the present rotation.
-

2.3 METHOD

2.3.1 Study site

The study was conducted in an even-aged plantation of Queen Charlotte Islands provenance Sitka spruce (*Picea sitchensis* (Bong.) Carr.). Griffin Forest, is located near Aberfeldy, Perthshire, UK (56°37"N, 3°48"W) and is a long-term site within the EU-funded CARBOEUROFLUX network. The site description is summarised in Table 2.1.

Site and Stand characteristics		No. of samples
Elevation (m)	340	
Mean annual temperature (°C)	8.2	
Mean annual precipitation (mm)	1200	
Inclination (°)	7	
Planting Year	1981	
Former Land Use	Moorland	
Soil Type (see Table 2.2)	Peaty-gley and Podsols	
Number of trees (ha ⁻¹)	2200 (600)	1040
Average tree height (m)	10 (2)	94
Average diameter at breast height (cm)	13 (5)	1040
Specific needle area (SNA) cm ² g ⁻¹	30-50	
Needle area index (m ⁻² m ⁻²)	6 (2)	
Average overbark basal area (m ² ha ⁻¹)	32 (13)	1040
Live Crown base height (m)	1.1(1)	94
Live Crown radius (m)	1.8 (0.5)	94

Table 2.1 Summary description of the site and stand characteristics of Griffin Forest during 2001. Diameters at breast height (D_{BH}) and numbers of trees per 0.01 hectare were based on measurements of all trees within 45 plots of 0.01 ha sampled systematically within 50 ha in the footprint of a flux tower. This number of samples were required to predict stand D_{BH} to meet the 10% upper bound on the error of estimation of the stand. Leaf area index was calculated from direct harvest and complementary allometric data available from the literature. Where available one standard deviation are provided in parentheses.

2.3.2 Forest structure

Leaf area determination

Samples for the determination of leaf area were collected on two occasions at Griffin Forest, the first during April 1998 and the second at the end of the gas exchange study period in August 2001. Eight individuals, from three different sites within the flux footprint were sampled intensively to characterise vertical leaf area distribution.

For each tree the top height (m) and respective height of each whorl on the trees were measured to create a whorl profile. Within each whorl the number of branches were recorded and two branches harvested from whorls at four levels in the canopy. Each branch was then measured for length and total fresh biomass (accuracy of $\pm 0.1\text{kg}$). For each needle cohort on a branch a sub-sample of needles were separated and measured for fresh biomass (g), specific needle area, SNA ($\text{cm}^2 \text{g}^{-1}$) and dry mass (g) after 48 hours of drying at 70°C . Projected needle area (cm^2) for sub-sampled fresh needles were then measured with a Li-Cor 3100 area meter (Li-Cor Inc., Lincoln, Nebraska). Total needle area for each cohort was determined by applying the cohort SNA, to the total mass of needles weighed for each cohort of the individual branches. The average mass and leaf area for the sampled branches ($n = 2$) were then assumed to represent all branches recorded on that whorl. The total leaf area in each cohort for the sub-sampled whorl was then calculated simply by multiplying the average leaf area per cohort by the number of branches in the whorl.

As the positions of all whorls in the sampled crown were determined, the leaf area for each cohort in the sub-sampled whorls could be interpolated by approximating the leaf area as a β -function with respect to a normalised crown height whereby the β -function was forced through the bottom and top of the crown system as follows,

$$L_A = a z_c^b (z_t - z_c)^c, \quad (\text{Eq 2.1})$$

where L_A represents the estimated projected leaf area for the cohort (cm^2), a , b and c are the fitted empirical parameters, z_t represents the top height of the tree normalised to = 1 and z_c represents the normalised height of the whorl ($0 < z_c < 1$) (Kellomäki *et al.*, 1980). The β -function was fitted using the PROC NLIN, SAS procedure for each cohort. Using the interpolated leaf areas and the relative crown positions of the whorls the total leaf area of the sample tree was estimated.

As the sample size for tree L_A was small ($n = 8$ individuals) the biometric data from each tree were pooled with other leaf area studies describing the biometry of pole-stage Sitka spruce in Scotland. The studies used to determine the allometric relationships between leaf area (L_A), sapwood area (S_A) and over-bark basal area (B_A) are presented in Table 2.2.

Site Id	Location	Stem Density	Age	Elev.	Prec.	Treatment	Reference
Benmore	NS139736	2900	27	315	2000	Fertilised	McIntosh, 1984
Wauchope	NY599058	3610	23	330	1200	Fertilised Spacing	McIntosh, 1984
Cloich*	55° 42' N	2500	26	360-400	800	n/a	Dunning, 1999
Forest	03° 16' W		28				
Cloich,	55° 42' N	2500	13	330-405	1100	Spacing	Sinclair, 1995
Forest	03° 16' W		15				
Glentrool	NX360792		30	122	1750	Fertilised	Edwards, 1980
Griffin	56° 37' N	2200	17	340	1200	n/a	Wingate, 1998 and 2001
	03° 48' W		20			recent N	

Table 2.2 Published datasets used in this study to characterise leaf area and sapwood area for pole-stage Sitka spruce in Scotland.

Above-ground biomass distribution

An inventory of woody biomass was made within the eddy covariance flux footprint, estimated to cover $\approx 50 - 100$ ha (Clement, 2003). During 1997, 45 plots of 0.01 ha were set out systematically within the flux footprint. These plots were sampled for species composition, stem density and D_{BH} for all trees present in the sampling unit. To meet the 10% upper bound on the error of estimation based on preliminary sampling of the stand, 55 plots of 0.01 ha would have required sampling. The 45 plots measured in 1997 were then re-measured annually to determine increases in the above ground biomass within the flux footprint.

The above-ground biomass of a stand is closely related to its over bark basal area. Mitchell, Proe & MacBrayne (1981) found the following relationship from harvest data for young Sitka spruce stands at an age of 13 – 22 years, yield class of 10 – 28 and stocking density of 2520 – 4160 trees ha^{-1} :

$$W_A = 2.30985 B_A + 0.0218 B_A + 5.90025, \quad (\text{Eq 2.2})$$

where W_A is the above-ground biomass in Mg ha^{-1} and B_A is the basal area of the stand in $\text{m}^2 \text{ha}^{-1}$. To estimate the total stock of carbon stored in above-ground biomass W_A was divided by a factor of 2, i.e., 50% of above-ground biomass.

Soil Structure

The ploughing regime used for the site preparation of Griffin Forest inverted material from furrows onto adjacent strips of land to form elevated ridges, resulting in three distinct surface areas: 'furrows', 'ridges' and undisturbed land, hereon referred to as 'flat' illustrated in Figures 2.1 and 2.2. Trees were planted on the ridges and

undisturbed ground at $\approx 2 \times 2$ m spacing so that there are usually two lines of trees between the furrows. Ridges occupy 50% of the total area, furrows and flat areas 25% each. Soil samples of 5.7 cm diameter were taken in a stratified random design from a 0.85 ha plot within the flux footprint, 40 from ridges, 20 from furrows and 20 from flat areas. Sampling depth was determined by the lower boundary of the lowest horizon enriched in organic carbon. This boundary was identified by the sudden change from dark brown to bright pale colour at the lower end of the original Aeh (or Ahe) horizon. In the deepest parts of the furrows, where this horizon has been completely removed by the plough, sampling depth was limited to the thickness of the L and Of horizons formed since ploughing. Average sampling depths were 10.7, 19.8 and 30.1 cm for furrows, flat and ridges, respectively (personal communication, F. Conen). Differences between ridge profiles, containing soil inverted from the furrow areas and flat were examined more closely to assess the carbon accumulation in the surface layers since site preparation. A description of the inverted profile and how this differs from the undisturbed is shown in Figures 2.1 and 2.2.

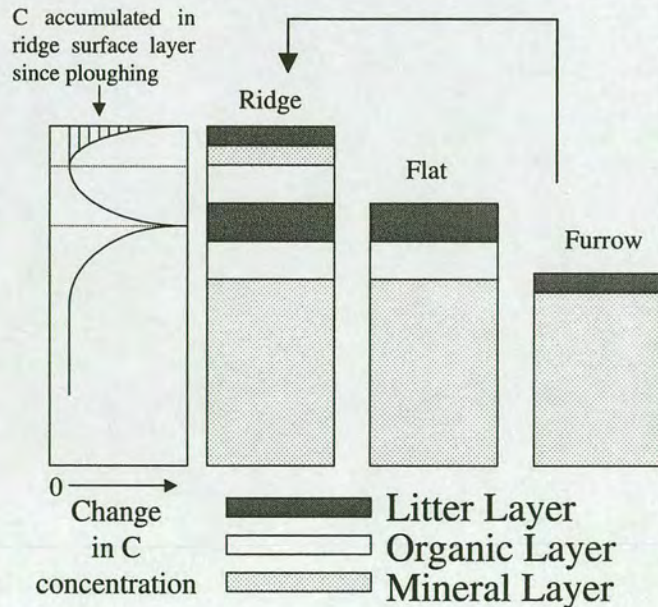


Figure 2.1 Location of soil layers in different areas after ploughing and the changes in C content within the profile caused by disturbance and organic matter accumulation.

Samples were dried to constant mass at 60 °C and crushed in a mortar. Roots (>0.5 mm diameter) and the few stones (> 4 mm) were removed and the remaining sample weighed, milled and mixed. Roots and stones were also weighed and roots were milled and mixed. A sub-sample of soil and root material (≈ 1 g) was further ground and mixed in an agate mortar before being sub-sampled again (≈ 10 mg) for analysis in an elemental analyser (Carlo Erba, Model, 1106, Milan).

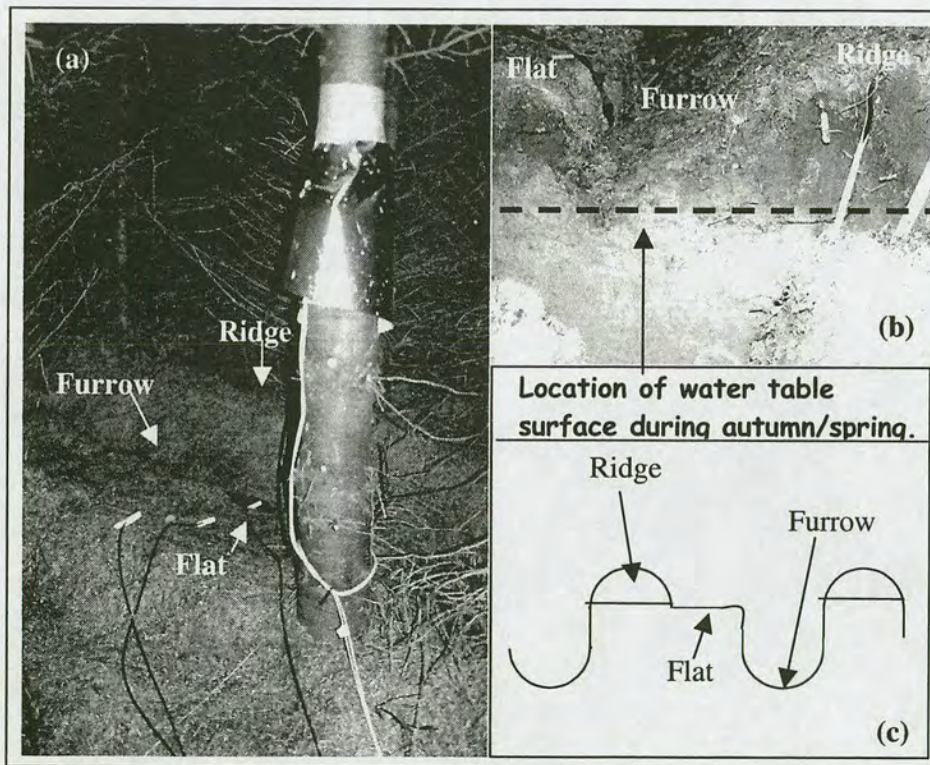


Figure 2.2 Description of soil surface at Griffin Forest (a) example of forest floor relief caused by site preparation (b) soil profile showing the organic and mineral soil layers within each area (c) cross section diagram highlighting the repetitive relief pattern and area sampled for structure, carbon content and soil surface CO₂ exchange.

2.4 RESULTS

2.4.1 Crown structure

Leaf area determination

Total L_A measured at Griffin Forest and the other Scottish plantations are presented in Figure 2.3. Griffin Forest values fell within the variation observed for all the study sites reviewed. The relationships between L_A , S_A and B_A were then determined using linear regression analysis PROC REG, SAS and are presented in Table 2.3.

Allometric Relationship	Intercept + 1SD	Slope + 1SD	n	r^2	P-value
B_A vs L_A	0.12 ± 1.8	10.36 ± 1.83	136	0.41	<0.0001
D_{BH} vs L_A	-2.07 ± 3.00	2.26 ± 0.23	136	0.41	<0.0001
S_A vs L_A	0.29 ± 2.04	0.28 ± 0.02	112	0.68	<0.0001
B_A vs S_A	6.50 ± 5.93	0.56 ± 0.03	92	0.75	<0.0001

Table 2.3 Linear regression parameters derived for pole-stage Sitka spruce allometric relationships used in this study for modelling L at Griffin Forest. See Figure 2.3 and Table 2.2 for further details of compiled datasets.

The relationship between L_A , S_A and B_A for Sitka spruce were significantly correlated with one another (Table 2.3). The relationship between S_A and L_A accounted for more of the observed variation than that between B_A and L_A . Most of the variation observed was most likely the result of the differing spacing and fertilisation treatments at each study site (Table 2.2). Justification for the use of this varied relationship comes from the knowledge that different compartments within the flux footprint of Griffin Forest have received fertilisation treatment in different years over the present rotation probably contributing to a certain degree of variation in growth.

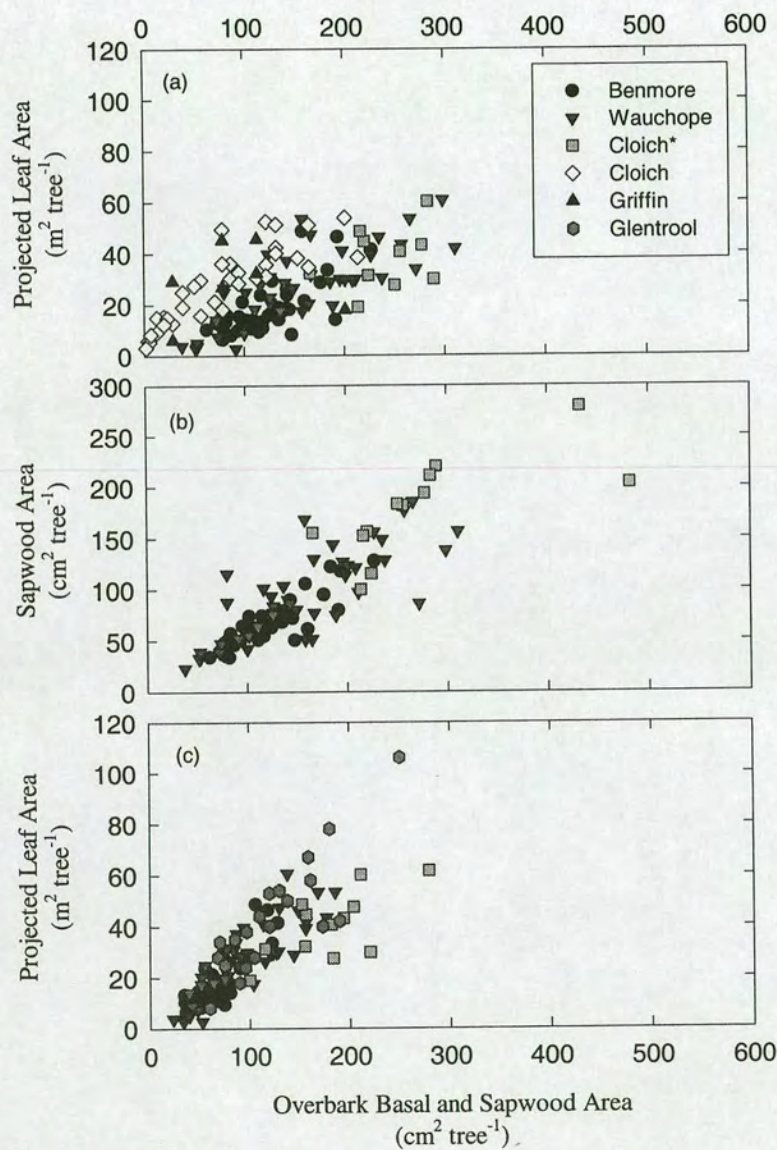


Figure 2.3 Allometric relationships between (a) basal area (B_A) and projected leaf area (L_A), (b) basal area and sapwood area (S_A) and (c) sapwood area and projected leaf area collected in pole-stage Sitka spruce plantations across Scotland. For site characteristics and published sources see Table 2.2.

Furthermore, the presence of *Calluna vulgaris* L. in some areas within the footprint has imposed varying degrees of ‘heather check’ i.e., competition for resources and was a likely contribution to the increased variation of growth and L_A for trees within the footprint.

Above-ground biomass distribution

An average stem density of $2200 \pm 600 \text{ ha}^{-1}$ ($\pm 1\text{SD}$, $n = 1040$) was determined for the flux footprint. The distributions of stem density within each plot measured are shown in Figure 2.4.

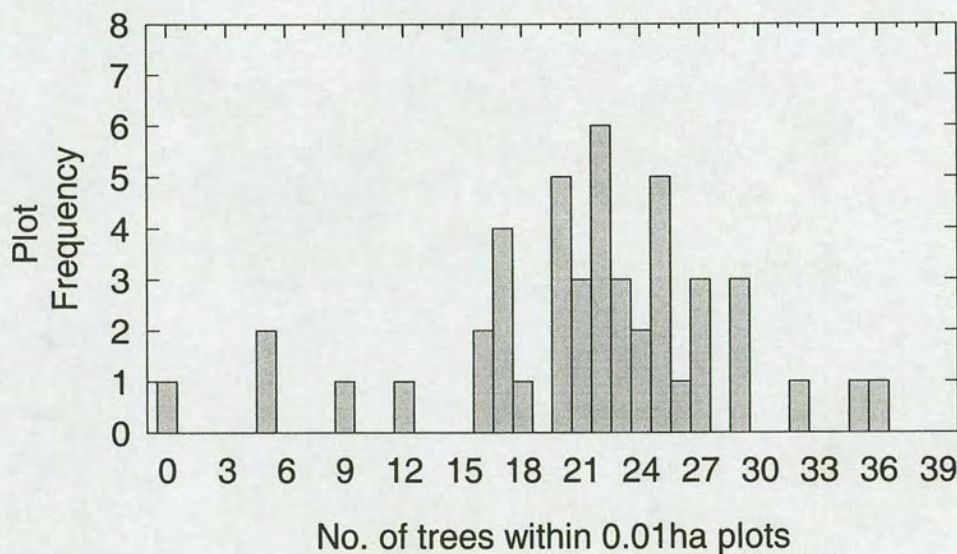


Figure 2.4 Stem density distribution measured in 45 plots within the flux footprint at Griffin Forest during 2001.

The basal area distribution within the flux footprint is presented in Figure 2.5. Based on this data the overbark basal area was calculated as $32 \pm 13 \text{ m}^2 \text{ ha}^{-1}$ ($\pm 1\text{SD}$, $n = 1040$). Using Eq 2.2 the estimated mean stock of above-ground biomass was 80 Mg ha^{-1} , equivalent to $\approx 40 \text{ Mg C ha}^{-1}$. Both the stem density distribution and basal area

within plots throughout the flux footprint displayed a high degree of variability, despite representing an even-aged monoculture. This variation is likely to result from the variations in nitrogen treatment and 'heather check' described above.

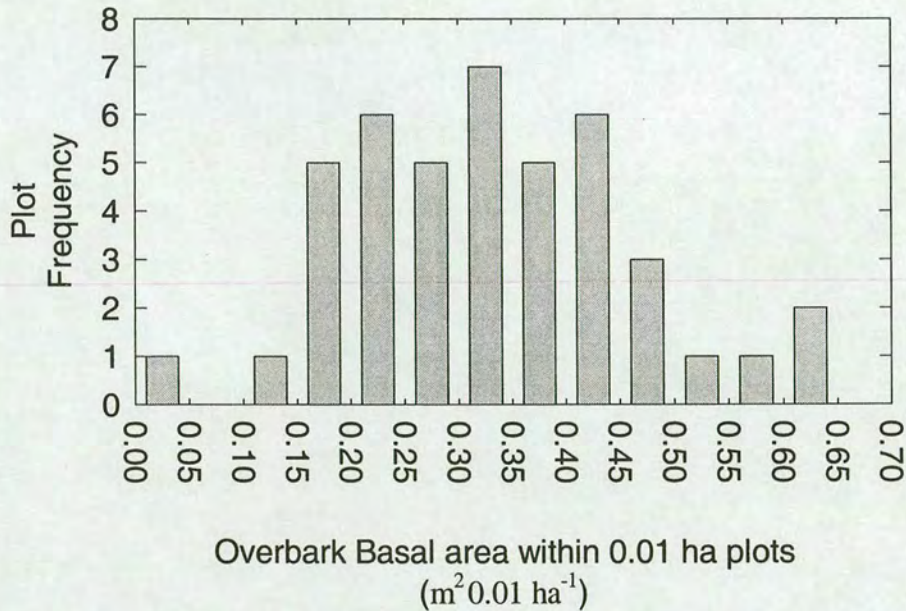


Figure 2.5 Basal area distribution measured in 45 plots within the flux footprint at Griffin forest during 2001.

The mean annual increment in D_{BH} measured at Griffin Forest was estimated at 0.7 ± 0.3 cm tree⁻¹ y⁻¹. This represented an increase in the above-ground biomass of *ca.* 13 Mg ha⁻¹ y⁻¹ equivalent to a 6.5 Mg C ha⁻¹ y⁻¹. Most of the increase in tree girth measured weekly from dendrometers, occurred between June and September after the period of bud-burst (Figure 2. 6). There were also substantial differences in the observed girth accumulation between sites of varying L and individuals of different size. The closed site had achieved full canopy closure prior to dendrometer installation in 2000 and substantial needle drop had occurred in the lower canopy, compacting the depth of the live crown to the uppermost region of the canopy. The

open site however, was relatively open with a deep live crown and interlocking branches only at the base of trees.

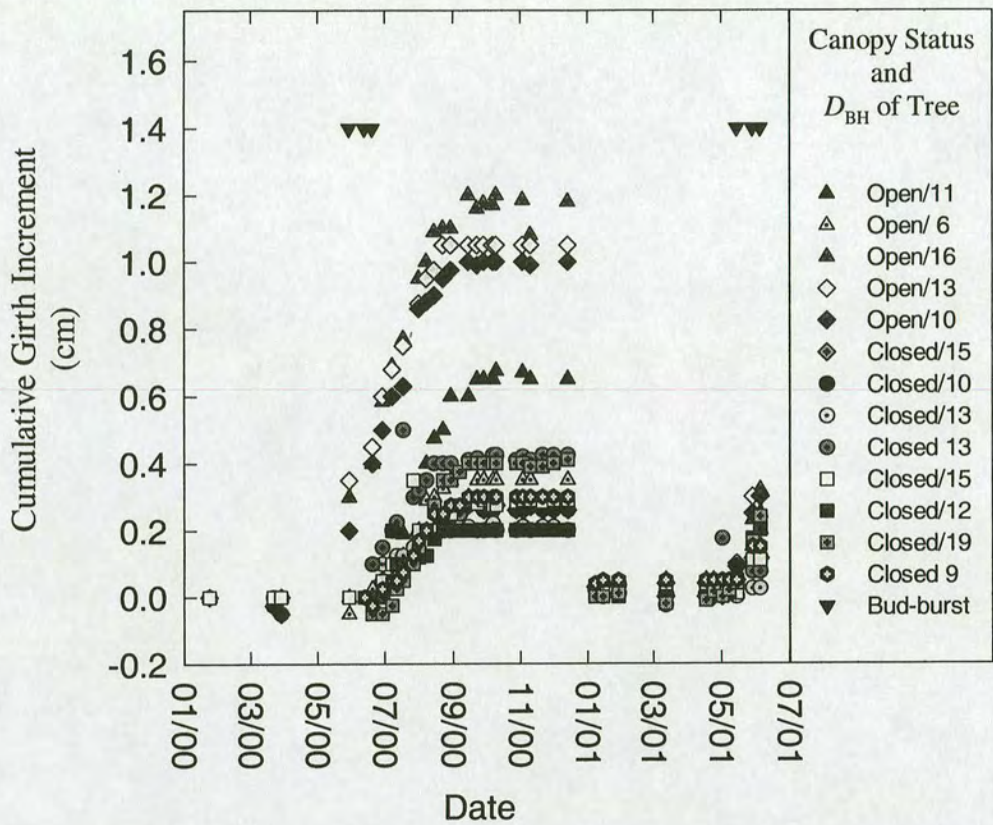


Figure 2.6 Cumulative girth increment measured at Griffin Forest during 2000-2001 at two sites with differing levels of canopy closure and variable D_{BH} . Down turned triangles represent periods of canopy bud burst.

Using the plot basal area information and the linear regression relationships established in Table 2.3, needle area index, L (m^2 projected leaf area m^{-2} ground area) was estimated for each of the 45 plots measured within the flux footprint (Figure 2.7). The mean L for the footprint was estimated as 6 ± 2 ($\pm 1SD$, $n = 45$).

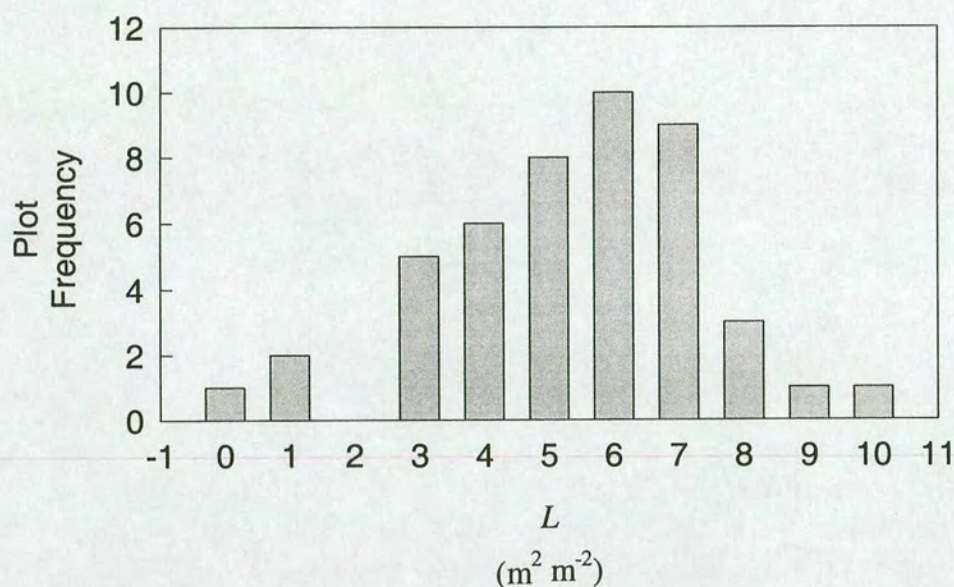


Figure 2.7 Distribution of modelled L using basal area as the predictor for 45 plots measured in the flux footprint at Griffin Forest during 2001.

2.4.2 Soil structure

Differences in the depths of organically enriched layers were found between the three distinct areas. The trend for organic layer depth was Ridge > Flat > Furrow. The differences in carbon content between areas was also pronounced with the Ridge containing greater carbon content than both the Flat and Furrow. The differences between the Furrow and Ridge were largest (Table 2.4). The distinct differences between areas with respect to temperature, volumetric soil water content and soil CO₂ efflux caused by soil carbon content, structure and forest management will be explored in Chapters 5 and 6.

Stratum	Sample size n	Sample depth (cm)	Soil mass (kg m ⁻²)	Carbon concn (%)	Carbon content	
					(individual samples) (kg m ⁻²)	(mean of soil mass x mean of C concn) (kg m ⁻²)
Furrow	20	10.7 (1.3)	65 (10)	6.5 (0.7)	3.8 (0.65)	4.2 (0.79)
Flat	20	19.8 (1.1)	87 (9)	13.1 (1.3)	9.8 (0.65)	11.4 (1.63)
Ridge	40	30.1 (1.5)	162 (10)	8.7 (0.8)	12.6 (0.90)	14.2 (0.17)
Total area	80	22.7 (0.9)	119 (6)	9.3 (0.5)	9.7 (0.51)	11.0 (0.46)

Table 2.4 Mean depth, soil mass, carbon concentration and content of the organically enriched layers of different strata in Griffin Forest. Numbers in brackets indicate one standard error. Data collected by F. Conen and R. Clement (University of Edinburgh).

The calculated carbon stock of the soil within the flux footprint was estimated at approximately 100 Mg C ha⁻¹. The calculated below-ground biomass of roots in ‘Open’ canopy sites were 8.7 ± 1.6 and 8.8 ± 0.5 Mg ha⁻¹ for Ridge and Flat areas, respectively and 6.7 ± 1.5 and 9.19 for Ridge and Flat areas in ‘Closed’ canopy sites. The mean % C for root biomass sampled by cores was 45 ± 2.6 %, and the C stock contained in root biomass was 3.10 ± 0.7 Mg C ha⁻¹ for closed sites and 3.65 ± 0.1 Mg C ha⁻¹ for open sites. Conservative estimates of carbon accumulation in the soil profile since planting in the Open canopy were 18.8 ± 2.6 , 0.2 ± 0.4 and $0.6 \pm >0.1$ Mg C ha⁻¹ for the litter, mineral soil and rootlet components, respectively. In closed canopies carbon accumulation was 15.8 ± 7.3 , 0.5 ± 1.2 and $3.1 \pm >0.7$ in the litter, mineral soil and root components, respectively. Therefore a conservative estimate of carbon gained below-ground at Griffin Forest since planting is approximately 19.5 Mg C ha⁻¹ (personal communication, F. Conen, University of Edinburgh).

2.5 DISCUSSION

Direct measurements of L_A were comparable to those in other Sitka spruce studies (Table 2.2) as was the range of L predicted for the site and individual plots.

However, other studies have predicted values somewhat higher than these results for Sitka spruce. Values of L from the literature range between 7 to 10 for Sitka spruce stands in Scotland (Landsberg *et al.*, 1973; Norman & Jarvis, 1974; Jarvis, 1981; Meir *et al.*, 2002).

Stand B_A was similar to harvest data published for young Sitka spruce stands between the age of 13 to 22 years (Mitchell, Proe & MacBrayne, 1981). However, as pointed out in the results section, B_A was fairly heterogenous across the footprint, it is likely that a number of environmental factors including nitrogen deficiency, water stress or suppression *via* 'heather check' have contributed to this variability. This variability was also apparent in the girth increment data shown for an Open and Closed site. Individuals had typically smaller girth in the Open site but larger girth increments in 2000. This may be the result of increased resource availability i.e. photon flux density (Q) and N availability *via* recent fertilisation completed in compartments with low basal area.

Many other studies on allometric relationships have reported weak relationships when using over-bark B_A as a weak determinant of L_A or S_A (Whitehead, 1978; Waring, 1983). This did not appear to be the case for young Sitka spruce as individual B_A correlated well with L_A and S_A . According to the pipe-model theory and evidence from other inventory studies, L_A is more likely to correlate with S_A than B_A through water supply constraints (Grier and Waring, 1974; Whitehead, 1978; Bartelink, 1996). Generally as trees age heartwood accumulates and S_A and L_A tend to reach an asymptote regulated by resource supply, thus B_A continues to increase and no longer correlates with S_A and L_A . However, in these young Sitka spruce stands the formation of heartwood is negligible and relationships between B_A , L_A and S_A persist.

Systematic mechanical ploughing at Griffin Forest, in preparation for afforestation created pronounced artificial micro-topography. This created three evenly spaced areas differing in organic layer depth, root distribution through the profile and total C content. It is hypothesised that the structural and chemical differences of the three areas will give rise to systematic differences in soil CO₂ efflux rate, and this will be explored in Chapters 5 and 6.

3. Daily variation of gas exchange and ^{13}C discrimination by Sitka spruce branches under field conditions – Theory and Methods

3.1 INTRODUCTION

Photosynthesis, stomatal conductance and ^{13}C discrimination

The primary processes responsible for the seasonal pattern of CO_2 and $\delta^{13}\text{C}$ in the Northern Hemisphere are photosynthesis, discrimination against ^{13}C during photosynthesis and the release of photosynthetic products during respiration. During photosynthetic uptake it has been postulated that plants conserve a balance between the demand for CO_2 during carboxylation and its supply of CO_2 and loss of water, via regulation of stomatal conductance (g_s) (Farquhar *et al.*, 1982). Fluctuations in environmental variables such as the photon flux density (Q) and temperature (T) cause changes in the rate of carboxylation (v_c). Consequently, changes in the concentration of CO_2 in a leaf relative to that in the ambient air (C_i/C_a) may be expected to occur. Wong *et al.*, (1979) on the contrary, were the first to conjecture that C_i/C_a in plant leaves may be nearly constant for a wide range of environmental conditions. In a series of experiments Wong *et al.*, (1979) found that perturbations in net CO_2 assimilation (A) resulted in parallel changes in g_s such that a nearly constant C_i/C_a was maintained for a wide range of environmental conditions.

In contrast, some studies provide evidence that the stomatal response to changing environmental conditions is much slower than the response of carboxylation (Barradas *et al.*, 1994; Barradas & Jones, 1996). For instance, the very different response times of g_s and A to changes in Q may lead to a wide variation of C_i

occurring under fluctuating Q in the field (Leverenz, 1981). Stomatal conductance can take 20 min to achieve steady-state following changes in irradiance (Barradas & Jones, 1996) and have been reported to take between 20 and 45 min for *P.sitchensis* (Ludlow & Jarvis, 1971; Neilson *et al.*, 1972). Decreases in g_s also occur with increasing saturation deficit at the leaf surface (Grace *et al.*, 1975; Sandford & Jarvis, 1989) and can cause large changes in C_i (Morison & Gifford, 1983). Indeed, any variable that changes g_s without at the same time having a corresponding, direct effect on mesophyll photosynthesis and *vice versa*, will cause a transient change in C_i and C_i/C_a .

Complementary studies measuring gas exchange and discrimination against ^{13}C have revealed that intercellular CO_2 concentration (C_i) governs the extent of Δ (Evans *et al.*, 1986). This study provided direct evidence for theory presented by Farquhar *et al.*, (1982) that established the link between the extent of discrimination in leaves with CO_2 supply and demand. All C_3 plants, including the coniferous species studied here, discriminate against ^{13}C relative to ^{12}C as they assimilate atmospheric CO_2 . This fractionation is related primarily to the differing diffusivities of $^{13}\text{CO}_2$ and $^{12}\text{CO}_2$ in air (Craig, 1953), and an intrinsically lower reactivity of ^{13}C during enzymatic CO_2 fixation (Whelan *et al.*, 1973; Estep *et al.*, 1978a, 1978b; Wong *et al.*, 1979b; O'Leary, 1981; Farquhar *et al.*, 1982; Roeske & O'Leary, 1984). When the plant supply of CO_2 is regulated by stomata, the ratio of $^{13}\text{C}/^{12}\text{C}$ in the CO_2 supplied and consequently fixed by the plant is correspondingly altered. This can be measured in plants as a depletion of ^{13}C in the soluble carbohydrates, or as a corresponding enrichment in the surrounding atmospheric CO_2 (Lauteri *et al.*, 1993; Evans *et al.*, 1986). However, observations of C_i/C_a and Δ on leaves *in situ* indicate that a simple model of Δ commonly used is not validated against instantaneous data

(Gillon *et al.*, 1997; Harwood *et al.*, 1998). This indicates a need for the re-evaluation of other processes associated with photosynthesis that potentially alter Δ .

Photorespiration and daytime dark respiration

During periods of high irradiance and temperature, high v_c combined with low g_s lead to reduced C_i (Farquhar *et al.*, 1980). Consequently, decarboxylation increases *via* glycine decarboxylase during photorespiration ($0.5v_o$, where v_o represents the rate of oxygenation) and *via* the tricarboxylic acid (TCA) cycle decarboxylases during daytime dark respiration (R_d). The fractionation of carbon occurs during photorespiration, and makes photorespired CO_2 5 to 9‰ more depleted in the heavier ^{13}C , relative to that of the recently fixed substrate (i.e., the composition of CO_2 becomes more negative) (Rooney, 1988; Gillon & Griffiths, 1997). Whether or not fractionation occurs during dark respiration, is debateable (von Caemmerer & Evans, 1991; Farquhar & Lloyd, 1993; Lin & Ehleringer, 1997; Duranceau *et al.*, 1999, 2001; Cernusak *et al.*, 2001). Measurement of v_c , $0.5v_o$, R_d and associated fractionations are logistically confined to controlled laboratory studies or models (Cornic & Jarvis, 1972; Laisk, 1977; Brooks and Farquhar, 1985; Atkin *et al.*, 1998; Atkin *et al.*, 2000; Rooney, 1988; Ivlev, 1996; Gillon & Griffiths, 1997; Duranceau *et al.*, 1999; Duranceau *et al.*, 2001). Given the differences between theory and observations at the leaf scale, quantification of respiratory processes and associated $\delta^{13}C$ of respired CO_2 may go some way towards reconciling observed discrimination *in situ* and improve understanding and prediction of the temporal and spatial links between the leaves and atmosphere.

Applications of integrated ^{13}C discrimination

An alternative strategy employed to estimate average C_i/C_a is the $\delta^{13}\text{C}$ of bulk organic matter based on the Farquhar *et al.* (1982) model of isotopic fractionation during photosynthetic gas exchange, mentioned above. Its validity for determining instantaneous C_i , is supported by the constant C_i/C_a theory presented by Wong *et al.*, (1979). Studies have used the isotopic composition of bulk organic material to infer photosynthetic or plant physiological characteristics like photosynthetic pathway, plant functional groups and provenance selection for comparative water use efficiency (Bender, 1968, 1971; Flanagan *et al.*, 1997; Farquhar *et al.*, 1982). However, what is still unclear is whether the integrated $\delta^{13}\text{C}$ composition of bulk needle material is appropriate for inferring instantaneous processes over hourly, daily and seasonal time-steps as applied in some gas exchange studies for example Flanagan *et al.*, (1997) and Katul *et al.*, (2000). As described previously stomatal conductance may not necessarily achieve steady-state during periods of the day when environmental variables are fluctuating, therefore patterns of C_i/C_a and Δ over the day are likely to be dynamic and not constant. Furthermore, comparative estimates of C_i/C_a obtained from instantaneous photosynthesis and stomatal conductance measurements and $\delta^{13}\text{C}$ composition of bulk material do not always agree, indicating other processes not related to stomatal conductance have a part to play in the $\delta^{13}\text{C}$ composition of bulk material (Francey *et al.*, 1985; Flanagan *et al.*, 1997).

Application of instantaneous ^{13}C discrimination

Numerical models of isotopic gas exchange between the terrestrial biosphere and the atmosphere at global and ecosystem scales rely on theoretical descriptions of isotopic gas exchange at the leaf or cellular scale. Very few attempts to measure Δ of leaves

in the field have been made, consequently a gap presently exists between theory and models. Published datasets of Δ measured *in situ* found that net observed discrimination (Δ_{obs}) deviated substantially from that of the theoretically modelled discrimination (Δ_{s}) based on the Farquhar *et al.*, (1982) model using C_i/C_a (Harwood, 1996; Harwood *et al.*, 1998). The authors showed that other processes substantially influenced the Δ_{obs} under field conditions, but unfortunately did not proceed to quantify the other processes and their likely isotope effects on Δ . The most promising result from this study was the systematic correspondence of Δ_{obs} with diurnal changes in measured environmental variables and net assimilation (A). This suggests that in the future we will be able to parameterise functional relationships between Δ , gas exchange and environmental variables.

3.2 CHAPTER AIMS

The aims for this chapter are:

- (i) to characterise the daily variations in environmental conditions and photosynthetic performance of branches, under field conditions in a Sitka spruce plantation in central Scotland;
 - (ii) to estimate gross photosynthetic CO_2 uptake and the proportion that is respired;
 - (iii) to describe a system capable of measuring instantaneous discrimination against $^{13}\text{CO}_2$ (Δ_{obs}) by branches under field conditions;
 - (iv) to characterise the daily variation of Δ_{obs} under field conditions;
-

- (v) to estimate the influence of other processes to Δ_{obs} ,
- (vi) validate the Farquhar model of photosynthetic ^{13}C discrimination for a field collected dataset and,
- (vii) model the daily variation in Δ using continuous environmental and photosynthetic gas exchange data.

3.3 METHOD

3.3.1 Gas exchange measurements

Four branch chambers were installed on two trees, within a 0.01 ha plot inside the footprint of the flux tower, during May and July 2001. During May bud burst was occurring, whilst in July shoot expansion was complete. Branches were investigated in May prior to bud-burst and were chosen as representative of the majority of sun-lit branches visible from the tower. Two branches were used in the upper canopy (at 10.5 m (Chamber 1, Upper) and 9.4 m (Chamber 3, Upper) height and one in the middle canopy at 8.1 m (Chamber 4, Middle) height. During the July campaign Chamber 4 was designated as a control chamber, placed at the same height in the canopy and sealed without any branch inside. The heights of the two trees were 13.62 and 9.50 m. Tree diameter at breast height was 16 cm and 10.5 cm, respectively. The chambers were supported in position by metal booms projecting from the canopy access tower and nylon cord. This arrangement allowed the chambers to move freely as the trees and branches moved with the wind. Each of the chambers were positioned on trees to the south of the tower to minimise shading effects of the tower. The chambers remained on the branches between 18th May 2001 until the 22nd July 2001. During this time the system for measuring gas

exchange was operated only periodically due to power constraints. However, in between gas exchange periods the chambers remained in an open position and continuously ventilated with canopy air.

The chambers (see Fig. 3.1 and 3.2) consisted of two 5 mm thick acrylic end pieces, ellipsoid in shape (600 mm major axis, 300 mm minor axis, 0.14 m² area), separated by five thin (5 mm diameter) stainless steel rods. This construction was covered with polypropylene film (ICI Propafilm, 34 µm thickness, ICI Propafilm, Dumfries), and sealed along the edges of the end pieces with silicone sealant. One end piece was made such that it could slide up or down the rods to adjust the bag length to suit the individual branch (chamber lengths were 0.89 m, 0.91 m, 0.92 m and 0.87 m for bags 1 to 4, respectively).

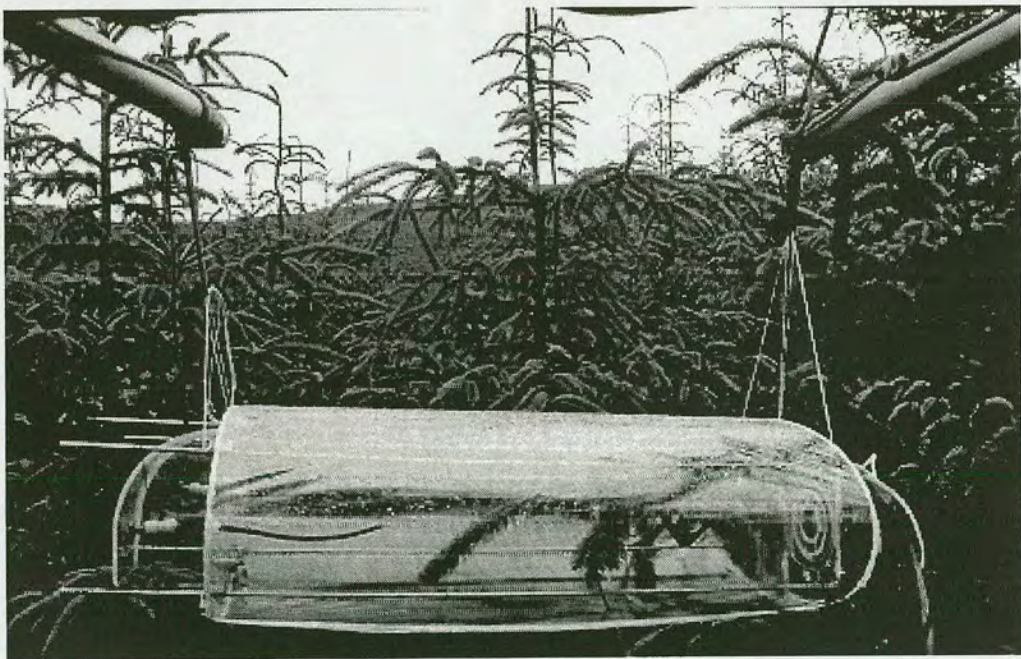


Figure 3.1 Assembled branch chambers used to measure gas exchange and sample stable isotopes at Griffin Forest during 2001.

An ellipsoid shape was chosen to minimise the dead volume within the chamber, to minimise the chamber's surface area to volume ratio (minimising any adsorption/desorption effects), to minimise attenuation of incoming light, to allow snow to slide off and to prevent water pooling on the top. The bottom of the chamber was left unsealed to allow placement of the chamber over the branch, thereafter it and the branch entry point were also sealed with silicone sealant.

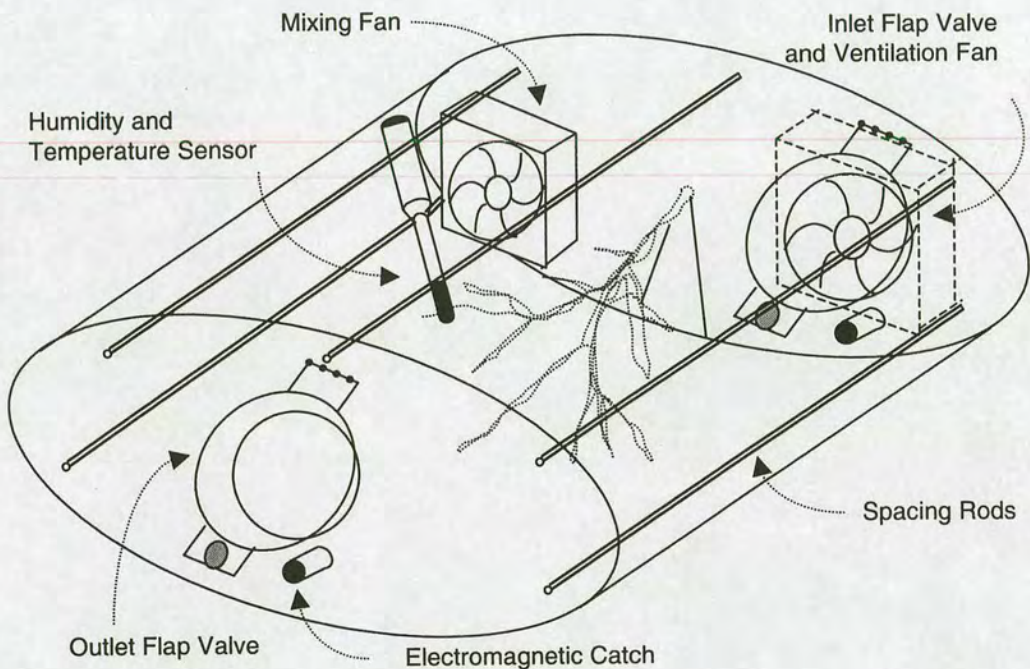


Figure 3.2 Schematic of branch bag construction. Re-produced with permission from Rayment, 1998.

A 12v electric fan (RS 250-1561, RS Components Ltd., Corby) was mounted at the trunk end of each bag, and blew air at a high flow rate ($30 \text{ dm}^3 \text{ s}^{-1}$; approximately 15 air changes min^{-1}) through the bag via large shrouded inlet and outlet ports. When a gas exchange measurement was to be made, the ventilation fan was switched off and an internal circulating fan was switched on. Thin "Perspex" flap valves dropped over the inlet and outlet ports and were shut tight with small electromagnetic catches. Air

was circulated ($5 \text{ dm}^3 \text{ min}^{-1}$) continuously between the bag under measurement and a box containing the IRGA and control system (mounted nearby on the tower), through loops of Bev-a-line tubing (1/4 inch i.d. Bev-a-line, Thermoplastic Processes Inc., Stirling, NJ). At measurement time a small amount of air ($0.2 \text{ dm}^3 \text{ min}^{-1}$) was diverted from the appropriate loop to the IRGA (LI-6262, LI-COR Inc., Lincoln, Nebraska) operating in absolute mode and the change in CO_2 concentration was measured over a 5 or 10 minute interval. The uptake or efflux of CO_2 was calculated from the rate of change of the CO_2 mole fraction and the molar volume of the chamber.

Within each bag, relative humidity and air temperature were measured (Vaisala HMB 30A, Vaisala (UK) Ltd., Cambridge), as was needle temperature in three locations within each chamber (0.2 mm diameter Cu-Con thermo-junction, referenced to the air temperature sensor). Photosynthetic photon flux density (Q) incident upon each branch was measured with a photosynthetic photon flux density sensor (SD101QV, Macam Ltd., Livingston) mounted in a vertical orientation directly onto the branch or above the chamber, midway along its length. Sensor outputs were recorded with a logger (CR10, Campbell Scientific (UK) Ltd., Shepshed, Leics.), which also initiated the measurement sequence. The gas analyser was calibrated prior to each measurement campaign. Nitrogen was used as the zero gas. The CO_2 span was set using bottles of CO_2 in air at ca. ambient CO_2 concentration. The concentrations of CO_2 in reference bottles were calibrated against a cascade of three Wösthoff mixing pumps (H.Wösthoff oHG, Bochum, Germany). H_2O vapour span was set using a dew point generator in the laboratory (LI-610, LI-COR Inc., Lincoln, Nebraska).

Sources of errors during gas exchange

Errors in the calculated fluxes are directly proportional to errors in needle area, bag volume and the span setting of the gas analyser. The LI-COR IRGA is a very stable instrument with a calibration drift of less than $1 \mu\text{mol m}^{-2} \text{s}^{-1}$ over four weeks; if the calibration of the analyser were to drift by $1 \mu\text{mol mol}^{-1}$ during the course of a five minute measurement, this would correspond to an error of less than $0.05 \mu\text{mol m}^{-2} \text{s}^{-1}$ in the calculated rate of photosynthesis (Rayment & Jarvis, 1999). This is very small compared to typical daytime fluxes of 5 to $10 \mu\text{mol m}^{-2} \text{s}^{-1}$, however, it can amount to large errors in the order of 10% for low flux rates observed in the dark or when Q is low at dawn and dusk.

Measurements of water vapour flux (and branch conductance) are subject to errors arising from any adsorption/desorption of water vapour to or from the inside of the bags if temperature changes during the measurement period. The use of "Propafilm" (having a low susceptibility to water adsorption/desorption) as the main material for the bags, together with the bags' high volume to surface area ratio, should have reduced this effect as far as possible.

The small temperature increases observed inside the bags compared with the ambient air temperature may have affected CO_2 and water vapour exchange, both directly (i.e., by acting on the biochemical activity of the branch) and indirectly (e.g., by increasing the humidity deficit of the air). Rayment & Jarvis, (1999) found no evidence of any systematic change in the temperature regime during the course of a measurement period, but during the daylight hours the temperature within each bag was consistently higher than the temperature immediately outside the bag. This effect was found to be a linear function of Q ($r^2 > 0.9$ upper bags, $r^2 > 0.7$ lower bags), and was therefore more pronounced in the bags experiencing higher radiation at the top of the canopy than in those positioned lower down. Air temperatures inside the lower bags were within 1°C of ambient temperature 90 % of the time and were

exceptionally (< 1 % of the time) up to 3 °C warmer than the ambient air. Inside the upper bags, air temperatures were within 1 °C of the ambient air temperature 75 % of the time, within 3 °C 90 % of the time and exceptionally (< 1 % of the time) were up to 6 °C warmer than the ambient air.

3.3.2 Sample collections

Needle area and biomass

At the end of the observation period (August 2001) the branches were cut off whole. Current-year-foliage was separated from older foliage and needle area, needle and wood dry mass were measured for each needle cohort and branch separately. Projected needle area for sub-sampled needles were measured with a LI-COR 3100 area meter. Total needle and wood dry mass was determined prior to and following 48 hours of drying at 70 °C in a ventilated oven. Estimates of specific needle area (SNA) were then determined from the relationship between projected leaf area and needle dry mass for the sub-sampled needle material. Total needle area for each branch was determined by applying the SNA for each needle cohort, to the total mass of needles in each cohort of the individual branch. Needle area and dry mass for each branch are presented in Table 3.1 below.

Field Campaign	Projected L_A Inside Chamber (cm ²)	Standard Deviation (\pm 1SD) (cm ²)	Branch Dry Mass (g)	Standard Deviation for A (\pm 1SD) ($\mu\text{mol m}^{-2} \text{s}^{-1}$)	Location (Chamber Id)
May	1309	8	115	0.06	Upper (1)
	1671	11	67	0.04	Upper (3)
	920	19	81	0.16	Middle (4)
July	3842	30	195	0.02	Upper (1)
	2464	34	104	0.01	Upper (3)

Table 3.1 Projected leaf area and dry mass present in branch chambers during May and July 2001. \pm 1SD estimates for projected leaf area, dry mass and calculated net assimilation rate as a result of errors in leaf area using the automated branch chamber system.

Needle, stem and soil collection for $\delta^{13}\text{C}$ analysis

Needle and suberised twig and soil samples were randomly selected at each time of branch chamber measurement from trees and soils accessed around the tower (including the trees under measurement). The needle and twig samples were taken from the same levels and adjacent to the branch chambers, at 10 m (top), 8 m (middle), and 6 m (low) height. Soil samples were taken from the top 5cm of soil extracted using a soil corer.

Air collection for CO_2 and $\delta^{13}\text{CO}_2$ analysis

The branch chambers were modified to circulate air between the chamber and a flask flushing system through loops of polyethylene-lined, PVC tubing (3/8" i.d. Dekabon 1300, Furon, Gembloux, Belgium). Prior to sampling, all loops were flushed with nitrogen from cylinders under pressure for approximately five minutes each to ensure the loops were dry and free from contamination. The loops were then connected to 3/8" i.d. Cajon fittings (Swagelok, Co., Ohio, USA) and chamber air was circulated through a stainless steel water trap filled with $\text{Mg}(\text{ClO}_4)_2$, a Gelman Filter (1 μm pore size) and two cylindrical flasks connected in series using air-tight connectors and polyethylene-lined, PVC tubing (1/4" i.d., Dekabon 1300, Furon, Gembloux, Belgium). The sampling containers used were 1 dm^3 glass flasks, each fitted with two valves at either end (Glass Expansion, Melbourne, Australia) and sealed with Teflon® PFA (perfluoroalkoxy alkane) O-rings. In July a combination of the above sampling containers and differently designed 1.3 dm^3 glass flasks each fitted with two valves (Hapers-Lowert, Netherlands) and sealed with Viton® O-rings (DuPont Dow Elastomers) were used in the campaign. Air was pulled through the flasks using a 12 V pump (PM 14625-86, KNF Neuberger GmbH, Freiburg, Germany) and

regulated at $3 \text{ dm}^3 \text{ m}^{-1}$ using a flow-meter and returned to the chamber. The residence time of gas in the lines was 6 - 8 seconds, dependent on chamber height.

At measurement time an initial sample, now referred to as the *Open* sample, was taken by flushing the flasks with air from inside the chamber whilst the chamber flaps were open and re-circulating the air from the flask back to the chamber. This ensured that pre-conditioning gas was quantitatively replaced with chamber air. After flushing both flasks for a duration of 5 minutes, the air flow was closed at the exhaust pressure control. The flasks were pressurised to 1 bar above ambient pressure over approximately 1 minute and then the valves were closed. One flask in-line was then removed for future lab analysis. A new flask was then placed in line and flushing of the two flasks was resumed for the second sample, referred to as the *Closed* sample. After one minute flushing, the branch chamber flaps closed and air modified by the branch was directed to the flasks for a further four minutes of flushing and pressurisation. Due to low respiratory fluxes at dusk and throughout the night, the period of chamber closure was extended to ten minutes, thereby maximising the difference in CO_2 concentration between the “*Open*” and “*Closed*” sample. Because of logistic restrictions, duplicate samples were not taken until the final sampling of the field campaigns. A schematic diagram of the sampling protocol is shown in Figure 3.3.

Flask samples were collected at intervals of approximately every three hours over a 24 h sampling period. Field campaigns were chosen to avoid days where strong wind or rain was predicted. However, showers were experienced during some sample runs and precautions were taken to ensure no water contamination. Inevitably some showers were persistent and heavy enough to cause sampling to cease, because of contamination risks and equipment failure. Branch exchange of CO_2 and H_2O could continue despite rainfall, however.

3.3.3 Stable isotope analysis

Needle, stem and soil $\delta^{13}\text{C}$ analysis

Cryogenically dried needle, twig and soil samples (soil analysis presented in Chapter 6) were ground with a ball mill to a fine homogeneous powder. Sub-samples of the powdered substances were then weighed and placed into tin cups and prepared for $\delta^{13}\text{C}$ analysis. The tin capsules were then transferred to the auto-sampler tray of an elemental analyser (NA 1110 CN, CE Instruments, Rodano, Italy), coupled via a open split interface (ConFlo III, Finnigan MAT, Bremen, Germany) to a mass spectrometer (Delta⁺XL, Finnigan MAT, Bremen, Germany) and analysed for carbon content and $\delta^{13}\text{C}$ at the Max-Planck-Institute for Biogeochemistry, Jena, Germany.

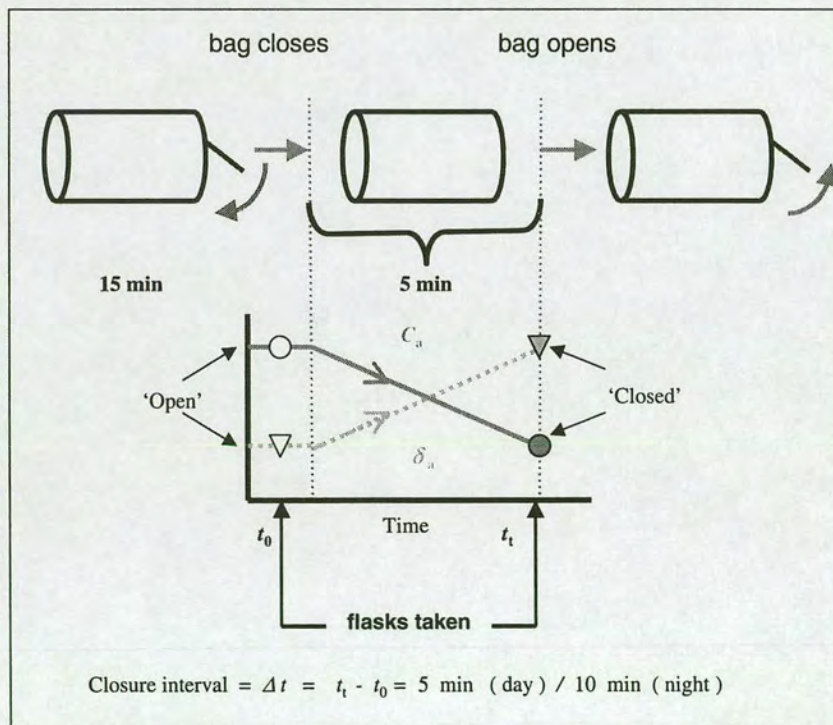


Figure 3.3 Schematic showing the protocol for sampling and hypothesised changes in CO₂ mole fraction (C_a) and $^{13}\text{C}/^{12}\text{C}$ ratio (δ_a) of chamber air head space.

The ratio of ^{13}C to ^{12}C in a plant or air sample was then determined relative to an accepted standard with a mass spectrometer, and expressed in δ notation in per mil units (‰):

$$\delta^{13}\text{C}_{\text{sample}} = \left(\frac{^{13}\text{C}/^{12}\text{C}_{\text{sample}}}{^{13}\text{C}/^{12}\text{C}_{\text{standard}}} - 1 \right) 1000, \quad (\text{Eq 3.1})$$

where $\delta^{13}\text{C}$ sample is the ratio of ^{13}C to ^{12}C in the sample, in this case needle and stem tissue (but also applicable to soil samples and flask air), expressed relative to the Pee Dee Belemnite (PDB) standard (‰). For further details of measurement, theory and units please refer to Appendix I. The calculated standard deviation for dry matter $\delta^{13}\text{C}$ was 0.05 ‰.

All organic matter analysis was completed at the Max-Planck-Institut für Biogeochemie, Jena, Germany. A full description of the analytical set-up is given by Werner et al. (1999).

Air sample CO_2 and $\delta^{13}\text{CO}_2$ analysis

Pre-conditioning and analysis of flask air was completed by staff at the GasLab and IsoLab of the Max-Planck-Institut für Biogeochemie in Jena, Germany. The CO_2 concentration of air samples was determined using gas chromatography. The analysis system is based on a gas chromatograph (HP 6890, Hewlett Packard, USA) equipped with two sets of chromatographic columns linked to a flame ionization detector (FID, for CO_2 analysis) and an electron capture detector (ECD, for N_2O analysis). The two sample loops (FID-line: 2.2 cm^3 ; ECD-line: 5 cm^3) were linked in series and kept at $\pm 0.1 \text{ }^\circ\text{C}$ in a tempering oven. From each flask 30 cm^3 of the air sample was flushed

through two sample loops. The gas in the loops equilibrated with ambient pressure, then injected onto the pre-column (Hayesep Q, 1.8 m * 3.2 mm) and passed through the main GC column (Porapak Q, 3.6 m * 3.2 mm) held at 60 °C. After chromatographic separation, CO₂ was converted to CH₄ over a hot nickel catalyst ("methanizer") using hydrogen before being detected by the FID. To increase precision, injections were made alternating between the sample gas and a reference gas. Reproducibility using this system yielded a standard deviation of $\pm 0.08 \mu\text{mol mol}^{-1}$ for CO₂.

Further samples of CO₂ were extracted cryogenically from flask air, using an automated sampling line ("BGC-AirTrap", MPI, Jena, Germany). The ¹³C / ¹²C ratio of the separated CO₂ was determined using a dual-inlet isotope ratio mass spectrometer (MAT 252, Finnigan MAT, Bremen, Germany). The analytical precision of $\delta^{13}\text{C}$ for separated CO₂ samples was a standard deviation of $\pm 0.012 \text{ ‰}$. Full details of the analysis procedure is given by Werner *et al.*, (2001). For a review of referencing strategies and techniques in isotope ratio mass spectrometry see Werner & Brand (2001).

Sources of error during isotopic sampling and analysis

Compared with errors introduced by the sampling procedure, uncertainties in the laboratory analyses were negligible. Likely sources of error in this study were contamination of branch chamber sample air with conditioning gas or other previous flask fillings. Interactions between the sample gas and tubing, pumps and branch chamber materials were identified as potential surfaces for adsorption/desorption and isotopic exchange in the system. Leaks from the experimental system and the influence of changing conditions inside the branch chambers on gas exchange characteristics during bag closure were also not ruled out. Feedback effects on

branch gas exchange caused by changing gas concentrations and environmental variables were minimised using short closure intervals and having a large chamber volume. Contamination caused by the release of flask air was minimised by releasing the contents of the flasks into large ventilated volumes (*ca.* 120 dm³). As both flasks were being flushed whilst the chambers were open and mixing with the atmosphere, dilution of flask air in the chamber would be rapid.

Combined estimates of uncertainties arising from the sampling procedure were obtained using control measurements from the empty branch chamber. Since this represents the standard sampling situation, it includes all error sources except the response of branches to changing environmental conditions in the chamber. Data for changes in the control chamber gas composition during closure are presented in Figure 3.4.

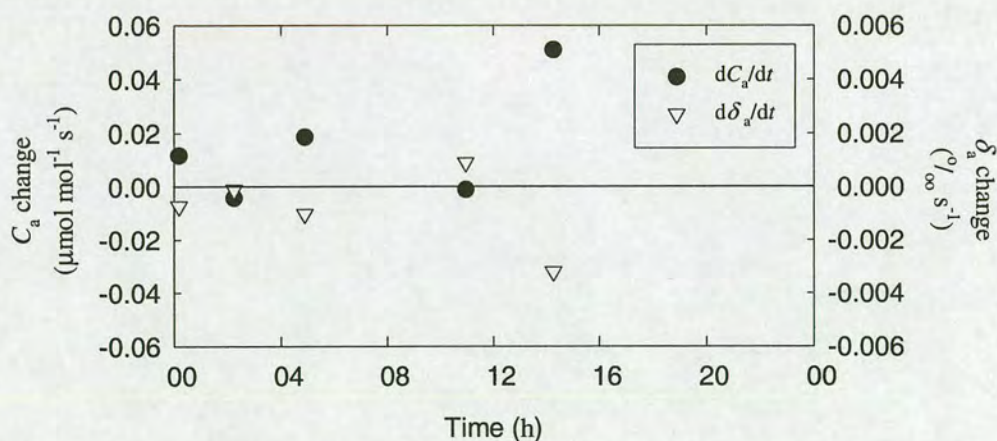


Figure 3.4 Change in the CO₂ mole fraction (C_a) and isotopic composition (δ_a) between ‘Open’ and ‘Closed’ flasks taken from the control chamber on 20th July 2001.

Observed dC_a/dt and $d\delta_a/dt$ were independent of CO₂ mole fraction, temperature and relative humidity. The observed differences between paired flasks during July 2001 indicated non-systematic errors with the sampling protocol (Figure 3.4). Sampling

uncertainty estimated using all control chamber measurements during the day and night were $1.3 \mu\text{mol mol}^{-1}$ for CO_2 and 0.1‰ for Δ values. Open chamber measurement uncertainties are more difficult to assess, therefore estimates are based on the standard deviations of laboratory analysis of duplicate flasks which were $0.15 \mu\text{mol mol}^{-1}$ for CO_2 , 0.01‰ for Δ . Combining this information with errors associated in leaf area measurement, overall uncertainties for net CO_2 fluxes were *ca.* $0.2 \mu\text{mol m}^{-2} \text{s}^{-1}$. Estimates of standard deviations (1SD) for CO_2 fluxes and Δ are listed in Table 3.2. Standard deviations for A were observed to be independent of flux rate. However, SD for Δ were inversely related to net CO_2 flux, as was C_i/C_a to a lesser extent.

	High flux rate	$\pm 1\text{SD}$	Medium flux rate	$\pm 1\text{SD}$	Low flux rate	$\pm 1\text{SD}$
A ($\mu\text{mol m}^{-2}\text{s}^{-1}$)	9.01	0.22	4.70	0.18	1.66	0.22
Δ (‰)	14.83	0.68	17.33	1.24	31.51	5.76
C_i/C_a (dimensionless)	0.41	0.03	0.51	0.05	1.06	0.23

Table 3.2 Standard deviations ($\pm 1\text{SD}$) for net assimilation rate (A), net observed discrimination against ^{13}C (Δ) and estimated C_i/C_a values from flask sampling procedure. All errors were calculated using Gaussian Error Propagation.

3.4 CALCULATIONS

3.4.1 *Relating to gas exchange*

The net rate of CO₂ assimilation (A) can be calculated from

$$A = \frac{dC_a}{dt} \cdot \frac{V}{L_A}, \quad (\text{Eq 3.2})$$

where the term dC_a/dt was calculated from the slope of the regression of gas concentration against time, V represents the temperature dependent molar volume of the branch chamber plus tubing and L_A is the projected needle air contained in the branch chamber. The convention adopted hereon in Chapter 3 and 4 is to express all fluxes as positive and on a projected leaf area basis.

The net rate of CO₂ assimilation can also be expressed as

$$A = v_c - 0.5v_o - R_d, \quad (\text{Eq 3.3})$$

where all processes contributing to the net exchange are considered as follows. Ribulose-1,5-bisphosphate carboxylase/oxygenase (Rubisco) catalyses the competing reactions of carboxylation (v_c) and oxygenation (v_o) of Ribulose-1,5-bisphosphate (RuBP). During carboxylation 1 mol of RuBP leads to the formation of 2 mol of 3-phosphoglycerate (PGA). The oxygenation (v_o) of 1 mol of RuBP leads to the formation of 1 mol of PGA and 1 mol of phosphoglycolate (PGly). The recycling of 1 mol PGly results in the release of 0.5 mol of CO₂ and thus it follows that the CO₂ mole fraction at which CO₂ uptake from carboxylation and CO₂ loss from photorespiration are equal, is that at which $v_c = 0.5v_o$ (Farquhar & Von Caemmerer,

1982). This CO₂ concentration has been called Γ_* (Laisk, 1977) and is distinguished from the CO₂ compensation point, Γ (CO₂ mole fraction where $A = 0 \mu\text{mol m}^{-2} \text{s}^{-1}$). Published studies have found Γ_* conservative across plant species and techniques (Laisk, 1977; Rasulov *et al.*, 1984; Brooks & Farquhar, 1985; Atkin *et al.*, 2000). Consequently, for this study Γ_* is assumed to follow the expression obtained from Brooks & Farquhar (1985),

$$\Gamma_* = 44.7 + 1.88 (T_i - 25) + 0.036 (T_i - 25)^2 \quad (\text{Eq 3.4})$$

where T_i is needle temperature (°C).

Mitochondrial respiration (R_d) associated with the TCA cycle also continues in the light, although not necessarily at the rate which occurs in the dark (Cornic & Jarvis, 1972; Sharp *et al.*, 1984; Brooks & Farquhar, 1985; Atkin *et al.*, 2000a). Thus R_d denotes day respiration, the rate of CO₂ evolution from processes other than photorespiration (Azcon-Bieto *et al.*, 1983).

As this study did not measure R_d directly, parameters published by Atkin *et al.*, (2000a) shown in Figure 3.5 for Snow gum (*Eucalyptus pauciflora* Sieb. Ex Spreng) were used. At present there are few published studies which comprehensively characterise the interactions of both light and temperature on the rates of day respiration (Brooks & Farquhar, 1985; Kirschbaum & Farquhar, 1987; Villar *et al.*, 1994; Villar *et al.*, 1995). Further discussion about assumptions and possible bias in using parameters for a different species are handled in the Discussion section of Chapter 4. The Atkin *et al.*, (2000a) study demonstrated that R_d was variable, and dependent on irradiance and temperature. Therefore, relationships describing the ratio of respiration occurring in the light relative to that occurring in the dark (R_d/R_n) for a given temperature and irradiance were used to calculate branch R_d .

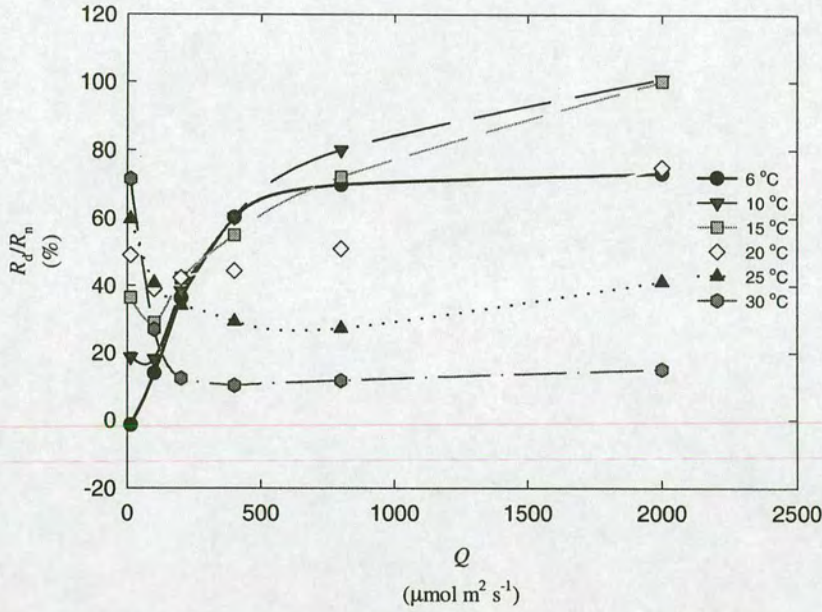


Figure 3.5 Effect of temperature on the relationship between photon flux density (Q) and the percentage of day respiration (R_d) relative to dark respiration (R_n) for *Eucalyptus pauciflora* Sieb. Ex Spreng. Re-produced from Atkin *et al.*, 2000.

Estimates for R_n were based on flux data obtained during periods when $Q < 0 \mu\text{mol m}^{-2} \text{s}^{-1}$. An Arrhenius “activation energy” temperature response (e.g., Lloyd & Taylor, 1994) was fitted to the branch data. The model followed the form

$$R_n = R_{20} \exp\left(\frac{E_0}{T_{20}\mathcal{R}}\right) \left(1 - \frac{T_{20}}{T_1}\right), \quad (\text{Eq 3.5})$$

where R_n is the nocturnal CO_2 efflux rate ($\mu\text{mol CO}_2 \text{m}^{-2} \text{s}^{-1}$) at needle temperature T_1 (K), R_{20} is the efflux rate at 20°C (K), \mathcal{R} is the gas constant ($8.314 \text{ J mol}^{-1} \text{K}^{-1}$) and E_0 is the activation energy ($56,734 \text{ J mol}^{-1} \text{K}^{-1}$ (Rayment *et al.*, 2002)).

Rates of CO₂ uptake during v_c and CO₂ release during $0.5v_o$ were calculated according to the method of Farquhar and von Caemmerer (1982):

$$v_c = \frac{A + R_d}{1 - \frac{\Gamma_*}{C_i}}, \quad (\text{Eq 3.6})$$

and

$$0.5v_o = 0.5v_c \left(\frac{2\Gamma_*}{C_i} \right), \quad (\text{Eq 3.7})$$

where C_i , the intercellular CO₂ mole fraction is calculated following von Caemmerer & Farquhar, (1981) as:

$$C_i = \frac{\left(g_c - \frac{E_L}{2} \right) C_a - A}{\left(g_c + \frac{E}{2} \right)}, \quad (\text{Eq 3.8})$$

whereby E_L is the transpiration rate per unit projected leaf area ($\text{mmol m}^{-2} \text{s}^{-1}$), g_c is the conductance to CO₂ and C_a is the mole fraction CO₂ of bulk air surrounding the branch.

Due to problems with absorption/desorption on the tubing walls IRGA water vapour mole fraction were unreliable for capturing the instantaneous changes inside the chamber. Therefore the rate of transpiration, E_L ($\text{mmol m}^{-2} \text{s}^{-1}$) from the branch were calculated from relative humidity data collected inside the branch chamber as follows:

$$E_L = \frac{d}{dt} \left(\frac{hP_{\text{sat}}}{P_{\text{atm}}} \right) \frac{V}{L_A}, \quad (\text{Eq 3.9})$$

where P_{sat} and P_{atm} are saturated vapour pressure at air temperature and atmospheric pressure (hPa), assumed constant, and h is the relative humidity. dh/dt was obtained from the derivative of a quadratic equation fit to relative humidity data ($r^2 > 0.99$ (July), > 0.9 (May)) at its initial phase of increase (corresponding to time zero) in the branch chambers. For flask sampling periods, the amount of water vapour removed in the drying cylinder was estimated from the flow rates of air circulated through the flask sampling unit.

Branch conductance to water vapour, g_s , ($\text{mmol m}^{-2} \text{s}^{-1}$) was calculated from the water vapour flux, E_L , and the needle to air mole fraction deficit, D_1 , expressed as a mole fraction deficit (mmol mol^{-1}). It is assumed D_1 can be estimated by the saturated mole fraction at the temperature of the leaf minus the mole fraction of ambient air surrounding the branch. Branch conductance is then calculated according to the following:

$$g_s = \frac{E_L}{D_1}, \quad (\text{Eq 3.10})$$

using only those data for which E_L exceeded $0.02 \text{ mmol m}^{-2} \text{s}^{-1}$ and D_1 exceeded $0.2 \text{ mmol mol}^{-1}$. Potential influences of the boundary layer on water flux were neglected because observations were conducted under conditions of high boundary layer conductance by constant air mixing (Rayment *et al.*, 2002). The water vapour flux cut-off value was determined as the value below which the calculated fluxes were not significantly different from zero. The humidity deficit cut-off point was chosen to eliminate spurious values when the denominator was very small.

The total branch conductance to CO₂, g_c , is then related proportionally to g_s by a factor of *ca.* 1.6 representing the binary diffusivities of CO₂ and H₂O in air (Andrussow, 1969) as follows:

$$g_c = \frac{g_s}{1.6}. \quad (\text{Eq 3.11})$$

It is important to note that this definition of conductance assumes molecules are traveling through still air. This assumption is violated during periods of high E . Equation 3.8 reconciles this departure, for the impact of the water vapour flux on the transport of CO₂.

3.4.2 Relating to net observed discrimination and $\delta^{13}\text{C}$ of respired CO₂

Net observed photosynthetic discrimination

The pair of flask samples represent the conditions in the chamber at the beginning (t_0) and the end (t_i) of a measurement period (see Figure 3.3). By comparing the trace gas composition of sample pairs, fractionation processes during gas exchange of branch chamber foliage could be determined. For daytime measurements, differences between sample pairs can be primarily attributed to photosynthesis. Calculation of photosynthetic discrimination against ¹³C (also applicable to ¹⁸O discrimination using this method) has to account for the isotope ratio of source CO₂ as it undergoes changes simultaneously with that of the product (see Appendix I for a definition of Δ). Photosynthetic gas exchange enriches (or depletes) air in the heavier isotope, ¹³C, and this air then becomes the new source for assimilation. In analogy to a Rayleigh process, the observed discrimination factor (D (‰)) against CO₂, in a closed chamber is calculated using the “Rayleigh” equation (after Kroopnick and Craig, 1976; Rooney, 1988; Guy *et al.*, 1993; Henry *et al.*, 1999):

$$D = \left(- \frac{\ln \frac{\delta_a}{\delta_{a0}}}{\ln \frac{C_a}{C_{a0}}} \right) 1000, \quad (\text{Eq 3.12})$$

where δ_a and C_a are the carbon isotope ratio and CO_2 mole fraction of the substrate at t_t contained in the ‘Closed’ flask, and δ_{a0} and C_{a0} are the initial carbon isotope ratio and CO_2 mole fraction of the substrate at t_0 contained in the ‘Open’ flask.

The discrimination factor is then re-expressed using “ Δ ” notation (Farquhar *et al.*, 1989) for carbon isotope discrimination by conversion of D as follows:

$$\Delta = \frac{D}{1 - \frac{D}{1000}} \quad (\text{Eq 3.13})$$

$\delta^{13}\text{C}$ of respired CO_2

During respiration, CO_2 released from foliage (also applicable to soils) accumulates within the closed chamber. The isotopic signature of the respiratory CO_2 flux reflects diffusion and respiratory fractionation processes as well as shifts in $\delta^{13}\text{C}$ due to changes in respiratory substrate (e.g., sugars, starch, lipids etc.). The carbon isotopic composition of respired CO_2 , δ_B for branches (δ_S in the case of soils), was calculated from a simple isotopic mass balance equation:

$$\delta_B = \frac{C_a \delta_a - C_{a0} \delta_{a0}}{C_a - C_{a0}}, \quad (\text{Eq 3.14})$$

An alternative method for estimating the respired CO₂ isotopic composition was to perform geometric mean regression between the isotopic composition, δ_a , and inverse of CO₂ mole fraction of air samples, ($1/C_a$) (i.e., "Keeling Plots") as:

$$\delta_a = C_{a0}(\delta_{a0} - \delta_B) \frac{1}{C_a} + \delta_B \quad (\text{Eq 3.15})$$

with δ_B as the intercept of the regression, i.e. at infinite C_a . For two data points (specifically, flask sample pairs), both equations are numerically equivalent, but the principle can be applied to other combinations of flasks (e.g., if one flask from a pair had a leak, then the other flask could still be included in this analysis, however, the mass balance approach could not be used). However, the "Keeling Plot" approach does require that δ_B remains constant at the temporal and spatial scale of study.

3.4.3 Relating to modelled photosynthetic ¹³C discrimination

Simple Model, Δ_s

The simplest (and most often used) model, describing the relationship of Δ to plant C_i at the leaf scale (hereon referred to as the "simple" model, Δ_s), was developed in Farquhar *et al.*, (1982) as:

$$\Delta_s = a + (b - a) \frac{C_i}{C_a}, \quad (\text{Eq 3.16})$$

where a is the fractionation resulting from diffusion of CO₂ in air into the leaf (≈ 4.4 ‰, Craig, 1953) and b is the combined net fractionation during carboxylation by Rubisco and phospho-enol-pyruvate carboxylase (PEPC) (30 ‰). Estimates of the

fractionation, b , can vary across species and have been reported in the range of 27 to 38 ‰ (Whelan *et al.*, 1973; Estep *et al.*, 1978a, 1978b; Wong *et al.*, 1979b; Roeske and O'Leary, 1984). For the purpose of this study, b is assumed to be 30 ‰.

The above model illustrates that when stomata place no limitation on CO₂ diffusion and $C_i/C_a \rightarrow 1$, C₃ leaves will discriminate against ¹³CO₂ by 30 ‰, with respect to the source air. In contrast, when stomatal closure is approached and resistance to CO₂ diffusion is high, $C_i/C_a \rightarrow 0$, and the discrimination against ¹³CO₂ decreases accordingly and will eventually reach 4.4 ‰, with respect to the source air. Thus, this model predicts the magnitude of ¹³C discrimination observed in C₃ plants is governed solely by C_i/C_a .

Comparison of the above model with automated gas exchange measurements is possible, by re-arranging Eqn 3.16 and making C_i/C_a the subject as follows:

$$\frac{C_i}{C_a} = \frac{\Delta_s - a}{b - a}. \quad (\text{Eq 3.17})$$

Respiration corrected model, Δ_{Rd}

The model described above (Eq 3.16) does not consider the possible fractionation associated with the concurrent processes of day respiration and photorespiration. It was shown by Farquhar *et al.*, (1982) that a more elaborate model can be constructed to deal explicitly with these additional processes. Hence Eq 3.16 can be replaced and Δ solved as follows:

$$\Delta_R = a + (b - a) \frac{C_i}{C_a} - f \frac{\Gamma^*}{C_a} - e \frac{R_d}{kC_a}, \quad (\text{Eq 3.18})$$

where e and f are the fractionation factors during dark respiration in the light and photorespiration (‰), respectively and k is the carboxylation efficiency ($\mu\text{mol m}^{-2} \text{s}^{-1}$). Following the definition of carboxylation efficiency (Farquhar *et al.*, 1982) the above equation can be rewritten as:

$$\Delta_R = a + (b - a) \frac{C_i}{C_a} - f \frac{\Gamma^*}{C_a} - e \frac{R_d}{A + R_d} \frac{C_i - \Gamma^*}{C_a}. \quad (\text{Eq 3.19})$$

For Eqn 3.19 it is assumed that the isotopic signature of the respiratory substrate used in photorespiration is the same or close to that recently fixed instantaneously during net assimilation. The isotopic signal of the photorespired CO_2 differs from that of the photosynthetic flux into the leaf by the magnitude of the fractionation factor, f , which is *ca.*, +7 to +8 ‰ (Rooney, 1988; Gillon & Griffiths, 1997, respectively). This positive fractionation factor creates photorespired CO_2 depleted with respect to its source, newly assimilated carbon. Thus, incorporating the isotope effects of photorespiration predicted photosynthetic discrimination would decrease in value. As the fractionation factor for photorespiration has not been established for Sitka spruce a value of +8 ‰ is assumed for f in this study.

As shown in Eq 3.19, day respiration has an impact on the net observed discrimination value only if there is intrinsic discrimination against ^{13}C during dark respiration, i.e., CO_2 respired is enriched (negative fractionation factor) or depleted (positive fractionation factor) with respect to its source. A consensus in opinion and evidence regarding respiratory fractionation has yet to be reached and estimates of e range from 0 to -6 ‰ (Lin & Ehleringer, 1997; Duranceau *et al.*, 1999, respectively) as mentioned previously. In this study, it was not possible to determine a fractionation factor during respiration. If e is assumed to be 0 ‰ in subsequent calculations, then Eq 3.19 cannot be applied as the dark respiration term on the far

right hand side of the equation would disappear. However, dark respired CO_2 originates from a substrate pool, representing an integral of Δ ($\int \Delta$) over some preceeding time interval that will be different from instantaneous Δ on most occasions. Therefore, even if there is no intrinsic fractionation during dark respiration, the isotopic signal of the day respired flux would still differ from that of the photosynthetic flux into the branch. Hence, an apparent fractionation factor for daytime respiration, e^* (‰), was defined as:

$$e^* = \delta_a - \delta_{\text{plant}} - \Delta, \quad (\text{Eq 3.20})$$

where δ_{plant} (‰) is the isotopic composition of the substrate pool of recently assimilated needle carbohydrates, derived from nocturnal measurements of the isotopic signature of dark respiration, $= \delta_b$ (this assumes no intrinsic fractionation during dark respiration occurs) and δ_a is the isotopic composition of ambient CO_2 in the canopy air space, varying around the background value of tropospheric CO_2 of ≈ -8 ‰ (Goodman & Francey, 1988). A more detailed derivation of Eq 3.20 is given in Appendix II.

Full model, Δ_F

Lastly, the above equation does not incorporate all isotope fractionations associated with the diffusion of CO_2 through a laminar boundary layer or internal CO_2 transfer through mesophyll cells to the chloroplasts, the site of carboxylation and enzymatic fractionation. These unaccounted fractionations can potentially alter the magnitude of photosynthetic ^{13}C discrimination. Because experiments were conducted under conditions of high boundary layer conductance (see Rayment *et al.*, 2000), the CO_2 at the needle surface, C_s , was assumed to be equal to C_a , so that fractionation associated with diffusion through a laminar boundary layer ($a_b = 2.9$ ‰) could be

neglected. Combining all the contributions described so far and the further contribution of mesophyll conductance, the "full" discrimination, Δ_F , was calculated using:

$$\Delta_F = a \frac{C_a - C_i}{C_a} + a_m \frac{C_i - C_c}{C_a} + b \frac{C_c}{C_a} - f \frac{\Gamma^*}{C_a} - (e^* + e) \frac{R_d}{A + R_d} \frac{C_i - \Gamma^*}{C_a}, \quad (\text{Eq 3.21})$$

where $a_m (= e_s + a_d)$ is the sum of the fractionation factors during internal CO_2 transfer, combining equilibrium fractionation of CO_2 entering solution ($e_s = 1.1 \text{ ‰}$ at 25 °C , Mook *et al.*, 1974) and fractionation during diffusion of dissolved CO_2 in water ($a_d = 0.7 \text{ ‰}$, O'Leary *et al.*, 1984). C_c is the chloroplast CO_2 mole fraction, C_i the CO_2 mole fraction in the stomatal cavities, assuming this is representative of that at the mesophyll cell wall surface (Farquhar & von Caemmerer, 1982).

The ^{13}C fractionation during internal CO_2 transfer is weighted by the drawdown of CO_2 mole fraction between stomatal cavities and the chloroplasts. In analogy to stomatal conductance, the two CO_2 mole fractions, C_i and C_c , are related to the net rate of CO_2 assimilation, A , and mesophyll conductance, g_w ($\text{mol m}^{-2} \text{ s}^{-1}$) according to:

$$A = g_w (C_i - C_c). \quad (\text{Eq 3.22})$$

Hence, mesophyll conductance can be derived from a regression of the difference between predicted discrimination (including concurrent respiratory contributions) and observed discrimination, $\Delta_R - \Delta_{\text{obs}}$, versus A/C_a , assuming that Δ_{obs} corresponds to the full derivation value of Δ_F as obtained from Eq 3.21. Subtracting Eq 3.21 from 3.19, and substituting $(C_i - C_c)$ from Eq 3.22, allows the calculation of mesophyll conductance, g_w , and thereby C_c , from the slope of the regression (see Evans and von Caemmerer, 1996):

$$\Delta_R - \Delta_{\text{obs}} = \Delta_R - \Delta_F = (b - a_m) \frac{C_i - C_c}{C_a} = \frac{(b - a_m)}{g_w} \frac{A}{C_a}. \quad (\text{Eq 3.23})$$

$\delta^{13}\text{C}$ of recently assimilated carbohydrates

Lastly, the isotopic composition of recently assimilated material, δ_D , reflects the time integrated signal of assimilation weighted ^{13}C discrimination as follows:

$$\delta_D = \frac{\int A(\delta_a - \Delta) dt}{\int A dt}, \quad (\text{Eq 3.24})$$

where Δ is the discrimination against ^{13}C weighted by the assimilation rate, A , during the photosynthetic period over the day. The weighting also incorporates the diurnal variations of δ_a , the isotopic composition of canopy CO_2 . Calculated values of δ_D also reflect the specific model used for calculating ^{13}C discrimination (i.e., Δ_s , Δ_R or Δ_F).

During photosynthesis, newly assimilated material is added to the carbohydrate pool of the needles. Hence, diurnal variations in the magnitude of discrimination will be reflected with changes in the isotopic composition of foliage carbohydrate pools in the needle. These changes in carbohydrate pools, will then directly influence observed discrimination values, Δ_{obs} , because of a feedback through the isotopic signature of day respiration which reflects the isotopic composition of the substrate source. Therefore, calculations of δ_{plant} were performed fully coupled with the concurrent discrimination predictions as follows:

$$\delta_{\text{plant}}(t) = \left(1 - \frac{\int A dt}{M_c}\right) \delta_{\text{plant}}(t-1) + \frac{\int A dt}{M_c} (\delta_a(t) - \Delta(t)), \quad (\text{Eq 3.25})$$

where M_c ($\mu\text{mol C m}^{-2}$) represents the total carbon content of branch foliage inside the chamber. Here, the assimilation rate A was integrated over one sampling interval, usually twenty minutes, assuming that the values for discrimination and δ_a remained constant throughout that time period. The isotopic composition of the needle carbohydrate pool from the previous time step, $\delta_{\text{plant}}(t-1)$, was then used as the isotopic signature of day respiration to calculate instantaneous values of discrimination in the next time step i.e. $\Delta(t) = f(\delta_{\text{plant}}(t-1))$.

When the initial value of δ_{plant} was prescribed from the isotopic composition of nocturnal dark respiration, δ_{plant} displayed strong drifts over short time periods because diurnal discrimination integrals were substantially different from initial δ_{plant} . Instead, an initial value was chosen such that drifts in δ_{plant} over time were minimised, i.e., the system was assumed to be in dynamic steady state.

4. Daily variation of gas exchange and ^{13}C discrimination in Sitka spruce branches under field conditions – Results and Discussion

4.1 RESULTS

4.1.1 *Branch micro-climate*

Figures 4.1 and 4.2 show examples of daily time courses of environmental variables measured within branch chambers during both field campaigns. Photosynthetic photon flux density (Q) during the May and July campaigns were very different. During May, in the upper canopy direct beam irradiance dominated, with intermittent cloud cover. However, in July diffuse irradiance dominated as indicated by low Q in the upper canopy (Figures 4.1a and 4.2a). However, intermittent breaks in cloud cover during July were observed, usually when solar elevation was low, and the horizon was not obscured by the cloud base. The branch chamber (4) characteristic of the middle canopy consistently measured Q values *ca.* 75% lower than those located in the upper canopy, particularly Chamber 1. The upper chambers experienced similar values of Q during the July campaign and on occasions during the May campaign, however during the morning and afternoons Chamber 3 measured Q values much lower than Chamber 1 partly because of shading from surrounding branches.

Despite overcast conditions in July, a diurnal pattern of within canopy air temperature (T_a) and humidity deficit (D_a) were observed (Figures 4.1 and 4.2, panels b and c) during both field campaigns. Temperatures were similar for both upper chambers (1 and 3) during May and July reaching *ca.* 15 to 25 °C over the midday period (10:00 – 14:00 hrs). The middle chamber (4) T_a were lower over the midday

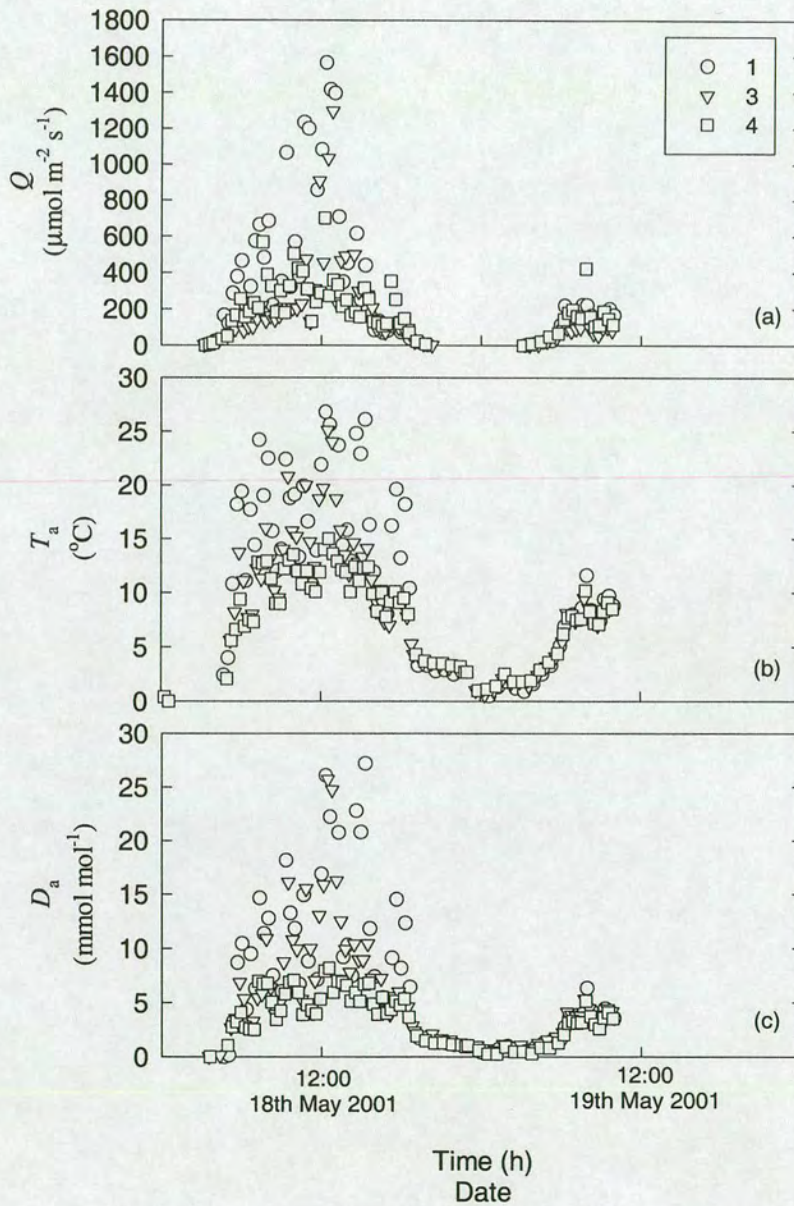


Figure 4.1 Daily variation of branch (a) photosynthetic photon flux density (Q), (b) air temperature (T_a) and (c) air humidity deficit (D_a) in each branch chamber during 18th and 19th May, 2001. Chamber 1 (upper) represented by (○), chamber 3 (upper) represented by (▽) and chamber 4 (middle) represented by (□). Each point represents the 5 min average for each environmental variable during chamber closure.

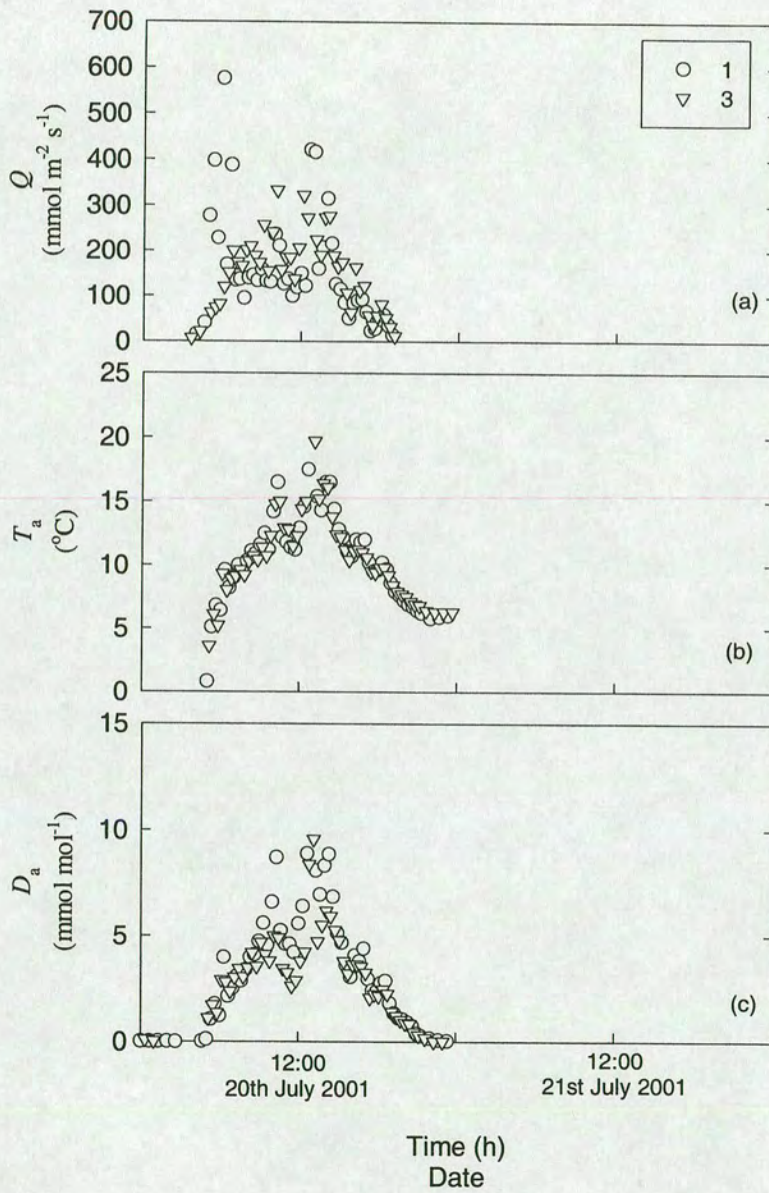


Figure 4.2 Daily variation of branch (a) photosynthetic photon flux density (Q), (b) air temperature (T_a) and (c) air humidity deficit (D_a) in each branch chamber during 20th July, 2001. Chamber 1 (upper) represented by (○) and chamber 3 (upper) represented by (▽). Each point represents the 5 min average for each environmental variable during chamber closure.

period during May, ranging between 10 to 15 °C. Air vapour pressure deficits (D_a) were also similar for both upper chambers during May and July. Values for D_a ranged between 10 to 15 mmol mol⁻¹ for the upper chambers and 4 to 10 mmol mol⁻¹ for the middle chamber during May. These were somewhat larger than values observed in the same chambers during July that ranged between 4 to 10 mmol mol⁻¹. Maximum D_a occurred after midday during May and July. Both Q , T_a and D_a were dependent on incoming solar radiation (data not shown). At night dew formation was observed on both the canopy and branch chambers.

4.1.2 Branch gas exchange

Field observed assimilation, stomatal conductance and C_i/C_a

Figures 4.3 and 4.4 show the daily time courses of gas exchange measurements for both field campaigns. During May, assimilation rates (A) were highest before midday when Q was high and D_a low. Assimilation rates tended to follow Q over the daily time course, with the exception of Chamber 3. Data from this chamber did not correspond with the general pattern observed in the other two chambers. Field notes indicated problems with the chamber between 09:00 and 10:40 and again between 12:30 and 15:00 (18th July 2001). This problem only affected CO₂ mole fraction (C_a) transported in the system tubing consequently all other measured variables (Q , T_a , D_a , g_s) remained unaffected. Maximum assimilation rates for May were larger than those observed in July (11 and 8 μmol m⁻² s⁻¹, respectively).

Calculated branch conductance (g_s) ranged between 100 and 250 mmol m⁻² s⁻¹ in the middle canopy and 30 to 170 mmol m⁻² s⁻¹ in the upper canopy during May (Figure 4.3b). In contrast values for g_s during July were much lower ranging between 50 and 150 mmol m⁻² s⁻¹ (Figure 4.4b). Maximum g_s were typically observed in the morning

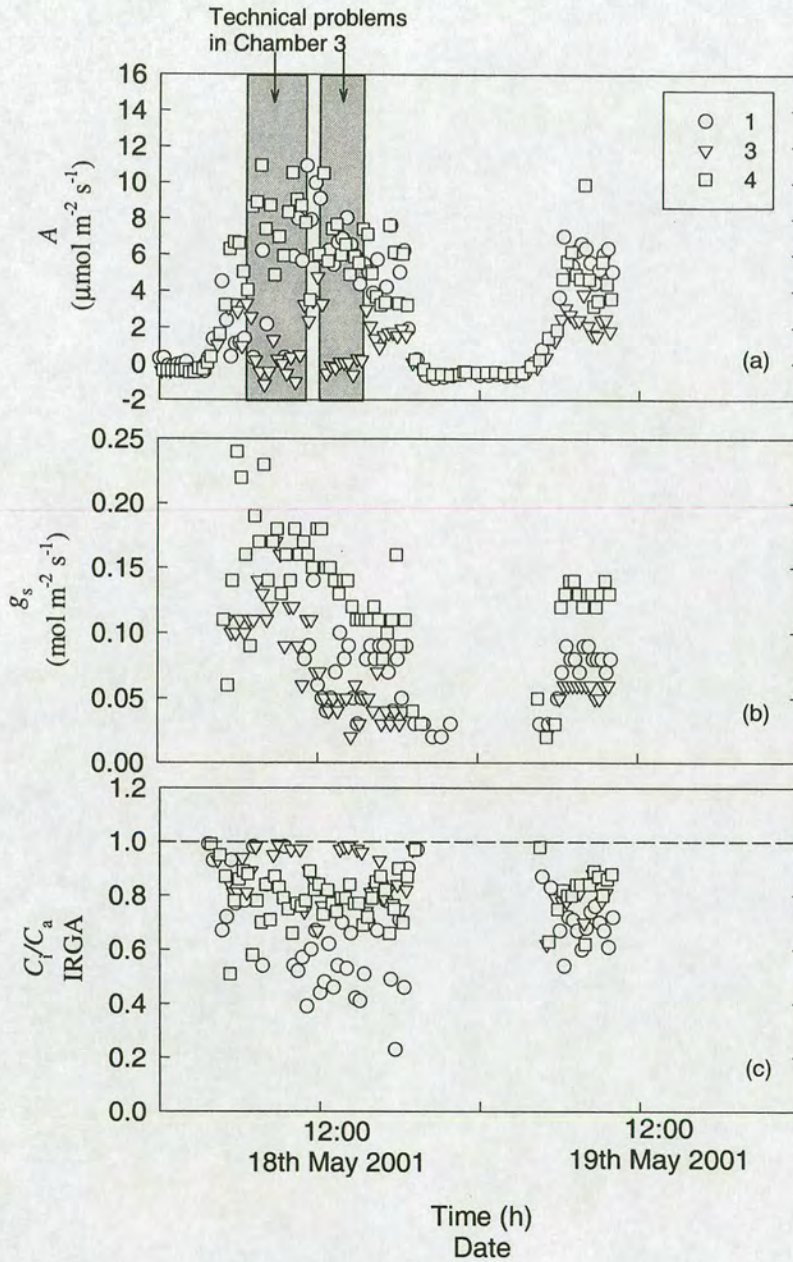


Figure 4.3 Daily variation of branch (a) assimilation rate (A), (b) branch conductance to water vapour (g_s) and (c) the ratio of intercellular to ambient CO_2 mole fraction (C_i/C_a) in each branch chamber during 18th and 19th May, 2001. Chamber 1 (upper) represented by (○), Chamber 3 (upper) represented by (▽) and Chamber 4 (middle) represented by (□).

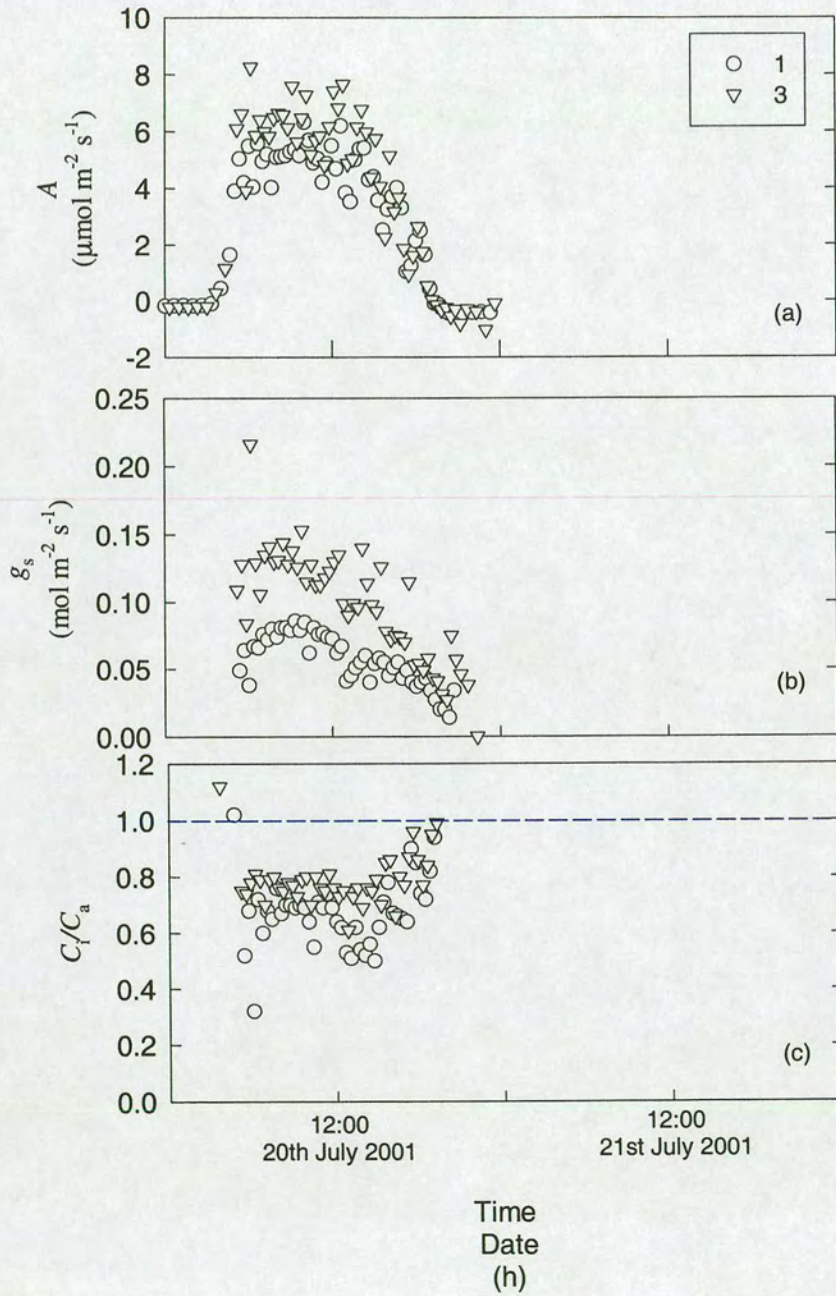


Figure 4.4 Daily variation of branch (a) assimilation rate (A), (b) branch conductance to water vapour (g_s) and (c) the ratio of intercellular to ambient CO_2 mole fraction (C_i/C_a) in each branch chamber during 20th July, 2001. Chamber 1 (upper) represented by (o) and Chamber 3 (upper) represented by (∇).

and gradually decreased over the day as T_a and D_a increased. After midday during the July campaign a transient increase in incoming solar radiation caused Q , T_a and D_a to increase and g_s to decrease. The ratio of intercellular to ambient CO_2 mole fraction (C_i/C_a) during May remained between 0.4 to 0.8 for the upper canopy and 0.7 to 0.9 for the middle canopy during May (Figure 4.3c). During July C_i/C_a was stable over the day and ranged between 0.5 and 0.8 for both branch chambers (Figure 4.4c). However, during dawn and dusk C_i/C_a was typically $0.8 \rightarrow 1$ as $Q \rightarrow 0 \mu\text{mol m}^{-2} \text{s}^{-1}$. At dawn, the large C_i/C_a occurred when values of A were low and g_s high, because Q and D_a were low. In contrast, at dusk large C_i/C_a occurred primarily because of low A rather than g_s (Figures 4.3 and 4.4).

Nocturnal branch respiration rates (R_n) observed during May 2001 were larger than those observed in July 2001 (Figures 4.5 and 4.6). Fitted parameter estimates for the nocturnal respiration rate at 20°C (R_{20}) during May were approximately double those estimated for July (Table 4.1).

Campaign Position (Id)	R_{20} \pm SE $\mu\text{mol m}^{-2} \text{s}^{-1}$	\pm 95% CI $\mu\text{mol m}^{-2} \text{s}^{-1}$	n	P
May	3.29	2.96 – 3.62	55	<0.0001
Upper (1)	\pm 0.17			
May	2.50	2.41 – 2.59	52	<0.0001
Upper (3)	\pm 0.04			
May	2.65	2.57 – 2.73	70	<0.0001
Middle (4)	\pm 0.04			
July	1.43	1.37 – 1.49	67	<0.0001
Upper (1)	\pm 0.03			
July	1.28	1.06 – 1.51	40	<0.0001
Upper (3)	\pm 0.11			

Table 4.1 Parameter values obtained from the relationship between needle temperature (T_i) and nocturnal branch efflux rates (R_n) from each branch chamber using Eq 3.5. Data collected during 18th/19th May 2001 and 19th/23rd July 2001 used for curve fitting.

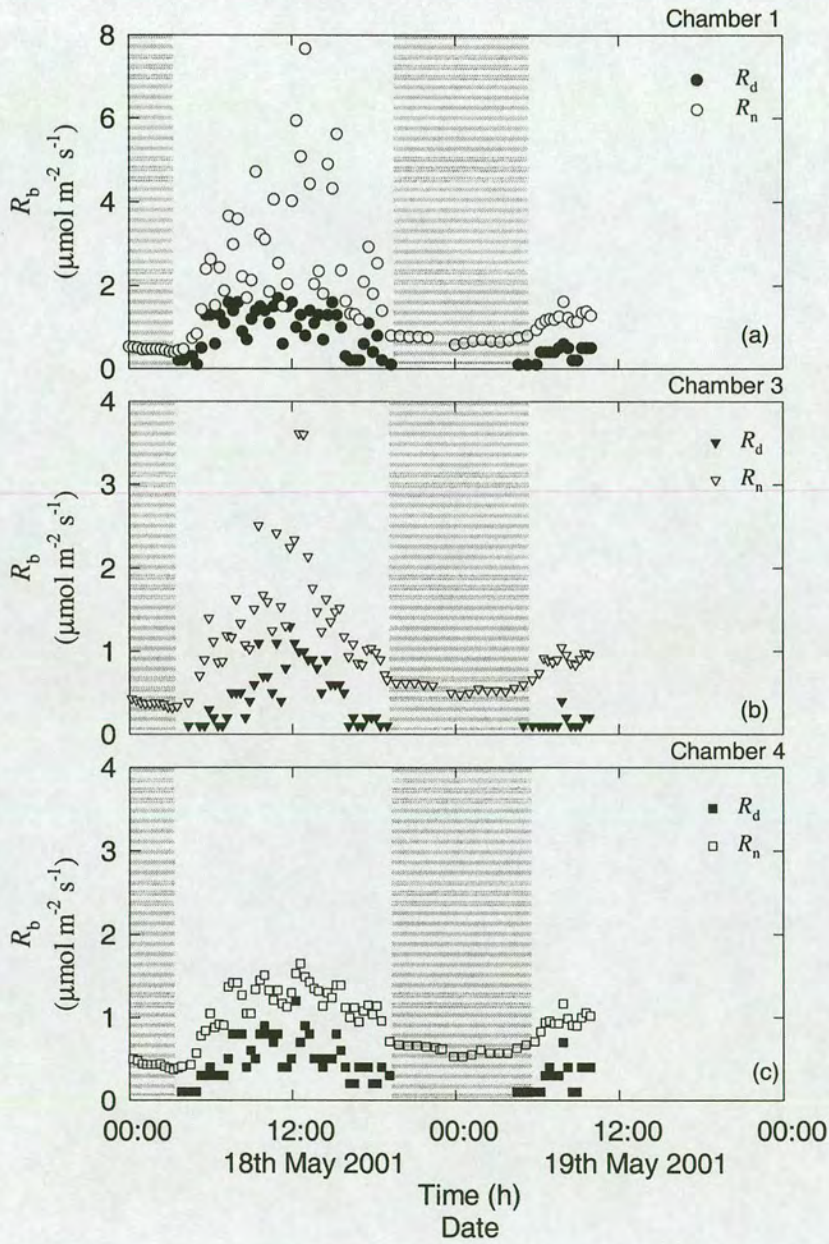


Figure 4.5 Daily variation in measured and modelled branch respiration rates assuming no inhibition of respiration during the day (R_n) or incorporating inhibition of daytime dark respiration (R_d) (see Section 3.4.1) for (a) Chamber 1 (\circ), (b) Chamber 3 (∇) and (c) Chamber 4 (\square) during 18th and 19th May 2001. N.B. R_n can only be measured when $Q < 0$ $\mu\text{mol m}^{-2} \text{s}^{-1}$, indicated with dark panels on the above graphs.

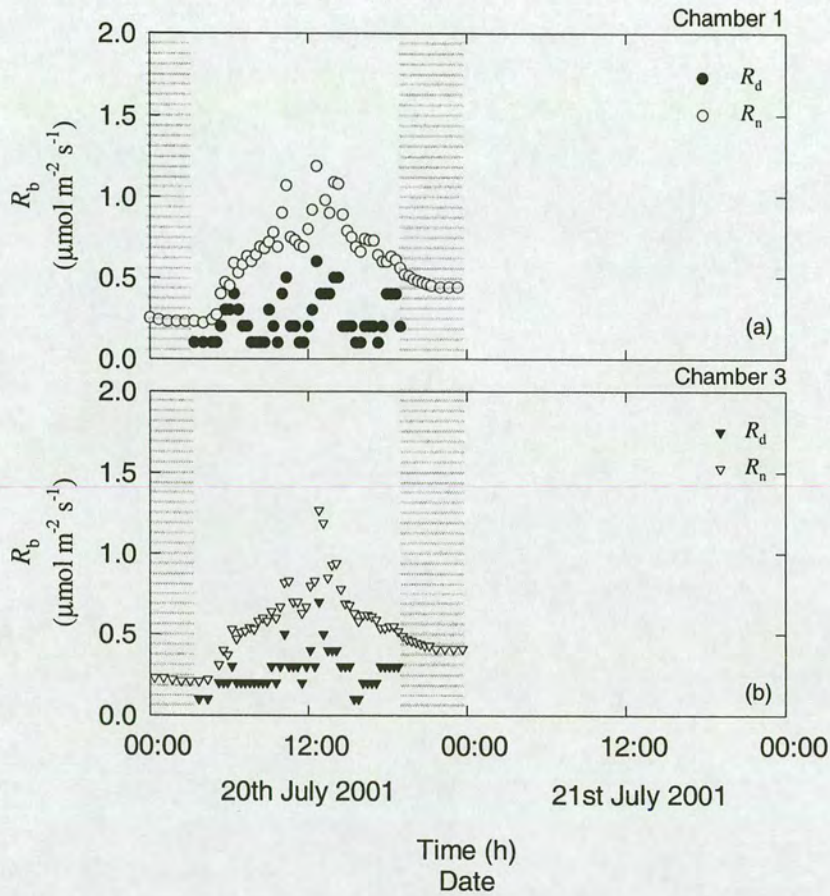


Figure 4.6 Daily variation in measured and modelled branch respiration rates assuming no inhibition of respiration during the day (R_n) or incorporating inhibition of daytime dark respiration (R_d) (see Section 3.4.1) for (a) Chamber 1 (\circ) and (b) Chamber 3 (∇) during 20th July 2001. N.B. R_n can only be measured when $Q < 0 \mu\text{mol m}^{-2} \text{s}^{-1}$, indicated with dark panels on the above graphs.

Figures 4.5 and 4.6 highlight the differences in modelled daytime dark respiration assuming no inhibition of branch respiration (R_n) and incorporating the inhibition function as a function of Q and T_1 (see Section 2.4.1). The largest differences between the two models occurred when T_1 and Q were largest. The largest respiration rates were observed in Chamber 1 during May and July (Figure 4.5a and

4.6a). However, during July differences between chambers were not as pronounced as for May.

Modelled component fluxes

Figure 4.7 provides an example of the estimated rates of CO₂ exchanged between the branch and the atmosphere as a consequence of carboxylation (v_c), day respiration (R_d) and photorespiration ($0.5v_o$). Maximum rates of carboxylation occurred in May and July, (16 and 9 $\mu\text{mol m}^{-2} \text{s}^{-1}$, respectively), when maximum assimilation rates and Q were observed. Losses of CO₂ via photorespiration were also largest at these times, with up to 41% of gross photosynthetic CO₂ uptake (i.e., v_c) respired in both May and July. Over the day, both carboxylation and photorespiration tracked Q closely with values ranging between 1-16 $\mu\text{mol m}^{-2} \text{s}^{-1}$ for v_c and 0.1-5.7 $\mu\text{mol m}^{-2} \text{s}^{-1}$ for $0.5v_o$, during both May and July. The percentage of v_c respired as a consequence of photorespiration ranged between 11-29% for the majority of both days, with a few exceptions, noted above, in high Q .

Differences in the estimated contribution of day respiration between field campaigns were considerable, both in pattern and magnitude. During May, R_d tracked the daily pattern of A , Q and T_i , to a greater extent than in July. Higher respiration rates observed during May coincided with canopy 'bud-burst'. Temperatures between May and July were similar during the night, but May T_a were larger than those of July. However, these temperature differences did not account for the higher branch respiration (R_b) indicated by R_{20} (Table 4.1). Additional losses of CO₂ via growth respiration were the most likely cause for this difference. The percentage of v_c respired as a consequence of inhibited dark respiration in the light, was largest at dawn, between 20–70%, and at dusk between 11-51%. At these times, Q and gross photosynthetic CO₂ uptake were at their lowest during the daytime period ($Q \rightarrow 0$

$\mu\text{mol m}^{-2} \text{s}^{-1}$). If no inhibition of daytime dark respiration occurred (R_n), between 20 – 70% of v_c was also lost, however there were occasions when predicted R_n exceeded A during the day when assimilation rates were low at dusk and dawn or when temperatures were largest leading to very large losses >100%.

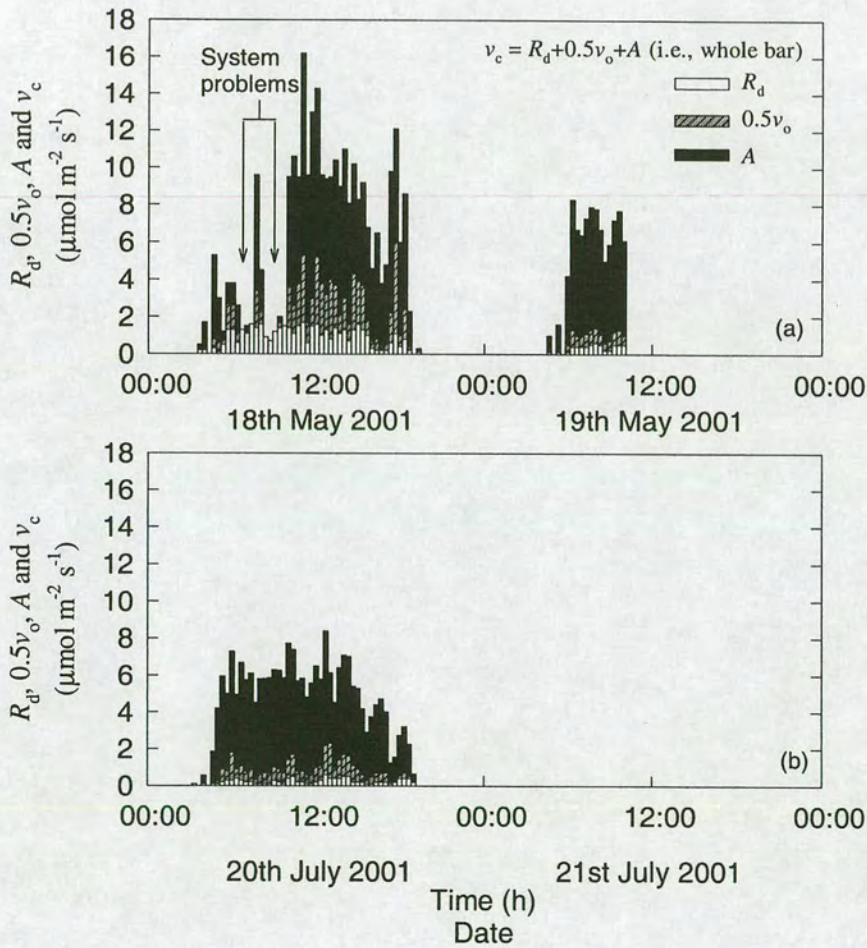


Figure 4.7 Daily variation in the contribution of day respiration (R_d), photorespiration ($0.5v_o$) and assimilation rate (A) to the carboxylation rate (v_c) estimated for Chamber 1 during (a) 18th May 2001 and (b) 20th July, 2001. N.B. Summing the contributions of R_d , A and $0.5v_o$, v_c is inferred (whole bars).

4.1.3 Flask method for stable isotope collection

Figure 4.8 shows values of C_a and δ_a for a sub-set of flask pairs collected during the May field campaign.

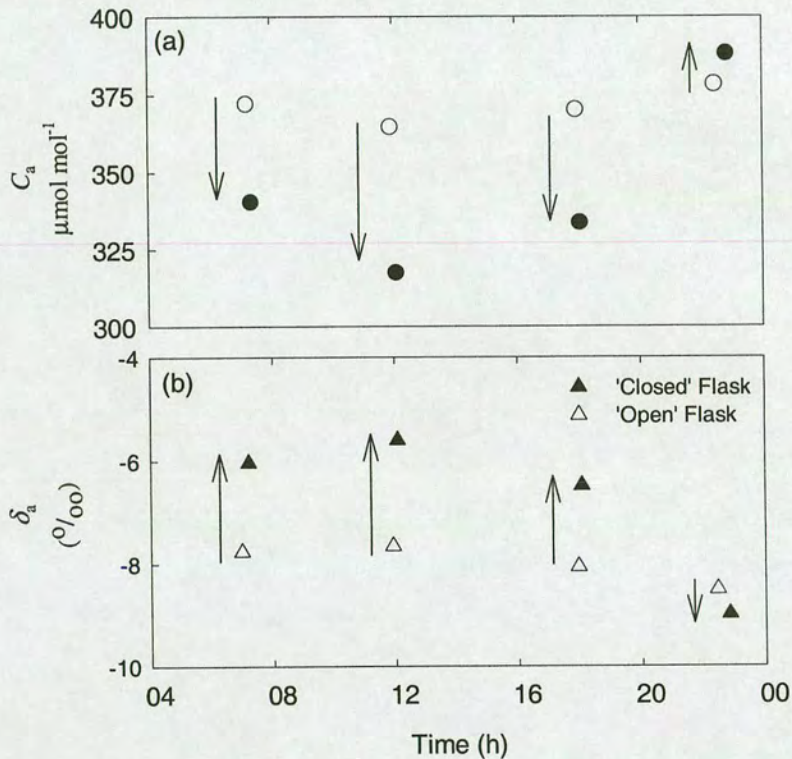


Figure 4.8 Daily variation in bulk air (a) CO₂ mole fraction (C_a) and (b) $^{13}\text{C}/^{12}\text{C}$ ratios (δ_a) of flask pairs collected on 18th May 2001 from a ventilated branch chamber when the chamber is 'Open' (open symbols) and 'Closed' (filled symbols). Data collected by L. Wingate (University of Edinburgh) and U. Seibt (Max Planck Institute for Biogeochemistry).

The data show clearly the differences between 'Open' and 'Closed' flasks for both C_a and δ_a during the daily time course. When photosynthetic processes dominate, a draw-down in C_a is observed over time, as CO₂ is taken up by the branch, leaving the

chamber air depleted in CO_2 (Figure 4.8a). The isotopic composition of substrate, δ_a , in the chamber is altered in concert with the uptake of CO_2 (Figure 4.8b). The data clearly show an enrichment of the heavier isotope, ^{13}C , between ‘Open’ and ‘Closed’ flasks, as the needles preferentially take up the lighter ^{12}C during photosynthesis. The arrows next to the flask pairs highlight the overall direction of change observed over time.

At dusk, respiratory processes start to dominate, as highlighted by the flask pair collected at 22:00 h. A build-up of CO_2 (C_a) is observed over time, reflecting the input of respired CO_2 from the branch. A corresponding change in δ_a is also observed, as CO_2 is released into the chamber. The data clearly show an enrichment of the lighter isotope, ^{12}C between ‘Open’ and ‘Closed’ flasks, as the plant releases CO_2 depleted in the heavier isotope, ^{13}C . These flask pairs were subsequently used to calculate Δ_{obs} following Eqs 3.12 and 3.13 and δ_b following Eq 3.14 (see Section 3.4.2 and Appendix I for more details on calculations and units).

4.1.4 Field observed instantaneous net discrimination against $^{13}\text{CO}_2$

Daily variation in the net observed instantaneous discrimination, Δ_{obs} from different branch bags was pronounced over both field campaigns (Figure 4.9). Maximum values of Δ_{obs} , ranging between 30 to 35‰, were observed at dusk and dawn on both days in the upper branch chambers (1 and 3). As Q and A increased during the morning Δ_{obs} decreased in value to an observed minimum of 15‰. Over midday and for sometime in the afternoon Δ_{obs} remained at this value during both field campaigns. Differences between Δ_{obs} were also apparent for different locations in the canopy. Δ_{obs} for the middle canopy were systematically larger than for the upper canopy at similar times of the day. During late afternoon Δ_{obs} values increased and were observed to fluctuate in concert with Q , D_a , A and C_i/C_a in the late afternoon.

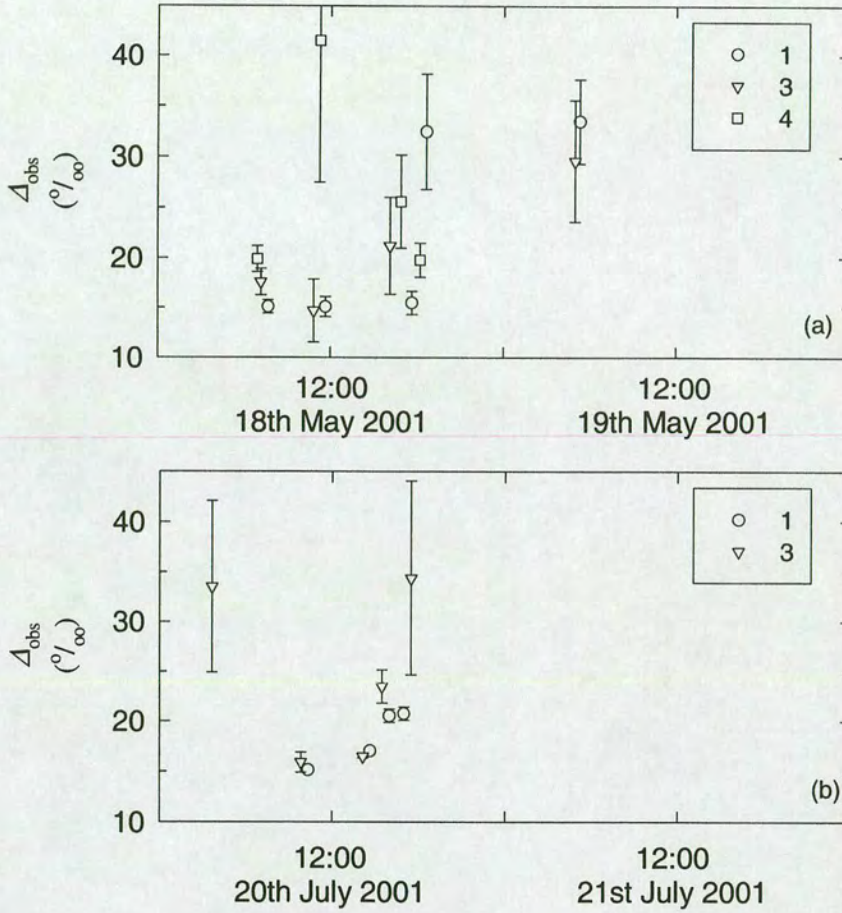


Figure 4.9 Diurnal variation in observed instantaneous net discrimination ($\Delta_{\text{obs}} \pm 1\text{SD}$) collected in different branch chambers during (a) 18th and 19th May 2001 and (b) 20th July 2001. Chamber 1 (upper) represented by (\circ), chamber 3 (upper) represented by (∇) and chamber 4 (middle) represented by (\square). Data collected by L. Wingate (University of Edinburgh) and U.Seibt (Max Planck Institute for Biogeochemistry).

During both field campaigns variation in Δ_{obs} was systematically related to changing environmental conditions, A and C_i/C_a (Figures 4.1, 4.2, 4.3 and 4.4). There were no observed differences in Δ_{obs} between field campaigns despite differences in Q and A observed using the automated gas exchange method (Figures 4.1, 4.2, 4.3 and 4.4).

Δ_{obs} and estimated uncertainties were typically largest at dawn and dusk ($>30\text{‰}$) (Table 3.2 and Figure 4.9). However, one observation from the middle bag at noon on the 18th May 2001, gave the largest value of Δ_{obs} (41 ‰) and was associated with the largest calculated uncertainty. This observation occurred during a transient period of low Q and A (Figures 4.1 and 4.3). Referring to the Simple model of photosynthetic discrimination (Eq 3.16) values $> 30\text{‰}$ indicate C_i/C_a values in excess of 1 during the day which indicate a reversal in the diffusion gradient of CO_2 , with C_i values higher than C_a .

There are three hypotheses put forward for these observations:

the enzymatic fractionation factor, b , assumed to equal 30 ‰, is inappropriate for *P. sitchensis* and could be $> 30\text{‰}$;

C_i could be higher than C_a if respiration rates exceeded carboxylation;

or the additional processes of concurrent photorespiration and day respiration could contribute to Δ_{obs} through the distinct isotopic composition of respired $^{13}\text{CO}_2$.

In this experiment it was not possible to establish b for *P. sitchensis*. Therefore, it is difficult to prove this is the appropriate fractionation factor, however, indirect data using branch respiration presented later suggests integrated values of b in this region. Furthermore, values of 41‰ for b although not impossible (Estep *et al.*, 1978) are extremely rare and unlikely for this species and environment.

Continuous field measurements of A indicated that the second hypothesis was also unlikely as a net CO_2 uptake (a prerequisite for Δ) was observed during these sampling occasions and calculated $C_i/C_a < 1$ (Figures 4.3 and 4.4).

Therefore, in this field study the most tenable hypothesis for explaining the high Δ_{obs} is the last one presented i.e., isotopic contributions through respiratory processes become increasingly important during these periods of the day. Thus, to relate Δ_{obs} to C_i/C_a one must consider the extensive models of photosynthetic discrimination which incorporate the contributions of respiration (Eq 3.19) and mesophyll conductance (Eq 3.21) (Also see Appendix II). Adopting this approach allows estimation of the discrimination against ^{13}C by photosynthesis alone (Δ), validates theoretical models describing field observations, and thereby provides a means to predict instantaneous discrimination over time and space using continuous gas exchange data or models of photosynthesis.

4.1.5 *Modelling the diurnal variation of discrimination against $^{13}\text{CO}_2$*

Stable isotope composition of canopy CO_2

Figures 4.10a and 4.11a show the predicted variation in carbon isotope composition of canopy CO_2 , δ_a . Daily cycles of δ_a were simulated using a geometric regression relationship fitted to 'Open' flask observations of C_a vs δ_a for May and July collected over the daily cycle, also shown in Figures 4.10a and 4.11a. The regression relationships used were:

$$\delta_a (\text{May}) = 11.54 (\pm 0.94) + -0.053 (\pm 0.002)C_a \quad r^2 = 0.96 \quad n = 17 \text{ and};$$

$$\delta_a (\text{July}) = 12.10 (\pm 0.64) + -0.054 (\pm 0.000)C_a \quad r^2 = 0.99 \quad n = 21.$$

No significant difference was found between the two regressions and the relationships described the distribution of observations well. Any observed differences between the regressed and predicted δ_a are probably the result of random differences between CO_2 mole fraction measured by the IRGA and in flask samples.

Apparent fractionation during daytime dark respiration

The calculated isotope signatures of daytime dark respiration for each branch with respect to canopy air (i.e., $\delta_e = \delta_a - \delta_{\text{plant}}$) were plotted in Figures 4.10b and 4.11b. The isotopic composition of the respiratory substrate, δ_{plant} , was assumed to be in dynamic steady state with discrimination as described in Section 3.4.3, Eq 3.25. The initial values for δ_{plant} were -26‰ (Chamber 1), -31.5‰ (Chamber 3) and -29.5‰ (Chamber 4) during May and -25‰ (Chamber 1) and -28‰ (Chamber 3) for July. From Figures 4.10b and 4.11b it is apparent that the average isotopic signal from day respiration was $\approx 22\text{‰}$. Variation in δ_e over the day was $\approx 1\text{‰}$, similar to δ_{plant} but smaller than δ_a ($\approx 2\text{‰}$).

The apparent fractionation factors of daytime dark respiration (e^*) presented in Figures 4.10c and 4.11c were calculated from the differences between $\delta_e - \Delta$ presented in Figures 4.10b and 4.11b (see Eq 3.20). The figures illustrating the apparent fractionation factor, show that when the isotopic signature of the respiratory contribution is equal to discrimination, e^* equals zero. When the contribution from dark respiration is substantial during dusk and dawn, e^* changes sign and becomes increasingly negative, thereby expressing an apparent negative fractionation factor. In contrast when the contribution from carboxylation dominates, e^* becomes an apparent positive fractionation factor. As with fractionation that occurs during photorespiration, a positive factor means that respired CO_2 is isotopically depleted in ^{13}C with respect to its substrate pool, whereas a negative fractionation factor indicates an isotopic enrichment of ^{13}C in the respired CO_2 . Therefore, incorporating the isotopic effects of daytime dark respiration would account for the larger values of Δ_{obs} at dusk and dawn not predicted by the simple model incorporating C_i/C_a only (Eq 3.16).

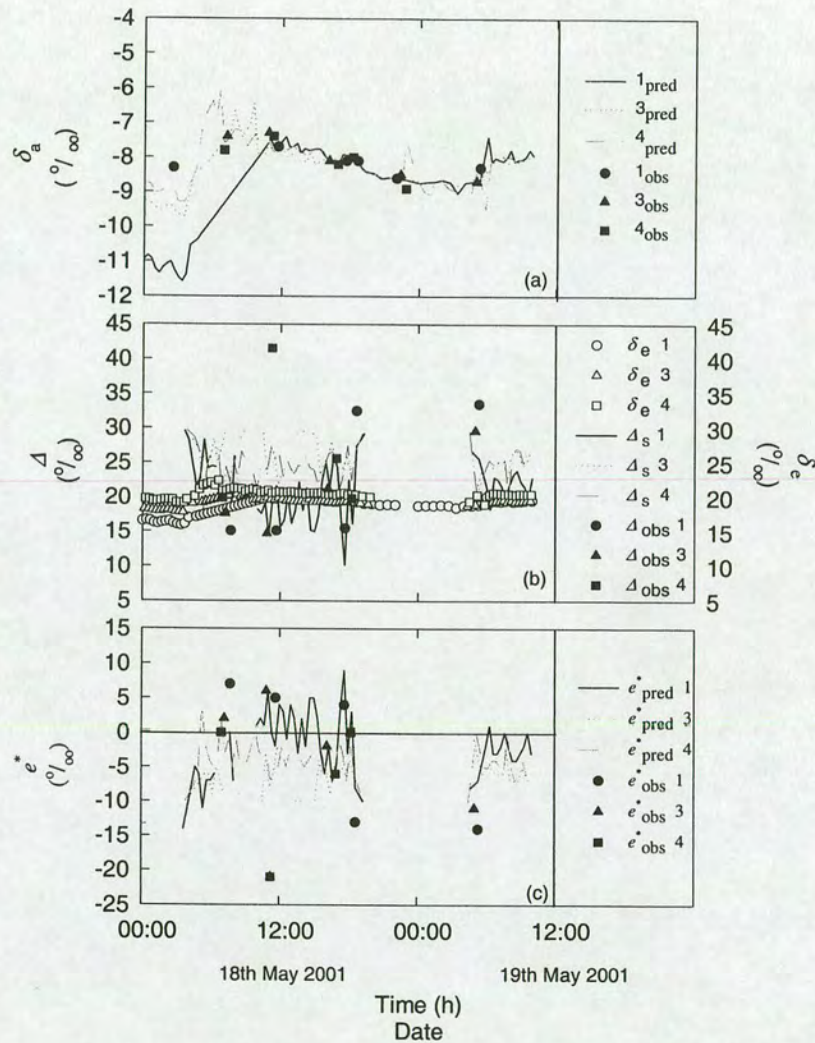


Figure 4.10 Daily variation in (a) δ_a of canopy CO_2 observed in ‘open flasks’ for Chamber 1 (●), Chamber 3 (▲) and Chamber 4 (■) or predicted from a regression between C_a and δ_a and simulated using C_a from Chamber 1 (solid line), Chamber 3 (dotted line) and Chamber 4 (dot/dash line) (b) the δ_e of day respiration with respect to δ_a predicted for Chamber 1 (○), Chamber 3 (△) and Chamber 4 (□), Δ_s predicted using the simple model (Eq 3.16) and C_i/C_a measured in Chamber 1 (solid line), Chamber 3 (dotted line) and Chamber 4 (dot/dash line) and Δ_{obs} for Chamber 1 (●), Chamber 3 (▲) and Chamber 4 (■) (c) the apparent fractionation factor, e^* (Eq 3.20), predicted from Δ_s in Chamber 1 (solid line), Chamber 3 (dotted line) and Chamber 4 (dot/dash line) and Δ_{obs} in Chamber 1 (●), Chamber 3 (▲) and Chamber 4 (■) during 18th/19th May 2001. Data collected by L. Wingate (University of Edinburgh) and U. Seibt (Max Planck Institute for Biogeochemistry).

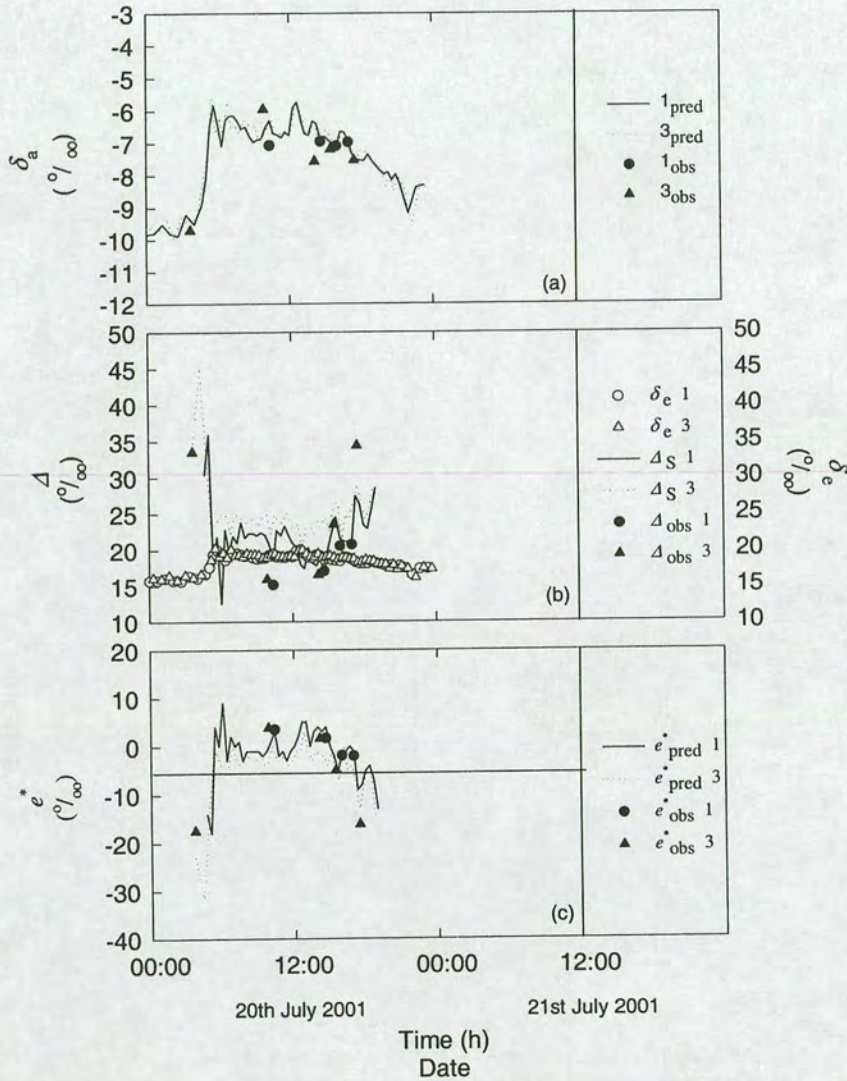


Figure 4.11 Daily variation in (a) δ_a of canopy CO_2 observed in ‘open flasks’ for Chamber 1 (●) and Chamber 3 (▲) or predicted from a regression between C_a and δ_a and simulated using C_a from Chamber 1 (solid line) and Chamber 3 (dotted line) (b) the δ_e of day respiration with respect to δ_a predicted for Chamber 1 (○) and Chamber 3 (Δ), Δ_s predicted using the simple model (Eq 3.16) and C_i/C_a measured in Chamber 1 (solid line) and Chamber 3 (dotted line) and Δ_{obs} for Chamber 1 (●) and Chamber 3 (▲) (c) the apparent fractionation factor, e^* (Eq 3.20), predicted from Δ_s in Chamber 1 (solid line) and Chamber 3 (dotted line) and Δ_{obs} in Chamber 1 (●) and Chamber 3 (▲) during 20th July 2001. Data collected by L.Wingate (University of Edinburgh) and U. Seibt (Max Planck Institute for Biogeochemistry).

Mesophyll conductance

The combined field measurements of Δ_{obs} , A and C_i/C_a were utilised to obtain estimates of mesophyll conductance, g_w . However, to do this it was necessary to use predictions of discrimination that included the contributions of photorespiration and dark respiration i.e., Δ_R (by combining Eqs 3.19 and 3.20). Thus differences between Δ_R and Δ_{obs} could be attributed to fractionation that occurred during internal CO_2 transfer. This regression method for estimating g_w , has been used successfully a number of times in both laboratory (Evans *et al.*, 1986; Evans and von Caemmerer, 1996) and field situations (Harwood *et al.*, 1998).

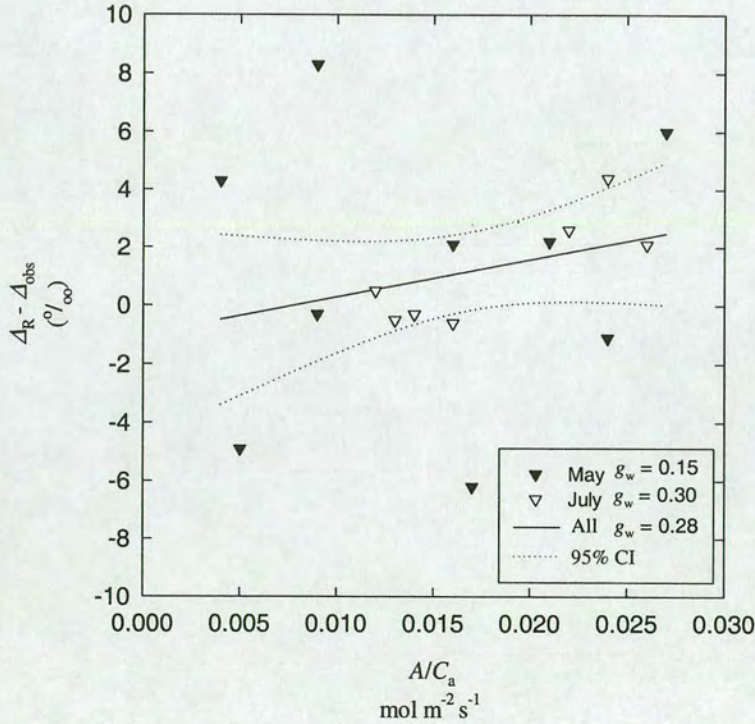


Figure 4.12 The relationship between the difference in respiration corrected predicted discrimination, Δ_R (combined Eqs 3.19 and 3.20) and net observed instantaneous discrimination, Δ_{obs} versus A/C_a in May (\blacktriangledown) and July (\triangledown) for data where $A/C_a > 0.001 \text{ mol m}^{-2} \text{ s}^{-1}$. Data collected by L.Wingate (University of Edinburgh) and U. Seibt (Max Planck Institute for Biogeochemistry).

Predictions for g_w ranged from $0.15 \text{ mol m}^{-2} \text{ s}^{-1}$ during May and $0.30 \text{ mol m}^{-2} \text{ s}^{-1}$ during July. The regression data used are presented in Figure 4.12 and only include A/C_a observations that were significantly different from zero ($<0.001 \text{ mol m}^{-2} \text{ s}^{-1}$). The mean g_w for both May and July data was $0.29 \text{ mol m}^{-2} \text{ s}^{-1}$, this conductance was very similar to the maximum g_s observed during the May experiment *ca.* $250 \text{ mol m}^{-2} \text{ s}^{-1}$, indicating a substantial resistance to CO_2 transfer. Incorporation of a constant g_w enabled the calculation of C_c using Eq 3.22. The average offset between $(C_i - C_c)/C_a$, was approximately 0.1 during periods of high A , in agreement with other published values for woody species (Syvertsen *et al.*, 1995).

Predicting the diurnal variation of discrimination against $^{13}\text{CO}_2$

Combining continuous estimates of v_c , $0.5v_o$, R_d and C_i/C_a with the above parameters, estimates for branch ^{13}C discrimination, Δ , were made using: the simple model, Δ_s ; a photorespiration corrected model, $\Delta_{0.5v_o}$; a day respiration corrected model, Δ_{R_d} ; a mesophyll conductance corrected model Δ_{g_w} and; a model incorporating all of the above processes, the full model, Δ_F . The five sets of predictions for branch discrimination are presented for Chamber 1 during May and July 2001 (Figures 4.13 and 4.14). For each panel in Figures 4.13 and 4.14, predicted discrimination are presented alongside uncorrected estimates of discrimination Δ_s and Δ_{obs} . This illustrates the changes caused by each individual correction relative to the most commonly implemented model.

Correcting discrimination for the effects of $0.5v_o$ typically decreased predicted discrimination values by about 0.5‰ . The impact of this correction increased throughout the morning, was largest at midday and decreased in the afternoon with Q and T_a changes. This change caused differences between observed and predicted

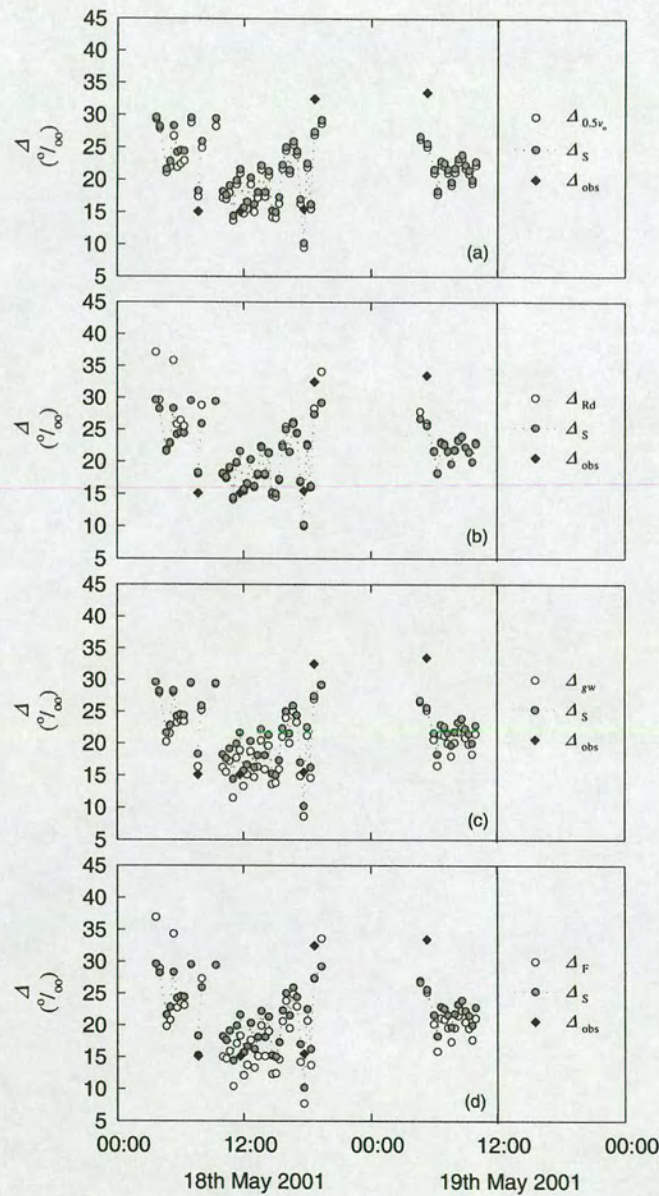


Figure 4.13 Daily variation in net observed instantaneous discrimination, Δ_{obs} (\blacklozenge) and the simple C_i/C_a model, Δ_s (\bullet) plotted against (a) the photorespiration corrected model, $\Delta_{0.5v_o}$ (\circ) (b) the day respiration corrected model, Δ_{Rd} (\circ) (c) the mesophyll conductance corrected model Δ_{gw} (\circ) and (d) a model incorporating all of the above processes, the full model, Δ_F (\circ) for Chamber 1 during 18th/19th May 2001. Data collected by L. Wingate (University of Edinburgh and U.Seibt (Max Planck Institute for Biogeochemistry).

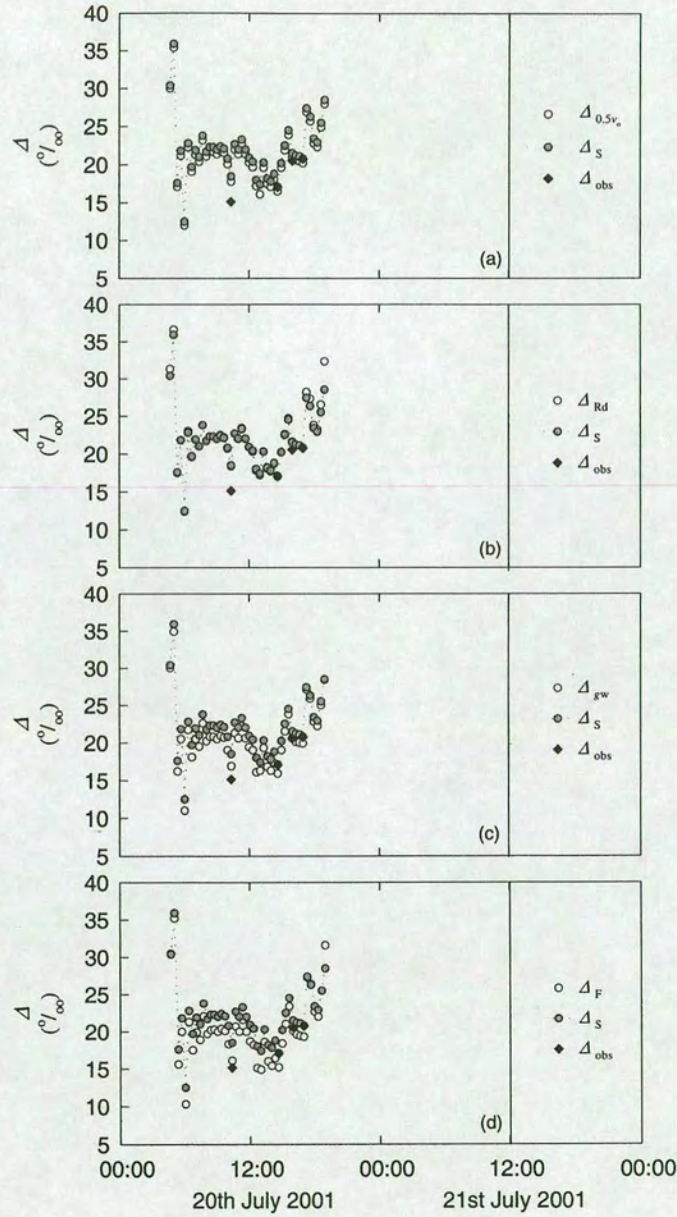


Figure 4.14 Daily variation in net observed instantaneous discrimination, Δ_{obs} (◆) and the simple C_i/C_a model, Δ_s (●) plotted against (a) the photorespiration corrected model, $\Delta_{0.5v_e}$ (○) (b) the day respiration corrected model, Δ_{Rd} (○) (c) the mesophyll conductance corrected model Δ_{gw} (○) and (d) a model incorporating all of the above processes, the full model, Δ_F (○) for Chamber 1 during 20th July 2001. Data collected by L. Wingate (University of Edinburgh) and U. Seibt (Max Planck Institute for Biogeochemistry).

discrimination to increase during the dusk and dawn periods indicated by the arrows but decrease during the midday period Figures 4.13a and 4.14a.

The impact of correcting discrimination for R_d during the majority of the day was minimal, when rates of dark respiration were small and when e^* values were close to zero. However, at dawn and dusk when R_d values were large relative to v_c and when e^* values were most negative, the largest differences between the simple and corrected predictions were observed. R_d corrected discrimination increased values by up to 10 ‰ relative to uncorrected predictions during these periods (Figures 4.13b and 4.14b). Incorporating the correction for R_d did not fully account for the highest values of discrimination during dawn and dusk.

Including the effects of fractionation during the transfer of CO_2 to the sites of carboxylation caused decreases in predicted discrimination relative to the simple model estimates (Figures 4.13c and 4.14c). The decrease in discrimination was typically 1 to 2 ‰ and varied over the day with A . Model results including the corrections for all the above processes are also shown in Figures 4.13d and 4.14d.

Validating theoretical models of discrimination against $^{13}\text{CO}_2$

Agreement between Δ_{obs} and predicted discrimination estimates described above are examined in Table 4.2. Linear regression between predicted and observed discrimination was performed initially including all data and then again with three points excluded when technical problems occurred with the continuous branch gas exchange system as highlighted in Figures 4.3a and 4.15. The regression analysis indicated that more observed variation was described by the corrected models in the following order, $\Delta_F > \Delta_{\text{gw}} = \Delta_{\text{Rd}} > \Delta_{0.5v_o} > \Delta_s$. This analysis indicates that a combination of corrections, Δ_F , that incorporate dark respiration during periods of

	Δ_{pred} vs Δ_{obs}	b $\pm 1\text{SD}$	Intercept $\pm 1\text{SD}$	r^2	n	P
May/July All data	Δ_{S} vs Δ_{obs}	1.0 ± 0.3	-0.7 ± 6.3	0.39	22	0.001
	$\Delta_{0.5\text{vo}}$ vs Δ_{obs}	1.0 ± 0.3	0.0 ± 6.0	0.40	22	0.001
	Δ_{Rd} vs Δ_{obs}	0.7 ± 0.2	5.8 ± 5.1	0.33	22	0.003
	Δ_{gw} vs Δ_{obs}	1.0 ± 0.2	1.9 ± 5.3	0.42	22	0.001
	Δ_{F} vs Δ_{obs}	0.6 ± 0.2	-8.8 ± 4.7	0.29	22	0.006
May/July 3 points removed	Δ_{S} vs Δ_{obs}	1.4 ± 0.3	-8.1 ± 6.3	0.56	19	<0.000
	$\Delta_{0.5\text{vo}}$ vs Δ_{obs}	1.4 ± 0.3	-7.0 ± 5.9	0.58	19	<0.000
	Δ_{Rd} vs Δ_{obs}	1.1 ± 0.2	-2.2 ± 4.4	0.63	19	<0.000
	Δ_{gw} vs Δ_{obs}	1.2 ± 0.2	-4.3 ± 4.8	0.63	19	<0.000
	Δ_{F} vs Δ_{obs}	1.1 ± 0.2	-0.4 ± 3.9	0.65	19	<0.000

Table 4.2 Linear regression parameters between predicted and observed discrimination for all branch chambers during May and July 2001 and with three points affected by technical problems removed. The three points removed are shown below in Figure 4.15.

low A and mesophyll conductance during periods of high A increase the overall agreement between modelled and observed results (Table 4.2 and Figure 4.15).

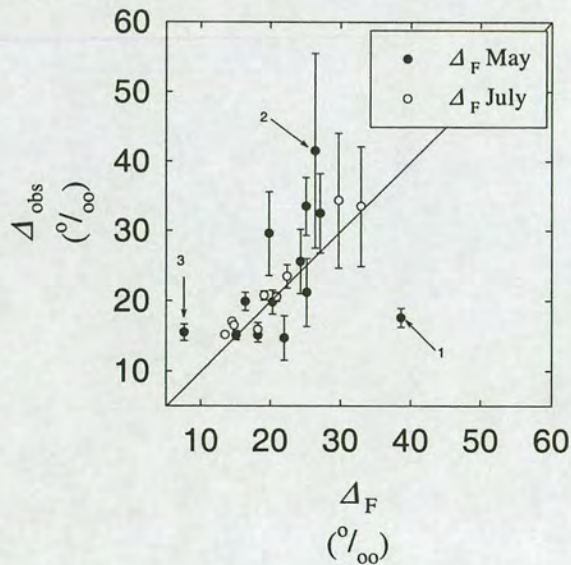


Figure 4.15 Relationship between predicted Δ_{F} and observed discrimination Δ_{obs} for all branch chambers during May and July 2001. Arrows indicate the three points removed during regression analysis due to technical problems encountered during field measurement. Data collected by L. Wingate (University of Edinburgh) and U. Seibt (Max Planck Institute for Biogeochemistry).

4.1.6 Modelling the diurnal variation of $\delta^{13}\text{C}$ composition in needle substrate pools

Because time lags between the assimilation of organic substrate and its use in respiration were unknown, variable daily average turnover times of needle carbohydrate pools were explored shown in Figure 4.16. Leaf carbohydrate turnover is a complex balance between the supply of carbohydrates via A and the demands for carbohydrates in both respiration and export out of the needles to other areas (i.e., buds, stems and roots) of the plant for maintenance or structural development. Daily integrated estimates of A were used to constrain estimates of CO_2 supply to the needle carbohydrate pool, and were used to calculate pool turnover times and isotopic mixing. Needle soluble carbohydrates constitute a small fraction of total needle mass in *P.sitchensis*, usually around 7% of dry weight, however this tends to vary with needle cohorts i.e., an age effect. Measurements of specific needle area for the sampled trees ranged from 30 to 50 $\text{cm}^2 \text{g}^{-1}$ across needle cohorts and constituted a carbohydrate pool of approximately 0.5 and 0.6 mol C m^{-2} for the top and middle chambers, respectively. Estimated daily A of 0.2 to 0.3 $\text{mol C m}^{-2} \text{d}^{-1}$, lead to a mean turnover time of approximately two days. If this were the case then the $\delta^{13}\text{C}$ of dark respired CO_2 would reflect the assimilation-weighted discrimination from more than one diurnal cycle. Therefore to develop understanding of the links and controls between instantaneous discrimination, substrate pools and $\delta^{13}\text{C}$ of respiration in the field, future studies will need to monitor environmental and gas exchange data from a number of days prior to instantaneous discrimination observations.

Continuous estimates of v_c , $0.5v_o$, R_d and C_i/C_a were combined with discrimination estimates, predicted using the full formulation. These values were then used to simulate the isotopic composition of daytime dark respiration i.e., δ_{plant} . Using Eq 3.25 and incorporating different turnover times for needle substrate pools, δ_{plant} was then predicted for the diurnal cycle and results are presented in Figure 4.16.

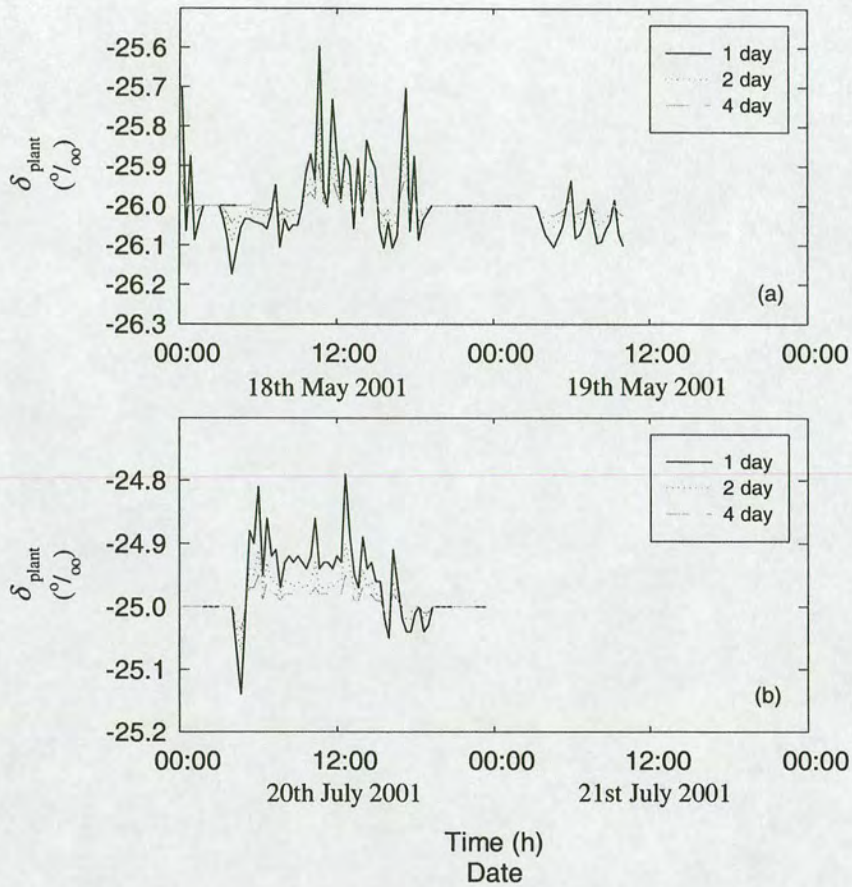


Figure 4.16 Daily variation in the $\delta^{13}\text{C}$ of soluble needle carbohydrates, δ_{plant} , predicted from fully corrected discrimination and $\delta^{13}\text{C}$ of daytime dark respiration in steady state, assuming a 1, 2 or 4 day turnover time of the carbohydrate pool for Chamber 1 during May and July 2001.

Needle carbohydrate pool sizes were explored by assigning values half or double the estimated turnover time described above. This corresponded to needle carbohydrate pool sizes of 0.25 and 1 mol C m⁻² and calculated turnover times for carbohydrate pools of one and four days, respectively. The magnitude of variation in δ_{plant} over the daily cycle was dependent on the pool size, with the largest pools displaying the smallest amplitude and smaller pools exhibiting the largest amplitude. Between

night variation (data not shown) resulted in shifts of $\delta^{13}\text{C}$ of recently assimilated carbohydrates of 0.6 ‰ assuming a 2 day turnover time, 1.1 ‰ for a 1 day turnover time and 0.3 ‰ for a 4 day turnover time. It is acknowledged that any fractionation during dark respiration in addition to the apparent fractionation factor would alter predictions, however, it was impossible to determine any fractionation given the uncertainties in measurements of Δ_{obs} and δ_{B} in the field, especially when fluxes are low at night.

Table 4.3 synthesises all methods employed to examine links between instantaneous and integrated estimates of the carbon isotope composition of bulk plant material (δ_{needle} and δ_{wood}) and recently assimilated plant organic material (δ_{D}).

Sampling Campaign	Bulk Needle δ_{needle} ‰	Bulk Wood δ_{wood} ‰	Nocturnal Dark Respiration $\delta_{\text{B}} = \delta_{\text{plant}}$ ‰	δ_{D} using $\int \Delta_{\text{S}}$ ‰	δ_{D} using $\int \Delta_{0.5\text{vo}}$ ‰	δ_{D} using $\int \Delta_{\text{gw}}$ ‰	δ_{D} using $\int \Delta_{\text{F}}$ ‰
May			-27.7	-29.0	-28.4	-27.3	-26.9
Upper (1)	-29.0	-27.7	± 4.4				
May	± 0.1	± 0.2	-27.4	-32.9	-32.3	-32.2	-31.7
Upper (3)	(4)	(4)	± 5.5				
May	-30.1	-	-26.1	-32.3	-31.7	-30.7	-30.2
Middle (4)	± 0.3 (4)		± 12.3				
May	-31.1	-30.4	-	-	-	-	-
Lower	± 0.1 (4)	± 0.0 (2)					
July			-25.7	-27.7	-27.1	-26.0	-25.4
Upper (1)	-29.0	-27.7	± 7.2				
July	$\pm 0.1^*$	$\pm 0.2^*$	-	-28.4	-27.7	-26.3	-25.6
Upper (3)							

Table 4.3 Measured carbon isotope composition of bulk needle and shoot wood, $\delta^{13}\text{C}_{\text{needle}}$ and $\delta^{13}\text{C}_{\text{wood}}$, nocturnal branch respiration δ_{B} estimated from mass balance (Eq 3.14), and diurnal integrals of newly assimilated material δ_{D} obtained from integrated photosynthetic discrimination, weighted by assimilation rates for each branch using the simple formulation, $\int \Delta_{\text{S}}$, correcting for photorespiration, $\int \Delta_{0.5\text{vo}}$, mesophyll conductance, $\int \Delta_{\text{gw}}$, and the full formulation incorporating photorespiration, day respiration and mesophyll conductance corrections $\int \Delta_{\text{F}}$ (Eq 3.21). (* values assumed equal to May data). Data collected by L. Wingate (University of Edinburgh) and U. Seibt (Max Planck Institute for Biogeochemistry).

The δ_B for individual branches were calculated using the mass balance method described in Eq 3.14. Because of low flux rates at night uncertainties in δ_B were large, especially for estimates made in Chamber 4 during May 2001. A further uncertainty when comparing values in Table 4.3 was introduced by the necessary assumption that the $\delta^{13}\text{C}$ of bulk material measured in May was representative for July. The main component of bulk material is represented by structural carbon which contains a $\delta^{13}\text{C}$ considered to be relatively stable over longer time-scales and unlikely to undergo major transformations under such short periods of 2 months. However, some studies have shown annual variation in the $\delta^{13}\text{C}$ of current year needles through developmental and environmental variations (Jäggi *et al.*, 2002). Given the bulk material was a pooled sample containing needles from all cohorts, it is likely that the addition of current needles and shoot wood in July to the pooled samples would slightly enrich the overall $\delta^{13}\text{C}$ for bulk material relative to May based on gradients found for age and 'sun'/'shade' morphology (Broadmeadow & Griffiths, 1993; Heaton & Crossley, 1995; Heaton, 1999). During May the gradient in $\delta^{13}\text{C}$ of bulk needle material with height was calculated by linear regression and was observed to increase by 0.5 ‰ for every metre down the canopy profile (Figure 4.17). The regression equation was $\delta_{\text{needle}} = -33.7 (\pm 0.3) + 0.5 (\pm 0.04) \text{ Tree Height}$ ($r^2 = 0.90$, $n = 17$, $P < 0.0001$). The $\delta^{13}\text{C}$ of bulk twig material, δ_{wood} , was typically enriched by 1 ‰ relative to δ_{needle} , but this did not represent a significant difference at the 5% level. These values were also similar to values of $\delta^{13}\text{C}$ in bulk material collected during September, 2000 (data not shown).

Values for δ_{needle} were always depleted in ^{13}C with respect to the $\delta^{13}\text{C}$ of nocturnal respiration, δ_B and the $\delta^{13}\text{C}$ of recently assimilated substrate, δ_D calculated using the daily integrals of discrimination predicted using different correction procedures for similar branches. Values for δ_D agreed with δ_B estimates better than with δ_{needle} . This would confirm the use of recently fixed labile assimilates as the substrate for

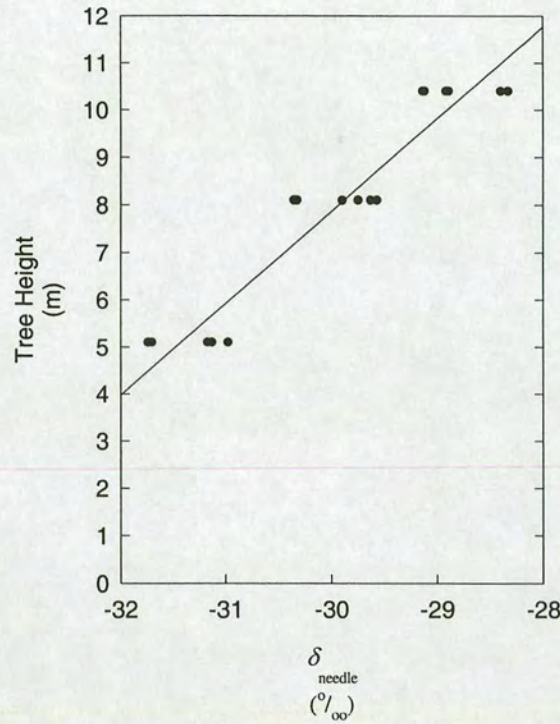


Figure 4.17 $\delta^{13}\text{C}$ variations with height for the needles of four 18-year-old Sitka spruce trees growing in Griffin Forest. Each point represents a sample of pooled needles from four different trees and three needle age classes.

nocturnal respiration and not structural carbohydrates and further indicates that if fractionation during dark respiration does occur its impact on δ_{B} may be minimal compared to fluctuations in the labile carbohydrate pool over time. Variation in δ_{B} between the simple model and the fully corrected model of discrimination, was in the region of 1.2 to 2.8 ‰ for different branches and field campaigns. This had the effect of enriching values of δ_{B} in ^{13}C and predicting estimates from the full model closer to δ_{B} values than the simple model. The simple model tended to predict values more depleted in ^{13}C , thereby making them closer to δ_{needle} . The effect of correcting instantaneous discrimination for photorespiration and mesophyll conductance enriched δ_{B} in ^{13}C relative to the simple model predictions by 0.5 to 1.5 ‰, thereby

also making δ_D estimates closer to δ_B . Correcting for daytime dark respiration is not presented in Table 4.3 as this did not affect daily integrated discrimination values as they were implicitly calculated in or close to, dynamic equilibrium with discrimination over the daily cycle (see Appendix II).

4.2 DISCUSSION

4.2.1 *Branch gas exchange*

Assimilation, stomatal conductance and C_i/C_a

Comparison of data presented above with previous studies of shoot CO_2 exchange, made on the same species may not be entirely appropriate. The enclosure of whole branches of species such as Sitka spruce, provides an estimation of the integrated gas exchange of different aged needle cohorts and both photosynthetic and non-photosynthetic woody material present. It has been shown there are systematic differences in the gas exchange capacity of differing needle age classes for Sitka spruce (Ludlow & Jarvis, 1971; Watts, Neilson & Jarvis, 1976; Leverenz *et al.*, 1982; Barton, 1997). This age effect in photosynthetic capacity is thought to result from higher stomatal resistances which may result from reduced stomatal reactivity, accumulation of wax tubes inside the stomatal ante-chamber and/or, the degradation of stomatal surfaces caused by the colonisation of microflora over the stomatal aperture (Jeffree *et al.*, 1971; Ludlow & Jarvis, 1971). Additionally, the redistribution of chlorophyll and macro-nutrients such as N to younger shoots, and phloem degradation, may also contribute to this effect (Barton, 1997).

Maximum photosynthetic rates over the development period vary for differing age-classes. Barton (1997) found that early in the growing season (May/June), average assimilation rates measured under natural conditions ($Q > 300 \mu\text{mol m}^{-2} \text{s}^{-1}$, leaf

temperature 20 °C) for one-year-old needles are higher than current year needles, (8 and 3 (average 5.5) $\mu\text{mol m}^{-2} \text{s}^{-1}$, respectively). Later in the growing season, current year assimilation rates rose above that for one-year-old needles, (to 7 and 5 (average 6) $\mu\text{mol m}^{-2} \text{s}^{-1}$, respectively). This seasonal and needle age effect on assimilation rate was also observed for Sitka spruce in a further study by Neilson *et al.*, (1972). Rates of assimilation observed during this study were comparable with those rates observed under natural conditions in the Barton study, with assimilation rates of between 4 to 6 $\mu\text{mol m}^{-2} \text{s}^{-1}$ over a Q range of 200–300 $\mu\text{mol m}^{-2} \text{s}^{-1}$ and leaf temperature *ca.* 15 °C. Despite the changes in photosynthetic capacity for different needle cohorts over the growing season, the integrated branch assimilation rates were unaltered and similar to the average assimilation rates observed in previous studies across needle-age. The above results indicate that on a projected leaf area basis branch assimilation rates tend to be seasonally conserved particularly in the upper canopy, despite changes in needle demography.

The maximum transpiration rates, and calculated conductances, measured in this study were also similar to others (Watts, Neilson & Jarvis, 1976; Leverenz *et al.*, 1982; Sandford & Jarvis, 1986; Barton, 1997). Stomatal conductance is also subject to needle age influences as mentioned previously. Leverenz *et al.*, (1982) found a systematic decrease in stomatal conductance with shoot age. Values reported for stomatal conductance were 175, 84 and 54 $\text{mmol m}^{-2} \text{s}^{-1}$, for needles of one, two and three-years-old, respectively. Values found in this study were between 20 and 100 $\text{mmol m}^{-2} \text{s}^{-1}$ over the diurnal period for both campaigns. As is the case for assimilation, the branches in this study contained a maximum of three age classes, with each age class conducting water and CO₂ at different rates. Thus, the integrated stomatal conductances observed in this study are comparable to the average conductance of 104 $\text{mmol m}^{-2} \text{s}^{-1}$ observed by Leverenz *et al.*, (1982). Despite the inability of the branch gas exchange method to resolve details in the specific capacity

of individual needle classes, it provides information that better represents the characteristics of a canopy containing multiple age-classes of needles, without a need for repeated shoot-scale measurements and additional scaling complexity.

C_i/C_a remained relatively stable over most of the day, because of coupled variation in A and g_s . The C_i/C_a ratios observed in the field were consistent with other published values for Sitka spruce using gas exchange methods. Barton (1997) also found C_i/C_a to be conservative in needles over a growing season and different CO_2 concentration treatments, with values ranging between 0.6-0.8 for current year needles and 0.65-0.8 for one-year old needles. In this study, during daylight values ranged between 0.4 to 0.9 during May for different chambers and 0.4 to 0.7 for July, values that are also similar in range to other published studies on Sitka spruce (Fan *et al.*, 1999; Silim *et al.*, 2001). Thus, I find that the Wong *et al.*, (1979) theory holds over the majority of the day except during the early morning period and late afternoon. When carboxylation is light-limited, rapid changes in C_i occurred as Q increased. At these times stomatal regulation was slower to respond, so that variations in C_i/C_a were observed (Figure 4.3 and 4.4). Around midday, g_s seemed to limit variation in C_i/C_a considerably, under changing assimilation rates. Later in the afternoon, changes in Q caused changes in carboxylation that could not be buffered by g_s . Thus in these conditions appreciable variations in C_i/C_a were observed and the Wong *et al.*, (1979) theory did not hold.

Modelled Component Fluxes

Before discussion of the modelled results, it is necessary to acknowledge some necessary assumptions made during this modelling exercise. It was assumed in this analysis that the branch represented a big leaf, despite the obvious inclusion of non-photosynthetic woody material. Pole-stage Sitka spruce possesses photosynthetic bark, around shoots, branches and the bole. In this and other species, the process of

corticular photosynthesis has been observed and is termed 're-fixation' (Ludlow & Jarvis, 1971; Schaedle, 1975; Levy & Jarvis, 1998; Cernusak & Marshall, 2000). This phenomenon in young trees is likely to be a means of improving their carbon balance with the advantages of very little water loss. Observations have shown corticular photosynthesis in Sitka spruce can maintain a neutral carbon balance over the natural range of Q (Ludlow & Jarvis, 1971). Furthermore, day respiration from photosynthetic bark is also assumed to become inhibited in the light. Therefore, the contribution of woody tissue photosynthesis and respiration to the integrated net CO_2 exchange and isotopic composition observed is likely to be negligible.

Datasets for respiration during the day, incorporating the interactions of both Q and T are rare. This is perhaps the reason why few studies attempt to partition the net CO_2 exchange observed *in situ*. In a study investigating the effects of oxygen of CO_2 exchange and stomatal resistance in Sitka spruce, Cornic & Jarvis, (1972) found evidence for reduced rates of daytime dark respiration. They observed a decline in CO_2 efflux by $\approx 85\%$, relative to dark respiration values at the same temperature and O_2 concentration from needles as irradiance increased. This observation in Sitka spruce could not be attributed to changes in either photorespiration or stomatal resistance. Thus they concluded inhibition of dark respiration in the light was the likely cause. Unfortunately, this experiment has not been repeated on Sitka spruce since to establish interactions between the rate of dark respiration in the light and other environmental variables. Thus it was necessary to make use of the best available dataset, which in this case was a study on the broadleaf species, *Eucalyptus pauciflora* Sieb. ex Spreng (Atkin *et al.*, 2000a). This particular study and others (Hurry *et al.*, 1996; Parnik *et al.*, 1988) demonstrated that leaf respiration is inhibited in the light and highly variable, being dependent on both irradiance and temperature. In contrast, Brooks and Farquhar (1985) reported that the degree of inhibition at a constant irradiance did not vary with temperature for spinach. Kirschbaum & Farquhar (1984) reported that light inhibited leaf respiration by a constant 40% in

controlled-environment-grown *E. pauciflora*, when measured across a temperature range of 15 °C to 35 °C. Consequently, there is still some uncertainty surrounding the effect of temperature in different species and with different experimental protocols. In this study, we assume the empirical relationships described by Atkin *et al* (2000a) to estimate the rates of non-photorespiratory respiration *in situ*, over a broad range of irradiance and temperature (see Section 3.4.1 and Figure 3.5).

Lastly, the component fluxes of carboxylation and photorespiration are mechanistically modelled using the method of Farquhar & von Caemmerer (1982) shown in Eqns 3.6 and 3.7. Estimates of these fluxes rely heavily on good measurements of A and C_i . They also require estimates for R_d as calculated above and estimates of Γ_* (something not measured during this study). Estimates of Γ_* have been modelled using the empirical relationship of Γ_* with temperature initially found by Jordan & Ogren (1984). This relationship with temperature (Eqn 3.4) was subsequently found in other studies, using different methods (Brooks & Farquhar, 1985; von Caemmerer *et al.*, 1994; Westbeek *et al.*, 1999; Atkin, 2000a). Despite the empirical nature of this model, it describes the observed parameter well. Moreover, Γ_* appears to be invariant across species and plant functional type (von Caemmerer *et al.*, 1994; Villar *et al.*, 1994; Brooks & Farquhar, 1985; Balaguer *et al.*, 1996; Westbeek *et al.*, 1999). In this study it has been assumed Γ_* follows the empirical relationship described in Eqn 2.4.

Differences between the two field campaigns for nocturnal respiration values, R_n , indicated a large influence of branch development on branch CO_2 efflux. Values for the parameter R_{20} during May were almost double that observed in July. Consequently, it is difficult to compare values of R_n measured in May to other estimates published for Sitka spruce, as the data would also need to reflect the change in R_n , during this shoot development phase. During the onset of bud-burst and

during shoot elongation, increases in the contribution of growth respiration are expected. During growth total respiration rates can be three to ten times higher than maintenance respiration rates (Larcher, 1995). Over the growing season, growth respiration ceases and rates of respiration drop to levels necessary for maintenance. Diurnal and seasonal acclimation of maintenance respiration has also been documented, in response to photosynthetic capacity and temperature (Atkin *et al.*, 2000b). Acclimation to temperature can occur within one day, in response to constantly changing weather, both in winter and summer (Billings *et al.*, 1971; *et al.*, 2000b), but, the mechanisms responsible for respiratory acclimation are presently unclear (Billings *et al.*, 1971; Atkin *et al.*, 2000b). Respiration in the light and dark is found to adjust faster to a new temperature regime than does photosynthesis (Zelawski & Kucharska, 1967; Rook, 1969; Pharos *et al.*, 1972; Neilson *et al.*, 1972).

Measured nocturnal respiration rates during July can be compared to previous studies that have measured R_n as there is more seasonal data available for outside the period of bud burst. Barton (1997) found respiration rates of 1 to 0.6 $\mu\text{mol m}^{-2} \text{s}^{-1}$, during August and September, respectively. These values were obtained during the day on pre-darkened shoots at 24 – 26 °C. Values of respiration rates during the night were also obtained during September and were $0.82 \pm 1.75 \mu\text{mol m}^{-2} \text{s}^{-1}$ at 16 °C. Values for R_n obtained in this study were comparable at 1.2 to 1.4 $\mu\text{mol m}^{-2} \text{s}^{-1}$ at 20 °C (Table 4.1). As discussed earlier some variation is expected over the course of the growing season through acclimation response, but values in this study are also an integrated rate representing different age classes of foliage and woody tissue. Other studies, e.g., Leverenz & Jarvis, (1979, 1980), found comparable values for R_n over different light treatments at around 0.6 $\mu\text{mol m}^{-2} \text{s}^{-1}$ @ 18.5°C (1980) and maximum rates of 2.5 $\mu\text{mol m}^{-2} \text{s}^{-1}$ at 15 °C in another study (1979). There are also some data available during the period after bud-burst in the study by Ludlow & Jarvis, (1971)

where values for R_n ranged from 1.7 in early June, 0.8 in mid June and $0.6 \mu\text{mol m}^{-2} \text{s}^{-1}$ at the end of September.

Estimates of modelled R_d were maximum when temperatures were moderate to high ($10^\circ\text{C} >$) and when Q was greatest. Rates of R_d were lowest when Q was greatest and temperatures were low. Had Q levels increased above those observed in concert with leaf temperatures, the degree of inhibition would have increased as predicted from the Atkin parameters. It has been argued that the inactivation of key enzymes during extreme T and Q are responsible for R_d inhibition (Budde & Randall, 1987, 1990; Hill & Bryce, 1992; Atkin *et al.*, 1998, 2000). In darkness and during low temperatures, rates of carbon input into the mitochondria are thought to be responsible for reduced values of R_n . An alternative, or additional, process responsible for reduced R_n , is the increased adenylate control of mitochondrial electron transport (because of reduced demand for adenosine triphosphate (ATP) at low temperatures (Atkin *et al.*, 2000a). Reduction in the activity of key enzymes that control substrate input into the mitochondria, such as pyruvate dehydrogenase complex (PDC) and NAD^+ -malic enzyme (ME), is likely to occur at low temperatures. Reduction in the activity of PDC and ME may explain why R_n is inhibited by low Q at all temperatures, as both are rapidly inactivated by light (Budde & Randall, 1990; Hill & Bryce, 1992). Atkin *et al.*, (1998) found that the time taken for inhibition by Q reflected the timing of inactivation observed for ME and PDC (Budde & Randall, 1987).

The difference in Q -inhibited and non-inhibited rates of mitochondrial respiration are considerable. For instance, during this study rates of R_d were between 0.9 and 2 for all chambers and $0.6 \mu\text{mol m}^{-2} \text{s}^{-1}$ for July. Rates of carboxylation were typically 8 to $10 \mu\text{mol m}^{-2} \text{s}^{-1}$ in May and 5 to $8 \mu\text{mol m}^{-2} \text{s}^{-1}$ during July. This loss of CO_2 through R_d represented 10-20% of gross CO_2 uptake during May and *ca.* 13% during July. If

in this study I had assumed no inhibition of daytime respiration, R_n , then maximum respiration rates during the day would increase to between 1.5 to 6 $\mu\text{mol m}^{-2} \text{s}^{-1}$ during May and 1 $\mu\text{mol m}^{-2} \text{s}^{-1}$ during July. Thus R_d were approximately 35 to 65% lower than R_n during May across all chambers and 40% lower during July. Unfortunately, we have no field or species-specific data to corroborate these modelled losses but perhaps future studies should be made to validate this modelled interaction of light and temperature on R_d for Sitka spruce.

4.2.2 *Flask method for stable isotope collection*

The method developed in this study to measure discrimination against $^{13}\text{CO}_2$, adopted the principles from laboratory studies of isotope fractionation that utilise closed chambers (O'Leary *et al.*, 1986; Rooney, 1998; Guy *et al.*, 1989; Robinson *et al.*, 1992; Henry *et al.*, 1999). The most popular method used to date in the observation of instantaneous Δ and concurrent gas exchange, consists of a normal through-flow gas exchange apparatus connected to a vacuum line, so that CO_2 exiting the leaf chamber can be collected, purified and isotopically analysed (Sharkey & Berry, 1985; Evans *et al.*, 1986). Typically the use of these systems has been confined to laboratory experiments. However, an *in situ* study adopted this method and adapted it to collect and equilibrate $\delta\text{H}_2^{18}\text{O}$ samples, at the same time as $\delta^{13}\text{C}^{18}\text{O}^{16}\text{O}$ samples (Harwood *et al.*, 1998). The method developed in this study has several advantages over the Harwood *et al.*, (1998) study including, differences in chamber volume, speed of sampling, automated gas exchange measurements, and reduced power, vacuum and cryogenic demands. Because the chamber volume in this study was relatively large in comparison to prior studies (*ca.* 200 x larger), any effects of leaks in the system were negligible and isotopic contamination was thereby minimised. The use of large chambers also had the advantage that more biomass could be accommodated inside. Large amounts of biomass, ensured large fluxes of

CO₂, necessary for the observation of isotopic change (Table 3.2 and Figure 4.8). As the time taken for large shifts in CO₂ mole fraction and isotope ratio was reduced, sampling could be rapid, minimising any physiological feedback effects. Furthermore, because of the large CO₂ concentration changes this method can also be used to monitor other important trace gases, e.g. O₂/N₂, and the oxygen isotope ratios of CO₂ and O₂.

4.2.3 Field observed instantaneous net discrimination against ¹³CO₂

Measured values of Δ_{obs} in Sitka spruce are within reported values for Δ_{obs} , in other published studies measuring at the leaf scale *in situ*. Harwood *et al.*, (1998) observed significant shifts in Δ_{obs} between 5 - 48 ‰ over a diurnal time-course for the species *Piper aduncum* in a tropical forest of Trinidad. Despite obvious differences in ecosystem and plant type a similar pattern was observed between Δ_{obs} and environmental variables over the day in the present study. Harwood (1996) also measured Δ_{obs} within a *Quercus petraea* canopy in Northumberland, UK, during 15th to 21st July 1995. Mean Δ_{obs} of 13.8, 17.4 and 12.5 ‰ were found at 1.5, 6.5 and 10 m height in the canopy, respectively, during exposure to low Q conditions $\approx 400 \mu\text{mol m}^{-2} \text{s}^{-1}$. Rates of mean Δ_{obs} typically increased at the same heights when exposed to higher $Q \approx 800 \mu\text{mol m}^{-2} \text{s}^{-1}$ with values of 17.1, 17.9 and 13.4 ‰ observed for 1.5, 6.5 and 10 m height in the canopy, respectively.

Harwood *et al.*, (1998) observed some very extreme values in the tropical forest for Δ_{obs} post dawn and over the midday period despite relatively conservative C_i/C_a . Comparison of these data with the simple Farquhar model highlighted a substantial discrepancy. As demonstrated by Eq 3.16, for the given range in C_i/C_a reported (0.6 – 0.8), Δ_{obs} would be expected to vary between 19 to 25 ‰ only and not 5 to 48 ‰ (assuming $b = 30\text{‰}$). One explanation for this discrepancy was explored using the

deviations between Δ_{obs} and predicted discrimination using the simple model (Δ_{S}). As already discussed above this would indicate the additional fractionation associated with the CO_2 transfer conductance from the leaf intercellular spaces to the chloroplast, g_{w} (Evans *et al.*, 1986; von Caemmerer & Evans, 1991; Lloyd *et al.*, 1992). However, the expected shift in Δ after accounting for g_{w} in *P. aduncum* was only 2 ‰, similar to the values reported for the present study. Thus additional processes were causing this large range of Δ_{obs} . The present study indicates that Δ_{obs} values reported by Harwood *et al.*, (1998) were most likely to have been caused by relatively large contributions of daytime dark respiration during the post dawn period, similar to results presented in Figures 4.13b and 4.14b.

However, as described in the method and results section, it is desirable when calculating mesophyll conductance in the field that the contribution of respiration on the predicted discrimination is included, thus constraining estimates of mesophyll conductance further, i.e., looking at the difference between $\Delta_{\text{R}} - \Delta_{\text{obs}}$ and not $\Delta_{\text{S}} - \Delta_{\text{obs}}$ as calculated by Harwood *et al.*, (1998). In the original equation (see Evans and Von Caemmerer, 1996), respiratory contributions are reflected in the intercept of the regression between $(\Delta_{\text{S}} - \Delta_{\text{obs}})$ vs A/C_{a} . This is only the case if respiratory contributions are constant over the full range of A/C_{a} , which can be assumed for photorespiration, but results obtained in this study suggest that this is unlikely to be the case for daytime dark respiration. However, differences in simple uncorrected and dark respiration corrected predictions were small, as corrections had most impact when A/C_{a} was not significantly different from zero, excluded from the regression analysis (Table 4.3 and Figure 4.15). The low values of discrimination in the afternoons observed by Harwood *et al.*, (1998) indicate the additional contributions of photorespiration and mesophyll conductance during this period. As demonstrated by Figures 4.13a/c and 4.14a/c, at these times of the day Δ_{S} tends to over-estimate instantaneous discrimination. Including the 2 ‰ shift calculated for g_{w} and including

a 0.5 to 1.5 ‰ shift for photorespiration, predictions of Δ_{obs} using C_i/C_a may have been improved substantially.

Discrepancies between Δ_{obs} measured in the field and predictions based on the simple C_i/C_a model were also observed during the study on *Q. petraea* (Harwood, 1996). Measurements of C_i/C_a over three heights in the canopy and for different light treatments varied by less than 10%. Using Eq 3.16, Harwood (1996) calculated a very similar Δ_s of ≈ 22.5 ‰ for all heights and *Q* treatments. As described above differences in mean Δ_{obs} varied between 12.5 and 17.9 ‰ over height and *Q*, leading to large differences between $\Delta_s - \Delta_{\text{obs}}$ ranging between 2 and 14 ‰. As Δ_{obs} was always less than Δ_s , it is likely that in this study, mesophyll conductance and photorespiration contributed significantly to Δ_{obs} , based on the analysis of the present study. Estimated g_w for *Q. petraea* for the Harwood (1996) study was appreciable at approximately $0.10 \text{ mol m}^{-2} \text{ s}^{-1}$. This is a much lower value for g_w than observed in the present study but, very similar to estimates derived for other woody species (Lloyd *et al.*, 1992; Loreto *et al.*, 1995). Therefore, the correction for mesophyll conductance in the Harwood (1996) study would be larger than the 2 ‰ estimated for the present study. Correcting Δ_{obs} for photorespiration and daytime dark respiration, estimates of Δ can be made. The values for Δ obtained in this study then become directly comparable to laboratory studies (Evans *et al.*, 1986).

Differences between fully corrected predictions of Δ_F and Δ_{obs} remained during dusk and dawn for a few samples. To account for these discrepancies whilst leaving C_i/C_a unchanged would require rates of daytime dark respiration to equal that of A , corresponding to $>50\%$ of v_c . This would require rates 10 to 20 times that of estimated R_d , a value higher than predicted R_n during the day and measured R_n . An alternative explanation could be actual C_i/C_a were higher than those calculated from continuous gas exchange measurements. If C_i/C_a values at these times were ≈ 0.95 ,

then R_d would only have to be twice that predicted, within the range of measured nocturnal respiration rates. These rates would correspond to 30% of v_c , similar to contributions observed at other times during the study. This indicates C_i/C_a values calculated at dawn and dusk were associated with large uncertainty.

4.2.4 Diurnal variation of needle substrate pool $\delta^{13}C$ composition

A gradient in δ_{needle} and δ_{wood} was found in this study, with bulk material more enriched in ^{13}C at the top of the canopy and becoming progressively depleted in ^{13}C towards the base of the crown (Figure 4.17). This result agrees extremely well with other studies on *P. sitchensis* in plantations within Scotland. Identical gradients of 0.5 ‰ m^{-1} with height were observed for δ_{needle} and δ_{wood} in closed plantation canopies at Penicuik, Edinburgh (Heaton & Crossley, 1995; Heaton, 1999). Similar values in δ_{needle} have been observed for *P. sitchensis* throughout its natural range, along the Pacific Northwest of USA and Canada (Fan *et al.*, 1999; Silim *et al.*, 2001; Bowling *et al.*, 2002) indicating δ_{needle} is fairly conservative within this species. Similar values and patterns for δ_{needle} have been reported for *P. abies* (Gebauer & Schulze, 1991; Broadmeadow & Griffiths, 1993; Högberg *et al.*, 1993; Jäggi *et al.*, 2002) and *P. mariana* (Brooks *et al.*, 1997) in temperate and boreal forests. This gradient occurs primarily because of changes in Q and D_a through the canopy profile and its influence on stomatal conductance and assimilation rates (Francey *et al.*, 1985; Broadmeadow & Griffiths, 1993; Harwood, 1996). However, Berry *et al.*, (1997) and Le Roux *et al.*, (2001) found significant variations in δ_{needle} without any significant variations in δ_a , T_a and D_a within a *Pinus resinosa* forest and within a *Juglans regia* L. crown, respectively. Broadmeadow & Griffiths, (1993) demonstrated on *P. abies* shoots under controlled conditions a negative correlation between instantaneous ^{13}C discrimination and Q under summer and winter conditions. Indirect secondary effects including the re-assimilation of respired CO_2

depleted in ^{13}C are now thought to play a minor role in maintaining this gradient in δ_{needle} (Francey *et al.*, 1985; Broadmeadow & Griffiths, 1993; Lloyd *et al.*, 1996). Another less explored theory is the fractionation associated with foliage senescence, for example during translocation processes (Francey *et al.*, 1985; Andreux *et al.*, 1990; Balesdent *et al.*, 1993; Buchmann *et al.*, 1997a, 1997b).

Observed differences between δ_{needle} and δ_{wood} have been reported for *P. sitchensis*, *P. abies* and Huon pine (Heaton, 1999; Jäggi *et al.*, 2002; Francey *et al.*, 1985). Francey *et al.*, (1985). Francey *et al.*, (1985) hypothesised that current year needle, δ_{needle} , values were ‘anomalous’ as they represent the isotopic composition of carbon fixed by immature tissues when C_i/C_a is high. Subsequently, these tissues mature and attain lower C_i/C_a by which time they begin to export carbon with a less negative composition, more representative of bulk wood and daily integrated discrimination. This hypothesis is partially supported by the present study, whereby predictions of daily integrals for recently fixed assimilates, δ_D , are typically closer to δ_{wood} .

Estimates of daily, and night to night variability in $\delta^{13}\text{C}$ of needle carbohydrates, δ_{plant} , are presented. These estimates were made using the fully coupled model described in Eq 3.25 using uncorrected and corrected predictions of instantaneous ^{13}C discrimination. Over short periods the diurnal variability of δ_{plant} was high and varied substantially between nights. This model could be validated using similar measurements developed in the present study for Δ_{obs} , nocturnal measurements of δ_B and additional direct measurements of the $\delta^{13}\text{C}$ of soluble carbohydrates (Lauteri *et al.*, 1993). This would provide a valuable link between environmental conditions, the composition of needle carbohydrates and changes in the isotopic composition of autotrophic respiration. Ekblad and Högberg (2001) illustrated indirectly the consequences of environmental conditions on the isotopic composition of autotrophic respiration in a *P. abies* and *Pinus sylvestris*, boreal forest. Measuring the variability

in $\delta^{13}\text{C}$ of soil respired CO_2 , δ_s , a correlation was made between δ_s and environmental variables measured four days previously for seasonal observations. Ekblad and Högberg (2001) concluded this provided evidence for a link between changes in photosynthetic discrimination *via* changes in environmental conditions and the isotopic signal of soil respired CO_2 . This has also been observed at the ecosystem scale, with variability in the $\delta^{13}\text{C}$ of ecosystem respired CO_2 also correlated with D_a (Bowling *et al.*, 2002). Therefore, the methods and models developed in the present study, executed over longer periods of time should provide direct evidence of the link between environmental conditions, canopy discrimination and the $\delta^{13}\text{C}$ of ecosystem respired CO_2 .

Table 4.3 highlighted differences in the isotopic composition of δ_B and δ_{needle} and differences between these and instantaneous values of discrimination. This is important because the isotopic composition of bulk leaf material is often used to derive an indirect measurement of C_i/C_a for plants under natural conditions. For example, Flanagan *et al.* (1997), assumed a constant C_i/C_a value from average δ_{needle} to predict canopy photosynthetic ^{18}O discrimination over diurnal cycles. The present study shows firstly that C_i/C_a may not be constant over the day and that δ_{needle} may not provide a reliable estimate of daily and instantaneous ^{13}C discrimination or C_i/C_a . The influence of changes in C_i/C_a on daily patterns of ^{18}O discrimination for the present study site and period are examined in Seibt, 2003.

4.3 CONCLUSIONS

Continuous measurements of branch gas exchange were implemented to characterise daily fluxes of CO_2 and H_2O in a temperate Sitka spruce forest. These data were then analysed to determine the daily variation in contributions of carboxylation, photorespiration and daytime respiration for branches. Furthermore, a method was

developed to monitor daily variations in instantaneous ^{13}C discrimination and branch respired $^{13}\text{CO}_2$. These measurements were then examined against existing theoretical models of photosynthetic ^{13}C discrimination. Predictions of instantaneous discrimination over time were then used to estimate fluctuations in the $\delta^{13}\text{C}$ of needle carbohydrates available for respiration and allocation.

The main conclusions drawn from this analysis were:

- Rates of carboxylation, photorespiration and respiration differed with canopy height becoming lower with depth in the canopy crown.
- Rates of carboxylation, photorespiration and daytime dark respiration differed between campaigns with rates in July lower than May.
- Respiration rates were higher in May than July indicating a significant contribution from growth respiration during bud burst.
- Estimates for Q -inhibited daytime dark respiration rates, R_d , were approximately 35 to 65% lower than estimated non-inhibited daytime dark respiration rates, R_n during May across all chambers and 40% lower during July.
- Predictions of mean branch mesophyll conductance, g_w was $0.29 \text{ mol m}^{-2} \text{ s}^{-1}$, this conductance was very similar to the maximum g_s observed and other published studies.
- It is desirable when calculating and constraining g_w in the field that the contribution of respiratory processes are quantified, and respiration corrected discrimination, Δ_R used instead of Δ_s .

- Including the effects of fractionation during the transfer of CO_2 to the sites of carboxylation caused decreases in predicted discrimination relative to the simple model, especially during the midday period.
- Correcting estimates of discrimination for the effects of photorespiration, $0.5v_o$, typically decreased predicted discrimination values relative to uncorrected values with the largest impact at midday.
- Discrimination corrected for daytime dark respiration typically increased predicted discrimination values relative to uncorrected values during dawn and dusk periods when the correction had the largest impact.
- This analysis indicated a combination of corrections incorporating dark respiration during periods of low A , and mesophyll conductance during periods of high A , increased the overall agreement between modelled and observed Δ .
- A gradient in δ_{needle} and δ_{wood} was found in this study, with bulk material more enriched in ^{13}C at the top of the canopy and becoming progressively depleted in ^{13}C towards the base of the crown.
- The present study showed that C_i/C_a may not be constant over the day and that δ_{needle} may not provide a reliable estimate of daily and instantaneous ^{13}C discrimination or C_i/C_a .
- To develop understanding of the links and controls between instantaneous discrimination, substrate pools and $\delta^{13}\text{C}$ of respiration in the field, it is desirable for future studies to monitor environmental and gas exchange data for a number of days prior to instantaneous discrimination observations.

- Methods and models developed in the present study to observe and predict instantaneous ^{13}C discrimination and the $\delta^{13}\text{C}$ of recently assimilated needle carbohydrates, should provide direct evidence of the link between environmental conditions, canopy discrimination and the $\delta^{13}\text{C}$ of ecosystem respired CO_2 when executed over longer sampling periods.

5. Daily variation of gas exchange and ^{13}C discrimination by a Sitka spruce plantation – Theory and Methods

5.1 INTRODUCTION

The one-way flux of gross photosynthesis typically constitutes the largest flux of carbon between vegetation and the atmosphere (Raich & Schlesinger, 1992). Direct measurement and quantification of this flux is difficult because of the on-going counter flux caused by respiration. Mechanistic models coupled with leaf scale measurements can describe the photosynthetic process in detail and aid in estimating the relative contributions of photosynthesis and respiration at the leaf scale. However, extrapolating relationships beyond the leaf to the forest or global scale can be challenging.

Measurements of the net exchange of CO_2 above forests and over regions reveal how the forest as a whole responds to changes in key environmental variables. Unfortunately, unlike leaf studies it is impractical to control environmental variables by experimental manipulation. However, more recent, large scale experiments are successfully controlling key variables that alter plant canopy function, e.g. Free Air CO_2 Enrichment (FACE) experiments (Hendrey *et al.*, 1999) and soil warming experiments (Bergh *et al.*, 1999). Findings from these studies then feed into current models of functional response of forests to changes in cloud cover, temperature and water availability giving an indication of the likely changes in key processes in future climate. However, these experiments are very ambitious and require the kind of resources unavailable to most. Therefore, the alternative is to observe forests and processes for longer periods of time in their natural environment. This allows the accumulation of large datasets of trace gas exchange under a wide range of weather

conditions, as systems become automated. The current methods used to extract useful information about photosynthesis and respiration at the forest scale consist of either direct measurement within the canopy using chambers and scaling appropriately to the amount of vegetation present in the system, or monitoring the exchange above forests. The latter approach attempts to quantify the flux of CO₂ leaving the system at night through the process of respiration. However, during the night many eddy covariance limitations occur and uncertainties regarding the magnitude of this flux remain. Thus the determination of total ecosystem assimilation and respiration by component summation is important for the independent verification of eddy covariance measurements over forests (Wofsy *et al.*, 1993; Goulden *et al.*, 1996; Lavigne *et al.*, 1997; Lindroth *et al.*, 1998).

More recently, theory, measurements and inverse models developed to monitor the change in ¹³C/¹²C of atmospheric CO₂ have been modified to investigate photosynthetic and respiratory fluxes of CO₂ at the leaf, ecosystem, regional and global scales (Harwood *et al.*, 1998; Lloyd *et al.*, 1996; Yakir & Wang, 1996; Bowling *et al.*, 2001; Francey *et al.*, 1995). Measurements of ¹³C/¹²C ratios in canopy air modified by photosynthetic and respiratory processes can provide independent information on the fluxes, thereby providing further constraints to chamber and eddy covariance methods used to investigate photosynthesis and respiration.

5.2 CHAPTER AIMS

The composite processes governing a forest's carbon balance will be considered in this chapter. Theory and method will be implemented to constrain estimates of photosynthesis and respiration from a Sitka spruce plantation during the summer of 2001.

The specific objectives within this chapter are:

- (i) to characterise the environmental drivers of H_2O and CO_2 exchange in a Sitka spruce plantation during a 5-day period in July 2001;
- (ii) to estimate the contribution of stand transpiration to the net ecosystem exchange of water vapour and to calculate the conductances of CO_2 and H_2O between the plant canopy and the atmosphere;
- (iii) to compare estimates of canopy assimilation (F_A), total ecosystem respiration (F_R) and the net ecosystem exchange (F_E) derived from eddy covariance and chamber methods;
- (iv) to explore some currently implemented protocols for determining F_A and F_R from F_E ;
- (v) to consider the growing evidence for inhibition of respiration at the leaf scale and apply a simple model to explore the effects of inhibition on F_A and F_R at the ecosystem scale;
- (vi) to estimate the contribution of soil CO_2 efflux and branch respiration to F_R ;
- (vii) to estimate the contribution of F_A and F_R using $^{13}\text{C}/^{12}\text{C}$ ratios combined with eddy covariance and chamber methods and compare these with the other two methods used in this study to estimate F_A ;
- (viii) to explore some theoretical assumptions underlying the partitioning of net ecosystem exchange using $^{13}\text{C}/^{12}\text{C}$ ratios, especially with respect to establishing the total canopy conductance to CO_2 ;
- (ix) to estimate the proportion of F_A lost from the system *via* F_R on days with variable weather;
- (x) to compare estimates of instantaneous canopy photosynthetic ^{13}C discrimination (Δ_C) obtained from the partitioning of $F_{E,D}$ to those observed and modelled from branch chamber data and;
- (xi) to explore the differential effects of assimilation and respiration on instantaneous ecosystem ^{13}C discrimination (Δ_E).

5.3 THEORY

5.3.1 Forest CO₂ exchange

Net ecosystem exchange

The flux of CO₂ measured across a plane above a plant canopy is the net result of all CO₂ fluxes occurring within the system. The normal convention in micrometeorology and followed in this chapter is that downward fluxes are negative and upward fluxes positive; hence net uptake from photosynthesis is a negative number during the day and respiration losses at night are positive. The change in the amount of CO₂ stored in the column of air between the system boundaries, $\rho dC/dt$, is treated as either positive if $\rho dC/dt$ increases, or negative if $\rho dC/dt$ decreases. This is commonly referred to as the storage flux of CO₂ and is important when atmospheric stability alters vertical mixing and allows the mean C_a within the system boundaries to change.

Because the flux across the system is the algebraic sum of the fluxes within the system, if we consider instantaneous fluxes within the forest depicted in Figure 1.5, Chapter 1, and assume a one-dimensional, horizontally uniform system then we can write

$$F_E = \overline{\rho w' C_a'} + \rho \frac{d}{dt} \int_0^{z_m} C_a(z) dz = F_A + F_R. \quad (\text{Eq 5.1})$$

Where F_E is the instantaneous net ecosystem exchange of carbon dioxide across a plane above the stand, $\overline{\rho w' C_a'}$ is total CO₂ flux (measured by eddy covariance), the overbar denotes Reynolds averaging, and ρ is air density. The primes denote fluctuations of instantaneous vertical velocity (w) and CO₂ mole fraction (C_a) from the mean vertical velocity ($w' = w - \bar{w}$) and CO₂ concentration ($C_a' = C_a - \bar{C}_a$). The

storage flux, $\rho dC/dt$ referred to previously denotes the time rate of change of CO_2 mole fraction between ground level (0) and the measurement height (z_m).

Canopy assimilation and respiration

The total amount of carbon dioxide assimilated by the vegetation per unit ground area and time, F_A is the sum of the net assimilation fluxes of all the individual leaves of all species, i.e. ,

$$F_A = \sum (A_{l,i} L_i) \quad (\text{Eq 5.2})$$

The total efflux of carbon dioxide from the system, F_R can be expanded to encompass respiring branches (net respiration of leaves and twigs, thereby assumed to represent a big leaf) (R_B) and tree trunks (R_W), plus the respiring roots and microbial activity in the soil (R_S),

$$F_R = R_B + R_W + R_S. \quad (\text{Eq 5.3})$$

The net gain in carbon by the plants comprises the CO_2 assimilated from the atmosphere above and that from microbial respiration in the soil. However, carbon dioxide respired within the system by branches, stems and roots etc. ($R_B + R_W + R_S$) and re-assimilated does not constitute a net gain to the vegetation, but is simply being re-circulated within the system.

At night, when $F_A = 0$, F_E changes direction and becomes a positive flux ($F_{E,N}$), constituting a net loss from the system. This loss should equal the sum of all the respiratory effluxes, including those from the leaves. Hence, the net loss of carbon dioxide becomes

$$F_{E,N} = F_R = R_B + R_W + R_S, \quad (\text{Eq 5.4})$$

$$R_B = \sum (R_{Bi} L_i) \quad (\text{Eq 5.5})$$

where R_B is the respiratory efflux from all branches within the canopy.

Thus, measurement of the net “biotic” CO_2 flux across the upper boundary of the forest (F_E) or summation of the component fluxes (F_A , R_B , R_W and R_S), can theoretically provide the instantaneous net gain or loss of CO_2 by the system.

Presently, methods to partition the net flux into its biotic components and quantify the magnitude and timing of photosynthesis and respiration are controversial. Three ways used to estimate respiration rates, F_R are described in the literature as:

(i) Determining F_R , as the mean value of F_E when $Q = 0$ using eddy covariance. This is then subtracted directly from daytime CO_2 fluxes, so that the Q response curve passes through the origin. For this case, the differences in respiration rate during the night and day, resulting from changes in temperature, have been neglected.

(ii) The relationship between $F_{E,N}$ and air (T_a) or soil (T_s) temperature is modelled and used to estimate the instantaneous F_R during the day for the appropriate temperature. This, however, assumes that leaf mitochondrial respiration rate and stem respiration measured in the dark continue at the same rate in the light for the same temperature. This approach may be an improvement on (i) but still assumes that respiration proceeds using the same pathways during the day and night.

(iii) Lastly, chamber methods have also been used extensively to provide independent estimates of the key components that contribute to F_R . A portion of the vegetation or an area of soil surface is enclosed from the outside environment in a

large chamber like that described in Chapter 3. This provides an estimate of the net flux from that component and can constrain estimates of the terms contained in Eqs 5.3 and 5.4 in the dark. In the light, the terms R_S and R_W can still be constrained as the net flux measured will be dominated by respiration. However, at the branch scale the net flux is dominated by photosynthesis making estimation of R_B a challenge. Consequently, R_B in the light is generally assumed to respond in the same way as observed during the dark.

Application of nocturnal models of respiration to predict daytime gross fluxes.

Are nocturnal models of respiration suitable for daytime estimates? Presently, there are a number of theories and growing experimental evidence to confirm respiratory inhibition processes occur in many different plant functional groups and across many woody species. Theory supporting a reduction in foliage respiration during the day was presented in Chapter 1, 3 and 4. This discussion accompanied modelling results for *P.sitchensis* branches under field conditions using relationships from the literature for another woody species *Eucalyptus pauciflora* as described in Chapter 3 (Atkins *et al.*, 2000a). The results indicate that the contribution from this process if it occurs could reduce the R_B term by as much as 30-60% at the branch scale of the nocturnal rate during the day. If an ecosystems total nocturnal losses (F_R) were composed of a large contribution from foliage and branches this decrease in respiration during the day for that component may be considerable at the canopy scale. For instance pole-stage coniferous forest in temperate regions have displayed very large contributions to total ecosystem respiration from the aboveground biomass. Van Wijk (2001) reports a 70% contribution of canopy respiration to the annual respiratory losses from a 30yr *P. menziessii* ecosystem, in the Netherlands. To illustrate this, if the total flux from the canopy at night was $10 \mu\text{mol m}^{-2} \text{s}^{-1}$ and 70% of this was respired by the canopy it would constitute $7 \mu\text{mol m}^{-2} \text{s}^{-1}$. For

daytime fluxes at the same temperature but reduced from its nocturnal rate by 50-80%, the flux of total ecosystem respiration could be reduced to 4.4 to 6.5 $\mu\text{mol m}^{-2} \text{s}^{-1}$. Of course this represents an extreme scenario as in most ecosystems soil respiration tends to dominate the total ecosystem respiration.

A further daytime complication may exist in the assumptions regarding the respiration rate of woody biomass the term, R_w . There is evidence collected in the field and in laboratory experiments to show that respiration from tree stems and branches decrease during the day. Negisi (1972, 1975, 1981, 1982) found that stem CO_2 evolution rates in several tree species were often lower than temperature-predicted rates by up to 50% on warm, sunny afternoons. This has also been found in many different temperate deciduous and coniferous species (Kakubari, 1988; Edwards and McLaughlin, 1978; Matyssek & Schulze, 1988; Martin *et al.*, 1994).

Typically rates of respiration from this component are small and represent *ca.* 10% of total ecosystem respiration. However, it is another term of the daytime carbon balance we may be over-estimating if nighttime relationships are applied during the day. If both of these inhibitions occur during the day then the consequence could represent a large overestimation of day-time respiration using the current models.

Uncertainties estimating nocturnal respiration rates

Net ecosystem exchange and forest carbon sequestration reflect the difference between two large fluxes, respiratory efflux and photosynthetic uptake during the day, a small underestimation of nocturnal flux can cause a large overestimation of long-term carbon uptake and vice versa. For instance, Goulden *et al.*, (1996) estimated errors in measurement and modelling of nocturnal respiration could alter annual respiratory estimates by 0.5 to 1.0 t C ha^{-1} . This led to changes in estimated

annual carbon sequestration from 3.7 t C ha⁻¹ to 2.8 t C ha⁻¹ for a temperate mixed deciduous forest, in Harvard Forest, Massachusetts, USA.

Previous experience has shown that eddy covariance works best during windy periods. Because of a tendency for the turbulent fluxes to underestimate F_E by 5 to 10 % and an additional ± 10 % added to account for uncertainties in the measurement of net radiation, used in the calculations of heat storage and correction of latent heat flux, confidence intervals for F_E measurements of all scalars during daytime turbulent exchange, are -20 to 0 %. The reasons for flux underestimation are numerous but will not be dealt with specifically in this thesis. A deeper analysis of the eddy covariance method and uncertainties in estimates of F_E at the Griffin Forest study site will be explored in Clement (2003). This thesis however, does provide scope for validation of $F_{E,N}$ and $F_{E,D}$ using chamber methods during periods of non-ideal mixing.

Evidence from the literature suggests that during poorly mixed periods, conveniently characterised by $U^* < 0.20$ m s⁻¹ there is a reduction in the measured vertical flux of CO₂ above forest canopies. The discrepancy is not entirely explained by an observed increase in the storage term and the possibility of CO₂ escaping via some undetectable route has been proposed (Goulden *et al.*, 1996; Goulden *et al.*, 1997). Numerous hypotheses exist to explain flux underestimation during stable periods, but they do not represent the focus of this thesis and reviews on the subject can be found in Goulden *et al.*, 1996, Moncrieff *et al.*, 1996, Massman & Lee, 2002 and Pattey *et al.*, 2002.

A recurring area of conflict within the flux community is what to do with $F_{E,N}$ data during stable conditions, should it be incorporated with data collected in well mixed conditions when modelling the nocturnal $F_{E,N}$ temperature response, or should it be left out? As highlighted above this can impact heavily on estimates for annual forest

carbon sequestration (Goulden *et al.*, 1996). Observations from chamber methods have also observed correlation between net CO₂ exchange and U^* inside soil and branch chambers (Rayment, 1998; Rayment & Jarvis, 2000). Therefore, reduction in $F_{E,N}$ measured by eddy covariance may in part be a consequence of reductions in respiratory processes and the transport of CO₂. Only by employing chamber methods concurrently with eddy covariance methods will this type of information be gathered, thereby reducing uncertainties in forest carbon balance in the future. Unfortunately, the work contained in this thesis is unable to resolve directly the consequences of low U^* at the chamber scale. This would have required a different soil respiration system capable of collection at a finer temporal resolution. However, this study can explore how well matched scaled chamber measurements and chamber parameterised models are with models of F_R derived from $F_{E,N}$ including or excluding low U^* values.

Modelling the ecosystem respiration response to temperature implicitly requires a reference temperature in the forcing. This temperature should be as close as possible to the temperature of the area or organ respiring. Presently, meta-analysis studies of flux data covering numerous biomes and plant functional groups commonly employ T_s to force the ecosystem temperature response (Valentini *et al.*, 2000; Falge *et al.*, 2002). The amplitude and timing of T_s and T_a can be very different over the day with obvious consequences for the timing and amplitude of F_R estimated. The use of T_s as an appropriate driver for all ecosystems, at possibly different stages of stand development is uncertain. In ecosystems characterised by open canopies of low L and large soil CO₂ efflux, T_s would indeed be the best variable to describe most of the variation in total ecosystem respiration. However, in ecosystems characterised by tall, dense canopies with a large L and above-ground biomass component, T_s may not be the best variable to describe short-term fluctuations in F_R and perhaps T_a would be a better suited driver. Within the scope of this study it will also be possible

to use the summed component fluxes to constrain the appropriate temperature reference location by comparison with F_R estimates derived from $F_{E,N}$ using T_s or T_a .

5.3.2 *Evaluating stable isotope methods to partition net ecosystem exchange*

More recently, stable isotopes have been used to trace plant physiological processes at the leaf, tree, ecosystem and regional scales. As described in previous chapters, the metabolic activity of plants and soil micro-organisms can cause not only diurnal fluctuations of CO_2 mole fraction but also changes in the $^{13}\text{C}/^{12}\text{C}$ and $^{18}\text{O}/^{16}\text{O}$ ratios of the surrounding atmosphere. In Chapter 4 direct observations showed how during the day photosynthetic discrimination against ^{13}C causes air within the canopy to become enriched in ^{13}C with respect to atmospheric CO_2 within and above the canopy when photosynthetic processes dominate. Whilst at night respiration causes the release of CO_2 depleted in the heavier carbon relative to atmospheric CO_2 . In principle the isotopic composition of CO_2 is a useful natural tracer which can enable identification of the likely source of CO_2 and give some estimate of canopy performance and processes.

Ecosystem respired $^{13}\text{CO}_2$

Many of the following equations require the ^{13}C composition of respired CO_2 , δ_R at the component or ecosystem level. To determine δ_R several methods can be used. One is to examine the isotopic composition of respiring organic material such as leaves, branches, trunks, roots, litter and soil organic matter (Sternberg, 1989; Lloyd *et al.*, 1996). Nevertheless, the possibility of isotope fractionation during respiration cannot be ruled out and caution should be exercised when adopting this approach (Farquhar & Lloyd, 1993).

A second option is to examine the relationship between the mole fraction (C_a) and the carbon isotope composition of CO_2 (δ_a) at night (Keeling, 1958, 1961; Lancaster, 1990). Keeling proposed that the composition of night-time air within a canopy could be interpreted as a simple mixing process of CO_2 , the mole fraction and isotopic composition of CO_2 in the air at any time, reflecting a mixture of CO_2 from an infinite reservoir (the troposphere) and that arising from ecosystem respiration. Keeling found that Eq 5.6 described the data for a single source of isotopic composition and a simple mixing process,

$$\delta_a = \delta_R + \frac{m}{C_a}, \quad (\text{Eq 5.6})$$

where m is a constant. Such an expression arises if

$$C_a \delta_a = C_T \delta_T + C_R \delta_R \quad (\text{Eq 5.7})$$

where C_T is the mole fraction of CO_2 in a background gas of composition δ_T , to which an additional mole fraction C_R , with composition δ_R is added. Eliminating C_R from Eq 5.13 and taking δ_R to be equivalent to the total ecosystem respiratory source $^{13}\text{CO}_2$ composition, Lancaster (1990) expressed Eqs. 5.6 and 5.7 as

$$\delta_a = \delta_R + \frac{(\delta_T - \delta_R)C_T}{C_a} \quad (\text{Eq 5.8})$$

where δ_a is the isotopic composition of the air within the “canopy layer”, and C_T and δ_T represent the CO_2 mole fraction and isotopic composition of the remaining troposphere, being an infinite background reservoir. The canopy layer does not need to be precisely defined in this case, but it must be close enough to vegetation for

diurnal cycles in nearby plants and soil to be measured. From Eq (5.8) it can be seen that if the isotopic composition of carbon entering and leaving plants is invariant over time, then a plot of δ_a versus $1/C_a$ gives a straight line relationship with a slope $(\delta_T - \delta_R)C_T$ and an intercept δ_R . Thus provided that δ_T and C_T remain constant during the observation period, and that there is no fractionation of CO_2 during plant or soil respiration, then from concurrent measurements of δ_a and C_a one can infer the carbon isotope composition of ecosystem respiration, δ_R . At the ecosystem scale, this value represents both the recent and historic signal of CO_2 fixed by species past and present within the forest system.

A third option is to measure the isotopic composition of respired CO_2 directly using either the mass balance or mixing models described above Eqs 5.7 and 5.8. This can be done through direct sampling of the component respiratory sources that contribute to the ecosystem respiration. Therefore, analogous to Eq 5.3 it would be desirable to compose a full $^{13}\text{CO}_2$ respiratory mass balance for all components individually as described below

$$F_R \delta_R = R_B \delta_B + R_W \delta_W + R_S \delta_S. \quad (\text{Eq 5.9})$$

Ecosystem discrimination against ^{13}C

As a next step one can re-arrange Eq 5.8 and use the information contained in the Keeling plot to make an estimate of the integrated carbon isotope discrimination of the entire ecosystem Δ_{KEELING} , (which includes all respiratory sources) as,

$$\Delta_{\text{KEELING}} = \frac{\delta_T - \delta_R}{1 + \delta_R}. \quad (\text{Eq 5.10})$$

Thus, Δ_{KEELING} integrates not only over Δ of all photosynthesising leaves but also includes information about the $\delta^{13}\text{C}$ of respiring organic matter. Equally, Δ_{E} can be re-expressed and defined for the instantaneous net result of isotopic fluxes during photosynthesis and respiration,

$$\Delta_{\text{E}} = \frac{A\Delta + R_{\text{W}}(\delta_{\text{W}} - \delta_{\text{a}}) + R_{\text{S}}(\delta_{\text{S}} - \delta_{\text{a}})}{A - R_{\text{W}} - R_{\text{S}}}. \quad (\text{Eq 5.11})$$

As described fully in Chapters 2 and 3 chamber techniques can provide direct measurements of the above isotopic fluxes and facilitate independent determination of instantaneous Δ_{E} .

Estimating F_{A} , F_{R} and canopy ^{13}C discrimination using the partitioning approach

The algebraic expression (Eq 5.1) describing the net biotic flux and the individual components of the carbon mass balance can be expanded to accommodate isotope ratios. Following theory developed in Bowling *et al.*, 2001 multiplying through by absolute isotope ratios the mass balance equations for $^{13}\text{CO}_2$ are obtained

$$\overline{\rho w'(r_{\text{a}}C_{\text{a}})}' + \rho \frac{d}{dt} \int_0^{z_{\text{m}}} r_{\text{a}} C_{\text{a}}(z) dz = F_{\text{R}} r_{\text{R}} + F_{\text{A}} \frac{r_{\text{a}}}{1 + \Delta}. \quad (\text{Eq 5.12})$$

where Δ is the extent of $^{13}\text{CO}_2$ discrimination by the foliage during net assimilation, and r_{R} and r_{a} refer to the absolute $^{13}\text{CO}_2/^{12}\text{CO}_2$ ratios of respired CO_2 and canopy air, respectively (see Appendix I). The terms on the left represent the net ecosystem exchange of $^{13}\text{CO}_2$, as a net eddy flux and a storage flux of $^{13}\text{CO}_2$ (analogous to Eq 5.1). The use of the absolute isotope ratio ($r = ^{13}\text{C}/^{12}\text{C}$) introduces the approximation that the $[^{13}\text{CO}_2] \approx (^{13}\text{C}/^{12}\text{C}) * [\text{total CO}_2]$. It is assumed that there is no fractionation of

$^{13}\text{CO}_2$ during autotrophic and heterotrophic respiration for $^{13}\text{CO}_2$ and that canopy air with the atmospheric $\delta^{13}\text{C}$ forms the substrate for CO_2 assimilation.

For consistency with other CO_2 mass balance studies the $^{13}\text{CO}_2$ exchange requires dividing by the isotopic standard, PDB- CO_2 , subtracting Eq 5.1 and re-expressing in delta notation ($\delta = r/r_{\text{PDB}} - 1$) ignoring terms in Δ^2 or smaller (Lloyd *et al.*, 1996), the following is obtained

$$\rho \overline{w'(\delta_a C_a)'} + \rho \frac{d}{dt} \int_0^{z_m} \delta_a C_a(z) dz = F_R \delta_R + F_A (\delta_a - \Delta). \quad (\text{Eq 5.13})$$

Although mass is conserved in both Eqs 5.1 and 5.13 the terms to the left no longer equal the net ecosystem exchange of $^{13}\text{CO}_2$ and, instead, their sum is the isoflux of $^{13}\text{CO}_2$, which represents the product of F_E and the isotopic composition (expressed in δ units) of that net exchange. Writing this explicitly, the isoflux referred to hereon as F_I is

$$F_I = F_R \delta_R + F_A (\delta_a - \Delta), \quad (\text{Eq 5.14})$$

where the term $F_R \delta_R$ represents the net isotopic flux of $^{13}\text{CO}_2$ added to the atmosphere through the process of ecosystem respiration from all components. This assumes a single isotopic composition, δ_R can be found that is representative of all components of ecosystem respiration (Keeling, 1958). The term $F_A (\delta_a - \Delta)$ represents the isotopic flux of $^{13}\text{CO}_2$ removed by photosynthesis, which is the net assimilation rate times the isotope ratio of that assimilated carbon, $(\delta_a - \Delta) \approx \delta_D$.

Using the linear regression, $\delta_a = mC_a + b$ between δ_a and C_a derived from flask measurements and assuming that $\overline{\delta_a} = m\overline{C_a} + b$, Bowling *et al.* (2001) verified empirically that F_I can be computed robustly using

$$F_I \approx (2m\bar{C}_a + b)\overline{\rho w' C_a'}. \quad (\text{Eq 5.15})$$

For more detail on the dependence of F_I on F_E see Eqs 11 – 16 of Bowling *et al.* (2001). Thus, using the eddy covariance measurements and a knowledge of δ_a , δ_R and C_a equations can be solved to derive F_A and F_R as detailed in Appendix III and the Appendix of Bowling *et al.*, (2001).

Very few studies have validated this technique with independent methods that measure F_A or Δ_C directly. By measuring F_A and Δ_C directly with chamber methods, comparisons can be made between the behaviour of the two methods. This type of validation will highlight potential problems with the experimental method and explore some of the theory assumptions. Furthermore, the use of partitioning approaches to obtain instantaneous estimates of F_A and Δ_C at the canopy scale will illustrate the dependence of these processes on environmental drivers and how they in turn impact the net isotopic signal from the ecosystem Δ_E .

5.4 METHOD

5.4.1 Net ecosystem exchange

Eddy covariance system

Fluxes of momentum, sensible heat, water vapour, CO_2 , and relevant canopy meteorological parameters were measured on a 15 m tall instrument tower by Mr R. Clement. This system forms part of a long-term CO_2 exchange study (CARBOEUROFLUX), and the instrumentation deployed throughout the forest has been described extensively elsewhere (Clement, 2003). Briefly, continuous above-canopy measurements of CO_2 , H_2O and wind velocity were employed in determining

30 min average fluxes. The University of Edinburgh Edisol flux measurement system (Moncrieff *et al.*, 1997) used throughout this study consisted of: a three-dimensional sonic anemometer mounted at 15.2 m (Solent A1002R, Gill Instruments Ltd., Lymington, England) to measure the vertical component of wind; a pumping unit to draw air at $6 \text{ dm}^3 \text{ min}^{-1}$ through 18 m of 6 mm i.d. heated tubing (Dekabon 1300, Furon, Gembloux, Belgium); a fast-responding closed-path infrared gas analyser (IRGA) to measure CO_2 and H_2O (LI-6262, Li-Cor Inc., Lincoln, Nebraska); a laptop using the EdiSol software (Moncrieff *et al.*, 1995); and a custom-built enclosure at the foot of the tower containing temperature and pressure transducers, tube heating control, and other accessories (Clement, 2003).

Unfortunately, because of instrument failure, vertical profiles of CO_2 mole fraction throughout the canopy were not possible. Instead, changes in CO_2 mole fraction within the canopy were determined from the start CO_2 mole fraction measured in branch chambers (see Chapter 3 and 4 for full description) and averaged over 30 minute intervals. Furthermore, air samples obtained from “Open” soil and branch chambers throughout the canopy were assumed representative of ambient canopy air for different heights. These samples were then used to evaluate the relationship between δ_a and CO_2 mole fraction, derive ecosystem δ_R and compute the ecosystem storage and eddy isofluxes according to Eqs 5.14 and 5.15.

Climatological data

A weather station was maintained throughout the field campaign (Clement, 2003). All data were recorded as half-hourly averages on dataloggers (CR10 and 21X, Campbell Scientific (UK) Ltd., Shepshed, England). All instrumentation, unless stated otherwise, was mounted to the south, at the top of the tower at 14.6 m. Temperature was measured using a combination of methods including: a psychrometer measuring the dry bulb temperature; a sonic anemometer described

above; and a thermocouple referenced to a thermistor. Humidity measurements were obtained using a ventilated thermistor psychrometer. In addition water vapour mixing ratio was measured by the IRGA as described above. A cup anemometer and sonic anemometer measured wind speed with the direction of wind measured with a wind vane at 12.2 m. Three net radiometers (Q*6 and Q*7, Radiation Energy Balance Systems, Washington) were projected on booms alongside two pyranometers (CM2 and CM5, Kipp & Zonen, Delft, The Netherlands) measuring incoming and reflected solar radiation. Incoming photosynthetic photon flux density (PPFD) was measured with two quantum sensors (SD101QV, Macam Ltd., Livingston), and rainfall was measured using two tipping bucket rain gauges (Campbell Scientific (UK) Ltd., Shepshed, England) both located in a clearing, with one elevated to 4 m and one at the soil surface.

Soil heat flux was measured using an array of seven soil heat flux plates (HFT-3, Campbell Scientific (UK) Ltd.) which were buried 5 cm below the soil surface. Soil temperature was measured over a depth 0 to 5 cm below the soil surface using a pair of RTD (PT100, RS Components, UK). Soil volumetric water content was obtained using six capacitance sensors (CS615, Campbell Scientific (UK) Ltd.) integrating over a depth of 15 cm from the soil surface. A full description of instrument calibration and maintenance is given by Clement, (2003).

Processing of eddy flux data - obtaining isofluxes

Flux and climate data were combined and used to calculate net ecosystem CO₂ exchange (F_E) as described in Eq 5.1. Isofluxes were estimated by combining fast (21 Hz) CO₂ time-series with a linear relationship between δ_a and C_a as described above in Eq 5.13 and 5.15. Appropriate processing corrections are described elsewhere (Clement, 2003) and were made prior to applying Eq 5.15. The net isoflux

was then calculated by adding the eddy isoflux and the storage isoflux following Eq 5.13.

5.4.2 Chamber measurements

Canopy assimilation, respiration and transpiration from chambers

Branch photosynthesis, transpiration, respiration and stomatal conductance were measured continuously on two branches using the branch chamber method described extensively in Chapter 3. The fluxes were then “scaled” simply to provide an estimate for the whole canopy by multiplying the instantaneous flux by the estimated needle area index ($6 \text{ m}^2 \text{ m}^{-2}$) of the canopy. Previous measurement campaigns from July 2000 (data not shown), indicated that branches lower in the canopy not only had different needle morphology but also different photosynthetic rates. To take account of these differences the canopy was initially split into a sun and shade portion, with 50 % of the canopy leaf area assumed to occur in each layer (Norman & Jarvis, 1974). Pooling all data collected in July 2000 it was found that the lower canopy rates of photosynthesis, transpiration and branch conductance were 24 ± 13 , 21 ± 18 and 28 ± 13 % of the upper canopy rates, respectively. Hence, each process in the shade layer of the canopy was assigned as a constant percentage of the sun layer. The contributions of carboxylation, photorespiration and dark respiration were then calculated following the method detailed in Chapter 3. This then allowed estimates of net photosynthetic discrimination and isofluxes associated with photosynthesis and respiration to be simulated.

A second method was also used to estimate canopy assimilation and stomatal conductance acknowledging the fact that chamber artefacts can create conditions inside chambers different from those outside (Denmead *et al.*, 1993). Firstly, branch chamber A versus incident Q response functions were constructed from data

collected under natural Q conditions. To describe the A/Q response function the data were fitted to a non-rectangular hyperbola (Ögren & Evans, 1993) as follows:

$$A = \frac{\phi Q + A_{\max} - \sqrt{(\phi Q + A_{\max})^2 - 4 \phi A_{\max} Q \Theta}}{2 \Theta} - R_d, \quad (\text{Eq 5.16})$$

where A is the instantaneous photosynthetic rate ($\mu\text{mol m}^{-2} \text{s}^{-1}$), Q is the incident photon flux density (PFD) ($\mu\text{mol m}^{-2} \text{s}^{-1}$), ϕ is the apparent quantum efficiency of photosynthesis ($\mu\text{mol CO}_2 \mu\text{mol}^{-1}$ quanta), A_{\max} ($\mu\text{mol m}^{-2} \text{s}^{-1}$) is the asymptotic maximum photosynthetic rate, Θ is the convexity coefficient describing the smoothness of the transition between PFD limited and PFD saturated rates of photosynthesis and R_d ($\mu\text{mol m}^{-2} \text{s}^{-1}$) is the daytime “dark” respiration rate (the day respiration). All fitted parameters were extracted from the data using the PROC NLIN, SAS procedures.

The next step was to use a simple light extinction model to simulate Q through a Sitka spruce crown with six separate layers of identical depth, each containing 1 m^{-2} projected needle area m^{-2} ground area. Meir *et al.*, (2002) fitted an exponential model to measured profiles of Q in a 13 yr old Sitka spruce stand at Glencorse Mains, Edinburgh. The spruce stand was 9 to 10 m high, with an L of ≈ 7 . The within canopy Q was estimated relative to incoming Q , at some live crown depth, H , relative to the maximum live crown depth, H_c of the canopy using the relationship

$$Q = e^{-Q_k H_c}, \quad \text{Eq (5.17)}$$

where Q_k is an extinction coefficient with a value of 4.08, and H refers to a value between 0 and 1 relative to H_c . The only input required for this model was the incident above-canopy Q . The model output presented in Figure 5.1 were then

coupled to the parameterised A/Q response above (Eq 5.16) to generate canopy assimilation rates (F_A) using Eq 5.2.

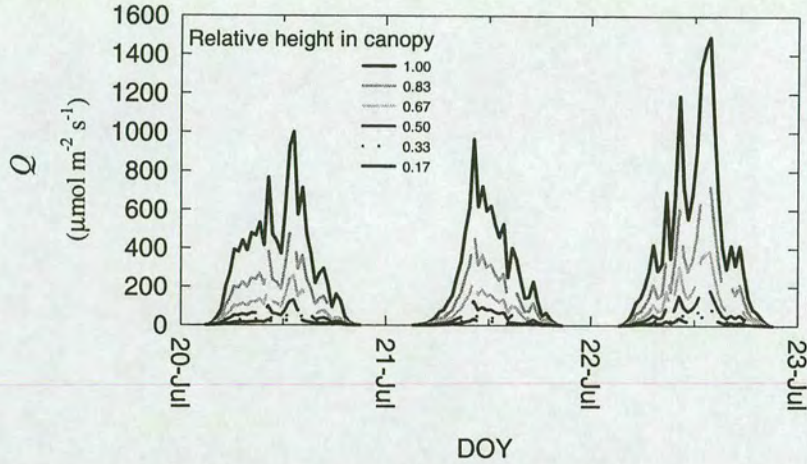


Figure 5.1 Daily variation in modelled Q within the canopy at Griffin Forest during July 2001 using Eq 5.17.

Lastly, the Leuning (1995) modified Ball, Woodrow and Berry (1987) model (L-BWB) was fitted to the pooled branch chamber g_s data. The model specifically relates g_s to A , C_a , and D_a as follows:

$$g_s = g_0 + \frac{a_1 A}{\left[(C_s - \Gamma_*) \left(1 + \frac{D_s}{D_0} \right) \right]}, \quad (\text{Eq 5.18})$$

where g_0 is the lowest conductance ($\text{mmol m}^{-2} \text{s}^{-1}$), i.e. the conductance remaining when $Q = 0 \text{ } \mu\text{mol m}^{-2} \text{s}^{-1}$. A is the assimilation rate ($\mu\text{mol m}^{-2} \text{s}^{-1}$) described above, Γ_* is the CO_2 compensation point described in Chapter 3. C_s is the CO_2 mole fraction at the leaf surface, which is equal to C_a in a ventilated branch chamber assuming a negligible aerodynamic resistance. D_s is the mole fraction humidity

deficit ($\text{mmol H}_2\text{O mol}^{-1} \text{ air}$) at the needle surface which $\approx D_a$ also assuming a negligible aerodynamic resistance. The parameters a_1 and D_0 are empirical coefficients (mmol mol^{-1} and dimensionless, respectively) which were determined through a least squares fit of the model to the branch data using PROC NLIN, SAS procedures. The model was then coupled with environmental data collected above the canopy and modelled A from above to calculate canopy stomatal conductance, G_s ($\text{mol m}^{-2} \text{ s}^{-1}$).

Soil CO₂ efflux and $\delta^{13}\text{C}$ of soil respired CO₂

Two soil systems were used during this observation period, one that would be used for establishing the $\delta^{13}\text{C}$ of respired soil CO₂ and another portable system for obtaining temporal and spatial information on soil CO₂ efflux. The former was a closed static system used to collect $^{13}\text{CO}_2$ respired from the soil surface during July 2001. The chambers were made of 5 mm thick clear acrylic, their volume was 384 dm^3 and area was 0.64 m^2 . Chambers contained a small 12V fan (RS 250-1561, RS Components Ltd., Corby) to provide a small amount of air mixing this was securely mounted on a bracket attached to one of the chamber walls. During sampling air was circulated between the chamber and a flask flushing system through 4 m of polyethylene-lined tubing (3/8" i.d. Dekabon 1300, Furon, Gembloux, Belgium). Chamber CO₂ mole fraction and $^{13}\text{C}/^{12}\text{C}$ ratios were sampled immediately prior to chamber closure and at 10 minutes after closure following the protocol set out in Chapter 3 and Figure 3.3 for the branch chambers. Care was taken not to breathe around the chamber during sampling time and when the lid was closed. The flasks were then sent to the Max Planck Institute for Biogeochemistry for analysis of CO₂ mole fraction and $^{13}\text{C}/^{12}\text{C}$ ratios following the procedure set out in Chapter 3.

Soil CO₂ efflux was also measured concurrently with a portable CO₂ analyser equipped with a soil chamber: the coupled SRC-1 and EGM-3 (PP Systems, Hitchin, Hertfordshire, England). This system consisted of a small, closed chamber fitted with an internal metal gauze to reduce the effects of the internal fan and a customised adaptor that allowed the chamber to be placed tightly onto PVC collars inserted 2 cm into the soil surface. Air was then drawn to a portable non-dispersive infrared gas analyser and dynamically sampled at 450 ml min⁻¹. The change in CO₂ mole fraction within the chamber over the measurement period (2 min) was monitored every 8 seconds and the CO₂ flux subsequently calculated. The chamber enclosed a surface area of 71 cm², and the volume of the chamber plus tubing was 1400 to 1500 cm³ variable with collar height above the soil surface. Soil CO₂ efflux was calculated by software included with the IRGA. The system is described further by Parkinson (1981) and Jensen *et al.*, (1996).

To avoid excessive soil surface disturbance during repeated measurements and to ensure repetition at identical locations, twelve plastic collars with a sharpened edge (100 mm tall, with wall thickness of 3 mm) were installed in a 0.01 ha plot. The collars were placed randomly within three distinct areas (refer to Chapter 2 for a description of the three areas). The collars were made to fit the inside diameter of a customised adapter fitted to the soil chamber to ensure no chamber leaks. Measurements were taken throughout the diurnal cycle coinciding with samples taken from the static closed chambers and pooled with other data collected over the course of the 2000-2001 growing season for the same locations. Further collars were placed in a further two sites varying in *L* with the same replication of 12 collars at each site and four collars randomly placed within the three distinct areas.

5.5 CALCULATIONS

5.5.1 Relating to canopy assimilation

Estimating F_A from $F_{E,N}$

Measurements of all F_E obtained during periods when $Q = 0 \mu\text{mol m}^{-2} \text{s}^{-1}$ ($F_{E,N}$) were fitted to the Arrhenius “activation energy” temperature response (Lloyd & Taylor, 1994) described in Eq 3.5. The model was modified slightly by establishing the efflux rate at 10 °C (R_{10}), both air (T_a) and soil (T_s) temperature were used as the independent variable. The Arrhenius temperature response was initially fitted to all $F_{E,N}$ data using both reference temperature locations. The $F_{E,N}$ data were then screened to remove all values with $U^* < 0.2 \text{ m s}^{-1}$ and the Arrhenius temperature response fitted again using both reference temperature locations.

Daytime estimates of F_R were then calculated from the resulting functions using measured daytime air and soil temperatures. Values for both F_R and observed $F_{E,D}$ were then applied to Eq 5.1 and F_A was solved as the residual. This was done using the relationships derived for F_R at night. This yielded four sets of data derived from $F_{E,N}$ for both F_R and F_A as follows:

$F_R (T_a)$ and $F_A (T_a)$ predicted from T_a including all U^* data;

$F_R (T_s)$ and $F_A (T_s)$ predicted from T_s including all U^* data;

$F_R (T_a \text{ and } U^*)$ and $F_A (T_a \text{ and } U^*)$ predicted from T_a excluding $U^* < 0.2 \text{ m s}^{-1}$ and;

$F_R (T_s \text{ and } U^*)$ and $F_A (T_s \text{ and } U^*)$ predicted from T_s excluding $U^* < 0.2 \text{ m s}^{-1}$.

Estimating F_A from combined eddy covariance and $^{13}C/^{12}C$ ratios

$F_{E,D}$ was calculated following Eqs 5.1 using the eddy covariance data and storage estimates as described above. F_I were then calculated using Eq 5.15 and the geometric mean regression of δ_a and C_a applied to the 30 min mean C_a measured above the canopy using the eddy covariance method. Air samples collected during the day from open chambers were used to construct this regression. This then left the flux terms F_A and F_R to be solved as shown in Eq 5.14. The isotope ratio of ecosystem respired CO_2 , δ_R , required for Eq 5.14 was obtained from the intercept of the geometric mean regression between δ_a and $1/C_a$. Air samples collected at night from open chambers were used to construct this regression.

Instantaneous canopy ^{13}C discrimination Δ_C was determined from two methods. The first method employed branch chamber observations of A , g_s and C_i scaled to the canopy as described above. Following the simplest (and most often used) formulation of ^{13}C discrimination described by Eq 3.16 in Chapter 3, Δ_C (Simple) is related to the ratio C_i/C_a (Farquhar *et al.*, 1982). In this formulation all respiratory terms and mesophyll conductance are neglected. The branch chamber data is then used in a more extensive formulation of ^{13}C discrimination, Δ_C (Full) described by Eq 3.21 in Chapter 3. This model explicitly includes the contribution of photorespiration, daytime mitochondrial respiration and mesophyll conductance. For further details on this modelling at the branch scale refer to Chapters 3 and 4.

The second method used to estimate Δ_C also uses the simple formulation of Eq 3.16, C_a above the canopy and eddy covariance data. To solve this equation at the ecosystem scale using eddy covariance methods, estimates of C_i are required for the canopy. A simplified version of Eq 3.8 in Chapter 2 can be made relating C_i to the instantaneous net assimilation rate and canopy conductance to CO_2 (G_c) as follows:

$$-F_A = G_c (C_a - C_i). \quad (\text{Eq 5.19})$$

The four equations of 5.1, 5.14, 3.16 and 5.19 collectively contain five unknowns (F_A , F_R , ΔC , C_i and G_c). If G_c is estimated, formal combination of the four equations provides a quadratic equation which has one realistic solution for F_A (Bowling *et al.*, 2001). The derived quadratic solution is given in Appendix III. Values for both F_A and observed $F_{E,D}$ were then applied to Eq 5.1 and F_R was solved as the residual.

Water vapour fluxes measured with the Edisol system (Clement, 2003), were used to calculate the bulk stomatal conductance of the canopy, on a half-hourly basis, by inversion of the Penman-Monteith equation to give:

$$\frac{1}{G_s} = \frac{s \left(\frac{1}{G_a} \right) (R_{\text{net}} - \lambda E) + \rho c_p D_a}{\lambda E \gamma} - \left(\frac{1}{G_a} \right) \quad (\text{Eq 5.20})$$

where G_s and G_a are stomatal and aerodynamic conductances (m s^{-1}), s is the slope of the saturation vapour pressure vs. temperature curve for water (Pa K^{-1}), R_{net} is net radiation (W m^{-2}), λE is the latent heat flux (W m^{-2}), ρ is density of dry air (kg m^{-3}), c_p is the specific heat of dry air ($\text{J kg}^{-1} \text{K}^{-1}$) and γ is the psychrometric constant (Pa K^{-1}). The aerodynamic resistance ($1/G_a$) was estimated for each measurement period as

$$\frac{1}{G_a} = \frac{U}{U^{*2}} \quad (\text{Eq 5.21})$$

where U is the mean horizontal wind speed at a reference height (m s^{-1}) and U^* is the friction velocity (m s^{-1}) (Thom, 1975). The relationship between conductance in molar units and resistance in s m^{-1} is

$$G_s = \frac{P_{\text{atm}}}{\Re T_a \left(\frac{1}{G_s} \right)} \quad (\text{Eq 5.22})$$

where P_{atm} is the atmospheric pressure (Pa), \Re is the universal gas constant (8.314 J mol⁻¹ K⁻¹). Canopy conductance to CO₂ (G_c) is then obtained using the factor 1.6 described in Eq 3.11 of Chapter 3.

Constraining estimates of F_A from combined eddy covariance and $^{13}\text{C}/^{12}\text{C}$ ratios

Water vapour exchange measured using eddy covariance is the net result of not only stand transpiration but also the evaporation of water from soil surfaces and canopy interception. The direct evaporation of intercepted water by foliage back to the atmosphere can form a significant contribution to the total water balance of a catchment. This is most pronounced in windy climates and for forests, which are well coupled to the atmosphere by virtue of their surface roughness (McNaughton & Jarvis, 1983). For the climate and vegetation type of the present study, it is typical for the annual interception losses to exceed 35 % of annual rainfall (Calder, 1977; Gash & Stewart, 1977; Gash, 1979; Calder, 1990). Furthermore, micrometeorological methods are difficult to use in wet conditions for several reasons, including: water on instruments such as the net radiometer and sonic anemometer; water droplets or condensation in tubes; sensors with water sensitive ‘windows’; very small saturation deficits (<1 mmol mol⁻¹); and very small gradients of specific humidity (Jarvis, 1993). For these reasons, estimates of canopy conductance during humid conditions are likely to overestimate the flux of water vapour from the plants alone to the atmosphere and consequently overestimate the uptake of CO₂ by the canopy. Therefore, estimates of canopy conductance should be

constrained where possible, using alternative methods, such as chamber gas exchange or sapflow methods. Alternatively, this approach may only prove accurate during dry periods, if independent methods of determining canopy conductance are unavailable.

Bowling *et al.*, (2001) in their formulation of canopy conductance to CO₂ as shown above in Eq 5.19 and Appendix III assume there is no further resistance in the pathway between the chloroplast and atmosphere once a CO₂ molecule reaches the stomatal cavity. However, evidence for many different species including *P.sitchensis* (see Results Chapter 4) indicate a further resistance encountered by CO₂ molecules between the intercellular air spaces and the site of carboxylation, r_w . The calculation of mesophyll conductance, $1/r_w$ was estimated at 0.29 mol m⁻² s⁻¹ in Chapter 4. Therefore, by incorporating this measure of mesophyll conductance at the canopy scale, the consequences of neglecting G_w in the estimation of F_A and Δ_c can also be explored.

Water vapour fluxes and estimates of stomatal conductance measured from branch chambers described in Chapter 3 and 4 were “scaled” to the canopy as described above. These half-hourly estimates of canopy conductance to H₂O, G_s were then converted to estimates of canopy conductance for CO₂, G_c . In order to represent the total canopy conductance to CO₂, another step including the mesophyll resistance must also be considered as follows

$$\frac{1}{G_T} = \frac{1}{G_a} + \frac{1}{G_c} + \frac{1}{G_w}, \quad (\text{Eq 5.23})$$

where the sum of all resistances through the boundary layer, stomatal cavity and mesophyll cell wall equals the total canopy resistance to CO₂, $1/G_T$. These chamber-based estimates of G_T were then exchanged with the eddy covariance estimates of G_c calculated from Eq 5.20, thereby constraining estimates of total canopy

conductance to CO₂ (G_T) with canopy transpiration and mesophyll conductance. Because the effects of mesophyll conductance are now included, Eq 5.19 must be modified to solve for F_A and becomes:

$$-F_A = G_T(C_c - C_a), \quad (\text{Eq 5.23})$$

where C_c represents the CO₂ mole fraction at the site of carboxylation.

It follows that to obtain an estimate of Δ_c , the incorporation of mesophyll conductance also requires that Eq 3.16 be modified accordingly to:

$$\Delta_c = \bar{a} + (b - \bar{a}) \frac{C_c}{C_a} = a_b \frac{C_a - C_s}{C_a} + a \frac{C_s - C_i}{C_a} + a_m \frac{C_i - C_c}{C_a} + b \frac{C_c}{C_a} \quad (\text{Eq 5.24})$$

where \bar{a} is the total fractionation resulting from diffusion of CO₂ from above the canopy to the sites of carboxylation. This can be re-expressed and expanded as shown above on the right to describe each fractionation during the diffusion pathway where, C_s is the mole fraction at the leaf surface, a_b is the fractionation associated with diffusion through a laminar boundary layer ($a_b = 2.9\%$, Farquhar, 1983), and a , a_m and b are the fractionation factors described in Chapter 3 (see Eq 3.21).

6. Daily variation in gas exchange and ^{13}C discrimination by a Sitka spruce plantation – Results and Discussion

6.1 RESULTS

6.1.1 *Driving environmental variables*

Figures 6.1 and 6.2 collectively, describe the weather conditions prevalent at the study site between the 18th and 23rd July 2001. The period started dry and sunny with R_{net} and Q reaching maximum values of $> 650 \text{ W m}^{-2}$ and $1500 \mu\text{mol m}^{-2} \text{ s}^{-1}$, respectively. The Q time series indicates clear skies in the mornings becoming progressively cloudy after midday (Figure 6.2). Wind speeds remained fairly regular at between 3 and 4 m s^{-1} during the first two days, resulting in maximum values for aerodynamic conductance of 3.5 and 4 $\text{mol m}^{-2} \text{ s}^{-1}$ (Figure 6.1). Both T_a and D_a exhibited pronounced daily patterns tied to incoming solar radiation (data not shown). Maximum T_a were between 13-15 °C and D_a reached a maximum 12 mmol mol^{-1} , but was more commonly ca. 8 mmol mol^{-1} .

In contrast, the period of study from the 20th onward was characterised by dull, warm and wet conditions. Values for R_{net} were consistently around 100 to 300 W m^{-2} and Q ca $< 600 \mu\text{mol m}^{-2} \text{ s}^{-1}$. Wind speeds reduced during this period, reaching 1 to 2.5 m s^{-1} . However, nocturnal conditions during this period were relatively turbulent compared to daytime conditions, with friction velocity reaching 0.7 m s^{-1} and wind speeds reaching 3.5 m s^{-1} and $\zeta < -3$. Aerodynamic conductance persisted at approximately 2 $\text{mol m}^{-2} \text{ s}^{-1}$ throughout this period. Despite the reduction of incoming radiation, daytime maximum temperatures remained at 14 °C, whilst minimum night-time temperatures increased to 12 °C and R_{net} remained close to zero.

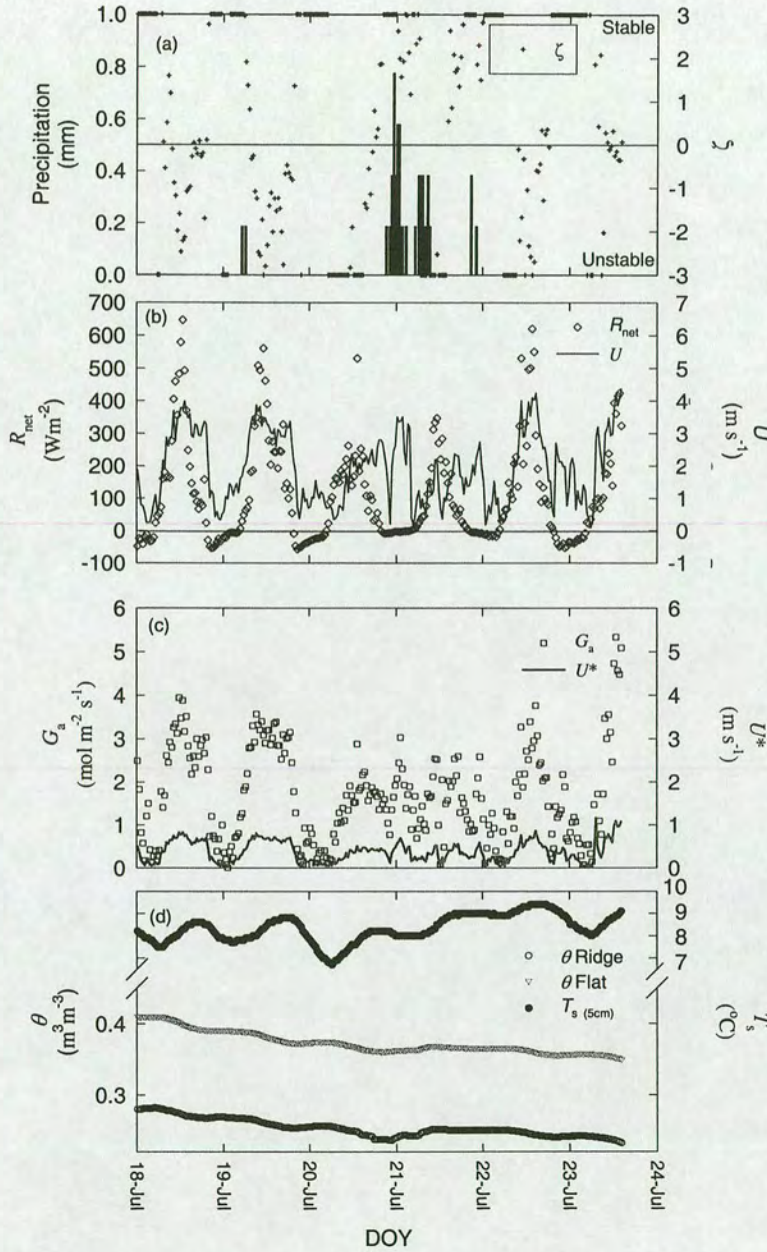


Figure 6.1 Daily variation of (a) precipitation[†] and a surface-layer scaling parameter (ζ), (b) net radiation[†] (R_{net}) and horizontal wind speed[†] (U), (c) aerodynamic conductance (G_a) and friction velocity[†] (U^*) and (d) soil temperature at 5 cm (T_s) and soil volumetric water content (θ) measured at Griffin Forest during July 2001. Each point represents the 30 min average for each environmental variable with the exception of precipitation which represents the total measured each 30 min. [†] indicates data collected by R. Clement (University of Edinburgh, UK).

Rainfall was intermittent between 20th - 21st July, with 6.5 mm measured over 24 h. This was enough rainfall to provide soil moisture recharge over the top 15 cm of the soil profile (Figure 6.1a and d). From the 22nd July onward environmental conditions returned to values similar to those observed at the beginning of the study period.

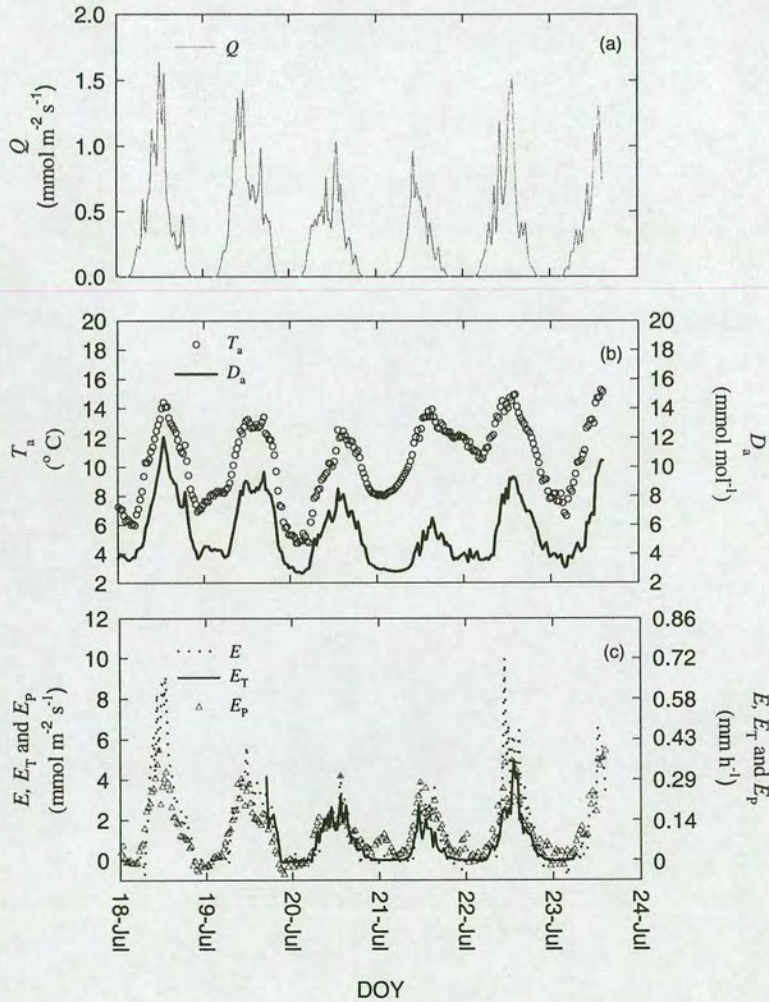


Figure 6.2 Daily variation of (a) above canopy Q , (b) canopy air temperature[†] (T_a) and air water vapour mole fraction deficit[†] (D_a), (c) eddy flux estimates of evapotranspiration[†] (E), scaled branch estimates of transpiration (E_T) and modelled Penman potential evaporation (E_P) for Griffin Forest during July 2001. Each point represents the 30 min average for each environmental variable. [†] indicates data collected by R. Clement (University of Edinburgh, UK).

6.1.2 Ecosystem water vapour exchange

A maximum evapotranspiration rate (E) of $9 \text{ mmol m}^{-2} \text{ s}^{-1}$ was measured on the 18th July when maximum D_a and U for the whole study period were observed. Despite similar T_a and U on the 19th July, E only reached a maximum of $5 \text{ mmol m}^{-2} \text{ s}^{-1}$ indicating either canopy sensitivity to D_a , or more likely an extra source of water in the system prior to the observation period displayed. Indeed rain gauges at the site collected approximately 23.5 mm between the 14th and 17th of July, confirming that the large water vapour fluxes were probably associated with evaporation of intercepted water (E_I) from the canopy and soil surface. Between the 20th to 21st July E measured above the canopy were depressed compared with the first two days. The reduction in G_a and D_a diminished the tree-atmosphere vapour pressure gradient and rates of E remained below $4 \text{ mmol m}^{-2} \text{ s}^{-1}$.

During the period 20th to 23rd July, branch transpiration (E_L) was measured and scaled to the canopy (E_T) using L as described Chapter 5. Given the uncertainties associated with L , stand heterogeneity and scaling assumptions necessary when splitting the canopy, estimates of E_T using different L values were compared against eddy flux estimates of evapotranspiration, E and are presented in Figure 6.3. Only daytime measurements obtained whilst the canopy remained dry were used for this comparison, as this flux should mostly represent canopy transpiration. At times when the canopy is wet other processes such as evaporation of intercepted water will tend to dominate (Penman, 1967; Jarvis & Stewart, 1979; Gash *et al.*, 1980; Calder, 1990; Jarvis, 1993).

Values of E_T for various canopy assumptions confirmed that the best description of foliage quantity and distribution was $6 \text{ m}^2 \text{ m}^{-2}$ during dry conditions. These data were evenly distributed along the 1:1 line for the independent methods and was significantly correlated ($r = 0.914$). Estimates using L values of 4 and $8 \text{ m}^2 \text{ m}^{-2}$ on

the whole under- and over-estimated E_T relative to the eddy flux estimates. Hence, on the 20th July when the canopy was dry, flux estimates were similar in magnitude and patterns, reaching maximum values of $3.2 \text{ mmol m}^{-2} \text{ s}^{-1}$ for branch-derived estimates compared to $4.3 \text{ mmol m}^{-2} \text{ s}^{-1}$ measured above the canopy (Figure 6.2). Mean rates of E and E_T were 1.5 ± 1.1 and $1.4 \pm 0.8 \text{ mmol m}^{-2} \text{ s}^{-1}$, respectively.

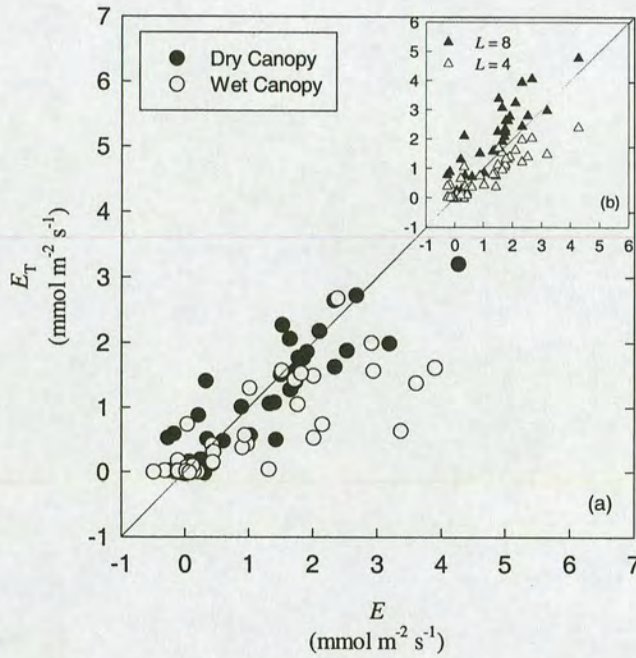


Figure 6.3 Comparison of daytime (a) eddy flux estimates of evapotranspiration[†] (E) and scaled branch estimates of transpiration (E_T) during wet and dry conditions and (b) eddy flux estimates of evapotranspiration[†] (E) and scaled branch estimates of transpiration (E_T) assuming different L for dry conditions. Each point represents the 30 min average and branch estimates are based on average evapotranspiration for two chambers located in the upper canopy. [†] indicates data collected by R. Clement (University of Edinburgh, UK).

During the rain events of the 21st July, estimates of E_T began to diverge from E as shown in Figures 6.2 and 6.3. Maximum values for E during rainfall reached $3.9 \text{ mmol m}^{-2} \text{ s}^{-1}$, whilst E_T estimates reached $2.7 \text{ mmol m}^{-2} \text{ s}^{-1}$ (Table 6.1). Despite little

difference in the maximum values early in the day, a gradual decrease in E_T caused differences between the methods to develop later in the afternoon (Figure 6.2).

↓ Method / Date →	Mean \pm 1SD and Maximum					
	Mn \pm 1SD (n)	Max	Mn \pm 1SD (n)	Max	Mn \pm 1SD (n)	Max
	20th		21st		22nd	
Eddy (E) (mmol m ⁻² s ⁻¹)	1.5 \pm 1.1 (30)	4.3	1.4 \pm 1.2 (27)	3.9	2.8 \pm 2.5 (31)	10.0
Scaled Branch (E_T) (mmol m ⁻² s ⁻¹)	1.4 \pm 0.8 (30)	3.2	0.9 \pm 0.71 (27)	2.7	1.6 \pm 1.3 (31)	4.9

Table 6.1 Daytime mean and maximum rates of evapotranspiration (E) and transpiration (E_T) during the daytime for a 3-day period during July 2001 using different methods.

This is also apparent in Figure 6.3 for the 21st July data which show points falling away from the 1:1 line as E_I plays a more important role in the overall exchange of water vapour from the ecosystem. Following the rainfall on the 22nd July, E rose dramatically in response to increased solar radiation and larger D_a . Maximum fluxes of E observed on the 22nd July above the canopy were 10 mmol m⁻² s⁻¹ and did not correspond in timing or magnitude to the scaled maximum for E_T . Maximum rates of scaled E_T during this sunnier day were 5 mmol m⁻² s⁻¹, the corresponding measurements above the forest for the same half hour was 6 mmol m⁻² s⁻¹ (Table 6.1).

Daytime rates of E from the forest were highest during bright sunny days (Table 6.2), with between 2.7 to 3.5 mm d⁻¹ lost. On overcast days, evapotranspired losses were between 1.2 to 1.4 mm d⁻¹, with the majority of the flux composed of transpired water. On all days except the 20th estimates of E were larger than estimated E_T . The contribution of E_I to the total flux from the forest was between 33 and 36% during and after rainfall.

Total amount of water lost during the day by evapotranspiration (E) transpiration (E_T) and evaporation of intercepted water (E_I) (mm d ⁻¹)					
Date → Method ↓	18th	19th	20th	21st	22nd
E	3.5	2.7	1.4	1.2	2.8
E_T	-	-	1.5	0.8	1.8
$E_I = E - E_T$			-0.1	0.4	1.0
(E_I as % of E)			(7%)	(33%)	(36%)

Table 6.2 Daytime ecosystem evapotranspiration loss (E) and the estimated contribution of evaporation (E_I) and transpiration (E_T) in Griffin Forest during the daytime, during July 2001.

6.1.3 Canopy Conductance

Modelling branch conductance

Data collected in branch chambers during July 2001 when $Q > 2 \mu\text{mol m}^{-2} \text{s}^{-1}$ and $D_a > 0.01 \text{ mmol mol}^{-1}$ were pooled and used to describe the response of branch conductance to environmental drivers. This was achieved by fitting the Leuning-modified Ball *et al.*, model (L-BWB) to the dataset using non-linear curve fitting (PROC NLIN, SAS) (see Eq 5.18 Chapter 5). Figure 6.4a shows the values of g_s measured in the branch chambers against those predicted from the fitted L-BWB model. The model gave a reasonable fit to the data in so far as the slope of the regression between predicted and actual g_s was very close to one, however, there was some variation around the slope. The regression equation between measurements and the model shown in Figure 6.4a was $g_s = 15.37 (\pm 6.86) + 0.88 (\pm 0.08) g_{s \text{ pred}}$, $r^2 = 0.55$ $n=98$.

Results for g_s over the July period seem to indicate a hysteresis phenomenon when inspected against D_a and Q . For instance Figures 5.4b and c show this phenomenon clearly for the 20th July. g_s measured at a D_a of 4 mmol mol^{-1} over the day were quite

different, with higher g_s observed in the morning. This undoubtedly contributes to the scatter in observed residuals against environmental variables.

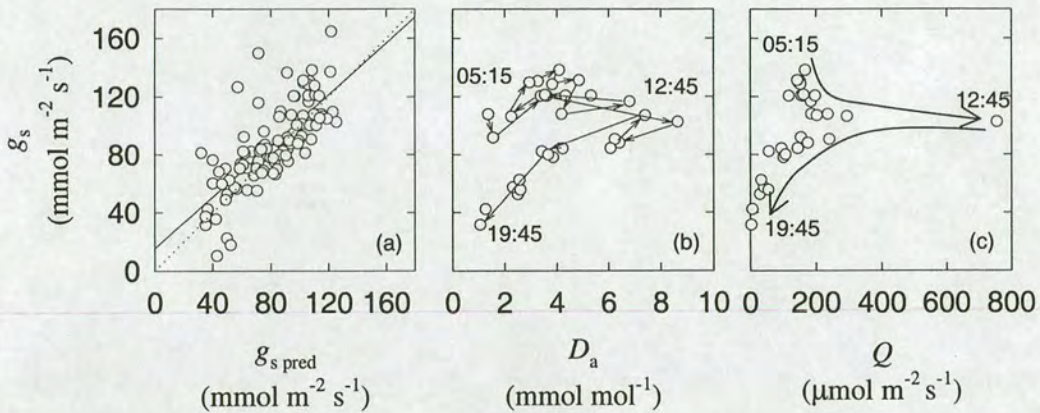


Figure 6.4 Daytime stomatal conductance predicted by the L-BWB model plotted against (a) measured stomatal conductance (b) ambient D_a and (c) Q from data obtained from two chambers in July 2001 and averaged see Table 5.3. $a_1 = 3508$, $D_0 = 30$ and $g_0 = 38$. The line shows the regression; $g_s = 15.37 + 0.88g_{s \text{ pred}}$, $r^2 = 0.55$, $n=98$. Broken line shows 1:1.

Chamber	n	a_1 $\pm 95\%$ CI (dimensionless)	D_0 $\pm 95\%$ CI (mmol mol ⁻¹)	g_0 $\pm 95\%$ CI (mmol m ⁻² s ⁻¹)
1	94	2340 2157 - 2523	44 16 - 73	36 33 - 39
3	92	4213 3803 - 4623	24 8 - 39	46 40 - 52
Average (1 and 3)	95	3508 3252 - 3764	30 15 - 46	38 34 - 42

Table 6.3 Parameter values for the L-BWB model fitted to two chamber data-sets collected under daytime natural conditions in Griffin Forest during July 2001.

Most of the variation in g_s was observed under conditions of very low D_a (< 0.5 mmol mol⁻¹) and branch transpiration (E_L) during early morning periods, leading to observed g_s both much larger and smaller than that predicted. This is possibly

because g_s estimated under these conditions are extremely noisy as the humidity probes are incapable of measuring very small changes in relative humidity at the extremes of the calibration range (McDermitt, 1990). Furthermore, at low D_a , g_s is likely to be large, so that a random error of the same proportion will be numerically larger than at high D_a . Therefore, the measured g_s at these times are most likely an artefact and unreliable as suggested by the plot of residuals against D_a (Figure 6.5c). The model also did not predict g_s well at higher D_a ($>8 \text{ mmol mol}^{-1}$) as there were few data available over this range for fitting the model Figures 6.5c and 6.6.

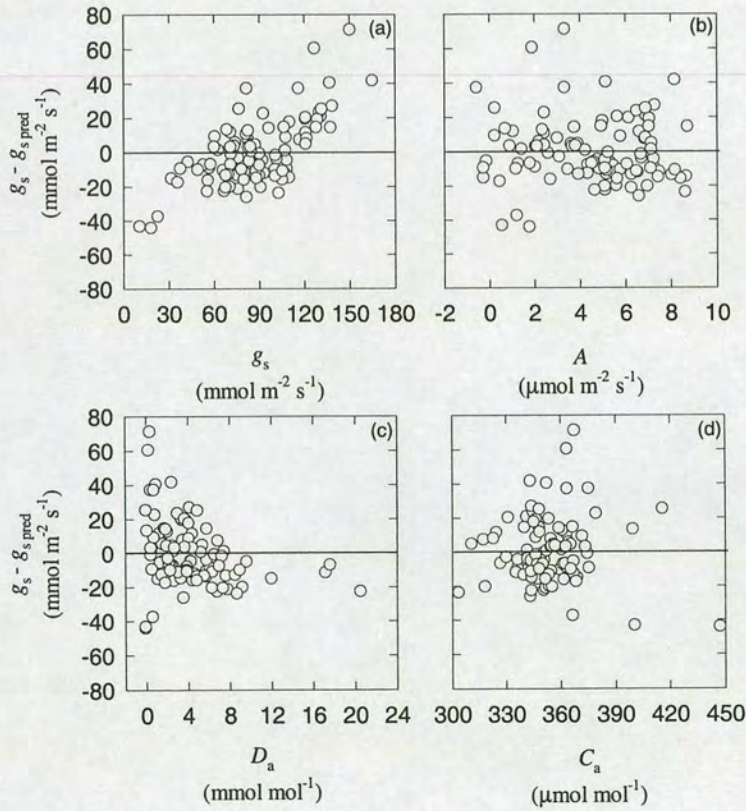


Figure 6.5 Plots of residuals (observed – predicted) against (a) g_s , (b) A , (c) D and (d) C_a for the L-BWB fit shown in Figure 6.4.

Consequently, this led to an overestimation of g_s by the model on the 22nd July, during brighter conditions (Figure 6.6). This is apparent in the residual plot which indicates a weak relationship between residuals and D_a . The regression equation was $g_s - g_{s \text{ pred}} = 7.00 (\pm 2.78) + -1.70 (\pm 0.51) g_s$, $r^2=0.09$, $n=98$. Furthermore, the residual plot, Figure 6.5a, displayed a positive correlation between g_s and the residuals. The regression equation for this observation was $g_s - g_{s \text{ pred}} = -39.18 (\pm 4.63) + 0.45 (\pm 0.05) g_s$, $r^2=0.44$, $n=98$. This indicated that when g_s are low the model tends to overestimate g_s and when g_s are high the model tends to underestimate g_s .

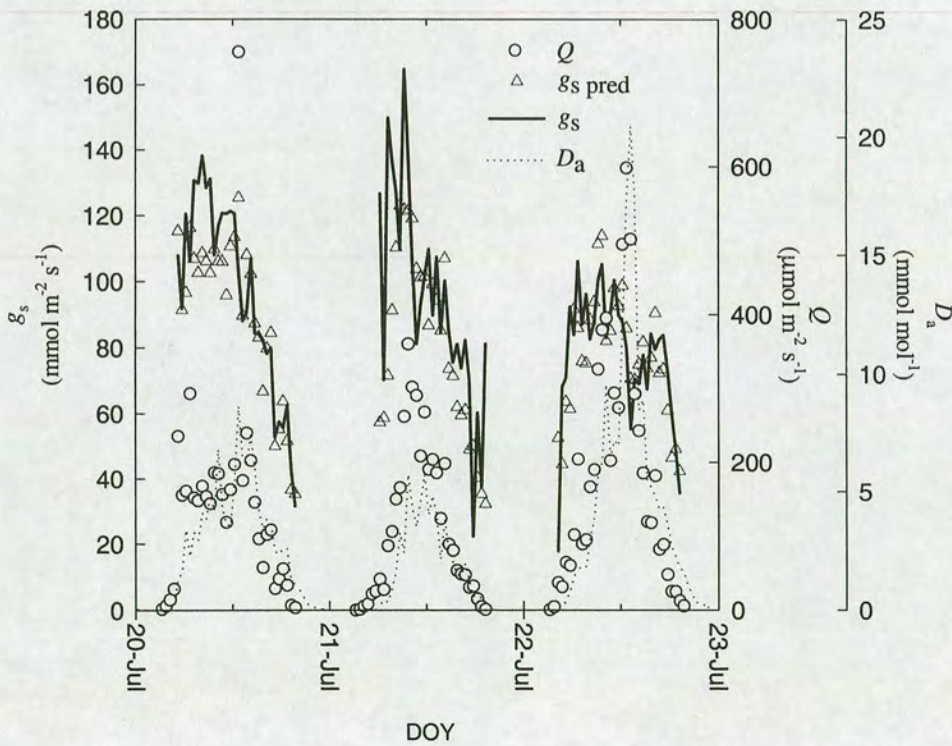


Figure 6.6 Daily variation of chamber Q , D_a , g_s and $g_{s \text{ pred}}$ predicted from the fitted L-BWB relationship for two chambers during July 2001 at Griffin Forest.

Eddy flux and chamber estimates

Values of canopy conductance to water vapour (G_s) were initially calculated for eddy covariance measurements using a one-dimensional inversion of the Penman-Monteith equation, thereby treating the canopy as a 'big leaf'. Where branch data was available, estimates of G_s were also made from branch chamber data using two approaches as described in Chapter 5. Briefly, the first approach scaled observed g_s for a two layered sun/shade canopy with L of $3 \text{ m}^2 \text{ m}^{-2}$ in each. The second approach used the fitted L-BWB relationship to predict g_s in a canopy of 6 layers each containing L $1 \text{ m}^2 \text{ m}^{-2}$. The fitted relationship was coupled to a simple radiation model that was used to predict A from a fitted non-rectangular hyperbola relationship.

G_s were highest early in the morning and gradually decreased over the course of the day (Figure 6.7). Maximum G_s values of 1.5 and $0.8 \text{ mol m}^{-2} \text{ s}^{-1}$ were calculated for the first two mornings, with values dropping to $0.4 \text{ mol m}^{-2} \text{ s}^{-1}$ around midday, eventually decreasing to around $0.3 \text{ mol m}^{-2} \text{ s}^{-1}$ later in the afternoon (Table 6.4). For the first two days of the study period no branch data was available for comparison. Estimates of G_s over the following calmer day were quite different between eddy covariance and branch-derived estimates (Figure 6.7). The patterns of G_s between methods were similar during the afternoon but differences of at times 50% between scaled up and L-BWB branch and eddy covariance estimates were apparent in the morning. This period was characterised by low D_a , R_{net} , ζ and U (Figure 6.1). Maximum values of 0.48 and $0.52 \text{ mol m}^{-2} \text{ s}^{-1}$ were estimated from scaled and modelled branch estimates, respectively (Table 6.4), whilst G_s from eddy covariance only reached a maximum of $0.35 \text{ mol m}^{-2} \text{ s}^{-1}$. Mean values for the branch methods were also similar to within $0.03 \text{ mol m}^{-2} \text{ s}^{-1}$, with mean eddy covariance estimates lower than the lowest chamber-based estimate by $0.19 \text{ mol m}^{-2} \text{ s}^{-1}$ (Table 6.4). In contrast on the 21st and 22nd July differences between means for each method were

smaller ranging from 0.31 to 0.38 mol m⁻² s⁻¹ for the 21st and 0.29 to 0.40 mol m⁻² s⁻¹ on the 22nd (Table 6.4). Maximum canopy conductance of 0.97 and 1.52 mol m⁻² s⁻¹ were observed for the 21st and 22nd, respectively. Over the 21st and 22nd branch modelled G_s tended to exhibit a similar pattern and values to Penman-Monteith estimates over the day, with a few exceptional points. However, the branch-derived methods gave slightly different estimates on the 22nd and were systematically offset by *ca.* 0.11 mol m⁻² s⁻¹, with L-BWB estimates predicting the higher G_s . There seems to be a discrepancy between the scaling approach rather than the performance of the L-BWB model itself. Figure 6.6 clearly shows that L-BWB and scaled branch measurements were well matched with one another and therefore scaling assumptions are responsible for the difference.

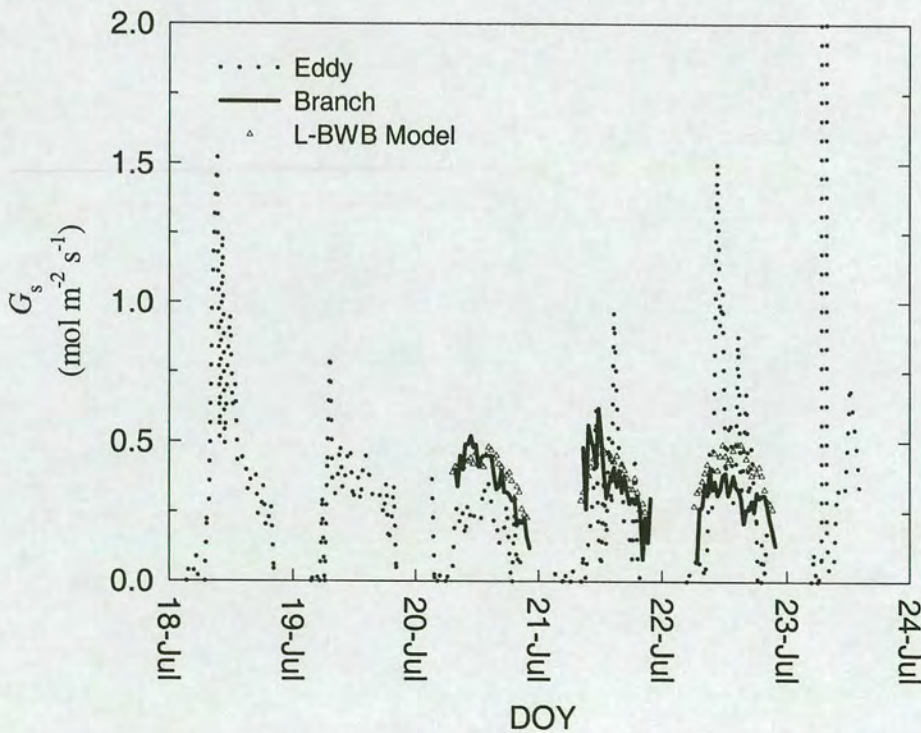


Figure 6.7 Canopy stomatal conductance (G_s) estimated from the inverted Penman-Monteith Model using measured environmental variables[†] and eddy covariance estimates for E^{\dagger} , scaled branch chamber measurements of g_s and fitted L-BWB predictions for conductance. [†] indicates data collected by R. Clement (University of Edinburgh, UK).

↓Method / Date →	Mean and Maximum Canopy Conductance (G_s mmol m ⁻² s ⁻¹)					
	(n)					
	Mn ± 1SD (n)	Max	Mn ± 1SD (n)	Max	Mn ± 1SD (n)	Max
	20th		21st		22nd	
Inverted Eddy	0.17 ± 0.11	0.35	0.31 ± 0.24	0.97	0.34 ± 0.37	1.52
Covariance	(32)		(21)		(33)	
Scaled	0.36 ± 0.11	0.52	0.36 ± 0.12	0.62	0.29 ± 0.07	0.40
Branch	(30)		(27)		(31)	
L-BWB	0.39 ± 0.07	0.48	0.38 ± 0.08	0.49	0.40 ± 0.07	0.49
Model	(30)		(27)		(31)	

Table 6.3 Daytime mean and maximum rates of canopy conductance (G_s) for a three-day period during July 2001 using different approaches.

6.1.4 Ecosystem respiration

Soil respiration

Sampling of CO₂ efflux from the soil surface was stratified into three distinguishable areas: Ridge; Flat; and Furrow illustrated in Figure 2.1. Soil CO₂ efflux was sampled at a number of sites with varying L ($n = 3$) each containing 12 soil collars, four placed randomly within each of the three areas (see section 5.4.2). The soil CO₂ efflux measured from each area was then tested using SAS, PROC ANOVA. Mean soil CO₂ efflux was found to differ significantly between areas ($P=0.004$) but was not significantly different between site (Figure 6.8). Mean soil temperature at 1 cm and 5cm (T_1 and T_5) and soil volumetric water content (θ_{6cm}) also measured at each collar location also did not differ significantly between sites. However, there were significant differences between areas for both T_{5cm} ($P=0.000$) and θ_{6cm} ($P=0.001$) (Figure 6.8).

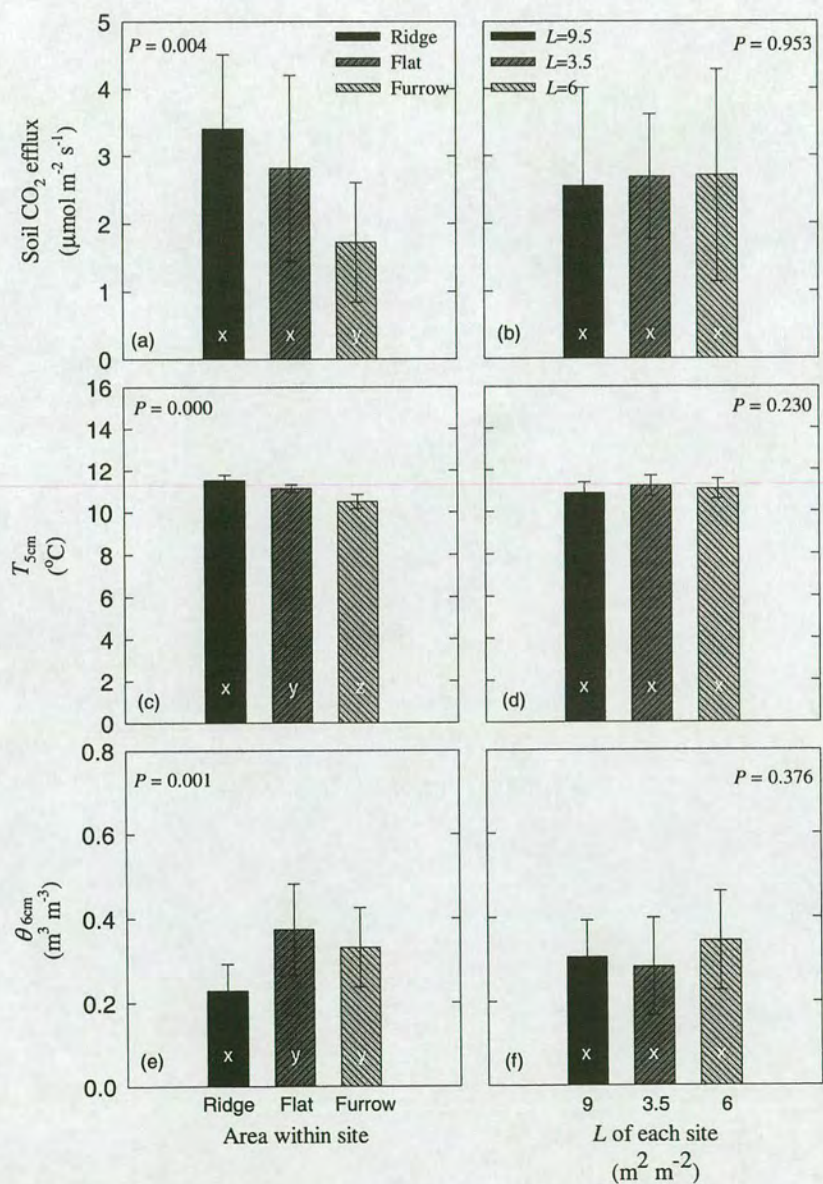


Figure 6.8 Variation in (a) soil CO₂ efflux, (c) soil temperature at 5 cm depth (T_5) and (e) soil volumetric water content at 0–6 cm depth ($\theta_{6\text{cm}}$) measured in three different areas and (b) soil CO₂ efflux, (d) soil temperature at 5 cm depth (T_5) and (f) soil volumetric water content at 0–6 cm depth ($\theta_{6\text{cm}}$) measured in three sites of varying L at Griffin Forest during July 2000. Each bar represents the mean value ± 1 SD for each variable with n=12. Bars with the same letter indicate no differences between sample means i.e. P>0.05.

The diurnal variation in soil CO₂ efflux was monitored on 20th July 2001 for 24 h (Figure 6.9a). The soil CO₂ efflux decreased in the order ridge > flat > furrow with mean soil efflux rates (\pm 1SD, n=24) of 2.27 ± 0.75 , 1.62 ± 0.80 and 1.13 ± 0.77 $\mu\text{mol m}^{-2} \text{s}^{-1}$, respectively and was conserved over the course of the day (Table 6.5). However, there was one sampling occasion at 18:00 h when this order broke down and furrow CO₂ efflux rates exceeded those for both the ridge and flat strata. Furrow CO₂ efflux rates maintained a close relationship with soil and litter temperatures over the period and consequently continued to increase with rising soil temperatures until reaching a maximum efflux for the 24 h period at approximately 18:00 h, coinciding with the maximum observed soil temperature. During this period of maximum soil temperature both the ridge and flat CO₂ efflux rates deviated from the soil temperature response followed up until this point. This deviation from the temperature response corresponded with a decrease in the volumetric water content for both the ridge and flat over the top 15 cm of soil, indicating a possible moisture constraint on efflux rates.

Analysis of soil CO₂ efflux data collected independently in static closed chambers over the ridge and flat areas also confirmed this decrease in CO₂ efflux rates during the soil temperature maximum. The static chamber sampling also showed a transient depletion in the $\delta^{13}\text{C}$ composition of soil CO₂ efflux at this time. This shift in $\delta^{13}\text{C}$ was approximately -9‰ from the calculated $\delta^{13}\text{C}$ composition of soil respired CO₂, -29.1 ± 0.3 ‰ (\pm 1SD n=19) observed over the rest of the day (Figure 6.9b). After this depletion in $\delta^{13}\text{C}$, a later sample then indicated an enrichment of soil respired CO₂ to -27.5‰.

The $\delta^{13}\text{C}$ of respired CO₂ between chamber locations differed by *ca.* 1‰, with static chamber 2 values significantly (P=0.01) more depleted than static chamber 1 values. Furthermore, there was no correlation between $\delta^{13}\text{C}$ of soil respired CO₂ and soil

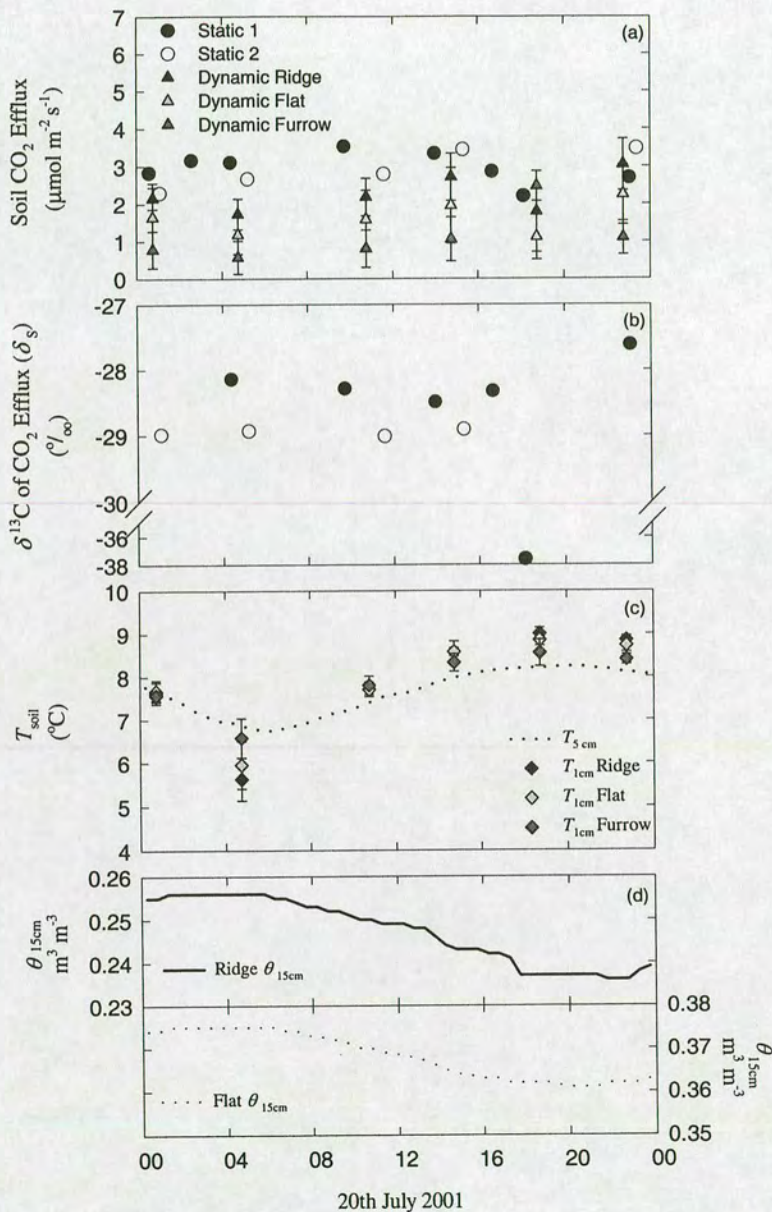


Figure 6.9 Variation in (a) soil CO₂ efflux, (b) δ¹³C of soil respired CO₂ (δ_s)(c) soil temperature at 1 cm and 5 cm depth (T₁) and (T₅) and (d) soil volumetric water content over 15 cm depth measured within different areas at Griffin Forest during July 2001. Each point for soil CO₂ efflux and T₁ represents the mean value for an area ±1SD for each variable with n=4. Continuous soil temperature and volumetric water content measurements represent the mean value for every 30 min. Static chamber symbols represent discrete point measurements over an area encompassing both ridge and flat areas.

CO₂ efflux rate. Differences in absolute flux rates calculated from the two methods were apparent over the 24 h period. The static chamber method tended to give slightly higher values than the dynamic ridge and flat estimates. However, on four out of the six sampling occasions the static efflux rates were within the error bars of the dynamic estimates. Furthermore, the temperature response of soil CO₂ efflux for static chambers was not as obvious as that for the dynamic chamber measurements. However, differences between methods on the two occasions during the morning were approximately, 0.5 to 1 $\mu\text{mol m}^{-2} \text{s}^{-1}$, and this represents a difference of between 15 to 30%. This might be expected given the substantial differences in chamber size, gas sampling method and measurement time for each method.

Modelling soil, branch and ecosystem respiration

Using parameters derived from measurements of nocturnal net ecosystem exchange ($F_{E,N}$), soil CO₂ efflux and nocturnal branch respiration (R_n) (Table 6.5), half-hourly respiration rates were modelled using air and soil temperature measurements. Exploring the differences of T , U^* and partial inhibition of daytime dark respiration yielded six sets of ecosystem respiration (see Chapter 5 for further details). In brief the following combinations were examined:

- estimating ecosystem respiration using the fitted relationship between nocturnal measurements of net CO₂ exchange ($F_{E,N}$) and soil temperature which included all U^* conditions ($F_R(T_s)$);
- estimating ecosystem respiration using the fitted relationship between nocturnal measurements of net CO₂ exchange ($F_{E,N}$) and soil temperature which excluded all U^* conditions $<0.2 \text{ m s}^{-1}$ ($F_R(T_s \text{ and } U^*)$);
- estimating ecosystem respiration using the fitted relationship between nocturnal measurements of net CO₂ exchange ($F_{E,N}$) and air temperature which included all U^* conditions ($F_R(T_a)$);

- estimating ecosystem respiration using the fitted relationship between nocturnal measurements of net CO₂ exchange ($F_{E,N}$) and air temperature which excluded all U^* conditions $<0.2 \text{ m s}^{-1}$ ($F_{R(Ta \text{ and } U^*)}$) ;
- estimating ecosystem respiration using relationships between CO₂ efflux and temperature observed in soil and branch chambers and scaled to the biomass using inventory data (see Chapter 2). Soil data used for fitting the temperature response were collected during both day and night conditions. Branch data observed continuously at night were used to fit the temperature response and applied during the day assuming no inhibition of daytime dark respiration rates ($F_{R(Rn)}$) and;
- the same as for $F_{R(Rn)}$ except for the inclusion of a model that simulates the partial inhibition of daytime dark respiration in response to fluctuations in Q and T_l ($F_{R(Rd)}$).

Values of the parameter describing $F_{R(Ta)}$, $F_{R(Ts)}$ at 10 °C (R_{10}) did not differ significantly, this was also the case for $F_{R(Ta \text{ and } U^*)}$ and $F_{R(Ts \text{ and } U^*)}$. However, estimates of R_{10} between U^* treatments did vary by ca. $1 \mu\text{mol m}^{-2} \text{ s}^{-1}$ with R_{10} higher when low U^* were excluded. A considerable amount of data collected at Griffin Forest during the night occurred under low U^* conditions. Approximately 42% of the available data was removed to calculate $F_{R(Ta \text{ and } U^*)}$ and $F_{R(Ts \text{ and } U^*)}$. Modelled respiration rates for soil and measured data from branches were summed for each 30 min period and compared with modelled $F_{R(Ta)}$, $F_{R(Ts)}$, $F_{R(Ta \text{ and } U^*)}$ and $F_{R(Ts \text{ and } U^*)}$ (Figure 6.10 and Table 6.6).

Scale of Measurement	R_{10} ($\mu\text{mol m}^{-2} \text{s}^{-1}$) 95% CI	n	Mean R ($\mu\text{mol m}^{-2} \text{s}^{-1}$) \pm 1SD	n
$F_{R(T)}$	4.37 4.29 – 4.45	9466	3.9 ± 0.9	61
$F_{R(Ts)}$	4.36 4.28 – 4.45	9313	3.7 ± 0.2	61
$F_{E,N}$			3.9 ± 4.4	70
$F_{R(T \text{ and } U^*)}$	5.23 5.15 – 5.30	5500	4.8 ± 1.1	48
$F_{R(Ts \text{ and } U^*)}$	5.34 5.27 – 5.42	5450	4.6 ± 0.2	48
$F_{E,N}$			5.6 ± 3.5	48
$R_{s(Ts)}$				
Ridge	2.6 2.37 – 2.81	128	2.3 ± 0.8	24
Flat	2.0 1.84 – 2.15	128	1.6 ± 0.8	24
Furrow	0.9 0.70 – 1.18	128	1.1 ± 0.8	24
$R_n(Tn)$	2.25 2.14 – 2.40	107	1.5 ± 0.7	107

Table 6.5 Parameters obtained from the relationship between temperature and 5 years of $F_{E,N}^{\dagger}$, 1 year of soil CO_2 efflux and 3 days nocturnal branch respiration data collected between 20th to 23rd July and used in the simulation of component and ecosystem respiration for Griffin Forest during 20th to 23rd July 2001. [†] indicates data collected by R. Clement (University of Edinburgh, UK).

Good correlations between chamber and eddy covariance estimates of F_R using T_a occurred during the night ($r^2 = 0.42$). The best agreement of F_R estimates occurred between $F_{R(Ta) \text{ Night}}$ and $F_{R(Rn)}$ especially at respiration rates $< 4 \mu\text{mol m}^{-2} \text{s}^{-1}$. Figures 6.10 and 6.11 show that the sum of soil and branch respiration rates were higher than estimates for $F_{R(Ta)}$, $F_{R(Ts)}$ and $F_{R(Ts \text{ and } U^*)}$. This is highlighted in Figure 6.12, which clearly shows total branch and soil respiration rates exceeding 100% of the flux estimated using $F_{R(Ta)}$, $F_{R(Ts)}$ and $F_{R(Ts \text{ and } U^*)}$ on occasion. In contrast, soil and branch respiration rates were generally between 70 to 90% of the filtered U^* star

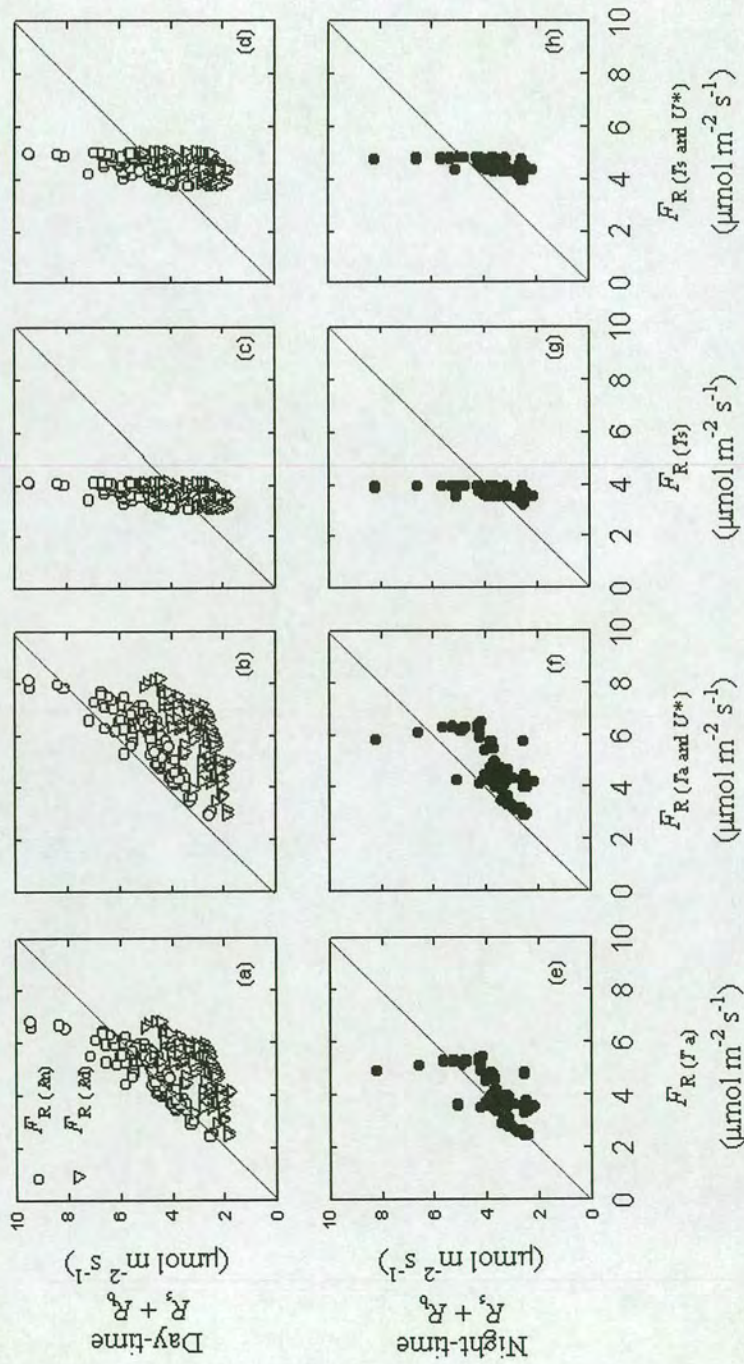


Figure 6.10 Ecosystem respiration rates predicted from fitted Arrhenius temperature responses for soil and branches assuming either inhibition or no inhibition of day respiration, plotted against F_R \dagger modelled using air temperature \dagger (a, b, e and f) or soil temperature \dagger (c, d, g and h) and including all U^* (a, c, e and g) or excluding $U^* < 0.2 \text{ m s}^{-1}$ (b, d, f and h). The solid line indicates the 1:1 slope. \dagger Indicates data collected by R. Clement (University of Edinburgh, UK).

estimates. In general, the range of fluxes observed between temperature treatments were very different with $F_{R(Ts)}$ maintaining a conservative range of $1 \mu\text{mol m}^{-2} \text{s}^{-1}$ compared with $>4 \mu\text{mol m}^{-2} \text{s}^{-1}$ for $F_{R(Ta)}$. The T_a range seemed to encapsulate the range observed for the summed components better.

Chamber models vs $F_{E,N}$ models		Slope $\pm 1\text{SD}$	Intercept $\pm 1\text{SD}$	r^2	n	Mean x	Mean y
$F_R(Ts \text{ and } U^*)$	vs $F_R(Rd)$	1.31 ± 0.21	-2.8 ± 0.9	0.19	172	4.55	3.21
$F_R(Ts \text{ and } U^*)$	vs $F_R(Rn)$	2.10 ± 0.30	-5.1 ± 1.4	0.22	172	4.55	4.45
$F_R(Ts \text{ and } U^*) \text{ Night}$	vs $F_R(Rn)$	2.43 ± 0.48	-7.4 ± 2.2	0.29	61	4.56	3.68
$F_R(Ts \text{ and } U^*) \text{ Day}$	vs $F_R(Rn)$	2.08 ± 0.32	-4.6 ± 1.5	0.27	111	4.54	4.88
$F_R(Ts \text{ and } U^*) \text{ Day}$	vs $F_R(Rd)$	0.99 ± 0.19	-1.5 ± 0.9	0.19	111	4.54	2.95
$F_R(Ts)$	vs $F_R(Rd)$	1.61 ± 0.25	-2.8 ± 0.9	0.19	172	3.71	3.21
$F_R(Ts)$	vs $F_R(Rn)$	2.57 ± 0.37	-5.1 ± 1.4	0.22	172	3.71	4.45
$F_R(Ts) \text{ Night}$	vs $F_R(Rn)$	2.97 ± 0.58	-7.4 ± 2.2	0.29	61	3.72	3.68
$F_R(Ts) \text{ Day}$	vs $F_R(Rn)$	2.55 ± 0.40	-4.6 ± 1.5	0.27	111	3.71	4.88
$F_R(Ts) \text{ Day}$	vs $F_R(Rd)$	1.21 ± 0.23	-1.5 ± 0.9	0.19	111	3.71	2.95
$F_R(Ta \text{ and } U^*)$	vs $F_R(Rd)$	0.31 ± 0.05	1.5 ± 0.3	0.18	172	5.48	3.21
$F_R(Ta \text{ and } U^*)$	vs $F_R(Rn)$	0.86 ± 0.05	-0.2 ± 0.3	0.62	172	5.48	4.45
$F_R(Ta \text{ and } U^*) \text{ Night}$	vs $F_R(Rn)$	0.64 ± 0.10	0.6 ± 0.5	0.42	61	4.78	3.68
$F_R(Ta \text{ and } U^*) \text{ Day}$	vs $F_R(Rn)$	0.88 ± 0.07	-0.3 ± 0.4	0.61	111	5.87	4.88
$F_R(Ta \text{ and } U^*) \text{ Day}$	vs $F_R(Rd)$	0.36 ± 0.03	0.4 ± 0.2	0.49	111	5.87	2.95
$F_R(Ta)$	vs $F_R(Rd)$	0.37 ± 0.06	1.5 ± 0.3	0.18	172	4.58	3.21
$F_R(Ta)$	vs $F_R(Rn)$	1.03 ± 0.06	-0.2 ± 0.3	0.62	172	4.58	4.45
$F_R(Ta) \text{ Night}$	vs $F_R(Rn)$	0.76 ± 0.12	0.6 ± 0.5	0.42	61	3.99	3.685
$F_R(Ta) \text{ Day}$	vs $F_R(Rn)$	1.06 ± 0.08	-0.3 ± 0.4	0.61	111	4.91	4.88
$F_R(Ta) \text{ Day}$	vs $F_R(Rd)$	0.53 ± 0.05	0.4 ± 0.2	0.49	111	4.91	2.95

Table 6.6 Linear regression parameters describing the relationship between ecosystem respiration[†] ($F_R(Ta)$, $F_R(Ts)$, $F_R(Ta \text{ and } U^*)$ and $F_R(Ts \text{ and } U^*)$) and the component sum of soil and branch respiration with ($F_R(Rd)$) and without ($F_R(Rn)$) inhibition of day respiration during 20th to 23rd July 2001. [†] indicates data collected by R. Clement (University of Edinburgh, UK).

During the day agreement between the estimates made with the different methods was variable, the greatest correlation observed being those using T_a and $F_R(Rn)$, $r^2 = 0.62$. Again T_s did not describe the predicted range of R_s and R_b during the day despite having a slightly larger range of $2 \mu\text{mol m}^{-2} \text{s}^{-1}$. Uncertainties regarding the extent of respiratory inhibition during the day can complicate both estimations of F_R and F_A . Respiration rates including the effect of partial inhibition by Q were always

lower than the rates estimated for $F_R(T_a)$, $F_R(T_s)$, $F_R(T_a \text{ and } U^*)$ and $F_R(T_s \text{ and } U^*)$ (Figures 6.10 and 6.11).

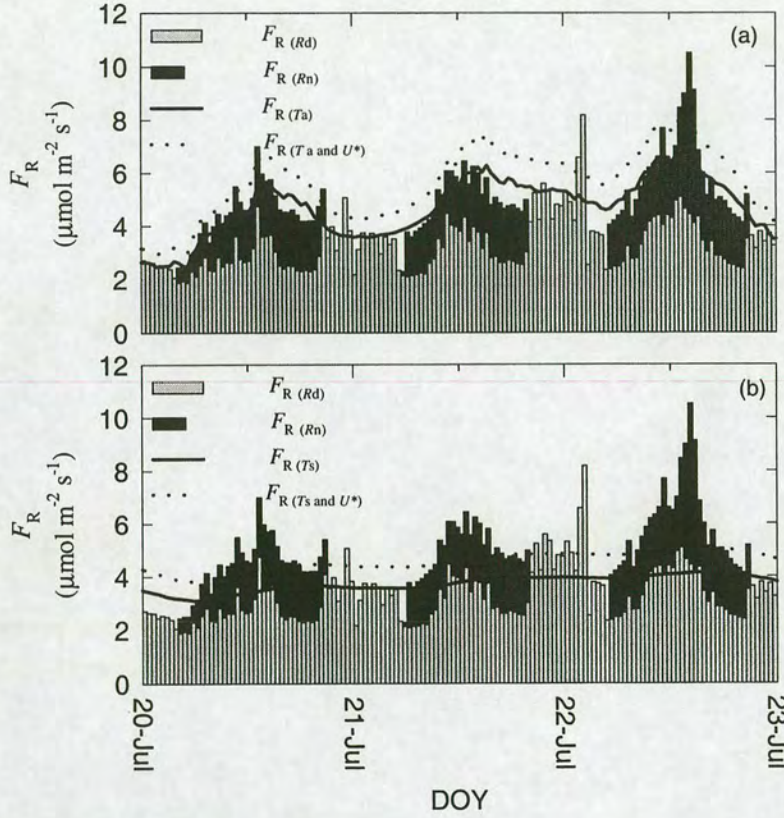


Figure 6.11 Daily variation in F_R estimated using the six different approaches (a) $F_R(T_a)$, $F_R(T_a \text{ and } U^*)$, $F_R(R_d)$, and $F_R(R_n)$, (b) $F_R(T_s)$, $F_R(T_s \text{ and } U^*)$, $F_R(R_d)$, and $F_R(R_n)$, for Griffin Forest, during July 2001.

Differences between the two methods were typically 1 to 2 $\mu\text{mol m}^{-2} \text{s}^{-1}$ most of the day but on occasion reached almost 5 $\mu\text{mol m}^{-2} \text{s}^{-1}$ when fluxes were high. $F_R(T_a)$ vs $F_R(R_d)$ values occasionally lay on the 1:1 line but were more commonly found below, with maximum differences of *ca* 2 $\mu\text{mol m}^{-2} \text{s}^{-1}$. Over the period, the influence of partial inhibition was most apparent in the evening when Q was low and T_a were highest (Figures 6.2 and 6.11). Maximum F_R of 5 and 11 $\mu\text{mol m}^{-2} \text{s}^{-1}$ were predicted by $F_{R(R_d)}$ and $F_{R(R_n)}$, respectively after midday when daytime temperatures

were highest on the 22nd July (Figure 5.1). However, estimates were more commonly between 3 and 5 $\mu\text{mol m}^{-2} \text{s}^{-1}$ for $F_{R(Rd)}$ and 5 and 7 $\mu\text{mol m}^{-2} \text{s}^{-1}$ for $F_{R(Rn)}$. If there was no inhibition of respiration then it is apparent that $F_{R(Ta)}$ best describes the magnitude, timing and pattern of the summed soil and branch components. Moreover, $F_{R(Ts)}$ describes a very different pattern and magnitude over time, especially compared to the no inhibition scenario. $F_{R(Ts)}$ does however, provide values similar to the inhibited scenario during the day but only at midday.

Modelled soil respiration contributed between 40 to 70% of the total flux estimated using $F_{R(Ta)}$, with the largest contribution from the soil component occurring at night when soil temperatures were highest. However, using T_s the soil component remained a constant $\sim 50\%$ of $F_{R(Ts)}$ and $\sim 45\%$ of $F_{R(Ts \text{ and } U^*)}$. If $F_{R(Ta \text{ and } U^*)}$ represented total ecosystem respiration, the contribution from the soil component never reached more than 60% of this value, with soil contributing between 30 to 50% of the total, for the remainder of the time. The measured branch contribution to respiration was substantial at night, accounting for approximately 30 to 50% of the total respiratory flux. This resulted in the contribution of soil and branch respiration equalling $F_{R(Ta)}$, $F_{R(Ts)}$, $F_{R(Ta \text{ and } U^*)}$ and $F_{R(Ts \text{ and } U^*)}$ at times (Figure 6.12). During the day inhibition of respiration altered the contribution of branch respiration considerably.

If respiration was indeed inhibited by Q the contribution from branches to the total flux was between 10 and 20 % of $F_{R(Ta \text{ and } U^*)}$, or between 20 and 30 % of $F_{R(Ta)}$. If T_s was used to force the relationship, the contribution of branch respiration was between 20 and 60%. In comparison if no inhibition occurred, then the contribution of branches to the overall respiratory flux was between 40 and 60% on average if T_a was used but 30 to 90% if T_s was used instead.

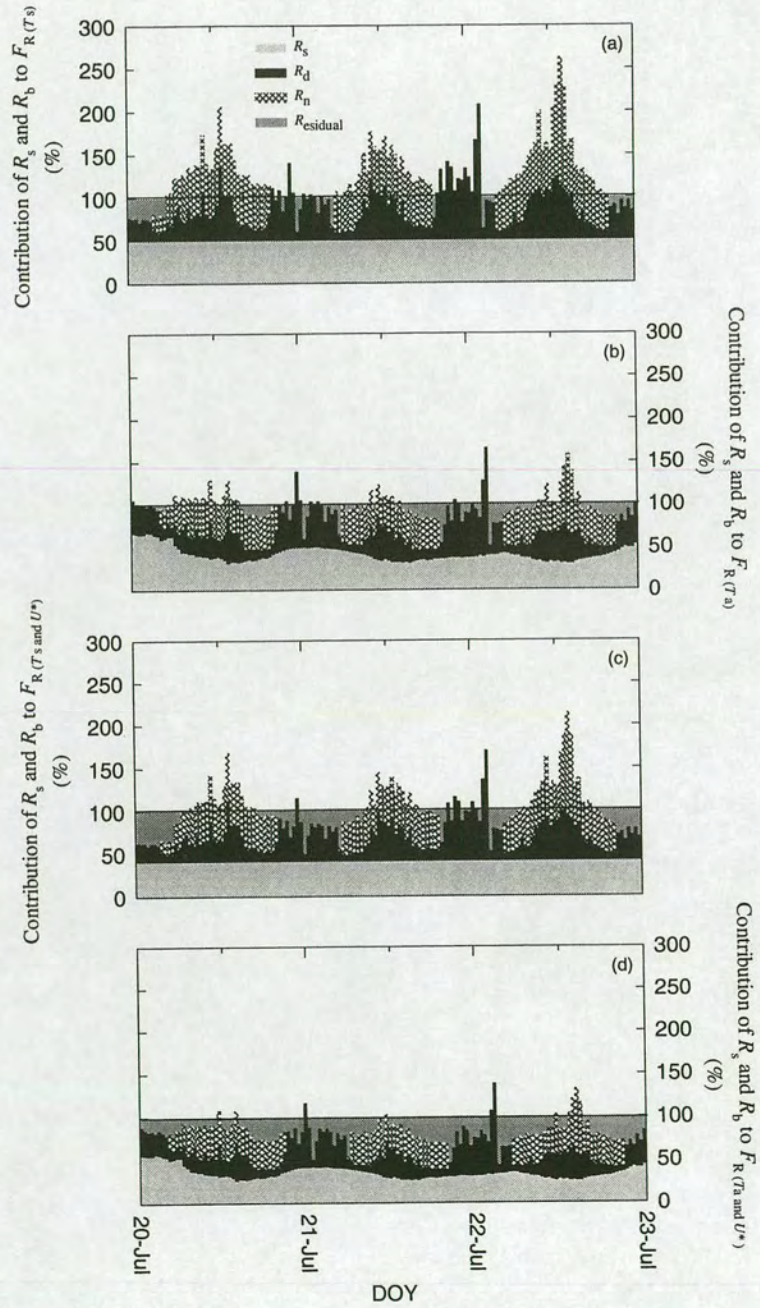


Figure 6.12 Daily variation in the component contribution of R_s , R_n and R_d to (a) $F_R(T_s)$, (b) $F_R(T_a)$, (c) $F_R(T_s \text{ and } U^*)$ and (d) $F_R(T_a \text{ and } U^*)$ for Griffin Forest, during July 2001.

Lastly, the difference between the chamber-derived estimates of ecosystem respiration and that measured by eddy covariance is named hereon as the 'residual flux' and is shown in Figure 6.12. This residual flux may account for CO₂ losses from other respiring organisms in the ecosystem, that were unmeasured during this study, e.g. tree stems and heather, moss and grass from areas where the canopy is open. The contribution of this flux to the total varied depending on the model used to describe $F_{E,N}$ with T . The mean contributions were 3 ± 25 , 6 ± 18 , 20 ± 21 and 21 ± 15 % for $F_{R(Ts)}$, $F_{R(Ta)}$, $F_{R(Ts \text{ and } U^*)}$ and $F_{R(Ta \text{ and } U^*)}$, respectively (± 1 SD, $n=62$). The fluxes corresponding to these contributions are 0.1, 0.2, 0.9 and 1.0 $\mu\text{mol m}^{-2} \text{s}^{-1}$ for the observation period.

6.1.5 Canopy photosynthesis

Modelling branch photosynthesis

All data collected in the branch chambers during July 2001 were pooled and used to describe the response of branch assimilation rates to Q , by fitting a non-rectangular hyperbola (e.g., Ögren & Evans, 1993) to the datasets using non-linear curve fitting (PROC NLIN, SAS) (see Eq 5.16, Chapter 5 for further details). Figure 6.13a shows the fit of the light response function to the measured assimilation rates. Linear regression results for measured A against A_{pred} were, $A = 0.022 (\pm 0.17) + 0.99 (\pm 0.03) A_{\text{pred}}$, $r^2 = 0.88$ ($n=110$). Figure 6.13b represents the Q response for upper canopy branches. Assimilation rate approximates a linear function of Q up to 200 $\mu\text{mol m}^{-2} \text{s}^{-1}$, after which the response began to saturate.

The average quantum requirement for branches was approximately 20 (± 5) photons per mole of fixed CO₂; the average assimilation rate under saturating Q was 7.02 (± 0.78) $\mu\text{mol m}^{-2} \text{s}^{-1}$; and the average apparent dark respiration for the branches was

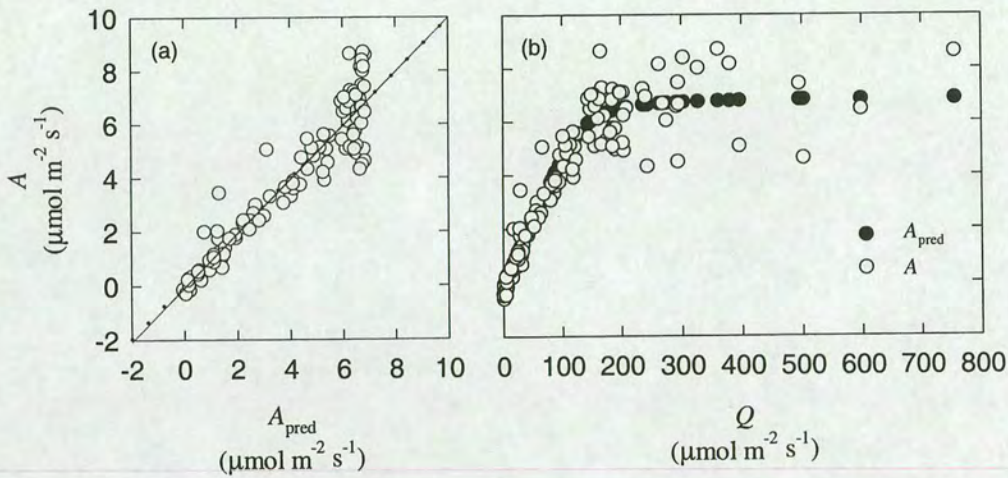


Figure 6.13 (a) Assimilation rate predicted by the A/Q function plotted against measured assimilation rate data obtained from two chambers in July 2001. The broken line shows the regression; $A = 0.022 + 0.99A_{\text{pred}}$, $r^2 = 0.88$. The solid line shows 1:1. (b) The relationship between observed and predicted assimilation rate and Q for branches in the upper canopy, measured under natural conditions during 20th to 23rd July 2001. Values are means for two branch chambers under various conditions of T_a and D_a . A_{pred} fitted using the parameters $A_{\text{max}} = 7.02$, $R_d = 0.12$, $\phi = 0.05$ and $\Theta = 0.97$

Chamber	n	A_{max} ($\mu\text{mol m}^{-2} \text{s}^{-1}$) ±95% CI	ϕ ($\mu\text{mol CO}_2 \mu\text{mol } Q^{-1}$) ±95% CI	R_d ($\mu\text{mol m}^{-2} \text{s}^{-1}$) ±95% CI	Θ ±95% CI
1	106	7.97 8.0 – 9.0	0.08 0.06 – 0.11	0.34 -0.22 – 0.90	0.89 0.75 – 1.03
3	104	7.09 5.7 – 8.5	0.04 0.03 – 0.06	0.24 -0.45 – 0.92	0.96 0.85 – 1.07
Average (1 and 3)	110	7.02 6.2 – 7.8	0.05 0.04 – 0.06	0.12 -0.33 – 0.57	0.97 0.90 – 1.03

Table 6.7 Parameter values for the A/Q function fitted to two chamber data-sets collected under natural light, during 20th to 23rd July 2001.

$0.12 (\pm 0.45) \mu\text{mol m}^{-2} \text{s}^{-1}$; errors are 95% confidence limits, $n=110$ (Table 6.7). The range of -0.33 to $0.57 \mu\text{mol m}^{-2} \text{s}^{-1}$ for average R_d measured over the natural temperature range compares well with the R_{10} , 95% confidence limits of between

0.57 – 0.64 $\mu\text{mol m}^{-2} \text{s}^{-1}$ (Table 6.5). The mean respiration rate R_d from the Q response curve was *ca* 80% lower than the night-time R_n rates of 0.6 $\mu\text{mol m}^{-2} \text{s}^{-1}$.

The residual plots in Figure 5.14a-f highlight three main features. Firstly they indicate little skew in the Q response function across the observed range of natural environmental variables. Secondly, data for warmer and drier conditions were under represented during this period and conditions of this type could cause an over-estimation of A by this model. Finally, because of the iterative fitting procedure that seeks to reduce the sum of squares, A_{max} was $< A$ on occasion. At times when conditions were optimal for A , e.g., when D_a was low (2 to 8 mmol mol^{-1}) and T_a (10 to 18 °C), then A was up to 2.5 $\mu\text{mol m}^{-2} \text{s}^{-1}$ higher than A_{max} .

Conversely, when temperatures exceeded 18 °C and $D_a > 10 \text{ mmol mol}^{-1}$, the function tended to overestimate A_{max} by 2.5 $\mu\text{mol m}^{-2} \text{s}^{-1}$. Linear regression analysis (PROC REG, SAS) of the residuals against all environmental variables found no significant relationships at the 5% level. An alternative fitting procedure could involve boundary line analysis or the creation of a more complicated multiplicative model that accounted for the effects of other environmental variables. However, as there were only a few occasions when environmental conditions caused such deviations during the period, this simple approach was adopted.

Eddy covariance and chamber-based estimates of canopy photosynthesis

Canopy photosynthesis (F_A) was calculated using two methods. The *first method* used relationships derived from the branch chamber data (Table 6.7). This was coupled to a simple radiation model to yield within canopy Q as a function of incoming Q using the parameters from Meir *et al.*, (2002) and described further in

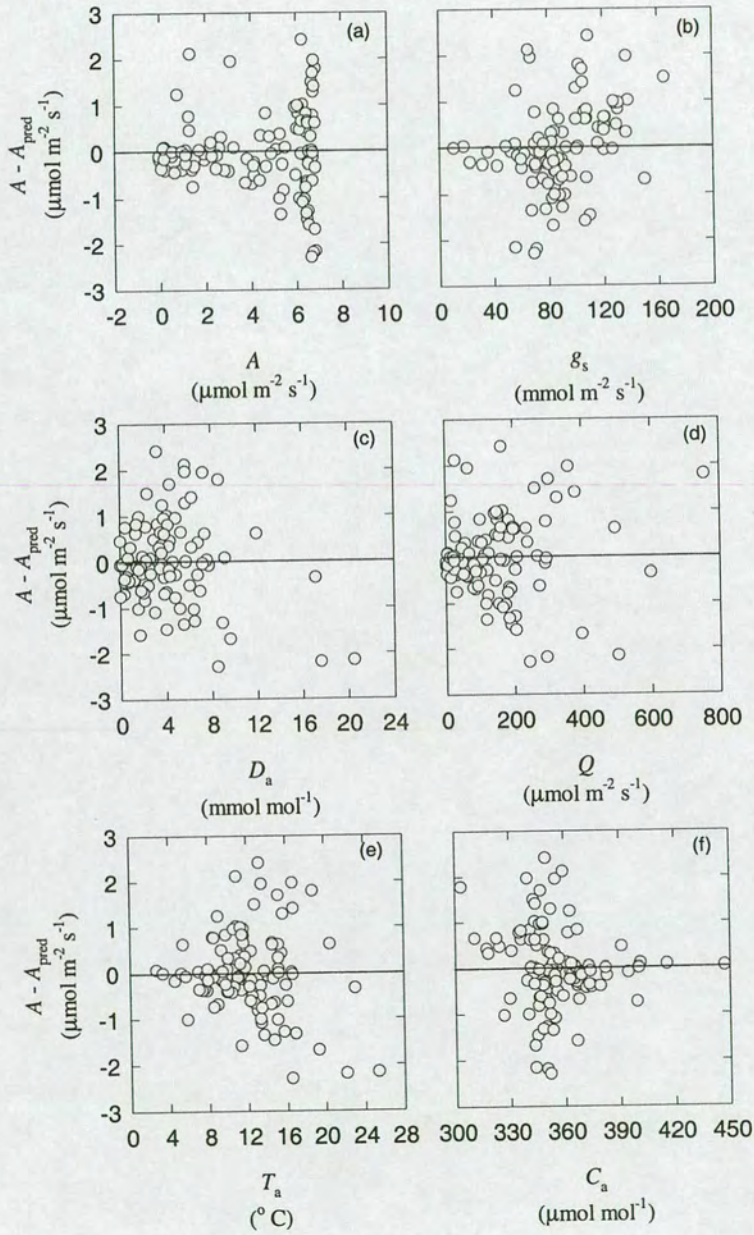


Figure 6.14 Plots of residuals (observed – predicted) against (a) A , (b) g_s , (c) D_a , (d) Q , (e) T_a and (f) C_a for the A/Q fit shown in Figure 6.13.

Chapter 5. Canopy carboxylation (v_c), photo-respiration ($0.5v_o$) and day respiration, with inhibited and non-inhibited mitochondrial respiration (R_d and R_n) during the day, were then calculated following the method described in Chapter 3. $F_{A(Rd)}$ and $F_{A(Rn)}$ were then calculated as $(v_c - 0.5v_o)$ accounting for both R_d or R_n , respectively. The fluxes of R_d and R_n directly contributed to $F_{R(Rd)}$ and $F_{R(Rn)}$, along with modelled soil CO_2 efflux for each 30 min interval. The *second method* used the results from $F_{R(Ta)}$, $F_{R(Ts)}$, $F_{R(Ta \text{ and } U^*)}$ and $F_{R(Ts \text{ and } U^*)}$ and the measurements of net ecosystem exchange measured during the day ($F_{E,D}$) to solve the CO_2 mass balance for $F_{A(Ta)}$, $F_{A(Ts)}$, $F_{A(Ta \text{ and } U^*)}$ and $F_{A(Ts \text{ and } U^*)}$.

Estimates of F_A using the different assumptions and methods followed closely the daily pattern in environmental variables (Figures 6.1, 6.2, 6.15 and 6.16) and $F_{E,D}$ measured above the canopy. The pattern of instantaneous fluxes estimated using tower and chamber methods, were similar for a given change in environmental variables. However, the absolute magnitude of the fluxes was somewhat different for each model. The mean of all values for $F_{A(Ta)}$ and $F_{A(Ta \text{ and } U^*)}$ were 29 to 43% lower than the mean fluxes predicted from $F_{A(Rd)}$ and $F_{A(Rn)}$ (Figures 6.15, 6.16, 6.17 and Table 6.8).

Comparison of Figures 6.15 and 6.16 indicate that $F_{A(Rd)}$ and $F_{A(Rn)}$ predict larger F_A occurring earlier in the morning and later in the evening than the eddy covariance methods. This could indicate that photosynthesis was re-assimilating some of the CO_2 released by nighttime respiration that was retained within the canopy volume and not exchanged with the atmosphere. This would indicate that the canopy is taking up CO_2 both earlier and later than is apparent from the eddy covariance data.

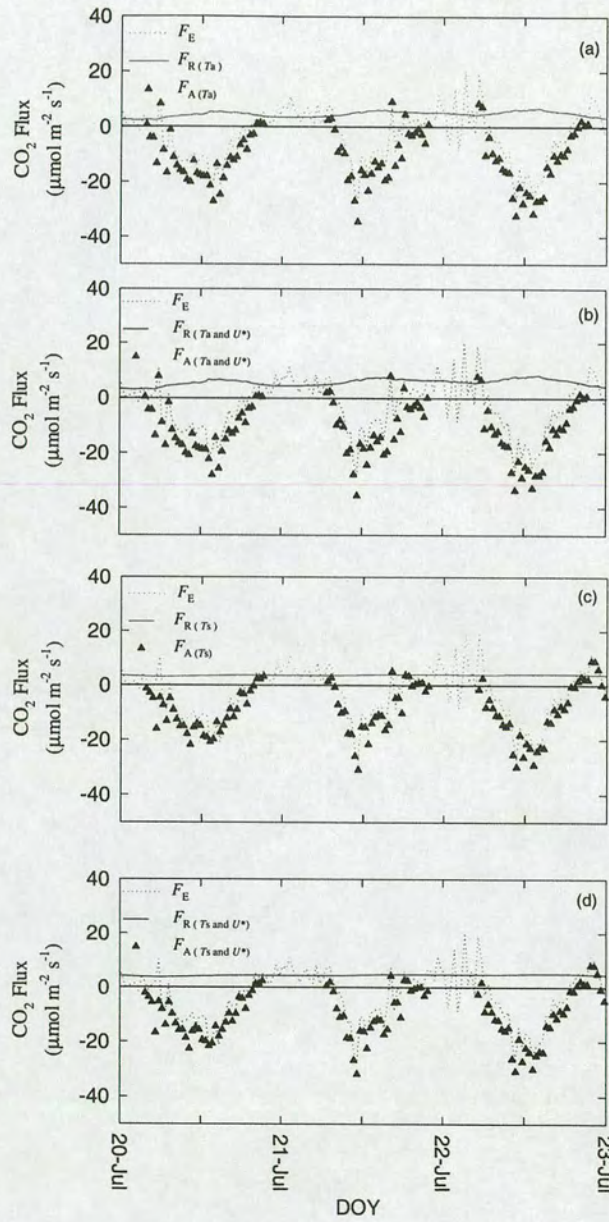


Figure 6.15 Daily variation in net ecosystem exchange (F_E)[†], canopy assimilation F_A and ecosystem respiration F_R (a) and (b) including all U^* (c) and (d) excluding $U^* < 0.2 \text{ m s}^{-1}$ (a) and (c) using T_s and (b) and (d) using T_a , July 2001. [†] indicates data collected by R. Clement (University of Edinburgh, UK).

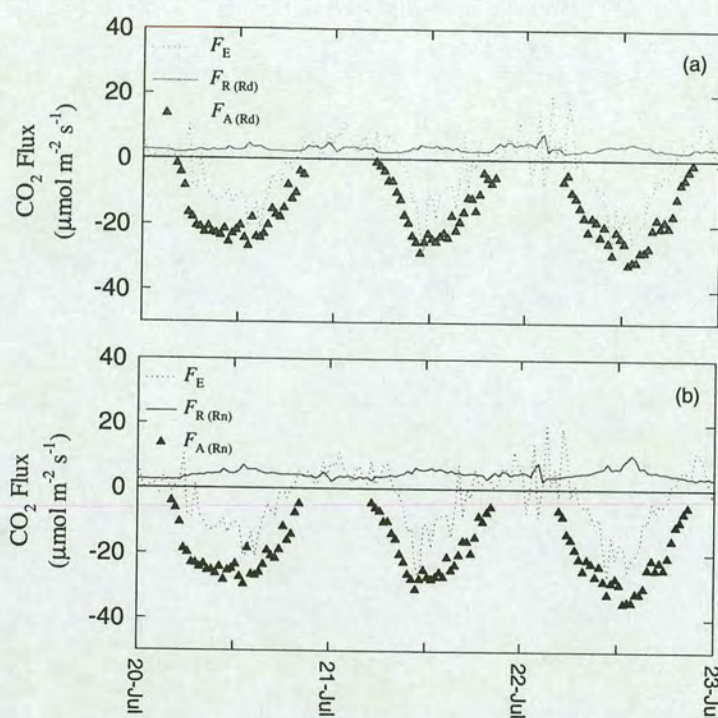


Figure 6.16 Daily variation in net ecosystem exchange (F_E)[†], canopy assimilation F_A and ecosystem respiration for chamber-based estimates of F_R (a) including inhibition of respiration (R_d) and (b) excluding inhibition of respiration (R_n), July 2001. [†] indicates data collected by R. Clement (University of Edinburgh, UK).

The closest between method agreement indicated from the mean values, was between $F_{A(Ta \text{ and } U^*)}$ and $F_A(R_d)$. Of the models generated using $F_{E,N}$ data, $F_A(Ta \text{ and } U^*)$ always resulted in larger values of F_A , but the means were not significantly different. This was expected given the higher value of R_{10} for $F_R(Ta \text{ and } U^*)$. Estimates of $F_A(Ta)$ were usually 4 to 20 % lower than those for $F_A(Ta \text{ and } U^*)$ over the day, with the largest differences between the two occurring during early morning and late afternoon periods, when fluxes were lowest (Figure 6.15). This difference was also observed for the model employing T_s . $F_A(T_s \text{ and } U^*)$ were typically 10 to 20% lower than $F_A(Ta \text{ and } U^*)$. After midday these differences reduced somewhat, primarily as a consequence of increasing soil temperatures and decreasing air temperatures.

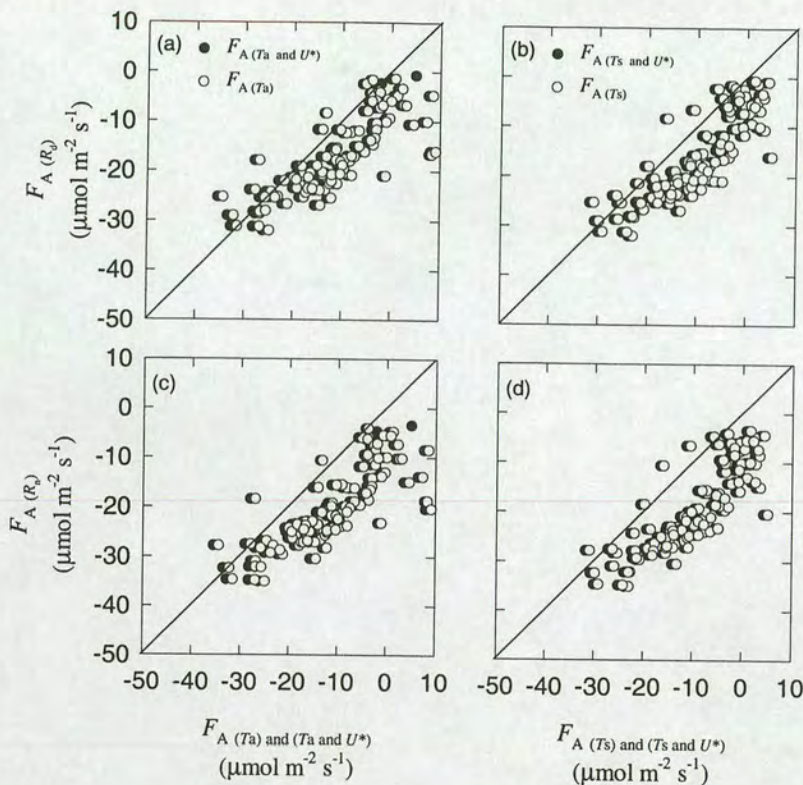


Figure 6.17 Assimilation rates predicted using chamber data relationships plotted against those predicted from $F_{E,n}^{\dagger}$ during the daytime period (a) and (b) assuming inhibition of day respiration (R_d); (c) and (d) no inhibition of day respiration (R_n); and using (a) and (c) T_a ; or (b) and (d) T_s . The line indicates the 1:1 slope. † indicates data collected by R. Clement (University of Edinburgh, UK).

Nocturnal $F_{E,N}$ models vs chamber-based models	Slope \pm 1SD	Intercept \pm 1SD	r^2	n	Mean x	Mean y
$F_A(T_s \text{ and } U^*)$ vs $F_A(R_d)$	0.85 ± 0.07	-8.2 ± 1.0	0.60	100	-11.7^a	-18.2^b
$F_A(T_s \text{ and } U^*)$ vs $F_A(R_n)$	0.91 ± 0.07	-10.1 ± 1.0	0.61	100	-11.7^a	-20.8^b
$F_A(T_s)$ vs $F_A(R_d)$	0.85 ± 0.07	-8.9 ± 0.9	0.60	100	-10.8^a	-18.2^b
$F_A(T_s)$ vs $F_A(R_n)$	0.91 ± 0.07	-10.8 ± 1.0	0.61	100	-10.8^a	-20.8^b
$F_A(T_a \text{ and } U^*)$ vs $F_A(R_d)$	0.75 ± 0.06	-8.4 ± 1.0	0.61	100	-12.9^a	-18.2^b
$F_A(T_a \text{ and } U^*)$ vs $F_A(R_n)$	0.81 ± 0.06	-10.3 ± 1.0	0.63	100	-12.9^a	-20.8^b
$F_A(T_a)$ vs $F_A(R_d)$	0.76 ± 0.06	-9.1 ± 0.9	0.61	100	-11.9^a	-18.2^b
$F_A(T_a)$ vs $F_A(R_n)$	0.82 ± 0.06	-11.0 ± 1.1	0.63	100	-11.9^a	-20.8^b

Table 6.8 Linear regression parameters describing the relationship between ecosystem assimilation estimated using different models. Similar superscripts indicate no significant differences between sample means, i.e., $P > 0.05$. Different superscripts indicate significant differences between sample means at the $P < 0.001$ level.

Estimates from chamber relationships correlated well with F_A (T_s and U^*), F_A (T_s), F_A (T_a and U^*) and F_A (T_a) (Table 6.8). Correlation with F_A (R_n) was best with some values falling on or close to the 1:1 line (Figure 6.17 and Table 6.8). Estimates of F_A from scaled branch relationships varied depending on the assumptions of dark respiration. Models generated from $F_{E,N}$ did not have significantly different means ($P>0.05$), whereas chamber-based estimates were significantly different from $F_{E,N}$ models at the $P<0.0001$ level (PROC ANOVA, SAS). Estimates assuming no inhibition of dark respiration during the day gave the largest estimates of F_A across all models (Figure 6.15, 6.16, 6.17 and Table 6.8).

Method ↓	Mean (\pm 1SD) and Maximum Canopy Assimilation Rates (F_A) ($\mu\text{mol m}^{-2} \text{s}^{-1}$)					
	Mn \pm 1SD (n)	Max	Mn \pm 1SD (n)	Max	Mn \pm 1SD (n)	Max
Date →	20th		21st		22nd	
F_A (T_s)	12.0 \pm 5.9 (31)	21.8	9.3 \pm 9.3 (28)	30.9	12.7 \pm 9.5 (32)	29.9
F_A (T_s and U^*)	12.7 \pm 5.9 (31)	22.6	10.1 \pm 9.3 (28)	31.8	13.6 \pm 9.5 (32)	30.8
F_A (T_a)	12.7 \pm 7.4 (31)	27.0	10.7 \pm 10.1 (28)	34.4	14.0 \pm 10.9 (32)	32.2
F_A (T_a and U^*)	13.5 \pm 7.5 (31)	28.0	11.7 \pm 10.2 (28)	35.5	15.2 \pm 11.0 (32)	33.5
F_A (R_d)	17.5 \pm 7.0 (33)	26.6	15.17 \pm 8.3 (31)	28.6	18.70 \pm 8.6 (33)	32.0
F_A (R_n)	20.3 \pm 7.1 (33)	29.6	18.4 \pm 8.2 (31)	30.9	22.4 \pm 8.7 (33)	35.0
F_A (Eddy Gc)	20.4 \pm 6.6 (20)	35.2	28.4 \pm 20.4 (18)	77.9	38.5 \pm 30.1 (25)	124.9
F_A (Eddy Gc and Gw)	14.5 \pm 4.5 (20)	24.8	16.1 \pm 7.5 (18)	30.3	18.9 \pm 8.8 (24)	32.0
F_A (Branch Gc and Gw)	19.6 \pm 5.7 (22)	29.0	20.4 \pm 4.4 (19)	28.8	18.6 \pm 3.8 (24)	25.0
F_A (L-BWB Gc and Gw)	20.26 \pm 4.9 (22)	29.9	21.4 \pm 3.8 (19)	28.6	21.3 \pm 3.7 (24)	25.5

Table 6.9 Daily mean and maximum rates of canopy assimilation (F_A) for a three day period during July 2001 using different models.

Maximum CO₂ uptake rates varied by 5 to 8 $\mu\text{mol m}^{-2} \text{s}^{-1}$ between days and 3 to 7 $\mu\text{mol m}^{-2} \text{s}^{-1}$ across all methods for each day (Table 6.9). There was no consistent pattern in the order of maximum values between methods over the three days. Maximum values ranged between -27 to -36 $\mu\text{mol m}^{-2} \text{s}^{-1}$ between days and methods. Mean uptake rates varied by 4 $\mu\text{mol m}^{-2} \text{s}^{-1}$ between days and 8 $\mu\text{mol m}^{-2} \text{s}^{-1}$ across methods for each day. In contrast for maximum estimates there was a consistent pattern to daily mean uptake rates which followed the order $F_{A(Rn)} > F_{A(Rd)} > F_{A(T \text{ and } U^*)} > F_{A(T)}$. Daily mean values ranged from -10 to -22 $\mu\text{mol m}^{-2} \text{s}^{-1}$ across all days and methods.

6.1.6 Application of Stable Isotopes

Isotopic composition of ecosystem respired CO₂

To partition F_E into F_A and F_R , information contained in the isotopic signature of respired CO₂ from the ecosystem and each measured component was determined. Figures 6.18a and b show all the flask data collected over the 24 h period. The solid line in Figure 6.18a describes the nighttime ecosystem respired signature and its relationship to different components at different times of the day. The regression equation for the line was $\delta_a = -29.54 (\pm 0.4) + 7953 (\pm 171)(1/C_a)$ $r^2=0.996$, $n=9$. The daytime data for branches on the plot are conspicuous, as they fall away from the integrated value of the ecosystem under the influence of photosynthetic ¹³C discrimination, which itself is variable over the day (see Chapter 3 and 4). The solid line in Figure 6.18b in contrast describes the net result of photosynthesis, respiration and turbulent transfer during the day. This solid line relationship was used to generate the above canopy values of $\delta^{13}\text{C}$ signature of net turbulent exchange, $\delta_{FC} = 2mC_a + n$ (see Bowling *et al.*, 2001, Eq 16). These data were derived from the regression of δ_a versus C_a mole fraction from air samples collected throughout the

canopy when chambers were open during the day. The relationship is described in Figure 6.18b and the regression equation is $\delta_a = 9.889(\pm 1.096) - 0.0482(\pm 0.002)(C_a)$ $r^2=0.960$ $n=20$. Because the goal was to derive rates of F_A , only daytime flasks of $^{13}\text{CO}_2$ were considered.

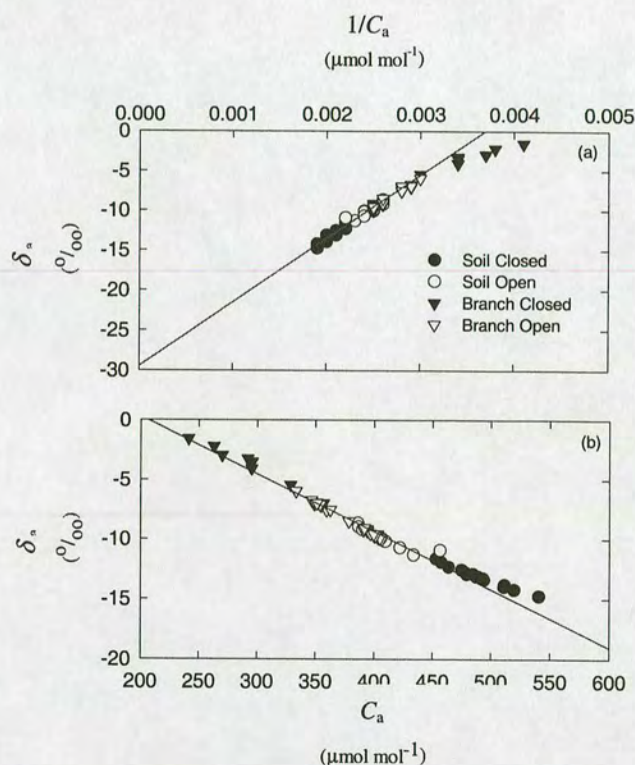


Figure 6.18 (a) A Keeling plot of flask samples collected from soil and branch chambers whilst open and closed. (b) δ_a of forest CO_2 vs C_a mole fraction for the same data. The solid line represents the geometric mean regression for (a) all open chamber samples collected during the night and (b) all open chamber samples collected during the day.

Isotopic composition of component respired CO_2

Flask measurements taken at night were used to characterise the $\delta^{13}\text{C}$ composition of branch and ecosystem respiration. In the case of soil CO_2 efflux only, all flasks collected were used to determine the δ_s . For each component the $\delta^{13}\text{C}$ signal of

respired CO_2 was determined using the Keeling model (Keeling 1961, see Chapter 5). In order to account for errors associated with both CO_2 mole fraction and $\delta^{13}\text{C}$ and to make the relationships comparable with other published studies, geometric mean regressions were calculated (Kermack & Haldane, 1950; Webb *et al.*, 1981). The isotopic composition of the respired CO_2 and substrate for respiration in each component are listed in Table 6.10.

Scale of Measurement	$\delta^{13}\text{C}$ of organic material (‰)	n	$\delta^{13}\text{C}$ of respired CO_2 (‰)	n
Ecosystem			-29.5 ± 0.4	9
Soil	-28.6 ± 0.3	8	-29.1 ± 0.3	19
Branch			-28.2 ± 1.3	6
Shoot Wood				
<i>Lower</i>	-30.4 ± 0.0	2		
<i>Upper</i>	-27.7 ± 0.2	4		
Mean	-28.6 ± 1.3	6		
Foliage				
<i>Lower</i>	-31.1 ± 0.1	4		
<i>Middle</i>	-30.1 ± 0.3	4		
<i>Upper</i>	-29.0 ± 0.1	4		
Mean	-30.1 ± 0.9	12		

Table 6.10 $\delta^{13}\text{C}$ of organic material collected in May 2001 and respired CO_2 measured during 20th July 2001, at Griffin Forest.

The most ^{13}C enriched values for foliage (δ_{needle}) and woody (δ_{wood}) material occurred in the upper canopy. These values were typically enriched by 2 to 3 ‰ relative to values found in the lower canopy. As described in section 4.1.6, Chapter 4 a gradient in δ_{needle} with height was calculated by linear regression SAS, PROC REG and was observed to increase by 0.5 ‰ for every metre down the canopy profile. The regression equation was $\delta_{\text{needle}} = -33.7 (\pm 0.3) + 0.5 (\pm 0.04)$ Crown Height ($r^2 = 0.90$, $n = 17$, $P < 0.0001$). The mean $\delta^{13}\text{C}$ composition of soil organic material (δ_{soil}) was the same as mean δ_{wood} . The $\delta^{13}\text{C}$ composition of respired CO_2

was also very similar to the respective signatures for the bulk substrate value in each component measured (Table 6.10).

The ecosystem respired signature was depleted in ^{13}C with respect to the soil and wood but enriched relative to the foliage composition (Table 6.10). The respired signature of lower branches could not be characterised. As discussed in Chapter 3, when fluxes become very small, errors tend to have a larger impact. CO_2 exchange rates of lower branches in July and September, 2000 (data not shown) were very low and little change in the δ_a was observed over 10 minutes of chamber closure. It would prove extremely difficult to identify a respiratory effect over any sampling errors confidently (see Chapter 3). Furthermore, although the $\delta^{13}\text{C}$ signature of organic material is depleted in the heavier ^{13}C , its overall contribution to the total ecosystem flux and isotopic composition is probably negligible. Seasonal differences between δ_s measured during September, May and July did not differ significantly for static 1 ($P>0.06$) or static 2 ($P>0.24$).

Canopy and ecosystem ^{13}C discrimination

Estimates of instantaneous canopy photosynthetic discrimination were calculated using the simple (Δ_{CS}) and full (Δ_{CF}) models of discrimination developed by Farquhar *et al.*, (1982) (Eq 3.16 and 3.21 see Chapter 3) and estimates for the component fluxes of A measured in branch chambers scaled to the canopy, as described in Chapter 3 and 5 (Figure 5.19). Briefly the simple model utilises estimates of C_i/C_a to determine Δ_{CS} , whereas the full model incorporates the effects of photorespiration, dark respiration and mesophyll conductance and thereby simulates the net canopy ^{13}C discrimination that would be observed in the field (see Chapter 4 for discussion). This model and branch gas exchange data explained the variation of Δ_{obs} for branches in July incredibly well $\Delta_{\text{obs}} = 0.51 (\pm 2.09) + 1.02 (\pm 0.10)$, $r^2 = 0.94$, $n=8$, $P<0.0001$. These estimates of Δ_{C} were coupled with

estimates of δ_s of soil CO_2 efflux, weighted by the efflux to generate an instantaneous estimate of ecosystem discrimination (Δ_E). The differential effects of photosynthesis and respiration on Δ_E could then be explored and used to highlight a potentially useful instantaneous model for predicting and validating daytime relationships of δ_a vs $1/C_a$ i.e., analogous to Keeling plots collected during the day under the influence of photosynthesis, respiration and turbulent exchange.

Over the observation period Δ_{CS} , Δ_{CF} and Δ_E were variable within and between days (Figure 6.19). The time course of Δ_C followed that of environmental variables, G_s and F_A closely. Values ranged from 16.5 to 30 ‰ for Δ_{CS} and 15 to 21.5 ‰ for Δ_{CF} . The highest Δ_C for both models occurred early in the morning and late in the afternoon as found at the branch scale. Maximum values of Δ_C varied between 26.3 and 29.4‰ for the simple model and 21.9 and 26.6‰ for the full model. Predicted Δ_{CS} was systematically larger than Δ_{CF} estimates. Minimum values also varied between days with Δ_{CS} ranging between 16.5 and 19.0‰ and Δ_{CF} values between 14.7 and 16.3‰. When Q was predominately diffuse and D_a low, Δ_C was largest. These conditions co-occurred with large G_s and despite the low light levels, F_A remained moderate. Δ_E values for the observation period were systematically lower than Δ_C , reflecting the contribution of soil respiration. As Δ_C enriches canopy CO_2 in ^{13}C and soil respiration continuously releases CO_2 depleted in ^{13}C , the net result reduces Δ_E relative to Δ_C . For example, when G_s is large in the morning and the relative contribution of F_A is greater than soil respiration, both Δ_C and Δ_E are large. In contrast, by late afternoon the relatively larger contribution of soil respiration is apparent from the gradual decrease in Δ_E , in contrast to Δ_C , which begins to increase tracking the pattern of C_i/C_a . Unlike Δ_C , minimum values of Δ_E occur at the end of the day and not at midday.

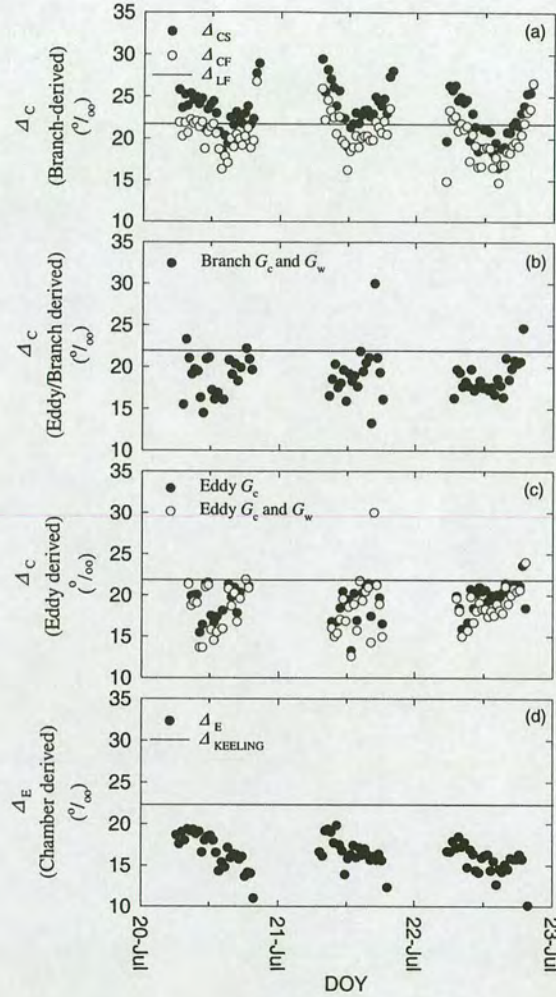


Figure 6.19 Instantaneous and integrated canopy and ecosystem ^{13}C discrimination estimated for the observation period using: (a) chamber-based estimates using a ‘Simple’ C_i/C_a model or a more detailed ‘Full’ model incorporating photorespiration, day respiration and mesophyll conductance; (b) the stable isotope partitioning approach substituting eddy covariance canopy conductance with chamber-based estimates; (c) the stable isotope partitioning approach using eddy covariance G_c only or also including mesophyll conductance; and (d) ecosystem discrimination including the effects of autotrophic and heterotrophic respiration. The solid line in (a) represents Δ_{LF} , the integrated canopy discrimination (‰) ($\Delta_{LF} \approx \delta_a - \delta_R$), where δ_R is calculated from the nocturnal Keeling Plot intercept and the daily average $\delta^{13}\text{C}$ composition of ambient canopy air available for F_A , δ_a , of -7.7 ± 1.2 ‰, $n=12$). δ_i determined from open flasks collected during the daytime from branch chambers. The solid line in (d) represents the integrated ecosystem discrimination, $\Delta_{KEELING}$ (‰) calculated as described by Eq 5.8 and from the nocturnal Keeling plot and assuming a δ_T of -7.8 ‰ for tropospheric composition.

Maximum values of between 18.5 and 19.3‰ were predicted for Δ_E and minimum values ranged between 10.9 and 12.3‰. The integrated values of $\int \Delta_{CS}$, $\int \Delta_{CF}$ and $\int \Delta_E$ calculated from chamber-based measurements are presented in Table 6.11 for each day.

Date → Method ↓	Average whole-canopy integrated photosynthetic discrimination, weighted by assimilation flux ($\int \Delta = \Sigma (\Delta F_A) / \Sigma (F_A)$)		
	20th	21st	22nd
$\int \Delta_{CS}$	22.82	23.49	21.22
$\int \Delta_{CF}$	20.10	20.45	18.84
$\int \Delta_C$ (Eddy Gc)	18.84	19.64	20.20
$\int \Delta_C$ (Eddy Gc and Gw)	17.34	17.89	18.29
$\int \Delta_C$ (Branch Gc and Gw)	18.44	18.24	18.24
$\int \Delta_E$	16.64	16.73	15.27
$\Delta_{KEELING}$	22.41		
Δ_{LF}	21.74		

Table 6.11 Whole canopy and ecosystem integrated discrimination for each day, weighted by F_A and F_R e.g. ($\int \Delta = \Sigma (\Delta \times F_A) / \Sigma F_A$). Integrated ecosystem discrimination, $\Delta_{KEELING}$ (‰) calculated as described by Eq 5.8 and from the nocturnal Keeling plot and assuming a δ_T of -7.8 ‰ for tropospheric composition. Δ_{LF} , the integrated canopy discrimination (‰) ($\Delta_{LF} \approx \delta_a - \delta_R$), where δ_R is calculated from the nocturnal Keeling Plot intercept and δ_i , the daily average $\delta^{13}C$ composition of ambient canopy air available for F_A , δ_a , of -7.7 ± 1.2 ‰, $n=12$). δ_a determined from open flasks collected during the daytime from branch chambers.

$\int \Delta_C$ and $\int \Delta_E$ varied by 1.5 and 1.6‰ between days under the various combinations of environmental variables. $\int \Delta_{CS}$ and $\int \Delta_{CF}$ estimates lay to either side of the estimate of 21.74 ‰ for $\Delta_{LF} \approx (\delta_I - \delta_R)$, where δ_R is calculated from the nocturnal Keeling Plot intercept and δ_i , the daily average $\delta^{13}C$ composition of ambient canopy air available for F_A , δ_i , of -7.7 ± 1.2 ‰, $n=12$. δ_I is determined from open flasks collected during the daytime from branch chambers. The simple model $\int \Delta_{CS}$ was larger than this on two of the three days, whereas the full model $\int \Delta_{CF}$, was systematically smaller than $\int \Delta_{LF}$.

The alternative estimates of Δ_C derived from eddy covariance measurements are also displayed in Figure 6.19b and c. The Bowling approach estimates of Δ_C assuming infinite mesophyll conductance, Δ_C (EDDY G_c), compared with estimates applying a mesophyll conductance, Δ_C (EDDY G_c and G_w), and substituting G_s , Δ_C (BRANCH G_c and G_w), led to slightly different patterns of Δ_C . The largest differences occurred in the mornings when eddy covariance derived values of Δ_C (Figure 6.19 b and c) were smaller than the chamber-based estimates (Figure 6.19a) especially when G_s were high. For instance, minimum Δ_C from eddy covariance-based approaches were observed before midday and reached values $<15\%$. The pattern of Δ_C from eddy covariance measurements seemed to correspond less with chamber-based estimates on diffuse radiation days. $\int \Delta_C$ for the eddy covariance approaches tended to be smaller relative to the chamber-based estimates and the long-term estimates of Δ_{LF} . The only exception to this occurred on the day characterised with high Q , when values for $\int \Delta_C$ (Eddy G_c) were much closer to the chamber-based estimates.

Canopy photosynthesis obtained from $\delta^{13}CO_2$

Using the quadratic equation of Appendix III and data for net ecosystem exchange during the day, ($F_{E,D}$), the calculated isoflux using Eq 5.15, (F_I), canopy conductance to CO_2 , (G_c), the $\delta^{13}C$ of ecosystem respired CO_2 , (δ_R) and the $\delta^{13}C$ of atmospheric CO_2 , (δ_a), canopy assimilation (F_A) and ecosystem respiration, (F_R) could be estimated for the ecosystem. Firstly, estimates of G_c from the inverted Penman-Monteith equation described earlier were used to solve for $F_{A(Eddy\ G_c)}$. Using this method and assuming an infinite mesophyll conductance, mean and maximum F_A for the three days were higher than for all other methods (Figure 6.20 and Table 6.9). However, $F_{A(Eddy\ G_c)}$ values were erratic over the observation period and reached maximums of -78 and $-125\ \mu mol\ m^{-2}\ s^{-1}$, on different days, as much as 2 to 4 times larger than the other F_A estimates for the same days. At these times, additional

evaporation sources, E_1 made an important contribution to the overall water exchange (Figure 6.2 and Table 6.1). Consequently, estimates for eddy covariance-derived G_c used in the solution for F_A exaggerated canopy CO_2 uptake (Table 6.9). Furthermore, at times the quadratic equation for $F_{A(\text{Eddy } G_c)}$ had no real solution. That is why, at times, F_R could not be calculated and the line becomes broken in Figure 6.20. Such a situation occurs when $(\delta_a - \Delta_c)$ is close to δ_R , this essentially describes an isotopic equilibrium situation (i.e. $\delta_a - \Delta_c = \delta_R$) analogous to the apparent fractionation factor e^* described in Chapters 3 and 4. Isotopic equilibrium is a situation most often satisfied in the morning and at dusk. Very early in the morning Δ_c values are high and typically $\delta_a - \Delta_c > \delta_R$. Rapidly after sunrise, C_i/C_a quickly decreases causing Δ_c values to become smaller and $\delta_a - \Delta_c < \delta_R$. Thus, early in the morning there is a brief period when $\delta_a - \Delta_c = \delta_R$, and isotopic equilibrium occurs. In the evening the reverse situation occurs as $C_i/C_a \rightarrow 1$ and $\delta_a - \Delta_c > \delta_R$. Hence when isotopic equilibrium is approached F_A estimates are not very accurate and when isotopic equilibrium occurs there is no solution to the quadratic. In essence this method should work best when isotopic dis-equilibrium is greatest i.e., when Δ_c approaches its minimum value when F_A is highest. It follows that maximum values for F_A using this approach are likely to agree closely to the other independent approaches used to estimate F_A .

The quadratic equation of Appendix III was modified to encompass a further conductance of $0.28 \text{ mol m}^{-2} \text{ s}^{-1}$ for CO_2 transfer to the sites of carboxylation, $F_{A(\text{Eddy } G_c \text{ and } G_w)}$ and used to calculate canopy assimilation. Mesophyll conductance (G_w) was determined using the relationship between Δ_{obs} and that predicted for respiration corrected Δ_R at the branch scale using the Farquhar model and C_i/C_a as described in Chapters 3 and 4. Mean and maximum estimates for $F_{A(\text{Eddy } G_c \text{ and } G_w)}$ became closer to those predicted from the eddy covariance and chamber models (Figures 6.15, 6.16,

6.20 and Table 6.9 and 6.12). Maximum F_A were -25 to $-32 \mu\text{mol m}^{-2} \text{s}^{-1}$ for the three day period with mean

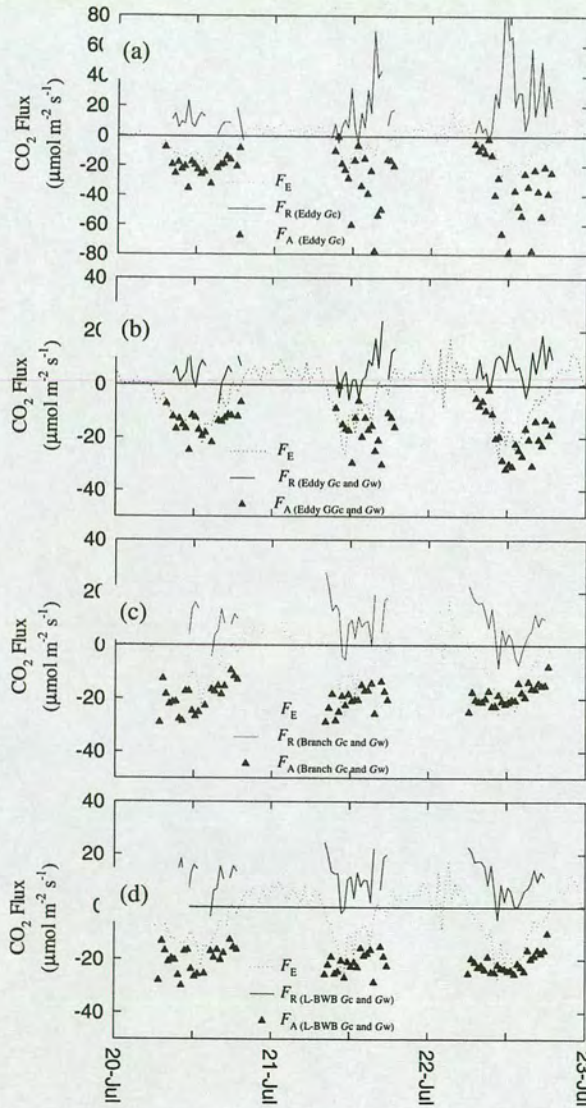


Figure 6.20 Daily variation in net ecosystem exchange (F_E), canopy assimilation (F_A) and ecosystem respiration (F_R) using the $^{13}\text{CO}_2$ partitioning approach: (a) with the inverted Penman-Monteith equation and infinite mesophyll conductance, (b) with the inverted Penman-Monteith equation and a constant mesophyll conductance ($0.28 \text{ mol m}^{-2} \text{s}^{-1}$), (c) with scaled branch measurements of G_c and G_w , and (d) with L-BWB modelled G_c and G_w for, July 2001.

values ranging between -14 and $-19 \mu\text{mol m}^{-2} \text{s}^{-1}$. Maximum and mean rates using this approach were most similar to $F_{A(Rd)}$ and $F_{A(Rn)}$ values; however, the mean rate of assimilation for the 20th July was somewhat lower than the rates predicted by chambers and was most similar to $F_{A(Ta \text{ and } U^*)}$.

¹³ CO ₂ partitioning approaches vs chamber and $F_{E,N}$ models	Slope $\pm 1\text{SD}$	Intercept $\pm 1\text{SD}$	r^2	n	Mean x	Mean y
F_A (Branch Gc and Gw) vs F_A (Ts)	0.76 ± 0.2	0.67 ± 4.4	0.15	62	-19.7	-14.3
F_A (Branch Gc and Gw) vs F_A (Ts and U*)	0.76 ± 0.2	-0.28 ± 4.4	0.15	62	-19.7	-15.2
F_A (Branch Gc and Gw) vs F_A (Ta)	0.85 ± 0.2	0.55 ± 4.6	0.18	62	-19.7	-16.1
F_A (Branch Gc and Gw) vs F_A (Ta and U*)	0.84 ± 0.2	-0.63 ± 4.6	0.17	62	-19.7	-17.2
F_A (Branch Gc and Gw) vs F_A (Rd)	1.01 ± 0.2	-1.92 ± 3.5	0.35	62	-19.7	-21.9
F_A (Branch Gc and Gw) vs F_A (Rn)	0.98 ± 0.2	-5.48 ± 3.7	0.31	62	-19.7	-24.9
F_A (Branch Gc and Gw) vs F_A (Eddy Gc)	0.02 ± 0.7	-29.7 ± 14.2	0.00	62	-19.7	-30.2
F_A (Branch Gc and Gw) vs F_A (Eddy Gc and Gw)	0.29 ± 0.2	-10.9 ± 4.4	0.01	62	-19.7	-16.6
F_A (Branch Gc and Gw) vs F_A (L-BWB Gc and Gw)	0.80 ± 0.0	-5.56 ± 1.0	0.79	62	-19.7	-21.3

Table 6.12 Linear regression parameters describing the relationship between ecosystem assimilation estimated using different approaches.

Canopy conductance estimates for water vapour (G_s) obtained from the inverted Penman-Monteith equation were then substituted with G_s estimates derived from scaled branch chamber measurements and those from the fitted L-BWB relationship to estimate the quadratic solutions for $F_{A(\text{Branch Gc and Gw})}$ and $F_{A(\text{L-BWB Gc and Gw})}$, respectively. Mean and maximum estimates of $F_{A(\text{Branch Gc and Gw})}$ and $F_{A(\text{L-BWB Gc and Gw})}$ were most similar to scaled $F_{A(Rn)}$ estimates (Figures 6.16, 6.20 and Table 6.9). Maximum assimilation rates were around -25 and $-29 \mu\text{mol m}^{-2} \text{s}^{-1}$, with mean uptake rates of $-19 \mu\text{mol m}^{-2} \text{s}^{-1}$. The most noticeable difference in values between $F_{A(\text{Branch Gc and Gw})}$ and $F_{A(\text{L-BWB Gc and Gw})}$ and all the other methods occurred in the early morning when values were larger than expected. This is probably because measurements of g_s below $30 \text{ mmol m}^{-2} \text{s}^{-1}$ at the branch scale were never observed. Consequently, the curve fitting procedure set the lowest conductance, g_0 observed as A and $Q \rightarrow 0 \mu\text{mol m}^{-2} \text{s}^{-1}$ to $38 \text{ mmol m}^{-2} \text{s}^{-1}$ (see Eq 5.18 in Chapter 5 and Table 6.3). Such a large value may result from incomplete stomatal closure and cuticular

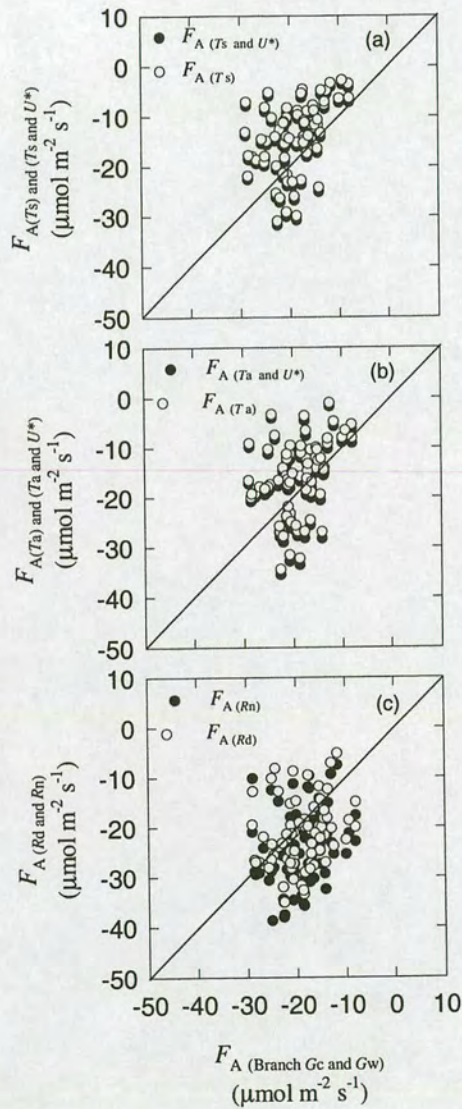


Figure 6.21 Canopy assimilation rates predicted using the stable isotope partitioning approach constrained with chamber G_c and G_w measurements plotted against those predicted from $F_{E,N}^\dagger$ over the day time period using (a) soil temperature, (b) using air temperature and, (c) from branch relationships assuming either inhibition of day respiration (R_d) or no inhibition of day respiration (R_n). The solid line indicates the 1:1 slope. † indicates data collected by R. Clement (University of Edinburgh, UK). All linear regression statistics for plotted data are provided in Table 6.12.

water losses or from moisture retained by foliage or bark when humid conditions persist. Also, the potential effects of evaporation from condensation on chamber walls in the early morning cannot be ruled out. This means that early in the morning $F_{A(\text{Branch } G_c \text{ and } G_w)}$ and $F_{A(\text{L-BWB } G_c \text{ and } G_w)}$ never start from zero like the other estimates for F_A .

There were also a few occasions when $F_{A(\text{Branch } G_c \text{ and } G_w)}$ and $F_{A(\text{L-BWB } G_c \text{ and } G_w)}$ predicted were lower than $F_{E,D}$, and F_R estimates became negative (Figure 5.20). These occasions coincided with drops in U , E and G_c leading to predicted values of F_A lower than $F_{E,D}$ observed.

6.1.7 Daily carbon balance

Estimates of daily ecosystem carbon uptake using the various methods differed between methods by 6, 6 and 12 g C m⁻² s⁻¹ for the 20th, 21st and 22nd of July, respectively (Figure 6.22). Mean daily uptake rates (mean \pm 1SD, $n=3$ days, g C m⁻² d⁻¹) for the different methods decreased in the order $F_{A(\text{Eddy } G_c)}$ (14.5 ± 5.5) $>$ $F_{A(Rn)}$ (14.2 ± 1.8) $>$ $F_{A(Rd)}$ (12.0 ± 1.6) $>$ $F_{A(\text{Branch } G_c \text{ } G_w)}$ (9.8 ± 0.9) = $F_{A(Ta \text{ and } U^*)}$ (9.8 ± 1.8) $>$ $F_{A(Ta)}$ (8.4 ± 1.7) $>$ $F_{A(\text{Eddy } G_c \text{ } G_w)}$ (8.1 ± 1.7) $>$ $F_{A(Ts \text{ and } U^*)}$ (8.0 ± 1.7) $>$ $F_{A(Ts)}$ (7.5 ± 1.7) (Note that the sign convention for daily C uptake is positive). Across the eddy covariance-derived estimates, uptake rates differed by a maximum of 1.83, 2.37 and 2.8 g C m⁻² d⁻¹ for the 20th, 21st and 22nd of July, respectively. Differences between chamber-based and $F_{E,N}$ derived estimates were between 2 and 4.5 g C m⁻² d⁻¹ assuming partial inhibition and between 4.5 and 6.5 g C m⁻² d⁻¹ with no Q inhibition. Estimates of uptake using the stable isotope partitioning approach for $F_{A(\text{Eddy } G_c)}$ gave greater uptake rates than $F_{A(Rn)}$ on the 22nd but lower uptake rates during the diffuse radiation days, this was a direct result of including periods when E_l was high.

Daily ecosystem carbon losses, were typically largest for the partitioning approaches (Figure 6.22). These were particularly noisy and required substantial smoothing. The nocturnal respiration for these estimates used $F_{E,N}$ which were also noisy with some very large instantaneous fluxes (Figure 6.20). For the chamber-based and $F_{E,N}$ derived estimates only, daily C loss rates (mean \pm 1SD, $\text{g C m}^{-2} \text{d}^{-1}$) for the different methods decreased in the order $F_{A(Ta \text{ and } U^*)}$ (7.3 ± 0.5) $>$ $F_{A(Ta)}$ (5.2 ± 0.4) $>$ $F_{A(Ts \text{ and } U^*)}$ (4.8 ± 0.1) $=$ $F_{A(Rn)}$ (4.8 ± 0.3) $>$ $F_{A(Ts)}$ (3.9 ± 0.1) $>$ $F_{A(Rd)}$ (3.4 ± 0.2). Across the $F_{E,N}$ derived estimates, loss rates differed by a maximum of 2.85, 3.81 and 3.58 $\text{g C m}^{-2} \text{s}^{-1}$ for the 20th, 21st and 22nd of July. Differences between chamber-based and $F_{E,N}$ derived estimates were between 0.6 and 4 $\text{g C m}^{-2} \text{s}^{-1}$ assuming inhibition and between 0.6 and 2.7 $\text{g C m}^{-2} \text{s}^{-1}$ with no inhibition.

The net result of these gains and losses are illustrated in Figure 6.22. Because of higher F_A and lower F_R chamber-based estimates gave the highest carbon balance estimates 9.4 ± 1.8 and 8.6 ± 1.8 , $\text{g C m}^{-2} \text{d}^{-1}$ for R_n and R_d , respectively. The net carbon balance estimates for each method were quite different between days, especially the rainy day of the 21st July. The net carbon gain for $F_{E,N}$ derived estimates decreased in the order $F_{A(Ts)}$ (3.6 ± 1.6) $>$ $F_{A(Ts \text{ and } U^*)}$ (3.3 ± 1.6) $>$ $F_{A(Ta)}$ (3.2 ± 1.8) $>$ $F_{A(Ta \text{ and } U^*)}$ (2.5 ± 1.9). The net carbon gain for chamber-based estimates were always larger when no inhibition occurred ($F_{A(Rn)} > F_{A(Rd)}$). The difference in net carbon balance between these two scenarios was $< 1 \text{ g C m}^{-2} \text{s}^{-1}$.

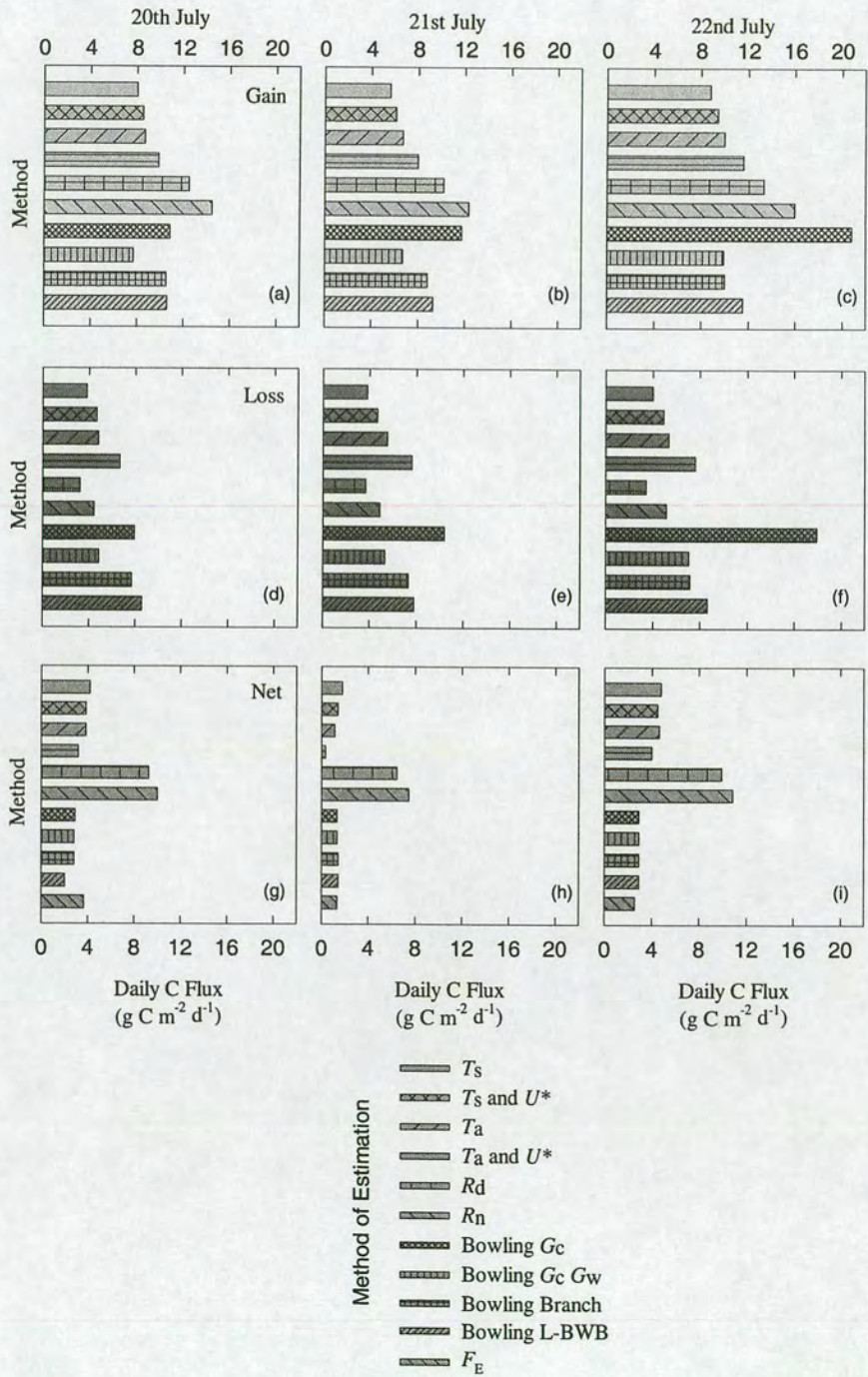


Figure 6.22 Daily carbon (a, b and c) gains, (d, e, and f) losses and (g, h and i) balance for different methods during July for Griffin forest.

6.2 DISCUSSION

6.2.1 Ecosystem water vapour exchange

Ecosystem evaporation

Rates of evapotranspiration from this canopy were similar to those found for another Sitka spruce plantation located in Fetteresso Scotland (3725 stems ha⁻¹) (James, 1977). During dry conditions and at high values of net radiation (400 to 600 W m⁻²), E was about 3.4 ± 1.5 mmol m⁻² s⁻¹ dropping down to 1 mmol m⁻² s⁻¹ at lower R_{net} values (<400 W m⁻²) (James, 1977). The E estimates in this study agreed well with these figures during dry conditions (Figure 6.2 and Table 6.1). During and after rainfall, values for E were also similar to rates found by James (1977) which were between 0.5 to 7.5 mmol m⁻² s⁻¹. Other studies on Sitka spruce at Rivoix, Scotland measured maximum evaporation rates of 7.5 mmol m⁻² s⁻¹ and daily rates of 4.4 mm d⁻¹ (Milne, 1979; Milne *et al.*, 1985). In the above study at Fetteresso daily rates of *ca* 3.0 mm d⁻¹ were measured (James, 1977). These values are also similar to values of E for temperate region *Picea abies* forests. Estimates of maximum E ranged between 7.1 and 9.7 mmol m⁻² s⁻¹, and daily rates of 2.8 and 4.1 mm d⁻¹ (Roberts, 1978; Tajchman, 1972, respectively). Estimates from *Picea mariana* in Boreal forests gave similar daily rates of 0.8 to 4.0 mm d⁻¹ with a mean \sim 2.3 mmol m⁻² s⁻¹, comparable with other spruce forests using flux-gradient and eddy covariance methods (Lafleur, 1992; Jarvis *et al.*, 1997).

The daily total for E on the dry day (20th July) was slightly less than that predicted by E_T , by about 7%. On the other two days E always exceeded E_T (Figure 6.2 and Tables 6.1 and 6.2). Scatter in the relationship between E and E_T shown in Figure 6.3 although considerable, displayed no systematic deviation from the 1:1 line over

the range of fluxes. Scatter in the relationship is understandable: as both methods are subject to considerable errors. On the one hand, there are sources of error in the assumptions and corrections involved in the derivation of E from the eddy covariance method and with instrumental errors whilst measuring fluxes. On the other hand, there are sampling errors in the estimation of both evaporation and L for the stand and errors inherent with chamber methods, e.g., chamber stickiness to water molecules (Dixon & Grace, 1982) and chamber alterations to the microclimate (Denmead *et al.*, 1993). Furthermore, one can also not be sure the chamber represents the footprint measured by the eddy covariance sensors. Despite these potential errors and uncertainties differences in the values of E by the two methods were comparatively modest.

Canopy transpiration

Transpiration rates (E_T) estimated during this study also compared well with others for Sitka spruce plantations, in the UK. E_T rates observed in this study were between 0.8 to 1.6 mmol m⁻² s⁻¹ compared with 0.4 to 2.1 mmol m⁻² s⁻¹ for daylight hours during winter and summer, respectively (Jarvis, James & Landsberg, 1976; Jarvis & Stewart, 1979). Daily rates of E_T published for coniferous plantations are typically between 0.3 and 2 mm d⁻¹ during winter and summer, respectively in the UK (Jarvis, James & Landsberg, 1976; Jarvis & Stewart, 1979). Over the three days measured in this study values of E_T were estimated 0.8 to 1.8 mm d⁻¹, within the range of published values. Furthermore, E_T modelled using MAESTRO for a Sitka spruce plantation with 1600 stems ha⁻¹, ranged from 1.25 to 3.25 mm day⁻¹ for July 1992 and annual estimates of 394 mm year⁻¹ were predicted (Kruijt *et al.*, 1999).

These values of E_T for *P. sitchensis* are comparable with other published studies for the genus *Picea* measured in temperate and boreal ecosystems. For a *P. mariana*

stand in Saskatchewan, Canada using branch chambers maximum E_T rates were estimated to lie between 0.4 and 4.4 $\text{mmol m}^{-2} \text{s}^{-1}$, and daily rates of 1.2 to 2.4 mm d^{-1} during July (Rayment, 1998). Sapflow studies in *P. abies* stands in Bavaria, Germany and central Sweden also found similar rates of E_T despite differences in latitude. In Bavaria, Alsheimer *et al.*, (1998) measured maximum E_T of 2.14 $\text{mmol m}^{-2} \text{s}^{-1}$ and 2 mm d^{-1} during June. Whilst, many studies published for the Swedish *P. abies* forest have shown a great deal of inter-annual variability for the month of July. Cienciala *et al.* (1998) found maximum E_T of 2.5 and 4.3 $\text{mmol m}^{-2} \text{s}^{-1}$ in a dry and wet year, respectively. Daily rates were 1-2 mm d^{-1} in the dry year and 2-4 mm d^{-1} in the wet year. However, a further study completed in the same forest during 1999 and 2000 also using sapflow methods found daily rates as low as 0.4 mm d^{-1} in July (Lagergren & Lindroth, 2002). Most of this variation will be the result of evaporative demand and soil water availability which are subject to variability at daily, seasonal and annual time-scales. However, the *Picea* genus appears to conserve daily rates of transpiration between 1 and 2 mm d^{-1} .

6.2.2 Canopy conductance to water vapour

Barton (1997) fitted the L-BWB model to Sitka spruce data collected at the shoot scale. These measurements were made at high Q and this made it difficult to establish g_s when $Q \rightarrow 0 \text{ } \mu\text{mol m}^{-2} \text{s}^{-1}$. Therefore, g_0 and Γ were fixed at 4 $\text{mmol m}^{-2} \text{s}^{-1}$ and 64.6 $\mu\text{mol mol}^{-1}$, respectively. It was possible to establish g_0 in this analysis, however estimates between this and the Barton (1997) study are an order of magnitude different. The value in the present study is by no means unusual for Sitka spruce as g_0 of 53 and 59 $\text{mmol m}^{-2} \text{s}^{-1}$ were found in two independent studies (Cornic & Jarvis, 1972; Jarvis, 1976). Furthermore, the mean *lowest* leaf conductance measured for a number of boreal forest conifers in the field was $38 \pm 16 \text{ mmol m}^{-2} \text{s}^{-1}$, $n = 3$. Whilst the mean *minimum* leaf conductance was $2.9 \pm \text{mmol m}^{-2} \text{s}^{-1}$, $n = 9$ (Korner, 1994).

It is useful to make a distinction between the lowest conductance measured in the field and the minimum conductance, that would occur if stomata were fully shut and under desiccation stress, as they are usually an order of magnitude different as highlighted above. Under most conditions in the field minimum conductance is rarely observed for two reasons. Firstly, in temperate regions water shortages and severe drought are fairly infrequent events, although in other climates where this is a persistent scenario, minimum conductance could be observed. Secondly, minimum conductance may not be observed in the field because of an obvious bias of erroneous values towards rather small conductance values. Minimum and lowest conductance is a difficult parameter to measure, because gas exchange systems and porometers are not accurate enough in their determination of low vapour fluxes under extreme conditions of humidity (McDermitt, 1990; Korner, 1994). This is apparent in the Figure 6.5 a-d which shows increased variability in g_s at D_a below 2 mmol mol⁻¹, as has been observed elsewhere (Pearcy *et al.*, 1989; McDermitt, 1990; Granier & Loustau, 1994; Arneth *et al.*, 1996). Therefore, typically for field modelling using L-BWB, g_0 should represent the lowest conductance observed in the field and not the minimum as this would cause g_0 to become underestimated as A and $Q \rightarrow 0$ $\mu\text{mol m}^{-2} \text{s}^{-1}$. Lastly, g_0 is not a measure of epidermal conductance g_e , which constitutes the extremely small loss of water from the plant cuticle. Rates of g_e in Sitka spruce are in the region of 0.5 to 1.5 mmol m⁻² s⁻¹ depending on the degree of abrasion to the needle surfaces (van Gardingen *et al.*, 1991).

Despite the differences in g_0 , the parameters D_0 and a_1 were similar to those found in the Barton (1997) study. Barton (1997) obtained values of between 12 and 40 for D_0 exposed to different CO₂ treatments, with values of 30 for ambient conditions. Values of a_1 also varied with CO₂ treatment between 2500 to 7500 and 2540 for ambient conditions. Barton (1997), concluded from his analysis that the L-BWB model did not perform well during changing environmental conditions of CO₂, D_a and Q , but performed better when conditions remained fairly constant. He attributed

these properties to incomplete stomatal adjustment. A similar study to this on *P. mariana* using shoot and branch chambers found variable results for parameters at the different scales of measurement (Rayment *et al.*, 2000). Lowest branch conductances were between 4.5 to 9 mmol m⁻² s⁻¹, but lowest shoot conductances were somewhat higher at between 8.7 to 30.5 mmol m⁻² s⁻¹ for the lower and upper locations in the canopy, respectively. However, this could be an artefact of the evaporation rate calculations. The present study found that if linear regression, instead of non-linear regression analysis, was used to determine E_L then fluxes were systematically underestimated. Consequently g_s would have also been in error (see Appendix 1 of Saugier *et al.*, 1997). Rayment *et al.*, (2001) obtained a reasonable fit to branch conductance data collected using the L-BWB model. Models of the L-BWB and Jarvis type model accounted for 29 and 12 % of the variation in observed conductance, respectively. Improvements of 26 and 33% to the static model fit were achieved by incorporating a pre-history of g_s and calculating the speed of the plant's response to changing environmental conditions. They concluded that the poor capacity of models used to describe stomatal behaviour of this species in the field indicated that other factors played an important role in controlling the stomatal function of this species, this echoes the findings of Barton (1997). For example, there is evidence that Sitka spruce stomata might make 70% of the steady-state response to a sizeable step change in environmental conditions in about 20 minutes. However the stomata may need about 45 minutes to achieve 90% of the steady-state response (Ludlow & Jarvis, 1971; Neilson *et al.*, 1972).

The L-BWB model of g_s is primarily a function of A and D_a . Although the model in this study accounted for 55% of the variation in measured stomatal conductance a lot of uncertainty in what drives the behaviour of stomata in this field site also still remains. Most noticeably, the variability in g_s at low D_a was substantial and probably precludes any attempt at accurate model prediction (e.g., Kelliher *et al.*, 1993;

Leuning, 1995; Arneth *et al.*, 1996). Moreover, something generally not accounted for in most models of conductance is the hysteresis phenomenon apparent in the diurnal course of g_s . For instance, a similar constellation of climatic conditions could produce a higher leaf conductance during the morning than in the afternoon, as found in this and in many other studies (e.g., Jarvis, 1976; Lange *et al.*, 1982; Pereira *et al.*, 1987; Arneth *et al.*, 1996). The afternoon reduction of g_s compared to morning values under equal climatic conditions was in the order of 20 to 35% in this study, similar to the reductions in the above references. The measured diurnal curve for g_s in this study approximated a triangular shape with a steep short ascent and a variable descent, a very common feature of g_s observed in the field. A plausible explanation of this phenomenon is changes to the flow resistance of the tree during the course of the day, higher resistances to flow occurring in the afternoon. The exact mechanism of this increased resistance within the tree is still conjectural but some hypothesise that the sources of available water in the plant itself shift lower during the day to places in the crown with increasing resistance (Jarvis, 1975). In the morning it is likely that sources of water for E_T are more readily available at the liquid-air interface primarily in the cells and leaves, then in the branches and sapwood of the crown region. As water is lost over the day the ability of the plant to supply water to the sites of evaporation is compromised, and hence the overall conductance of the tree decreases as does E_T (Jarvis, 1976; Whitehead & Jarvis, 1981; Williams *et al.*, 1996). These technical and mechanistic uncertainties will inevitably lead to models that imperfectly reflect the environmental regulation of stomata in the field.

Schulze *et al.*, (1994) investigated the relationship between maximum stomatal conductance and maximum surface conductance for different land surface covers, and found that maximum surface conductance was typically three times maximum stomatal conductance. The conductances found in this study ($g_s = 150 \text{ mmol m}^{-2} \text{ s}^{-1}$; $G_s = 500 \text{ mmol mmol m}^{-2} \text{ s}^{-1}$) follow this prediction. Moreover, evergreen conifers typically have quite low maximum g_s values of between 100 and 300 $\text{mmol m}^{-2} \text{ s}^{-1}$

(Korner, 1994). Sandford & Jarvis, (1986) also found this range of g_s for Sitka spruce shoots exposed to variable D_1 ranging from 5 to 25 mmol mol⁻¹. Maximum g_s values for this study were within this range over the three days. Mean maximum conductance estimated from the measurement of 26 conifer species across a number of biomes was 234 ± 99 mmol m⁻² s⁻¹ (Korner, 1994). This is also not so different from the global mean of 218 ± 24 mmol m⁻² s⁻¹ for the most important groups of woody vegetation. This would suggest that maximum conductance is a fairly conservative parameter within coniferous and woody species and the larger part of biome and ecosystem variability in measured canopy conductance is usually a function of L , canopy structure and daily and seasonal variations in g_s mediated by atmospheric and soil water content change. Maximum stomatal opening which regulates the uptake and release of CO₂ and water vapour, usually occurs at much lower Q of approximately 200 μ mol m⁻² s⁻¹, as was also found at Griffin Forest (Ludlow & Jarvis, 1971; Ng & Jarvis, 1980; Jarvis & Morison, 1981;).

Comparison of methods used to estimate canopy conductance to water vapour did agree well at times over the observation period. First of all, predictions made with L-BWB at the branch scale for all three days were very good. However, during the scaling of L-BWB deviations were apparent on the 22nd July. Up until that point estimates at both the branch and canopy scales were very similar in pattern and magnitude, as a result similar values of measured and modelled A persisted despite different scaling assumptions. However, on the 22nd July modelled and scaled canopy estimates diverged somewhat in both magnitude and pattern over the day. As already mentioned the L-BWB modelled g_s is largely dependent on prevailing A which in turn is a function of Q . As Q increased A , modelled g_s became correspondingly larger than that estimated from the simple two-layered canopy model. This implies that there is some uncertainty regarding the distribution of radiation within the canopy and, depending on how this is modelled, different estimates of A , and hence g_s , will result. In these circumstances it may be desirable to

use a more detailed radiation model, like that of MAESTRO or MAESTRA, which simulates both direct and diffuse radiation within the crown (Wang & Jarvis, 1990).

The branch and canopy estimates of stomatal conductance were extremely responsive to increases in Q and D_a especially apparent over a period of approximately two hours on the 22nd July (Figures 6.6 and 6.7). When both Q and D_a started to increase a transient reduction of *ca* 50 mmol m⁻² s⁻¹ in measured g_s was observed at the branch scale and was modelled very well by the L-BWB model. This behaviour was also evident at the canopy scale and a transient reduction of 125 mmol m⁻² s⁻¹ was observed. This transient decrease in conductance appeared to be in direct response to the increase in D_a , and opposed to the increase in the Q which would usually stimulate opening of stomata. However, closure was observed and this would have caused the $C_i/C_a \rightarrow 0$. After the peak in D_a passed, a gradual opening of stomata was observed allowing the supply of CO₂ to increase again and $C_i/C_a \rightarrow 1$. However, g_s did not go back to the values prior to this transient response but to some value below that on the afternoon trajectory.

The inverted Penman-Monteith estimates for G_s at times did not agree well with the branch-derived estimates. First of all, the Penman-Monteith equation makes use of E , which should represent the flux resulting from transpiration alone. When extra sources of water, like that of intercepted rainfall or soil evaporation are included in this flux then an overestimation of G_s will occur. This was illustrated in Figure 6.2 by occasions where $E \gg E_T$. Secondly, further discrepancies between the Penman-Monteith estimates and the branch-derived estimates were examined in conjunction with the Monin-Obukhov surface layer scaling parameter (ζ) (Monin & Obukhov, 1954). This indicated that a lot of the differences occurred when $\zeta < -3$. On the morning of 20th July, ζ remained < -3 until midday at which time the surface layer became suitably unstable and better conditions for eddy covariance resumed. Thus

the most accurate estimates of G_s from eddy covariance measurements will be obtained from dry canopies in unstable to neutral conditions ($\zeta = -3$ to 0).

6.2.3 Ecosystem Respiration

Soil respiration

Spatial variability

Chambers offer both advantages and disadvantages for dealing with spatial heterogeneity of fluxes. Where variation within the landscape is recognisable, chamber deployment can be stratified to measure the importance of that variability. The variability of soil CO₂ efflux measured within plots was high and coefficients of variation (CV) were approximately 58% and independent of L , with the exception of the site with $L = 3.5$, which had a CV of only 34% (Figure 6.8). As there were no significant differences in CO₂ efflux between the sites measured but there were significant differences between the areas within the sites, the dynamics of CO₂ efflux from the different areas was characterised during the observation period and over a longer period. Although a large number of flux measurements are the ideal, logistical constraints on labour and time limited the number of measurement locations that could be used for capturing the daily cycle in soil CO₂ efflux and confidently scaling to the flux footprint and consequently the scaled up fluxes must be regarded as tentative.

The observed within-site variability (Figure 6.8) was attributed primarily to the pronounced artificial micro-topography created by systematic mechanical ploughing in preparation for afforestation. The ploughing gave rise to three evenly spaced areas, distinct with respect to soil depth, soil mass (expressed on an area basis) and carbon content of the surface layers (Table 2.4). This topography is typical in

plantations of this age and older. However, because this type of ploughing effectively reduce root spread, with the furrows acting as barriers to root growth (Booth, 1973), windthrow becomes a problem, and therefore site preparation is now somewhat different, e.g., mounding rather than ploughing. As described in Chapter 2 the ridge areas arose from the overturning of soil which previously occupied the furrow area. The trees were systematically planted on this ridge. This site management accounted for the main differences in soil characteristics found and formed the basis for sampling stratification. The other contributing factor to the significant differences between the furrow and the other two areas, was the seasonal location of the water table. This site during the autumn and winter months is usually waterlogged, but surface water pooling is usually confined to the furrow area. These areas can become the conduits for runoff during heavy rain and experience lateral flow of water through the profile (personal observation). These factors physically prevent litter accumulation on the soil surface but also flush the roots with water from areas up slope in the catchment. Secondly, the effect of standing water gives rise to anaerobic and gleying conditions below the level of the water table. Hence, studies have found that although Sitka spruce is potentially a deep rooting species when planted on suitable soils (e.g., brown earths), when planted on stagnogley and stagnohumic gley soils there are very obvious relationships between the depth of the permanent root system and the shallow layer of well-oxygenated soil above the water table (Day, 1963; Fraser & Gardiner, 1967; Boggie, 1977; Armstrong *et al.*, 1976; Pyatt & Smith, 1983; Nisbet *et al.*, 1989; Soulsby, 1993). These soils are extensive, accounting for some 35-40% of the area in upland afforestation. The water table has a root pruning effect during the winter months but also during any periodic fluctuations of the water table during the growing season as active Sitka spruce roots are unable to tolerate anaerobiosis and quickly die (Coutts & Philipson, 1978; Sanderson & Armstrong, 1980).

The structural, biological, chemical and hydrological differences between the three areas created significant differences in T_s , θ and soil CO_2 efflux. Many field studies have shown that temperature and moisture are the most important factors regulating soil- CO_2 fluxes in both disturbed and “undisturbed” sites (Schlesinger, 1977; Edwards & Ross-Todd, 1983; Gordon *et al.*, 1987; Dorr & Munnich, 1987; Meir, 1996; Fang, 1997; Rayment, 1998). Fluxes from the ridge and flat areas were significantly higher than those from the furrow. Typically these areas contain most of the tree roots and successfully accumulate litter, an asset of their raised height. Thus they contain a lot of potential substrate for microbial respiration and a large amount of biomass that requires maintenance. Furthermore, these areas tend to be warmer during the summer months and this increases metabolic activity and they are better aerated at all times of the year, providing a constant supply of O_2 . This leads to the higher rates of respiration measured in this study. However, areas of high porosity and extensive root biomass are most likely to suffer from moisture deficits during prolonged periods of evapotranspiration losses. Low availability of soil water inhibits the metabolic activity of microbes and roots, producing lowered respiration rates (Froment, 1972; Schlesinger, 1977). This was a possible constraint on the soil CO_2 efflux at this site observed during summer (Figure 6.9). On the other hand θ did not constrain CO_2 efflux from the furrow areas during this field campaign or at any other time observed over the summer months (data not shown). However, soil CO_2 efflux from the furrow areas was constrained by θ at other times of the year (data not shown). High moisture content also causes inhibition of CO_2 efflux when oxygen becomes limiting to the microbes, as pore spaces fill with water (Glinsky & Stepniewski, 1985). Data collected over the period July 2000 to August 2001 did show that θ constrained CO_2 efflux from each area at values $> 0.45 \text{ m}^3 \text{ m}^{-3}$. At $\theta < 0.45 \text{ m}^3 \text{ m}^{-3}$, temperature regulated the extent of CO_2 losses from the soil surface.

Temporal variation

Daily variation in soil CO₂ efflux and $\delta^{13}\text{C}$ of soil respired CO₂ can vary depending on soil type and vegetation cover. The observed daily variation in soil CO₂ efflux at this site was $\leq 0.5 \mu\text{mol m}^{-2} \text{s}^{-1}$, which corresponded to a 3.5 °C change in T_s and a change in $\theta < 2\%$. A similar range of daily soil CO₂ efflux was observed in *P. abies* sites in Germany and Italy. Matteucci *et al.*, (2000) reported soil CO₂ efflux rates of 1.2 – 4.1 $\mu\text{mol m}^{-2} \text{s}^{-1}$ at different *P. abies* stands for different times of the day during the active growing season. The daily variation in observed rates at individual forests were typically $< 0.5 \mu\text{mol m}^{-2} \text{s}^{-1}$ with a daily CV of 1.5% and 5.1% for two of the stands (Waldstein and Renon, Germany, respectively). This variation was trivial compared with the CV calculated for individual hours in the same stands of 35 and 26%, for the two stands. Their study concluded that R_s at both sites appeared to be mostly controlled by T_s over the growing season. Soil water content was always non-limiting, apart from minor effects at minima in June at the Waldstein forest and in August at the Renon site (θ ca. 0.2 $\text{m}^3 \text{m}^{-3}$). On these occasions R_s was observed to decrease despite increasing or constant temperature. Buchmann (2000) also reported relatively stable daily soil CO₂ effluxes $< 0.25 \mu\text{mol m}^{-2} \text{s}^{-1}$ whilst within-site variation $< 1.6 \mu\text{mol m}^{-2} \text{s}^{-1}$ for four *P. abies* plantations of different age in Fichtelgebirge, Germany. Such results are not confined to temperate ecosystems but have also been observed in tropical forests. Davidson *et al.*, (2000), for example, found very little daily variation in soil CO₂ efflux and environmental variables in heavily shaded forest typical of eastern Amazonia.

Soil CO₂ efflux rates from the Griffin site were quite low considering the high growth rates and carbon assimilation observed for this pole-stage tree species. Similar results, confirming the low rates observed here have been found for the same species in the UK and in Denmark. Ritchie (1971), in a Sitka spruce site located

near Stonehaven, UK found soil CO₂ efflux R_{10} of 0.75 $\mu\text{mol m}^{-2} \text{s}^{-1}$. Further studies in the UK have also found similarly low rates of soil respiration in Sitka spruce sites at Harwood Forest, Northumberland. Ball *et al.*, (unpublished data) found soil CO₂ efflux rates of *ca* 0.96 $\mu\text{mol m}^{-2} \text{s}^{-1}$ in a 20-year-old Sitka spruce stand planted on peaty gley with low soil temperatures (<10 °C). Such low values at those sites can be attributed to persistently high water tables throughout the entire growing season. Therefore, it seems that soil CO₂ efflux rates from afforested, poorly drained soils under UK climatic conditions tend to have low emission rates even in the summer and autumn months when soils are warmest. It would appear that the dynamics of the hydrological regimes in ploughed forest soils of the uplands exert a considerable constraint on CO₂ losses from these ecosystems. These efflux rates are also in agreement with studies completed outside the UK, in similar oceanic climates. Jensen *et al.*, (1996) measured a range of 0.7 to 2.3 $\mu\text{mol m}^{-2} \text{s}^{-1}$ in a 30-year-old Sitka spruce, Norway spruce and *Fagus sylvatica* stand in Denmark situated on loamy sand during April and May. Despite the free drainage provided by sandy soils the range of soil CO₂ efflux rates were still within the range of values observed in the present study. Unfortunately, no soil temperature or θ accompanied their data to allow any more detailed comparisons.

Low rates of soil CO₂ efflux were also found in other *Picea* forests located in temperate regions of Europe but higher rates in boreal forest ecosystems. As shown above, forests in Germany had similar ranges of soil CO₂ efflux to that found in this study. The maximum range observed at Griffin forest site during a single visit occurred between days 230 and 240 in two different years 2000 and 2001. Temperatures were between 9 and 12 °C and mean soil CO₂ efflux rates of 1, 2.5 and 4 $\mu\text{mol m}^{-2} \text{s}^{-1}$ were observed for the furrow, flat and ridge areas, respectively. A similar range was described for the Waldstein and Renon sites by Matteucci *et al.* (2000). The R_{10} for *P. abies* sites were also similar to Griffin forest with 2.5 ± 0.2

$\mu\text{mol m}^{-2} \text{ s}^{-1}$ for the Waldstein site and 2.9 ± 0.4 for the Monte di Mezzo site, located in Italy (Matteucci *et al.*, 2000). Buchmann (2000) observed R_{10} of 2, 2.3, 2.6 and 3 $\mu\text{mol m}^{-2} \text{ s}^{-1}$ for *P. abies* stands of age 146, 47, 87 and 111 years respectively in Fichtelgebirge, Germany. These values are also similar to mixed coniferous/deciduous forests soil CO_2 efflux rates at a mixed *Pinus sylvestris* site in Belgium were 1.5 and 2.0 $\mu\text{mol m}^{-2} \text{ s}^{-1}$ measured during July in areas without and with understorey presence of small trees. At 10 °C at these sites soil CO_2 efflux rates were between 0.6 and 0.7 $\mu\text{mol m}^{-2} \text{ s}^{-1}$ for the two situations (Janssens *et al.*, 2000a).

In contrast forest sites with similar tree species situated in the boreal climate have much higher rates of soil CO_2 efflux. Moren & Lindroth (2000), gave values for a *P. abies* and *P. sylvestris* mixed forest in Sweden ranging from 4 to 14 $\mu\text{mol m}^{-2} \text{ s}^{-1}$ during the month of July and R_{10} of 4.3 $\mu\text{mol m}^{-2} \text{ s}^{-1}$, double the rates found in this study. Similarly in another *P. abies* stand within Sweden the daily range of values was between 4 to 6.5 $\mu\text{mol m}^{-2} \text{ s}^{-1}$ measured at night during June. However, these rates also included the respiration rates of moss and only account for rates measured during the nocturnal period (Strömberg, 2001). Interestingly this study also found R_{10} varied between 1.5 and 4.5 $\mu\text{mol m}^{-2} \text{ s}^{-1}$ over the June to September period, in two separate years and for different irrigation and fertiliser treatments. Other boreal sites with *Picea* species had similarly higher soil CO_2 efflux rates than the temperate sites with R_{10} values between 1.1 – 3.4 $\mu\text{mol m}^{-2} \text{ s}^{-1}$ for *P. mariana* (Goulden & Crill, 1997; Lavigne *et al.*, 1997; Rayment & Jarvis, 1997).

Soil system differences

This study employed two different methods for collecting information on soil gas exchange, to enable the complementary observation of the $\delta^{13}\text{C}$ of soil respired CO_2 . As two methods were used at the same time any disparity between estimates were

subject to scrutiny. A growing number of publications, reviewing the many different chamber designs, calculations and associated artefacts are available (Ewel *et al.*, 1987; Bekku *et al.*, 1997; Rayment, 2000; Hutchinson & Livingstone, 2002; Davidson *et al.*, 2002). The use of portable IRGAs is becoming increasingly common and is widely considered the method of choice for chamber-based soil respiration measurements. However, concerns remain regarding the artefacts and biases that accompany each method. The coupled SRC1 and EGM3 soil respiration system used throughout this fieldwork has been compared to other systems in a number of studies with variable results and conclusions (Jensen *et al.*, 1996; Arneth *et al.*, 1998; Kelliher *et al.*, 1999; Le Dantec *et al.*, 1999; Matteucci *et al.*, 2000; Janssens *et al.*, 2001).

Comparisons between similar dynamic chamber systems reported in the literature are variable. Arneth *et al.*, (1998) measuring soil respiration in a *Pinus radiata* plantation after clearcutting in New Zealand on stony sandy loam found a very good relationship between the LI-COR and PP Systems coupled system $LI-COR = 1.06 * PP \text{ Systems} (\pm 0.43; r^2 = 0.96)$. Average efflux values for this clearcut site were $2.2 (\pm 0.5)$ and $2.3 (\pm 0.6) \text{ mmol m}^{-2} \text{ s}^{-1}$ for the PP Systems and LI-COR, respectively. Arneth *et al.*, (1998) also expanded the range of efflux that could be measured by taking measurements on a loamy soil in fertilised pasture after adding aqueous glucose solution to the soil surface and measuring two and five days later. Arneth *et al.*, (1998) also reported higher fluxes measured by the LI-COR on a glucose-irrigated soil. This resulted in soil CO_2 effluxes $>7 \mu\text{mol m}^{-2} \text{ s}^{-1}$ and disagreement between the two methods with the LI-COR estimating higher absolute values than the PP Systems. In contrast Janssens *et al.*, (2000) found the opposite result on wet sandy soils in Belgium. A homemade chamber (based on the model proposed by Norman *et al.*, 1992) linked to an IRGA (LI-6250 Li-Cor, Inc., Lincoln, NE) and a control console (Li-Cor LI-6200) produced similar results to the commercially available system sold by Li-Cor (LI-6000-09). How similar the results

were to the commercial Li-Cor is unknown as no data or statistical analysis of these results were reported in the publication nor cited in any other. Janssens *et al.*, (2000) reported that the PP Systems systematically gave soil CO₂ efflux rates 50% higher than the replica Li-Cor system and this was also in agreement with a further study by Le Dantec *et al.*, (1999) that found estimates 30% higher than the LiCor replica. Most of this difference was attributed to fan speeds inside the SRC1 chamber and the authors concluded this system should have fan speeds reduced to resemble turbulence outside the chamber. However, this disparity in results is not convincing enough to warrant chamber adjustments. Soil porosity and moisture content may yet have some role to play in these differences and an across the board change to fan speeds in one situation may improve the agreement between methods at some sites, but not at others.

No direct comparison of the PP System with the exact, non-steady state, chamber method used in this study could be made from the literature. The static method also mixed the air inside the chamber with both a fan and a pump that continually circulated air through lengths of Dekabon tubing entering and leaving the chamber close to the fan. The most obvious differences between the two methods were the volume and surface area measured by the two methods. The PP system was considerably smaller than the home-made chamber with a volume difference of 382830 cm³ and a soil surface area difference of 6329 cm². The chambers were also made of different materials with the home-made chamber constructed from transparent Perspex and not opaque like the PP Systems. The sampling protocol was also different as only two concentrations were collected at the beginning before chamber closure and after 10 minutes of CO₂ enrichment within the chamber. Hence, the agreement between the two methods for the majority of the time was good considering these potential differences. Lastly, the spatial and temporal variability for any sampling occasion was not established using the large customised chambers because of the constraints on the number of flasks available for sampling

the δ_a from both soils and branches. These chambers served the primary purpose which was to establish the mean $\delta^{13}\text{C}$ signature of respired CO_2 from the soil surface and were not designed for modelling spatial or temporal dynamics of the soil CO_2 efflux rates. However, the information that was collected using this independent method did provide confirmation of unusual observations which may have been considered noisy or erroneous. For example, the drop in soil respiration rates in the early evening observed for the ridge and flat areas indicating θ limitations.

Ecosystem respiration

Comparing eddy covariance and chamber-scaled methods

The determination of F_R values by component summation is important for the independent verification of eddy covariance measurements over forested areas (Wofsy *et al.*, 1993; Goulden *et al.*, 1996; Lavigne *et al.*, 1997; Lindroth *et al.*, 1998). This is particularly true during stable conditions at night when limitations to eddy covariance measurements occur (Massman & Lee, 2002; Pattey *et al.*, 2002). Some of these limitations are instrumental whilst others are meteorological. Agreement between component-summed-estimates of F_R and those derived from $F_{E,N}$ following protocols often adopted, gave variable results during the night.

Firstly, comparison of the methods indicated that using T_a to force the Arrhenius model instead of T_s , gave a similar range and pattern to the summed component estimate. This could be an attribute of the 'current' canopy structure at Griffin Forest. At the time of measurement, canopy closure was occurring throughout the flux footprint, and L was high. The canopy exhibits high F_A and to sustain this level of productivity a correspondingly high level of metabolic maintenance should be required. This will undoubtedly lead to a substantial contribution of respiration from

aboveground components, influenced predominantly by the surrounding air temperature and not that of the soil. The data presented here indicate that currently above and belowground respiratory losses contribute equally to the overall flux during the night at this site. This was also shown to be the case for a 30-year-old *Pseudotsuga menziessii* (Mirb.) Franco in the Speuld forest, Netherlands (van Wijk, 2001). Scaled chamber measurements also showed that the dominant component of respiratory losses was located in the above-ground canopy (70% >) (Van Wijk, 2001). This could be a reason why soil temperature is perhaps not the best variable to describe F_R for 30 min periods. It may therefore prove a gross simplification to choose a unique location as the reference temperature, given that the respiring elements are spread throughout the ecosystem and experience different temperatures at different times and with different magnitudes. This highlights the importance of choosing an appropriate temperature driver on an individual basis for an ecosystem, appropriate to canopy structure and component contributions. Despite these concerns, it seems meta-analysis of eddy covariance data across many sites, in every major biome and vegetation type, have adopted the protocol of using soil temperature as the principle driver of total ecosystem respiration (Falge *et al.*, 2002; Law *et al.*, 2002). The potential errors incurred by adopting this protocol will obviously depend on the overall contribution of forests like Griffin and Speuld to global calculations of CO₂ sequestration.

For some time we have also been aware that F_E measured using eddy covariance methods declines at low wind speeds and low U^* at night. For long-term ecosystem studies, with limited instrument deployment, it appears to be more appropriate to use eddy covariance fluxes measured during windy nights to either develop or verify mathematical algorithms in order to estimate respiration for a continuous time-series. There is a need to be careful about making a standard set of corrections at different sites. For instance, it has been shown that low U^* is correlated with low measurements of soil CO₂ efflux in open-type soil chambers (Fang & Moncrieff,

1996; Rayment & Jarvis, 1997) and with nocturnal branch respiration (Rayment, 1988). Goulden *et al.*, (1997) showed for a temperate mixed deciduous and coniferous forest that by replacing data below $U^* < 0.17 \text{ m s}^{-1}$, with modelled estimates derived from $U^* > 0.17 \text{ m s}^{-1}$ and T_s , annual respiration estimates increased by $0.5 - 1.0 \text{ t C ha}^{-1}$ over one year. This had the overall effect of reducing the net carbon balance from 3.7 t C ha^{-1} to 2.8 t C ha^{-1} (Goulden *et al.*, 1996). In contrast, Valentini (1999) reported that differences caused by including or excluding low U^* made as little as 7% difference on the total carbon balance. A 7% difference at Griffin Forest would constitute some 0.4 t C ha^{-1} , based on a net annual CO_2 uptake of ca. 6 t C ha^{-1} . Given the many hectares of land this species is planted on, a 7% systematic bias quickly mounts up. However, Valentini (1999) did point out that such bias is probably site specific, and particular care should be taken at those sites with especially small net ecosystem exchange. Fluxes estimated from $F_{E,N}$ utilising all U^* conditions at this study site compared best with the summed component rates. Low U^* conditions constituted $>40\%$ of all nocturnal measurements at this site. Therefore, the choice of method correction, and indeed, whether to make any correction at all, is of considerable importance.

Rayment (1998) reported data for a *P.mariana* forest in Saskatchewan, Canada that suggested a definite reduction in efflux of CO_2 from the canopy and soil during periods of low U^* . Therefore, part of the reduction in F_R measured by eddy covariance may in part be a consequence of reductions in respiratory processes and transport of CO_2 and only partially a measurement artefact. There is a growing body of literature describing the behaviour and direct mechanisms for the existence of a positive correlation between turbulence and soil CO_2 transport (Kimball & Lemon, 1971; Baldocchi & Meyers, 1991; Arneth *et al.*, 1998; Rayment & Jarvis, 2000). However, correlation between respiration inside branch enclosures and turbulence appears to be indirect. Rayment (1998) showed that U^* tends to be significantly correlated with Q , and F_A and R_b are also significantly correlated with Q . Moreover,

periods of low U^* during the day usually lead to low U^* conditions the following night, creating an indirect link between night-time U^* and branch respiration. Furthermore, soil temperature is usually not correlated with low U^* , therefore it would not account for the reductions in respiratory release from the soil and aboveground components during low turbulence. As most studies reported in the literature tend to opt for replacement of flux data measured during low turbulence, a potential bias in ecosystem respiration values may currently exist, and this which could represent a systematic over-estimation of F_R . At Griffin Forest, differences in the R_{10} parameter of 20% were calculated for different U^* scenarios. This highlights a pressing need to consider alternative parameters in addition to the classical parameters used so far, such as U^* and σ_w when constructing respiration algorithms. Given the complications of establishing the respiration relationship and that studies critically depend on this flux for studying canopy physiology, perhaps it would be a good idea for sites to report relationships derived from all $F_{E,N}$ and those excluding $U^* < 0.2 \text{ m s}^{-1}$. Furthermore, the deployment, validation and development of independent chamber methods will allow the dependence of biological processes on climate and other physical variables to be explored.

One of the acknowledged drawbacks from this study was the omission of measurements describing the contribution of stem respiration. It is therefore impossible to say which estimate derived for this site is the 'true' flux, as a component is missing and remains uncharacterised. The contribution of stems to the overall carbon budget of a forest is generally regarded as small. Studies estimating the contribution of woody biomass confirm that this flux represents a small component. Meir, (1996) estimated a 10% contribution of stem CO_2 efflux to the total CO_2 losses in tropical forests of Brazil and Cameroon. The rates observed were 0.7 and $0.6 \mu\text{mol m}^{-2} \text{ s}^{-1}$ expressed on a ground area basis for Brazil and Cameroon, respectively. In a temperate deciduous forest, (Harvard Forest, Massachusetts) a 5% contribution was estimated with typical rates of $0.3 \mu\text{mol m}^{-2} \text{ s}^{-1}$ (Goulden *et al.*,

1996). In the BOREAS campaign six Canadian boreal sites of young and old *Pinus banksiana* Lamb and *P. mariana* contributed between 5 to 15% from woody biomass with rates ranging from 0.1 to 0.4 $\mu\text{mol m}^{-2} \text{s}^{-1}$ (Lavigne *et al.*, 1997). Lastly, two separate studies in 70 and 30-year-old *P. abies* stands in northern Sweden estimated a 6 and 26% contribution for stems respectively (Moren, 1999; Stockfors & Linder, 1998; Wallin *et al.*, 2001). Rates at 10 °C were also very different for the two sites at 0.6 and 1.8 $\mu\text{mol m}^{-2} \text{s}^{-1}$, respectively. Apart from the northern Sweden site, across every major biome stem respiration appears to be conservative at between 5 to 15%. Review of most stem studies suggests that stem biomass, although a major carbon store, generally requires less than 10% of annual gross primary production to maintain the small fraction of living cells associated with xylem parenchyma, cambium and phloem (Ryan, 1991; Ryan *et al.*, 1995). Assuming the residual flux calculated for this study represents stem CO_2 efflux, a comparative contribution could be anywhere between 3, 6, 20 or 21% using $F_{\text{R}}(T_s)$, $F_{\text{R}}(T_a)$, $F_{\text{R}}(T_s \text{ and } U^*)$ and $F_{\text{R}}(T_a \text{ and } U^*)$, respectively. Fluxes corresponding to these contributions would be approximately 0.1, 0.2, 0.9 and 1.0 $\mu\text{mol m}^{-2} \text{s}^{-1}$ for the observation period, all falling within the range of studies reported above, with the exception perhaps of $F_{\text{R}}(T_s)$ which some may regard as extremely small.

Usually disagreements between chamber-based estimates and eddy covariance are reported for nocturnal periods. Lavigne *et al.*, (1997) found the two methods to correlate poorly ($r^2 = 0.06\text{--}0.27$) and for eddy covariance to give consistently lower estimates than scaled chamber estimates (27% on average). This underestimation by eddy covariance methods has also been observed in a range of other ecosystems: temperate deciduous forest; temperate coniferous; and tropical forests (Goulden *et al.*, 1996; Law *et al.*, 1999; Meir 1996). In this study the eddy covariance temperature model did not under-estimate the summed components from the soil and branches measured and modelled.

The rates of total ecosystem respiration from this site compare well with rates from other temperate coniferous forests studied. Beverland *et al.*, (1996) measured nocturnal fluxes from a Sitka spruce stand at Rivoix Forest, located in south-west Scotland. Maximum fluxes ranged from 2, 5 and 6 $\mu\text{mol m}^{-2} \text{s}^{-1}$ over a three night field campaign. Another study located in the south-east of Scotland on a 13-year-old Sitka spruce stand at Blairadam Forest found that ecosystem respiration rates at 10 °C ranged from 0 to 10 $\mu\text{mol m}^{-2} \text{s}^{-1}$ (Massheder *et al.*, 1993). Four out of six nights observed in June had maximum values of *ca* 6 $\mu\text{mol m}^{-2} \text{s}^{-1}$ whilst on the other two nights maximums of *ca* 3 and 12 $\mu\text{mol m}^{-2} \text{s}^{-1}$ were observed. For another Sitka spruce stand, Fetteresso, in north-east Scotland respiration rates for the ecosystem were estimated to be *ca* 18 $\mu\text{mol m}^{-2} \text{s}^{-1}$ at 10 °C, a somewhat larger rate than observed in this study (Jarvis, 1994). Very few ecosystems could be found in the literature with similarly high rates of respiration. Correspondingly high seasonal maximum F_R of 16 $\mu\text{mol m}^{-2} \text{s}^{-1}$ were found for a temperate coniferous forest at the Brasschaat site in Belgium; 21.5 $\mu\text{mol m}^{-2} \text{s}^{-1}$ at a temperate deciduous forest at the Vielsalm site in Belgium and 15 $\mu\text{mol m}^{-2} \text{s}^{-1}$ in agricultural crops and grasslands in the USA (Falge *et al.*, 2002). Falge *et al.*, (2002) found that most temperate coniferous forests, with the exception of the Brasschaat site described above, had seasonal maximum rates of F_R between 3.6 and 7.3 $\mu\text{mol m}^{-2} \text{s}^{-1}$. This meta-analysis included analysis of 1997 data from Griffin Forest which was reported to have a seasonal maximum F_R of 5.3 $\mu\text{mol m}^{-2} \text{s}^{-1}$. Griffin forest also fell within the range reported for Boreal coniferous forests of 4.0 to 12.8 $\mu\text{mol m}^{-2} \text{s}^{-1}$.

The computation of GPP from a net CO_2 flux requires that fluxes from all components respiring in the ecosystem be accounted and, in particular, would take into account any metabolic differences between day and night-time leaf and stem respiration when significant (Ruimy *et al.*, 1995; Aubinet *et al.*, 2000). For instance, these differences may be more important in ecosystems containing large amounts of

photosynthetically active aboveground biomass. Unfortunately differences between daytime and nighttime respiration cannot be deduced from $F_{E,N}$ measurements and additional work would be required to measure all the component fluxes in the field and accompany these with controlled laboratory experiments. If there are differences between day and nighttime respiration, at the same temperature, the sum currently reported as GPP is theoretically and quantitatively erroneous.

It is apparent from experimental evidence growing in the literature for woody species, that partial inhibition of respiration during daytime is highly likely. Sitka spruce has exhibited both corticular refixation of CO_2 at the shoot scale (Ludlow & Jarvis, 1971) and inhibition of dark respiration, independent from changes in photorespiration and stomatal conductance (Cornic & Jarvis, 1972). In both cases these could prove highly advantageous attributes for plants to have evolved, as losses of CO_2 from the plant would be minimised. The potential reduction in CO_2 losses resulting from the above processes has yet to be explored rigorously at the scale of the ecosystem. Consequently, their potential impact on the overall carbon balance for forests possessing these processes is currently unknown.

The model results for respiration during the day indicated large differences between chamber-based and eddy covariance estimates, especially when inhibition of respiration was assumed. Mean inhibited respiration rates were 21, 40, 35 and 50% lower than $F_{R(Ts)}$, $F_{R(Ta)}$, $F_{R(Ts \text{ and } U^*)}$ and $F_{R(Ta \text{ and } U^*)}$, respectively. In contrast, when no inhibition was assumed and soil temperature was used to force respiration during the day, $F_{R(Ts)}$ and $F_{R(Ts \text{ and } U^*)}$ estimates were 30 and 7 % lower than the chamber-based estimates. If air temperature was the reference temperature then chamber-based estimates were only 1 and 17% lower than $F_{R(Ta)}$ and $F_{R(Ta \text{ and } U^*)}$, respectively. Therefore, if no inhibition occurred application of the nighttime relationship during daytime will estimate very closely rates from the independent methods. However, if inhibition does occur estimates for instantaneous, daily and annual CO_2 losses could

be somewhat smaller than those currently published for ecosystems with high L . Couple this with the potential reductions in stem respiration during the day and ecosystem respiration rates could be currently over-estimated.

6.2.4 *Canopy photosynthesis*

Sitka spruce evolved in the Pacific North West of North America and Canada, a region characterised by a predominantly diffuse radiation regime throughout the year, mainly the result of the large amount of cloud and fog cover experienced along maritime temperate coastlines. It is therefore unsurprising that Sitka spruce also grows well in the maritime temperate climate of the UK. The benefits provided by a maritime climate are multiple for this species. Firstly, diffuse light does not produce the shading that direct beam radiation casts down the canopy, but instead scatters and reflects radiation within the canopy. Secondly, diffuse radiation days with small amounts of direct beam radiation are also correlated with warm air and relatively low evaporative demand (Jarvis, 1994). Furthermore, the distinctive arrangement of clumped branches and foliage in the canopy facilitates efficient distribution of radiation within the canopy to the extent that almost all non-reflected incoming radiation is absorbed in stands with L of 10 (Norman & Jarvis, 1974). The needles at the bottom and middle of the canopy are usually well acclimated to their Q environment and consequently maintain a moderate carbon gain, because of their low compensation points and efficient photosynthesis (Jarvis & Leverenz, 1980; Meir *et al.*, 2002). As a consequence needles, shoots and crowns of Sitka spruce maintain high A_{\max} in diffuse light conditions, despite the sometimes large reductions of incoming Q (Jarvis, 1994).

This forest experienced Q of $<500 \mu\text{mol m}^{-2} \text{s}^{-1}$ during predominantly diffuse radiation conditions compared with $>1500 \mu\text{mol m}^{-2} \text{s}^{-1}$ during predominantly direct

beam irradiation. A 60 - 70% reduction in Q only caused a systematic reduction in mean F_A ca. 15 to 20% for all methods (Table 6.9, Figures 6.16 and 6.17). Maximum rates of F_A did not change systematically with changes in Q . For instance, under the diffuse radiation of the 21st July, $F_{E, N}$ derived estimates $F_{A(Ts)}$, $F_{A(Ta)}$, $F_{A(Ts \text{ and } U^*)}$ and $F_{A(Ta \text{ and } U^*)}$ were higher than values observed on the 22nd July when Q was relatively higher. This was not the case for the chamber-based estimates that always predicted higher F_A under sunnier conditions.

The largest differences between chamber-based and eddy covariance estimates of F_A noticeably occurred on the mornings of the 20th and 22nd July and the afternoon of the 21st July. Chamber-based modelling suggested larger rates of uptake during this period than was derived by the eddy covariance methods. These periods were characterised with $Q < 500 \mu\text{mol m}^{-2} \text{s}^{-1}$ and relatively low $U < 2 \text{ m s}^{-1}$. At these times other meteorological conditions may have placed limitations on the eddy covariance measurement, therefore reducing confidence in the estimates of F_A . During diffuse conditions like this it would not be unreasonable to hypothesise that substantial CO_2 assimilation was occurring throughout the plant canopy in the predominantly diffuse conditions. Undetected assimilation has been observed at boreal sites (Jarvis *et al.*, 1997) and is expected to occur more often in dense canopies that are likely to become de-coupled from atmospheric exchange in lower regions of the canopy (Jarvis & McNaughton, 1986; McNaughton & Jarvis, 1991; Meir, 1996). However, it is not possible to rule out other potential reasons for the observed discrepancies. Firstly, heterogeneity in F_A throughout the flux footprint may be poorly represented by the point measurements made by the branch chambers. Uncertainties in the estimate of L and biomass distribution are also likely over a flux footprint the size of 50 to 100 hectares, which may become even larger during stable conditions. However, despite these possible and probable errors in the scaling of point measurements, the methods correlated well and gave closely similar results at certain times during the observation period. This was especially the case when fluxes were

high on the 20th and 21st July, when chamber-based and eddy covariance estimates using T_a were very similar with < 10% difference.

Values of F_E and F_A found in this study were comparable with results from other Sitka spruce stands measured in Scotland. $F_{E,D}$ measured above Rivox forest during July 1990 gave net influxes between 27 and 32 $\mu\text{mol m}^{-2} \text{s}^{-1}$ at midday decreasing over the afternoon to *ca* 9 $\mu\text{mol m}^{-2} \text{s}^{-1}$ by 17:00 h (Jarvis & Moncrieff, 1992). A further study at Rivox by Beverland *et al.*, (1996) also measured maximum net influxes of between 18 to 25 $\mu\text{mol m}^{-2} \text{s}^{-1}$ during July, 1993 and an apparent canopy quantum requirement of 22 photons (molecule CO_2)⁻¹ for the canopy. This compared well with 23 and 43 photons (molecule CO_2)⁻¹ also measured at Rivox by McCracken (1993). Jarvis, (1994) estimated for Fetteresso Forest an A_{max} of 34 $\mu\text{mol m}^{-2} \text{s}^{-1}$ at 10 °C and an apparent quantum requirement of 18 photons (molecule CO_2)⁻¹. A study in Blairadam Forest, south-east Scotland on a Sitka spruce stand slightly younger than Griffin forest found comparable rates of F_E during the months of June with maximum rates of *ca* 20 $\mu\text{mol m}^{-2} \text{s}^{-1}$ when $Q > 700 \mu\text{mol m}^{-2} \text{s}^{-1}$, T_a was between 12 and 18 °C, and D_a between 5 and 15 mmol mol^{-1} . The apparent quantum requirement measured at the branch scale in Griffin Forest was on average 20 photons (molecule CO_2)⁻¹, within the range of values quoted above for Sitka spruce stands throughout Scotland. These values are also similar to shoot studies completed on Sitka spruce (Leverenz & Jarvis, 1979; Barton, 1997) and those of other C_3 plants. This seems to be a fairly conservative parameter for Sitka spruce across scales.

Falge *et al.*, (2002) found that most temperate coniferous forests had seasonal maximum rates of F_A between 16 and 25 $\mu\text{mol m}^{-2} \text{s}^{-1}$. This meta-analysis also included 1997 data from Griffin Forest of seasonal maximum F_A of 16 $\mu\text{mol m}^{-2} \text{s}^{-1}$. This figure is somewhat smaller than the maximum values observed during this study and others, independent of the method used for calculation. Employing criteria similar to those used by Falge *et al.*, (2002), (i.e., $F_{A(T_s \text{ and } U^*)}$ with a high turbulence

filter), maximum values of $F_{A(Ts \text{ and } U^*)}$ for Griffin forest were between 23 and 32 $\mu\text{mol m}^{-2} \text{s}^{-1}$ over the three days. Mean diurnal rates of GPP for temperate coniferous forest were also slightly lower than rates estimated for Griffin Forest for the same time of year. Griffin Forest also fell within the range reported for Boreal coniferous forests with GPP of 13 to 30 $\mu\text{mol m}^{-2} \text{s}^{-1}$.

6.2.5 *Integration of flux and stable isotope methods at the canopy and ecosystem scale*

$\delta^{13}\text{C}$ of respired CO_2

At the ecosystem scale we have a limited understanding of factors influencing the carbon isotope ratio of respired CO_2 . As evidence for isotope effects during dark respiration are largely inconclusive (Lin & Ehleringer, 1997), the carbon isotope ratio of canopy respired CO_2 should simply represent the relative efflux rates and isotopic composition of foliage, root and soil respiration. However, separating component respiratory sources using their $\delta^{13}\text{C}$ signatures in a 'Keeling plot' approach might be difficult because different sources often have similar isotopic compositions, as shown for this forest. For example, foliage and root respiration are both supplied from soluble carbohydrates which may be isotopically indistinguishable (Ekblad & Högberg, 2001). Literature reviews describe considerable variation among the carbon isotope ratios of different carbon compounds that are broken down during plant and soil respiration (O'Leary, 1981). This is primarily because many enzymes involved in secondary carbon metabolism discriminate against carbon isotopes; thus different chemical components have different carbon isotope ratios (for example lipids and lignins have depleted ^{13}C contents of 3 to 6 ‰ relative to bulk plant tissue. In contrast sucrose, starch, and cellulose tend to be slightly enriched in ^{13}C (O'Leary, 1981)). Another current

research enquiry is the short-term variation in photosynthetic discrimination caused by changes in meteorological conditions. This potentially alters the composition of the recently fixed assimilate that forms the substrate for instantaneous photo- and dark respiration. If autotrophic respiration forms a significant component of the overall ecosystem respiration, this could theoretically create transient changes in the composition of respired CO₂ over the growing season. This is especially the case for ecosystems that might experience changeable weather systems on short time scales of days to weeks or have distinct seasonality in precipitation, soil moisture deficits and evaporative demand on longer timescales, of weeks to months. These transient changes at the leaf scale can also affect the soil respired CO₂ signature when phloem transport of recent assimilates reaches the roots (Ekblad & Högberg, 2001; Bowling *et al.*, 2002). Because of these differences in the timing and magnitude of plant and soil respiratory processes, and associated variation in the chemical nature of the carbon-containing molecules that get broken down there may be significant spatial and temporal variation in the carbon isotope ratio of respired CO₂ in terrestrial ecosystems and further investigation of these processes will increase our understanding of how the atmosphere interacts with the plant and soil and how carbon compounds are allocated within a plant or forest.

Despite these potential differences in respired CO₂, the few studies reported indicate that the signature of organic material is correlated with integrated photosynthetic discrimination at the leaf scale. Consequently, as this material forms the litter and substrate for auto- and heterotrophic respiration the measured efflux should also be correlated. This study found very little variation in the $\delta^{13}\text{C}$ composition between the soil, wood and needle material from the upper canopy. Almost identical values were observed for a mixed *P. sitchensis* and *Tsuga heterophylla* stand located within the natural range of the species in Oregon, Pacific North West America (Bowling *et al.*, 2002). Bowling *et al.*, (2002) observed $\delta^{13}\text{C}$ compositions of -29.0, -31.5, -27.2,

-29.6, -28.8 and -27.2 ‰ for sun needles, shade needles, fine roots, fresh litter, old litter and soil organic matter in the top 5 cm of soil, respectively. These results demonstrate genetic conservation of photosynthetic discrimination through plant physiological characteristics, in the same species and different regions of the world. Furthermore, the similarities in the integrated $\delta^{13}\text{C}$ composition of the various tree components would suggest that maritime climates of the UK and Pacific Northwest are congruent.

A pattern of needle $\delta^{13}\text{C}$ composition from the top to the bottom of the canopy is commonly observed in dense canopies such as that of plantations. This gradient occurs primarily because of changes in Q and D_a through the canopy profile and their influence on stomatal conductance and assimilation rate (Francey *et al.*, 1985; Broadmeadow & Griffiths, 1993). Broadmeadow & Griffiths (1993) demonstrated a negative correlation between instantaneous ^{13}C discrimination and Q in both summer and winter conditions in a *P. abies* canopy. Indirect secondary effects of re-assimilating respired CO_2 depleted in ^{13}C are now thought to play a negligible role in maintaining this gradient in needle $\delta^{13}\text{C}$ composition (Francey *et al.*, 1985; Broadmeadow & Griffiths, 1993; Lloyd *et al.*, 1996). Another less explored theory is fractionation associated with translocation during foliage senescence, (Andreux *et al.*, 1990; Balesdent *et al.*, 1993; Buchmann *et al.*, 1997a, 1997b). Further studies on *P. sitchensis* in plantations within Scotland have found similar values for gradients of up to 0.5 ‰ m^{-1} with height for needles and branch wood in closed canopies (Heaton & Crossley, 1995; Heaton, 1999). Similar values and patterns for needle $\delta^{13}\text{C}$ have been reported in temperate *P. abies* (Gebauer & Schulze, 1991; Broadmeadow & Griffiths, 1993; Högberg *et al.*, 1993; Jäggi *et al.*, 2002) and in *P. mariana* boreal forests (Brooks *et al.*, 1997).

The relationship between $\delta^{13}\text{C}$ of respired CO_2 and that of the corresponding substrate has been shown to differ. Smith (1971) reported a depletion by 1 ‰ in respired CO_2 with respect to whole plant material of wheat, radish and pea. Park and Epstein (1961) reported a 2 to 5 ‰ enrichment with respect to bulk leaf material of whole tomato plants. Duranceau *et al.*, (1999) reported a 6 ‰ enrichment with respect to sucrose in leaves of bean plants. Duranceau *et al.*, (2001) and Ghashghaie *et al.*, (2001) found respired CO_2 isotopically enriched by 2 to 6‰ with respect to soluble carbohydrates and whole leaves of tobacco and sunflower, and concluded that direction and magnitude of respiratory fractionation of CO_2 may vary depending on environmental conditions and species. In this study, the $\delta^{13}\text{C}$ of soluble carbohydrates was not measured directly and therefore only tentative conclusions can be drawn from any comparison between, $\delta^{13}\text{C}$ composition of the respired CO_2 and the bulk material. However, in general respired CO_2 was enriched compared to bulk needle material by 1.5 to 3 ‰, in general agreement with the direction and magnitude observed by Park & Epstein (1961), Duranceau *et al.*, (1999, 2001) and Ghashghaie *et al.*, (2001).

The similarity of $\delta^{13}\text{C}$ of soil respired CO_2 to that of autotrophic respiration renders the isotopic imprint of soils on the atmosphere a possible tool in tracing the role of soils in the global CO_2 budget (Amundson *et al.*, 1998). Santruckova *et al.*, (2000) showed in laboratory experiments on soils from a North-South transect in Australia that soil microbial carbon tended to be more enriched in $\delta^{13}\text{C}$ than the soil organic carbon. This was balanced by an inverse isotope shift in the $\delta^{13}\text{C}$ value of respired CO_2 resulting in the $\delta^{13}\text{C}$ value of respired CO_2 being approximately similar to that of the $\delta^{13}\text{C}$ of soil organic carbon. For instance, Flanagan *et al.*, (1996) found the $\delta^{13}\text{C}$ of soil respired CO_2 quite similar to the $\delta^{13}\text{C}$ of the humus and mineral soil at a *P. mariana* site in Canada. Signatures for the soil respired CO_2 and organic matter at 0-10 and 10-20 cm, were ca. -25, -26.6 and -25.5 ‰, respectively. In contrast to this

result, Ekblad & Högberg (2001) found for a mixed *P.abies* and *P. sylvestris* site in Sweden marked differences between the soil respired $\delta^{13}\text{C}$ composition and that of the soil organic matter, which, over the season, measured between -21.6 to -26.5 ‰, from a soil with $\delta^{13}\text{C}$ of -28.2‰ for the upper organic soil and -27.4 ‰ lower in the profile (Ekblad & Högberg, 2001). Ekblad & Högberg, (2001) concluded from this result that at least 65% of total soil respiration came from root respiration using currently fixed photo-assimilates as the substrate.

Soil organic matter consists of a mixture of plant and microbial biomass. Evidence for preferential utilisation of available biomolecules by soil microbes and any potential discrimination during microbial metabolism is currently sparse, posing substantial technical and theoretical obstacles when extrapolated to the collection of field data. However, laboratory experiments show that fractionation during microbial degradation of organic material can induce a shift in the $\delta^{13}\text{C}$ composition of soil organic carbon. Santruckova *et al.*, (2000) concluded that this shift can be induced by both the selective use of organic compounds and isotope discrimination during microbial metabolism. The extent of isotopic discrimination during metabolism was found to be dependent on microbial population. Bulk soil organic matter tends to become enriched in ^{13}C relative to the aboveground plant material that forms the starting signature for decomposition (for a review see Ehleringer *et al.*, 2000). This ^{13}C enrichment has been shown for soil and forest types similar to those studied at Griffin forest. Bol *et al.*, (1999) showed for podsoles and stagnohumic gleysol from British uplands, ^{13}C enrichments of 1 to 2.5 ‰ over 25 cm depth, respectively. Bowling *et al.*, (2002) also measured a 3‰ increase in $\delta^{13}\text{C}$, also over 25cm depth. In this study $\delta^{13}\text{C}$ soil respired CO_2 was similar to soil organic matter and did not vary significantly between field campaigns. There was however, a shift in δ_s observed when temperatures were high and soil moisture availability low, that lowered δ_s relative to soil organic matter and the average $\delta^{13}\text{C}$ value for soil respired

CO₂. This point observation may be the result of some sampling artefact, for instance an input of human respired CO₂ when the chamber was being closed. Furthermore, as the flux rates had dropped the reliability of the measurement was perhaps compromised, as errors tend to increase with smaller fluxes (see Chapter 3). However, this strange observation was accompanied by curiosities in other, independent, measurements made at the same time; this may be coincidental but perhaps not. We know from many observations in the literature what happens to flux rates under water stress, but we know little about what happens to the community of organisms respiring. Was the drop in flux rate caused by a shortage of preferential substrate and switch to another? For instance, lignins are typically more depleted in ¹³C and abundantly found in coniferous ecosystems. Was it a switch in the community of organisms responsible for the respiration, perhaps to organisms with drought tolerance? This may perhaps indicate a potential area in need of research especially in ecosystems vulnerable to drought under future climate change; resulting changes in $\delta^{13}\text{C}$ of soil respired CO₂ may be a potential tracer for changes in soil respiration.

$\delta^{13}\text{C}$ of ecosystem respiration and ¹³C discrimination

Values for $\delta^{13}\text{C}$ of ecosystem respiration ($\delta^{13}\text{C}_\text{R}$) were conservative over three sampling campaigns and similar to the $\delta^{13}\text{C}$ of the measured soil CO₂ efflux. Values for $\delta^{13}\text{C}_\text{R}$ were -28.8 ± 0.5 , -29.3 ± 1.0 and $-28.8 \pm 0.2\text{‰}$ in September 2000, May and July 2001, respectively. These values were consistent with results from a study on two sites of 30 and 150-year-old *P. sitchensis* and *T. heterophylla* in the Pacific Northwest (Bowling *et al.*, 2002). These two sites represented the wettest sites in a transect across a moisture gradient in Oregon and had the most depleted δ_R composition relative to other sites on the transect. The younger stand had a mean δ_R composition of $-28.5 \pm 0.5\text{‰}$, whilst the older stand had a mean δ_R composition of –

$26 \pm 0.5\text{‰}$. Bowling *et al.*, (2002) concluded that on the older site $\delta^{13}\text{C}$ values were enriched because of processes involved in the age-related decline in aboveground productivity. Such an age-related change in $\delta^{13}\text{C}$ values was observed for *P. menziesii* forests ranging in age from 20 to >450 years in Washington, USA (Fessenden & Ehleringer, 2002).

Temperate and boreal regions are typically characterised by pronounced seasonal differences of incoming radiation, and temperature. Thus differences in $\delta^{13}\text{C}_\text{R}$ and Δ_KEELING values throughout the growing season are to be expected. For instance, Bowling *et al.*, (2002) found a wide range of $\delta^{13}\text{C}_\text{R}$ over the growing season, -27 to -31‰ for the 30-year-old site and -24 to -29‰ for the 150-year-old site although SD indicated possibly larger ranges than the means cited above. These values were not found to correlate significantly with either the previous months' precipitation or leaf pre-dawn water potential, as found for other sites of *P. menziesii* and *P. ponderosa* along the transect, indicating other mechanisms for the observed changes in signature with time for the *P. sitchensis* sites. In contrast to this, the seasonal course of $\delta^{13}\text{C}_\text{R}$ in Griffin forest did not vary much across the three sampling occasions. The apparent stability in Δ_KEELING (calculated from $\delta^{13}\text{C}_\text{R}$ and δ_a see Eq 4.14) has also been observed for other temperate and coniferous stands. Buchmann *et al.*, (1997) found for three *Abies amabilis* forests in the Pacific Northwest very weak patterns throughout the growing season of Δ_KEELING . Although shifts in composition were small, the directions were consistent across all three stands with higher values in August compared with those of June and September. The values for Δ_KEELING ranged from 18.9 to 19.8‰ across the three stands of *A. amabilis* with differing L and across the season (Buchmann, 1997). Further studies in *P. mariana* stands in boreal forest also showed very little seasonality in $\delta^{13}\text{C}_\text{R}$ for both northern and southern study sites in Canada. Both sites consistently gave values of -26‰ during spring, summer and autumn (Flanagan *et al.*, 1996). Calculated Δ_KEELING for the sites were also

conservative and ranged from 18.7 to 19.6 ‰. Both these values are somewhat lower than the values of Δ_{KEELING} calculated for Griffin forest of *ca* 21.6 ‰ for July (calculated assuming a tropospheric composition of -7.8 ‰ in July 2001). The exact composition of the atmospheric source air presently remains undetermined. Buchmann *et al.*, (1998) reviewed the published literature and compiled estimates of Δ_{KEELING} for temperate ecosystems. Values ranged between 16 and 20 ‰, slightly lower than the value found at the Griffin site. The value for Griffin forest fell within those typically found for tropical forests, between 19 and 21‰. Kaplan *et al.*, (2001) modelled values of 15.7 ± 2.2 and 17.6 ± 2.56 ‰ for temperate evergreen needle-leaf forest and cool evergreen needle-leaf forest, respectively. These were compared with a collection of measurements from these biomes of 17.8 ± 0.93 and 16.8 ± 1.00 , respectively. However, a global distribution map of Δ_{KEELING} produced by Kaplan *et al.*, (2001) predicted values in the region of 20 - 22‰ for vegetation in Scotland. Differences of 1-2‰ might be attributable to site-specific conditions, and are within the expected variability of the modelled values. Furthermore, as this site is only 20-year-old, site history may play some role, as this integrated signal includes a 'memory effect' of past vegetation cover incorporated in the soil organic matter, which accumulated under heather moorland.

Instantaneous canopy photosynthetic discrimination, (Δ_{C}) and instantaneous ecosystem discrimination (Δ_{E}) simulated for the observation period were variable over the day and between days (The latter which differs from Δ_{C} and represents the combined influences of photosynthetic and (both) autotrophic and heterotrophic respiratory fluxes on canopy air, Lloyd *et al.*, 1996). Fluctuations in Δ_{C} and Δ_{E} occurred in response to changing environmental conditions and give some indication of how persistent weather systems might cause temporal changes in Δ_{C} and Δ_{E} . When Q was predominately diffuse and D_{a} low, values of Δ_{C} were relatively larger than for conditions with direct Q and higher D_{a} . G_{s} values were typically larger under the

former conditions and despite the low Q maintained substantial A . These conditions consequently led to greater expression of enzymatic ^{13}C discrimination. The daily rhythms of F_R and G_s were apparent in Δ_C and Δ_E . For instance, in the mornings when T_s and F_R were low and G_s high, Δ_E resembled that of Δ_C and F_A dominated. However, when F_R increased and G_s decreased in the afternoon, Δ_C and Δ_E also decreased; the increasing contribution of R_s at this time is apparent from the difference between Δ_C and Δ_E . During periods of high Q and T_a the influence of soil respiration was even more pronounced in the afternoons as Δ_C started to increase after midday minima regulated by C_i/C_a . However, this increase did not transfer to Δ_E because of increases in R_s .

Values for integrated canopy photosynthetic discrimination ($\int \Delta_C$) and integrated ecosystem photosynthetic discrimination ($\int \Delta_E$) for each day, varied by as much as 1.6‰ for the canopy and 1.5‰ for the ecosystem. Modelling studies have also predicted various values of $\int \Delta_C$ for similar biomes. Lloyd & Farquhar, (1994) predicted values of 15.4‰ for cool/cold coniferous forest whilst Fung *et al.*, (1997) predicted Δ_C of 20.5‰ for needle-leaved evergreen forest. The main difference between these two studies was that the former model explicitly included mesophyll resistance while the latter did not; this difference was thought to explain the contrast in results. However, the present study also incorporated mesophyll conductance, photorespiration and dark respiration by the canopy explicitly, yet values in the present study are somewhat higher than 15.4‰, with canopy values varying between 18.8 and 20.4‰ over the three days. Lloyd & Farquhar (1994) modelled discrimination over regional spatial and annual temporal scales. Thus direct comparison between our localised measurements at a fine temporal resolution may not be directly comparable to this coarser simulation. Furthermore, Griffin Forest has been shown to differ from more continental stands of similar species at the same

latitude in its carbon dynamics, primarily because of its maritime proximity (Valentini *et al.*, 2000).

Comparable values for daily variations in Δ_C are currently available for two published studies. Lloyd *et al.*, (1996) measured gas exchange and the stable isotope composition of canopy air for a tropical forest in Brazil and a boreal forest in Siberia. The tropical forest had maximum values of 20‰ for Δ_C in the morning when G_s was at a maximum. By midday G_s had decreased and A was maximum, and calculated Δ_C reached a minimum of 17.7‰; thereafter Δ_C increased to values observed during the morning as G_s continued to decrease with A . In contrast, the boreal forest exhibited erratic behaviour in A and G_s over the diurnal period and this led to erratic Δ_C . Low G_s accompanied by low A , were observed in the morning with low Δ_C of 14.9‰. These values increased as G_s and A increased and Δ_C values reached a maximum of 20.0‰. At midday a drop in A caused a sharp drop in Δ_C to values of 14‰, thereafter increasing to a maximum of 17.0‰. These results are similar in magnitude and pattern to the results for the different days presented in this study with the exception of slightly higher Δ_C values predicted in the mornings at Griffin Forest.

In a biome study with comparable temporal resolution Bowling *et al.*, (2001) using eddy covariance and profile measurements to establish F_E and collection of $^{13}\text{CO}_2$ above and within the canopy used the partitioning approach in a temperate deciduous ecosystem in Tennessee, USA. Assimilation-weighted discrimination [Δ_C for this forest during July was 16.8 ± 4.7 to 17.1 ± 3.5 ‰, dependent on the canopy conductance calculation used. Notable strong diurnal patterns were calculated, with higher Δ_C of *ca* 17.5 to 19.5‰ in the early morning and lower Δ_C of 16 to 17‰ in the afternoon. Using a value of -8‰ for the atmosphere they estimated [Δ_{LF} of 18.1 ± 3.0 ‰, slightly higher than for daily-integrated values by 1‰. No measurements of A , g_s or Δ_{obs} were measured directly by independent methods by Bowling *et al.*

(2001), unlike the present study or Lloyd *et al.* (1996). Furthermore, data presented for each variable represented a 20-day bin ensemble. These data were then additionally smoothed, thereby removing short term fluctuations in the environmental variables and dependent processes usually observed over a day. For this approach to be satisfactory it is essential that isotopic relationships derived at one point in time are also applicable at another during a 20-day period. This could be a problem if any of the points raised in the discussion above occur. Bowling *et al.*, (2001) also did not consider the additional processes that occur during the day when calculating Δ_C , mainly the contributions of day respiration, photorespiration and the role of mesophyll resistance. However, the results from the 20 day averaged, daily cycles are similar to those results presented here, but only for certain methods and under particular conditions. Results from this study indicate that the Bowling partitioning approach tends to give Δ_C values lower than those observed and modelled from the branch data.

Bowling *et al.*, (2001) concluded that canopy conductance was one of the largest uncertainties with this approach to calculating Δ_C . This is especially true when canopies are wet as shown earlier. The contribution of evaporated water to eddy covariance estimates of canopy conductance were substantial at times, causing Δ_C to decrease. In this instance, the removal of data when canopies are wet from any bin-average would be justified, as inclusion of these data may lead to underestimation of Δ_C and overestimation of F_A . This could represent a problem in ecosystems that experience persistent rainfall like those of tropical rainforest and temperate maritime forests. On the whole, $\int \Delta_C$ and F_A estimates using this approach compared with branch scaled estimates differed by <10% for $\int \Delta_C$, but by up to 75% for maximum F_A and by 51% for mean daily F_A .

The further uncertainty regarding canopy conductance for CO_2 not addressed by Bowling *et al.*, (2001) was the potential effect of mesophyll resistance. Bulk mesophyll conductance is a hard parameter to estimate in the field but it appears to play an important role in the partitioning exercise. By neglecting this extra resistance encountered by CO_2 as it diffuses to the site of carboxylation, Δ_C is potentially underestimated for the canopy and daily mean F_A is consequently overestimated by as much as 50% on certain days. Therefore, it is crucial to obtain some estimation of the relative importance of mesophyll conductance compared with that of stomatal conductance when using this approach for constraining values of F_A . In the present study independent estimates of canopy conductance and mesophyll conductance were obtained from the branch chamber through the combined measurement of A , E , and Δ_{obs} . Estimates for G_w are found to vary with photosynthetic capacity, and values found for other species using a similar stable isotope method typically range between 200 to 550 $\text{mmol m}^{-2} \text{s}^{-1}$ (Lloyd *et al.*, 1992; Evans *et al.*, 1986; Evans & Von Caemmerer, 1996; Loreto *et al.*, 1992; Harwood *et al.*, 1999). Jarvis, (1994) estimated a mesophyll conductance value of 201 $\text{mmol m}^{-2} \text{s}^{-1}$ for CO_2 during the active growing season for a Sitka spruce plantation in Scotland compared with the value of 290 $\text{mmol m}^{-2} \text{s}^{-1}$ estimated for the Griffin Forest canopy. However, G_w may change seasonally through changes in photosynthetic capacity and leaf anatomy, that will certainly occur between bud burst and the end of shoot elongation, indicating the need for repeated measurements of this parameter if the partitioning approach is to be used over the growing season. Reductions in G_w would translate into greater Δ_C and lower F_A .

6.2.6 Ecosystem carbon balance

Daily ecosystem carbon balance

Differences in the modelled daily carbon balance for this forest were striking. Estimates of daily uptake differed by 45 to 55% over the three days using the extreme scenarios of F_A (T_s) and F_A (R_n). The highest daily C losses were predicted using the method most commonly applied at flux sites F_R (T_a and U^*). These losses differed from the chamber-based estimates by ca. 50%. These disturbing uncertainties and disagreements between methods indicate an urgent need for additional constraints on estimates of F_A and F_R . In particular, efforts should be focussed on F_R , especially during the day. This analysis highlights that canopy respiration is not a simple empirical process but is likely to be as complex as that of photosynthesis. Furthermore, it may prove difficult to demonstrate that some of the partial processes occur in the field. This will place a lot of emphasis on modelling and on generating laboratory evidence that these processes do exist across plant species, functional groups and biomes. There is also a need to confirm changes in canopy assimilation and respiration during periods when limitations to eddy covariance measurements occur during day and night. It was apparent that similar values of F_A between methods were found, under certain conditions, but, mean F_A values over the day could be very different, mainly because of periods of higher F_A that were observed in chambers was not detected by the eddy covariance method, especially in the morning and late afternoon.

Some modelling studies have incorporated differences in daytime respiration when estimating daily and annual carbon balance for forests. Daily net photosynthesis modelled with MAESTRO by Kruijt *et al.*, (1999) for a Sitka spruce plantation ranged from 4.8 to 10.8 g C m⁻² d⁻¹ for July. Comparable estimates from this study (corrected for soil respiration) were between 8.4 and 12.9 g C m⁻² d⁻¹ for the three

days. Kruijt *et al.*, (1999) also simulated the effects of elevated CO₂ (700 $\mu\text{mol mol}^{-1}$) and increased temperature (+3 °C). This exercise increased daily net photosynthesis to 14.4 g C m⁻² d⁻¹. Daytime respiration in this model was assumed to be reduced to 60% of nighttime rates at the same temperature, as a result of switching to chloroplastic ATP supply (Brooks and Farquhar, 1985). However, they did not explore the effects of ignoring inhibition of respiration. Furthermore, the extent of inhibition may not be constant over the day as discussed throughout this study. Falge *et al.*, (2002) in their meta-analysis estimated mean daily C balance at Griffin Forest of 1.95 g C m⁻² d⁻¹ and mean F_A rate of 6.27 g C m⁻² d⁻¹. As these represent mean values for the year it is difficult to compare with the present contribution.

Annual carbon balance

Kruijt *et al.*, (1999) estimated annual GPP values of 13.4 t C ha⁻¹ yr⁻¹ for ambient CO₂ and temperature conditions using MAESTRO. Valentini *et al.*, (2000) estimated annual GPP values for 1997 and 1998 at Griffin of 19.9 and 19.2 t C ha⁻¹ yr⁻¹ and annual estimates of total ecosystem respiration of 13.2 and 13.5 t C ha⁻¹ yr⁻¹, respectively. It was noted in this particular synthesis that, Griffin Forest had the largest values for GPP and total ecosystem respiration out of all the 18 sites studied across Europe. These high process rates were attributed to disturbance during site preparation, the favourable maritime climate and N fertilisation. These values were obtained using respiration rates which excluded $U^* < 0.2 \text{ m s}^{-1}$. This present contribution demonstrates that these respiration rates are indeed the largest estimates over all methods used here, particularly if T_a was used to force the functional relationship. Using data collected over the year, only for the soil component, losses constituted approximately 4.7 t C ha⁻¹ yr⁻¹, however, it is difficult to estimate the foliage contribution for the year without a more elaborate model. If 55% of the total

ecosystem respiration came from above ground components annual ecosystem respiration would account for losses of $\approx 10 \text{ t C ha}^{-1}$, slightly less than recent values of 12.5 t C ha^{-1} for Griffin Forest (Figure 6.23) (personal communication, R. Clement). To account for this difference in annual ecosystem respiration a decrease

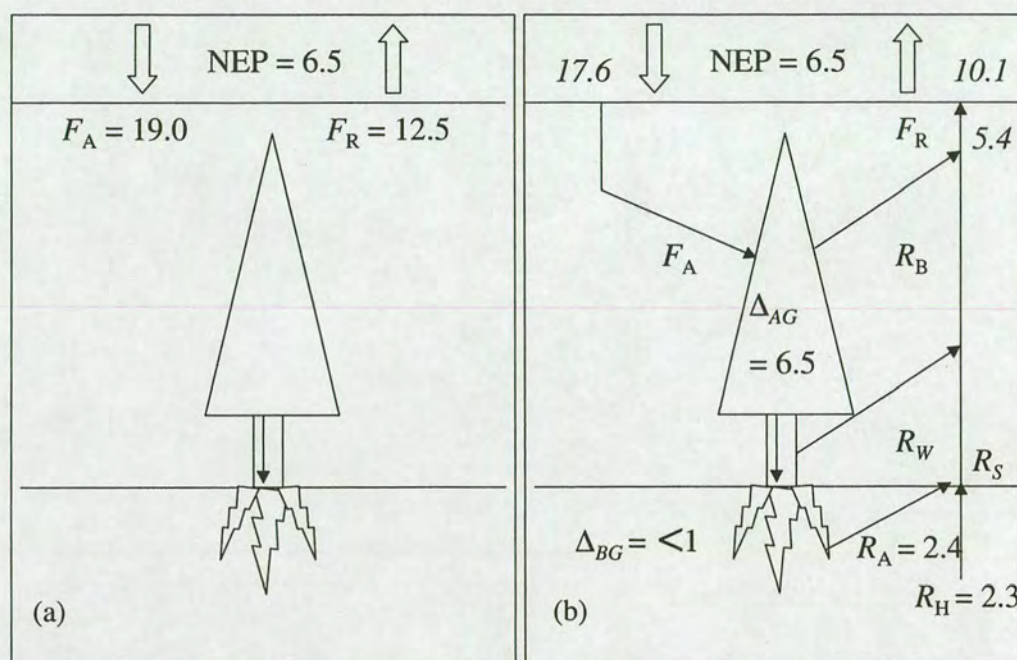


Figure 6.23 Tentative estimates for annual total carbon flows for Griffin Forest. All units are $\text{Mg C m}^{-2} \text{ y}^{-1}$ and Symbols are described in Figure 1.1. The data for (a) are derived from eddy covariance measurements and a fitted function between T_a and $F_{E,N}$ excluding low U^* data. The data for (b) are derived from basal area inventories collected over 5 years in 45 plots within the flux footprint, disturbed and undisturbed soil profiles within the flux footprint and soil respiration measurements collected over 2000/2001 within the flux footprint. Foliage and stem respiration are assumed to account for 55% of annual ecosystem respiration with measured soil respiration accounting for the remaining 45% split evenly between autotrophic and heterotrophic respiration (Hogberg *et al.*, 2001)

in GPP or increase in net ecosystem productivity (NEP) would be required as shown in Figure 6.23b for the former scenario. Average annual net ecosystem productivity (NEP) for the site estimated from 5 years of eddy covariance measurements is approximately $6.5 \pm 1.3 \text{ t C ha}^{-1}$ ($\pm 20 \%$). This value compares favourably with the

observed mean increment in above- and below-ground C (Figure 6.23b). The observed increase in above-ground C was $6.5 \pm 11 \text{ t C ha}^{-1}$ ($\pm 1\text{SD}$) (see Chapter 2), and the increment in below-ground C was conservatively estimated 19 t C ha^{-1} over the current rotation (≈ 20 years), assuming this increments evenly over the rotaion this equates to $ca < 1 \text{ t C ha}^{-1} \text{ y}^{-1}$ indicating the measurement of NEP using eddy covariance is comparable with inventory methods for estimating changes in forest C stocks and unlikely to account for the discrepancy in annual ecosystem respiration.

6.3 CONCLUSIONS

Three methods were used to estimate the daily ecosystem carbon balance from a temperate Sitka spruce forest: (a) a summation of branch and soil chamber observations (b) the eddy covariance method and (c) the partitioning of net ecosystem exchange using stable isotopes. Efforts to explore the sensitivity of ecosystem processes to presently adopted protocols have been made. These included the consequences of: (a) removing low U^* data, (b) applying different temperature reference locations, and (c) including inhibition of dark respiration during the day. The main conclusions drawn form this analysis are:

- Summed nocturnal chamber measurements agree well with eddy covariance estimates, especially when T_a and all U^* are used to estimate total ecosystem respiration.
- The range and pattern of nocturnal F_R was best described in relation to T_a .
- Excluding low U^* data systematically increased F_R estimates by $1 \mu\text{mol m}^{-2} \text{ s}^{-1}$.

- The contribution of aboveground components to the total ecosystem respiration equalled that of the belowground components.
- Structural characteristics of the soil gave rise to systematic differences in soil CO₂ efflux rates. The soil characteristics were influenced profoundly by the local hydrology and earlier forest planting practices at the site.
- Simulations indicated that inhibition of respiration during the day could potentially result in F_R up to 50% lower than currently modelled daytime rates.
- Branch chamber-based estimates indicated higher assimilation rates than eddy covariance based estimates of F_A when conditions were calm.
- The stable isotope partitioning approach was simple to apply in the field, but its applicability and reliability at determining instantaneous Δ_C and F_A observations has yet to be established.
- Mesophyll conductance at the canopy scale appeared to play an important role in the calculation of F_A using the partitioning approach. Neglect of this extra resistance will almost certainly lead to over-estimation of canopy F_A .
- The contribution of E_I when calculating G_s led to over-estimations of G_s and under-estimations of Δ_C .

7. Concluding remarks

Continued observation and increased understanding of the processes governing fluxes of CO₂ between the terrestrial biosphere and the atmosphere may prove to be one of the most important scientific pursuits in the next few decades. The terrestrial biosphere can sequester large amounts of CO₂ from the atmosphere *via* photosynthesis and store this carbon in potentially longer-lived products. Quantifying the sequestration potential of forests and their role in the global carbon cycle has now become a political necessity and recognised as a resource that could be managed to either mitigate or exacerbate future climate change.

Data were presented in this thesis to quantify the daily pattern of environmental variables and their effect on rates of key physiological processes monitored from branches, soil and the entire canopy of a Sitka spruce plantation.

At the forest scale daily patterns and estimates of canopy photosynthesis and ecosystem respiration were determined using three approaches (Chapters 5 and 6):

- fitting relationships to nocturnal net ecosystem exchange and temperature using the eddy covariance method, thereby estimating daytime respiration and facilitating mass balance calculation of canopy photosynthesis;
- scaling relationships between gas exchange and environmental variables observed in branch and soil chambers to the forest using biomass inventories and (Chapters 2, 3, 4, 5 and 6);

- combining canopy $^{13}\text{CO}_2$ measurements with daytime net ecosystem exchange data to estimate canopy photosynthesis, thereby facilitating mass balance calculation of ecosystem respiration rates (Chapters 3, 4, 5 and 6).

Daily patterns of canopy photosynthesis were comparable in magnitude and timing between methods and tightly coupled to incoming photon flux density, vapour pressure deficit and temperature. Daily maximums for canopy photosynthesis ranged from -20 to $-30 \mu\text{mol m}^2 \text{s}^{-1}$ and were similar to other published studies. Estimates for ecosystem respiration were variable between methods, depending on e.g. inhibition of day respiration and effects of low turbulence. Good correlation between derived estimates of nocturnal ecosystem respiration and chamber estimates were observed, but only when air temperature was used to predict ecosystem respiration. Furthermore, including low turbulence measurements of nocturnal net ecosystem exchange when fitting the temperature function for ecosystem respiration reduced discrepancies between the two methods (Chapters 5 and 6).

The present study also highlighted a gap in present knowledge concerning daytime dark respiration fluxes. There is evidence for inhibited rates of dark respiration during the day in Sitka spruce but models describing the behaviour of this process under variable environmental conditions are rare. Using the best dataset available to describe the interaction of photon flux density and temperature on daytime dark respiration, estimates of inhibited daytime respiration were made at the branch and canopy scale (Chapters 3 and 4). At the branch scale rates of daytime respiration were typically 35 to 65% lower than those predicted using a fitted relationship between nocturnal CO_2 efflux from branches and temperature for different locations in the canopy and during different field campaigns. When this relationship was scaled to the canopy estimates of ecosystem respiration were $\approx 50\%$ lower than if dark respiration was assumed to continue at the same rate during the day as observed during the night for the same temperature (Chapters 5 and 6). Hence there is a necessity for improvements in the measurement and modelling of respiratory fluxes

from Sitka spruce and within ecosystems, especially during the day where most of the uncertainty still remains.

Although the $^{13}\text{CO}_2$ partitioning approach is simple to apply in the field compared to chamber methods, its applicability and reliability at determining instantaneous canopy photosynthesis and canopy photosynthetic ^{13}C discrimination (Δ_c) is questionable for two reasons that could be addressed using additional field observations (Chapters 5 and 6). Firstly, this method is extremely sensitive to variations in canopy conductance to CO_2 (G_c) estimated indirectly from water vapour fluxes. When the canopy surface becomes wet, the contribution of intercepted water can cause a substantial overestimation of G_c , which in turn causes an overestimation of canopy photosynthesis and underestimation of Δ_c . This study concludes that this method is best suited to dry observation periods. Using independent methods capable of estimating transpiration during all weather conditions could constrain estimates using this approach alternatively, the development of site parameterised models of G_c could be used to fill gaps in data when canopies are wet (Chapter 5 and 6).

Secondly, mesophyll conductance (G_w) at the canopy scale appears to play an important role in the calculation of F_A using the $^{13}\text{CO}_2$ partitioning approach. Data presented in this study showed neglecting this extra resistance led to a substantial overestimation of F_A . G_w may also change seasonally through changes in photosynthetic capacity and leaf anatomy, which will certainly occur between the period of bud burst and the end of shoot elongation. This would indicate a need for repeated measurements of G_w if the partitioning approach is to be used reliably over the growing season or alternatively some proxy for g_w , like V_{\max} or leaf nitrogen be established. It also follows that if G_w scales with photosynthetic capacity, substantial spatial variability will exist between needles of different age and position in the canopy. Thus spatial measurements of mesophyll conductance in the canopy would also be desirable to constrain estimates of canopy assimilation and photosynthetic discrimination as demonstrated at both the branch and canopy scale (Chapters 3, 4, 5

and 6. In this study the measurement of photosynthetic discrimination conveniently provided a means of estimating an average G_w .

A method was also developed to measure the carbon isotope composition of CO_2 in air exchanging directly with branches (Chapters 3 and 4). Daily patterns in instantaneous ^{13}C discrimination (Δ_{obs}) and the $\delta^{13}\text{C}$ of respired CO_2 were combined with environmental data and continuous gas exchange to explore theoretical models describing photosynthetic discrimination, Δ . This analysis showed that commonly used simple models relating Δ solely to intercellular CO_2 concentration, typically underestimated Δ when compared against field observations during morning and evening periods when the relative contribution of daytime dark respired $^{13}\text{CO}_2$ was large. Furthermore, the simple model typically overestimated Δ when compared with field observations during the midday period, when CO_2 assimilation rates were high. This study demonstrated fractionation associated with photorespiration and mesophyll conductance were important for explaining differences between Δ_{obs} and that predicted using the simple model at these times.

Models were then developed and parameterised to predict daily cycles of instantaneous ^{13}C discrimination and $\delta^{13}\text{C}$ of recently assimilated needle carbohydrates (Chapters 3 and 4). This dynamically simulated the links between environmental conditions, canopy discrimination and the $\delta^{13}\text{C}$ of ecosystem respired CO_2 . Providing both a method and model to directly test hypotheses concerning the environmental regulation of autotrophic respiration measured above-ground and from soil surfaces, potentially leading to a clearer understanding in the temporal variability in observed ecosystem Δ and $\delta^{13}\text{C}$ of ecosystem respired CO_2 . Furthermore, these bottom-up estimates of canopy ^{13}C discrimination provided a means of comparison with top-down estimates calculated from a recently developed approach incorporating the eddy covariance method and profiles of δ_a and CO_2 .

REFERENCES

- Allison C.E., Francey R.J. and Meijer H.A.J. (1995) Recommendations for the reporting of stable isotope measurements of carbon and oxygen in CO₂. In: *References and intercomparison materials for stable isotopes of light elements*. International Atomic Energy Agency., Vienna.
- Alsheimer M., Kostner, B., Falge, E. and Tenhunen, J.D. (1998) Temporal and spatial variation in transpiration of Norway spruce stands within a forested catchment of the Fichtelgebirge, Germany. *Annales des Sciences Forestieres.*, **55**, 103-124.
- Amundson R., Stern, L., Baisden, T. and Wang, Y. (1998) The isotopic composition of soil and soil-respired CO₂. *Geoderma*, **82**, 83-114.
- Andreux F., Cerri, C.C., Vose, P.B. and Vitorella, V.A. (1990) The distribution of ¹³C and ¹⁵N in plants and soil profiles. In: *Nutrient cycling in terrestrial ecosystems*. (ed A.F. Harrison, Ineson, P., Heal, O.W.), pp. 262-265. Elsevier, The Netherlands.
- Armstrong W., Gaynard, E.J. (1976) The critical oxygen pressure for respiration in intact plants. *Physiologia Plantarum*, **37**, 200-206.
- Arneth A., Kelliher F.M., Bauer G., Hollinger D.Y., Byers J.N., Hunt J.E., McSeveny T.M., Ziegler W., Vygodskaya N.N., Milukova I., Sogachov A., Varlagin A. and Schulze E.D. (1996) Environmental regulation of xylem sap flow and total conductance of *Larix gmelinii* trees in eastern Siberia. *Tree Physiology*, **16**, 247-255.
- Arneth A., Kelliher F.M., Gower S.T., Scott N.A., Byers J.N. and McSeveny T.M. (1998) Environmental variables regulating soil carbon dioxide efflux following clear-cutting of a *Pinus radiata* D. Don plantation. *Journal of Geophysical Research-Atmospheres*, **103**, 5695-5705.
- Arrhenius S. (1896) On the influence of carbonic acid in the air upon the temperature of the ground. *The London, Edinburgh and Dublin Philosophical Magazine and Journal of Science*, **41**, 237-276.
- Atkin O.K., Evans, J.R., Ball, M.C., Lambers, H. and Pons, T.L. (2000) Leaf respiration of Snow gum in the light and dark. Interactions between temperature and irradiance. *Plant physiology*, **122**, 915-923.

- Atkin O.K., Evans, J.R. and Siebke, K. (1998) Relationship between the inhibition of leaf respiration by light and enhancement of leaf dark respiration following light treatment. *Australian Journal of Plant Physiology*, **25**, 437-443.
- Aubinet M., Grelle, A., Ibrom, A., Rannik, U., Moncrieff, J., Foken, T., Kowalski, A.S., Martin, P.H., Berbigier, P., Bernhofer, C., Clement, R., Elbers, J., Granier, Grunwald, T., Morgenstern, K., Pilegaard, K., Rebmann, C., Snuders, W., Valentini, R. and Vesala, T. (2000) Estimates of the annual net carbon and water exchange of forests: The EUROFLUX Methodology. *Advances in Ecological Research*, **30**, 114-175.
- Azcon-Bieto J., Lambers, H. and Day, D.A. (1983a) Effect of photosynthesis and carbohydrate status on respiratory rates and the involvement of the alternative pathway of leaf respiration. *Plant physiology*, **72**, 598-603.
- Azcon-Bieto J. and Osmond, C.B. (1983b) Relationship between photosynthesis and respiration. *Plant physiology*, **71**, 574-581.
- Bakwin P.S., Tans P.P., White J.W.C. and Andres R.J. (1998) Determination of the isotopic (C-13/C-12) discrimination by terrestrial biology from a global network of observations. *Global Biogeochemical Cycles*, **12**, 555-562.
- Balaguer L., Afif, D., Dizengremel, P. and Dreyer, E. (1996) Specificity factor of ribulose carboxylase/oxygenase of *Quercus robur*. *Plant Physiology and Biochemistry*, **34**, 879-883.
- Baldocchi D.D., Hicks B.B. and Meyers T.P. (1988) Measuring biosphere-atmosphere exchanges of biologically related gases with micrometeorological methods. *Ecology*, **69**, 1331-1340.
- Baldocchi D.D. and Meyers, T.P. (1991) Trace gas exchange above the floor of a deciduous forest - 1: evaporation and CO₂ efflux. *Journal of Geophysical Research-Atmospheres*, **96**, 7271-7285.
- Balesdent J. and Mariotti, A. (1996) Measurement of soil organic matter turnover using ¹³C natural abundance. In: *Mass spectrometry of soils*. (ed T.W. Boutton, Yamasaki, S.I.), pp. 83-111. Marcel Dekker, New York.
- Ball J.T., Woodrow, I.E. and Berry, J.A. (1987) A model predicting stomatal conductance and its contribution to the control of photosynthesis under different environmental conditions. In: *Progress in Photosynthesis Research* (ed I. Biggins), pp. 221-224. Martinus Nijhoff Publishers, Netherlands.

- Barradas V.L. and Jones, H.G. (1996) Responses of CO₂ assimilation to changes in irradiance: laboratory and field data and a model for beans (*Phaseolus vulgaris* L.). *Journal of Experimental Botany*, **47**, 639-645.
- Barradas V.L., Jones, H.G. and Clark, J.A. (1994) Stomatal responses to changing irradiance in *Phaseolus vulgaris* L. *Journal of Experimental Botany*, **45**, 931-936.
- Barton C. (1997) *Effects of elevated atmospheric carbon dioxide concentration on growth and physiology of Sitka spruce (Picea sitchensis (Bong.) Carr.)*. PhD, University of Edinburgh.
- Bartelink H.H. (1996) Allometric relationships on biomass and needle area of Douglas-Fir., **86**, 193-203.
- Battle M., Bender M.L., Tans P.P., White J.W.C., Ellis J.T., Conway T. and Francey R.J. (2000) Global carbon sinks and their variability inferred from atmospheric O-2 and delta C-13. *Science*, **287**, 2467-2470.
- Bekku Y., Koizumi, H., Oikawa, T. and Iwaki, H. (1997) Examination of four methods for measuring soil respiration. *Appl. Soil Ecol.*, **5**, 247-254.
- Bender M.M. (1968) Mass spectrometric studies of carbon-13 variations in corn and other grasses. *Radiocarbon*, **10**, 468-472.
- Bender M.M. (1971) Variations in the 13C/12C ratios of plants in relation to the pathway of carbon dioxide fixation. *Phytochemistry*, **10**, 1239-1244.
- Bergh J. and Linder, S. (1999) Effects of soil warming during spring on photosynthetic recovery in boreal Norway spruce stands. *Global Change Biology*, **5**, 245-253.
- Berry, S.C., Varney, G.T. and Flanagan, L.B. (1997) Leaf $\delta^{13}\text{C}$ in *Pinus resinosa* trees and understorey plants: variation associated with light and CO₂ gradients. *Oecologia* **109**, 499-506.
- Beverland I.J., Milne, R., Boissard, C., O'Neill, D.H., Moncrieff, J.B. and Hewitt, C.N. (1996) Measurement of carbon dioxide and hydrocarbon fluxes from a sitka spruce forest using micrometeorological techniques. *Journal of Geophysical Research*, **101**, 22807-22815.
- Boggie R. (1977) Water-table depth and oxygen content of deep peat in relation to root growth of *Pinus contorta*. *Plant and Soil*, **48**, 447-454.

- Bol R.A., Harkness, D.D., Huang, Y. and Howard, D.M. (1999) The influence of soil processes on carbon isotope distribution and turnover in the British uplands. *1999*, **50**, 41-51.
- Booth T.C. (1973) Tree pulling. *Report on Forest Research*, 72-73.
- Bousquet P., Ciais P., Peylin P., Ramonet M. and Monfray P. (1999) Inverse modeling of annual atmospheric CO₂ sources and sinks 1. Method and control inversion. *Journal of Geophysical Research-Atmospheres*, **104**, 26161-26178.
- Bousquet P., Peylin P., Ciais P., Ramonet M. and Monfray P. (1999) Inverse modeling of annual atmospheric CO₂ sources and sinks 2. Sensitivity study. *Journal of Geophysical Research-Atmospheres*, **104**, 26179-26193.
- Bowling D.R., Baldocchi, D. D. and Monson, R. K. (1999) Dynamics of isotopic exchange of carbon dioxide in a Tennessee deciduous forest. *Global Biogeochemical Cycles*, **13**, 903-922.
- Bowling D.R., McDowell, N.G., Bond, B.J., Law, B.E. and Ehleringer, J.R. (2002) ¹³C content of ecosystem respiration is linked to precipitation and vapor pressure deficit. *Oecologia*, **131**, 113-124.
- Bowling D.R., Tans P.P. and Monson R.K. (2001) Partitioning net ecosystem carbon exchange with isotopic fluxes of CO₂. *Global Change Biology*, **7**, 127-145.
- Broadmeadow M.S.J. and Griffiths, M.S.J. (1993) Carbon isotope discrimination and the coupling of CO₂ fluxes within forest canopies. In: *Stable isotopes and plant carbon-water relations*. (ed J.R. Ehleringer, Hall, A.E., Farquhar, G.D.), pp. 109-130. Academic Press, Inc., California.
- Broecker W.S., Takahashi T., Simpson H.J. and Peng T.H. (1979) Fate of fossil fuel carbon dioxide and the global carbon budget. *Science*, **206**, 409-418.
- Brooks A. and Farquhar G.D. (1985) Effect of temperature on the CO₂/O₂ specificity of ribulose 1,5-bisphosphate carboxylase oxygenase and the rate of respiration in the light: estimates from gas exchange measurements on spinach. *Planta*, **165**, 397-406.
- Brooks J.R., Flanagan L.B., Varney G.T. and Ehleringer J.R. (1997) Vertical gradients in photosynthetic gas exchange characteristics and refixation of respired CO₂ within boreal forest canopies. *Tree Physiology*, **17**, 1-12.
- Buchmann N. (2000) Biotic and abiotic factors controlling soil respiration rates in *Picea abies* stands. *Soil Biology & Biochemistry*, **32**, 1625-1635.

- Buchmann N., Brooks, J.R., Flanagan, L.B. and Ehleringer, J.R. (1998) Carbon isotope discrimination of terrestrial ecosystems. In: *Stable Isotopes: integration of biological, ecological and geochemical processes*. (ed H. Griffiths), pp. 203-221. BIOS Scientific Publishers, Ltd., Oxford.
- Buchmann N., Guehl J.M., Barigah T.S. and Ehleringer J.R. (1997) Interseasonal comparison of CO₂ concentrations, isotopic composition, and carbon dynamics in an Amazonian rainforest (French Guiana). *Oecologia*, **110**, 120-131.
- Buchmann N., Hinckley T.M. and Ehleringer J.R. (1998) Carbon isotope dynamics in *Abies amabilis* stands in the Cascades. *Canadian Journal of Forest Research-Revue Canadienne De Recherche Forestiere*, **28**, 808-819.
- Buchmann N., Kao W.Y. and Ehleringer J. (1997) Influence of stand structure on carbon-13 of vegetation, soils, and canopy air within deciduous and evergreen forests in Utah, United States. *Oecologia*, **110**, 109-119.
- Calder I.R. (1977) A model of transpiration and interception loss from a spruce forest in Plynlimmon, Central Wales. *Journal of Hydrology*, **33**, 247-265.
- Calder I.R. (1990) *Evaporation in the Uplands*. John Wiley & Sons, Chichester.
- Cernusak L.A., Marshall, J.D. (2000) Photosynthetic refixation in branches of Western White Pine. *Functional Ecology*, **14**, 300-311.
- Cernusak L.A., Marshall, J.D., Comstock, J.P. and Balster, N.J. (2001) Carbon isotope discrimination in photosynthetic bark. *Oecologia*, **128**, 24-35.
- Ciais P., Denning A.S., Tans P.P., Berry J.A., Randall D.A., Collatz G.J., Sellers P.J., White J.W.C., Troler M., Meijer H.A.J., Francey R.J., Monfray P. and Heimann M. (1997) A three-dimensional synthesis study of $\delta^{18}\text{O}$ in atmospheric CO₂. 1. Surface fluxes. *Journal of Geophysical Research-Atmospheres*, **102**, 5857-5872.
- Ciais P., Tans P.P., Denning A.S., Francey R.J., Troler M., Meijer H.A.J., White J.W.C., Berry J.A., Randall D.A., Collatz G.J., Sellers P.J., Monfray P. and Heimann M. (1997) A three-dimensional synthesis study of $\delta^{18}\text{O}$ in atmospheric CO₂. 2. Simulations with the TM2 transport model. *Journal of Geophysical Research-Atmospheres*, **102**, 5873-5883.
- Ciais P., Tans P.P., White J.W.C., Troler M., Francey R.J., Berry J.A., Randall D.R., Sellers P.J., Collatz J.G. and Schimel D.S. (1995a) Partitioning of ocean and

- land uptake of CO₂ as inferred by $\delta^{13}\text{C}$ measurements from the NOAA Climate Monitoring and Diagnostics Laboratory Global Air Sampling Network. *Journal of Geophysical Research-Atmospheres*, **100**, 5051-5070.
- Ciais P., Tans P.P., White J.W.C., Trolier M., Francey R.J., Berry J.A., Randall D.R., Sellers P.J., Collatz J.G. and Schimel D.S. (1995b) Partitioning of Ocean and Land Uptake of CO₂ As Inferred By Delta-C-13 Measurements From the NOAA Climate Monitoring and Diagnostics Laboratory Global Air Sampling Network. *Journal of Geophysical Research-Atmospheres*, **100**, 5051-5070.
- Cienciala E., Kucera, J., Ryan, M.G. and Lindroth, A. (1998) Water flux in boreal forest during two hydrologically contrasting years; species specific regulation of canopy conductance and transpiration. *Annales des Sciences Forestieres.*, **55**, 47-62.
- Clement R. (2003) *Long term micrometeorological measurements of mass and energy exchange of a Sitka spruce plantation in complex topography*. PhD, University of Edinburgh..
- Conway T.J., Tans P.P., Waterman L.S., Thoning K.W., Kitzis D.R., Masarie K.A. and Zhang N. (1994) Evidence for interannual variability of the carbon cycle from the NOAA/CMDL global air sampling network. *Journal of Geophysical Research*, **99**, 22,831-822,855.
- Cornic G. and Jarvis P.G. (1972) Effects of Oxygen on CO₂ exchange and stomatal resistance in Sitka spruce and maize at low irradiances. *Photosynthetica*, **6**, 225-239.
- Coutts M.P. and Philipson, J.J. (1978) Tolerance of tree roots to water-logging. I. Survival of Sitka spruce and Lodgepole pine. *New Phytologist*, **80**, 63-69.
- Craig H. (1953) The geochemistry of the stable carbon isotopes. *Geochimica et Cosmochimica Acta*, **3**, 53-92.
- Craig H. (1957) The natural distribution of radiocarbon and the exchange time of carbon dioxide between atmosphere and sea. *Tellus*, **9**, 1-17.
- Davidson E.A., Verchot, L.V., Cattanio, J.H., Ackerman, I.L. and Carvalho, J.E.M. (2000) Effects of soil water content on soil respiration in forests and cattle pastures of eastern Amazonia. *Biogeochemistry*, **48**, 53-69.
- Day W.R. (1963) The development of Sitka spruce on shallow peat. *Scottish Forestry*, **17**, 219-236.

- Denmead O.T., Dunin, F.X., Wong, S.C. and Greenwood, E.A.N. (1993) Measuring water use efficiency of Eucalypt trees with chambers and micrometeorological techniques. *Journal of Hydrology*, **150**, 649-664.
- Dixon M. and Grace, J. (1982) Water uptake by some chamber materials. *Plant, Cell and Environment*, **5**, 323-327.
- Dorr H. and Munnich, K.O. (1987) Annual variation in soil respiration from selected areas of the temperate zone. *Tellus Series B-Chemical and Physical Meteorology*, **39**, 114-121.
- Dunning S.M. (1999) *The application of the Pipe Model Theory to predict leaf area in Sitka spruce (Picea sitchensis (Bong.) Carr.)*. BSc, University of Wales.
- Duranceau M., Ghashghaie, J., Badeck, F., Deleens, E and Cornic, G. (1999) $\delta^{13}\text{C}$ of CO_2 respired in the dark in relation to $\delta^{13}\text{C}$ of leaf carbohydrates in *Phaseolus vulgaris* L. under progressive drought. *Plant Cell and Environment*, **22**, 515-523.
- Duranceau M., Ghashghaie, J. and Brugnoli, E. (2001) Carbon isotope discrimination during photosynthesis and dark respiration in intact leaves of *Nicotiana sylvestris*: comparisons between wild type and mitochondrial mutant plants. *Australian Journal of Plant Physiology*, **28**, 65-71.
- Edwards N.T. and McLaughlin, S.B. (1978) Temperature-independent diel variations of respiration rates in *Quercus alba* and *Liriodendron tulipifera*. *Oikos*, **31**, 200-206.
- Edwards N.T. and Ross-Todd, B.M. (1983) Soil carbon dynamics in a mixed deciduous forest following clear-cutting with and without residual removal. *Soil Science Society of America Journal*, **47**, 1014-1021.
- Edwards W.R.N. (1980) *Flow of water in trees*. PhD, University of Edinburgh.
- Ehleringer J.R., Buchmann N. and Flanagan L.B. (2000) Carbon isotope ratios in belowground carbon cycle processes. *Ecological Applications*, **10**, 412-422.
- Ekblad A. and Hogberg, P. (2001) Natural abundance of ^{13}C in CO_2 respired from forest soils reveals speed of link between tree photosynthesis and root respiration. *Oecologia*, **127**, 305-308.
- Estep M.F., Tabita, F.R. and Van Baalen, C. (1978a) Carbon isotope fractionation by ribulose-1,5-bisphosphate carboxylase from various organisms. *Plant physiology*, **61**, 680-687.

- Estep M.F., Tabita, F.R. and Van Baalen, C. (1978b) Purification of ribulose-1,5-bisphosphate carboxylase and carbon isotope fractionation by whole cells and carboxylase from *Cylindrotheca* sp. (Bacillariophyceae). *Journal of Phycology*, **14**, 183-188.
- Evans J.R., Sharkey T.D., Berry J.A. and Farquhar G.D. (1986) Carbon Isotope Discrimination Measured Concurrently With Gas-Exchange to Investigate CO₂ Diffusion in Leaves of Higher-Plants. *Australian Journal of Plant Physiology*, **13**, 281-292.
- Evans J.R. and Von Caemmerer S. (1996) Carbon dioxide diffusion inside leaves. *Plant Physiology*, **110**, 339-346.
- Ewel K.C., Cropper, Jr.W.P. and Gholz, H.L. (1987) Soil CO₂ evolution in Florida slash pine plantations. I. CHanges through time. *Canadian Journal of Forstry Research*, **17**, 325-329.
- Falge E., Baldocchi D., Tenhunen J., Aubinet M., Bakwin P., Berbigier P., Bernhofer C., Burba G., Clement R., Davis K., Elbers J.A., Goldstein A., Grelle A., Granier A., Guomundsson J., Hollinger D.Y., Kowalski A.S., Katul G.G., Law B.E., Mahli Y., Meyers T.P., Monson R.K., Munger J.W., Oechel W., Paw K.T., Pilegaard K., Rannik U., Rebmann C., Sukyer A., Valentini R., Wilson K. & Wofsy S.C. (2002) Seasonality of ecosystem respiration and gross primary production as derived from FLUXNET measurements. *Agricultural and Forest Meteorology*, **113**, 53-74
- Fan S., Grossnickle, S.C. and Sutton, B.C. (1999) Relationships between gas exchange and carbon isotope discrimination of Sitka x interior spruce introgressive genotypes and ribosomal DNA. *Tree Physiology*, **19**, 689-694.
- Fang C. (1997) *The measurement and simulation of CO₂ efflux in a Florida Slash pine plantation*. PhD, University of Edinburgh.
- Fang C. and Moncrieff, J.B. (1996) An improved dynamic chamber technique for measuring CO₂ efflux from the surface of soil. *Functional Ecology*, **10**, 297-305.
- Farquhar G.D. (1983) On the nature of carbon isotope discrimination in C₄ species. *Australian Journal of Plant Physiology*, **10**, 205-226.
- Farquhar G.D., Caemmerer S.V. and Berry J.A. (1980) A biochemical model of photosynthetic CO₂ assimilation in leaves of C₃ species. *Planta*, **149**, 78-90.
-

- Farquhar G.D., Ehleringer J.R. and Hubick K.T. (1989) Carbon Isotope Discrimination and Photosynthesis. *Annual Review of Plant Physiology and Plant Molecular Biology*, **40**, 503-537.
- Farquhar G.D. and Lloyd J. (1993) Carbon and oxygen isotope effects in the exchange of carbon dioxide between terrestrial plants and the atmosphere. In: *Stable Isotopes and Plant Carbon-Water Relations* (eds J.R. Ehleringer, A.E. Hall, & G.D. Farquhar), pp. 47-70. Academic Press, NY.
- Farquhar G.D., O'Leary, M.H. and Berry, J.A. (1982) On the relationship between carbon isotope discrimination and the intercellular carbon dioxide concentration in leaves. *Australian Journal of Plant Physiology*, **9**, 121-137.
- Fessenden J.E. and Ehleringer, J.R. (2002) Age-related variations in $\delta^{13}\text{C}$ of ecosystem respiration across a coniferous forest chronosequence in the Pacific Northwest. *Tree Physiology*, **22**, 159-167.
- Flanagan L.B., Brooks J.R. and Ehleringer J.R. (1997) Photosynthesis and carbon isotope discrimination in boreal forest ecosystems: a comparison of functional characteristics in plants from three mature forest types. *Journal of Geophysical Research-Atmospheres*, **102**, 28861-28869.
- Flanagan L.B., Brooks J.R., Varney G.T., Berry S.C. and Ehleringer J.R. (1996) Carbon isotope discrimination during photosynthesis and the isotope ratio of respired CO_2 in boreal forest ecosystems. *Global Biogeochemical Cycles*, **10**, 629-640.
- Francey R.J., Gifford, R.M., Sharkey, T.D. and Weir, B. (1985) Physiological influences on carbon isotope discrimination in huon pine (*Lagarostrobos franklinii*). *Oecologia*, **44**, 241-247.
- Francey R.J. and Tans P.P. (1987) Latitudinal variation in oxygen-18 of atmospheric CO_2 . *Nature*, **327**, 495-497.
- Francey R.J., Tans P.P., Allison C.E., Enting I.G., White J.W.C. and Troler M. (1995) Changes in Oceanic and Terrestrial Carbon Uptake Since 1982. *Nature*, **373**, 326-330.
- Fraser A.I. and Gardiner, J.B.H. (1967) Rooting and stability in Sitka spruce. *Forestry Commission Bulletin*, **40**.
- Froment A. (1972) Soil respiration in a mixed oak forest. *Oikos*, **23**, 273-277.

- Fung I., Field, C.B., Berry, J.A., Thompson, M.V.,m Randerson, J.T., Malmstrom, C.M., Vitousek, P.M., Collatz, G.J., Sellers, P.J., Randall, D.A., Denning, A.S., Badeck, F. and John, J. (1997) Carbon 13 exchanges between the atmosphere and biosphere. *Global Biogeochemical Cycles*, **11** (4), 507-533.
- Gardingen P.R.V., Grace, J. and Jeffree, C.E. (1991) Abrasive damage by wind to the needle surfaces of *Picea sitchensis* (Bong.) Carr. and *Pinus sylvestris* L. *Plant Cell and Environment*, **14**, 185-193.
- Gash J.H.C. (1979) An analytical model of rainfall interception by forests. *Quarterly Journal of the Royal Meteorological Society*.
- Gash J.H.C. and Stewart, J.B. (1977) The evaporation from Thetford Forest during 1975. *Journal of Hydrology*, **35**, 385-396.
- Gash J.H.C., Wright, I.R. and Lloyd, C.R. (1980) Comparative estimates of interception loss from three coniferous forests in Great Britain. *Journal of Hydrology*, **35**, 385-396.
- Gebauer G. and Schulze, E.-D. (1991) Carbon and nitrogen isotope ratios in different compartments of a healthy and a declining *Picea abies* forest in the Fichtelgebirge, NE Bavaria. *Oecologia*, **87**, 198-207.
- Ghashghaie J., Duranceau, M., Badeck, F.W., Cornic, G., Adeline, M.T. and Deleens, E. (2001) $\delta^{13}\text{C}$ of CO_2 respired in the dark in relation to $\delta^{13}\text{C}$ of leaf metabolites: comparison between *Nicotiana sylvestris* and *Helianthus annuus* under drought. *Plant, Cell and Environment*, **24**, 505-515.
- Gillon J.S., Borland, A., Harwood, K.G., Roberts, A., Broadmeadow, M.S.J. and Griffiths, H. (1997) Respiratory CO_2 and instantaneous discrimination against ^{13}C in plants: a source to be reckoned with? In: *Stable isotopes: integration of biological, ecological and geochemical processes*. (ed H. Griffiths), pp. 111-132. Bios Scientific Publishers, Oxford.
- Gillon J.S. and Griffiths H. (1997) The influence of (photo) respiration on carbon isotope discrimination in plants. *Plant, Cell and Environment*, **20**, 1217-1230.
- Glinski J. and Stepniewski, W. (1985) *Soil aeration and its role for plants*. CRC Press Inc., Florida.
- Gordon A.M., Schlentner, R.E. and Van Cleve, K. (1987) Seasonal patterns of soil respiration and CO_2 evolution following harvesting in the white spruce forests of interior Alaska. *Can. J. For. Res.*, **17**, 304-310.

-
- Goulden M.L. and Crill, P.M. (1997) Automated measurements of CO₂ exchange at the moss surface of a black spruce forest. *Tree Physiology*, **17**, 537-542.
- Goulden M.L., Daube B.C., Fan S.M., Sutton D.J., Bazzaz A., Munger J.W. and Wofsy S.C. (1997) Physiological responses of a black spruce forest to weather. *Journal of Geophysical Research-Atmospheres*, **102**, 28987-28996.
- Goulden M.L., Munger J.W., Fan S.M., Daube B.C. and Wofsy S.C. (1996) Measurements of carbon sequestration by long-term eddy covariance - methods and a critical evaluation of accuracy. *Global Change Biology*, **2**, 169-182.
- Grace J., Malcolm D.C. and Bradbury I.K. (1975) Effect of wind and humidity on leaf diffusive resistance in sitka spruce seedlings. *Journal of Applied Ecology*, **12**, 931-940.
- Granier A. and Loustau, D. (1994) Measuring and modelling the transpiration of maritime pine canopy from sap-flow data. *Agricultural and Forest Meteorology*, **71**, 61-81.
- Greco S. and Baldocchi D. (1996) Seasonal variations of CO₂ and water vapour exchange rates over a temperate deciduous forest. *Global Change Biology*, **2**, 183-198.
- Grier C.C. & Waring R.H. (1974) Conifer foliage mass related to sapwood area. *Forest Science*, **20**, 205-206.
- Guy R.D., Fogel M.L. and Berry J.A. (1993) Photosynthetic Fractionation of the Stable Isotopes of Oxygen and Carbon. *Plant Physiology*, **101**, 37-47.
- Harwood, K.G. (1996) *Variation in the stable isotopes of oxygen and carbon within forest canopies*. PhD thesis, University of Newcastle-upon-Tyne.
- Harwood K.G., Gillon J.S., Griffiths H. and Broadmeadow M.S.J. (1998) Diurnal variation of Delta(CO₂)-C-13, Delta(COO)-O-18-O-16 and evaporative site enrichment of delta(H₂O)-O-18 in *Piper aduncum* under field conditions in Trinidad. *Plant Cell and Environment*, **21**, 269-283.
- Heaton T.H.E. (1999) Spatial, species, and temporal variation in ¹³C/¹²C ratios of C3 plants: Implication for palaeodiet studies. *Journal of Archaeological Science*, **26**, 637-649.
- Heaton T.H.E. and Crossley, A. (1995) Carbon isotope variations in a plantation of Sitka spruce, and the effect of acid mist. *Oecologia*, **103**, 109-117.
-

- Hendrey G.R., Ellsworth, D.S., Lewing, K.F. and Nagy, J. (1999) A free-air enrichment system for exposing tall forest vegetation to elevated atmospheric CO₂. *Global Change Biology*, **5**, 293-310.
- Henry B.K., Atkin O.K., Day D.A., Millar A.H., Menz R.I. and Farquhar G.D. (1999) Calculation of the oxygen isotope discrimination factor for studying plant respiration. *Australian Journal of Plant Physiology*, **26**, 773-780.
- Hogberg P., Johansson, C., Hallgren, J.-E. (1993) Studies of ¹³C in the foliage reveal interactions between nutrients and water in forest fertilization experiments. *Plant and Soil*, **152**, 207-214.
- Hogberg P., Nordgren A., Buchmann N., Taylor A.F.S., Ekblad A., Hogberg M.N., Nyberg G., Ottosson-Lofvenius M. and Read D.J. (2001) Large-scale forest girdling shows that current photosynthesis drives soil respiration. *Nature*, **411**, 789-792.
- Hurry V.M., Keerberg, O., Parnik, T., Oquist, G. and Gardestrom, P. (1996) Effect of cold hardening on the components of respiratory decarboxylation in the light and in the dark in leaves of winter rye. *Plant physiology*, **111**, 713-719.
- Hutchinson G.L. and Livingston, G.P. (2002) Gas flux. In: *Methods of Soil Analysis: Part I, Physical Methods* (ed J.H. Dane, Topp, G.C.). Soil Science Society of America, Madison.
- IPCC (1996) *Climate change 1995: The science of climate change*. Cambridge University Press, Cambridge.
- Ivlev A.A. (1996) Fractionation of carbon (¹³C/¹²C) isotopes in glycine decarboxylase reaction. *FEBS Lett*, **386**, 174-176.
- Jaggi M., Saurer, M., Fuhrer, J. and Siegwolf, R. (2002) The relationship between the stable carbon isotope composition of needle bulk material, starch, and tree rings in *Picea abies*. *Oecologia*, **131**, 325-332.
- James G.B. (1977) *Exchanges of mass and energy in Sitka spruce*. PhD, University of Edinburgh.
- Janssens I.A., Kowalski, A.S., Longdoz, B. and Ceulemans, R. (2000) Assessing forest soil CO₂ efflux: an *in situ* comparison of four techniques. *Tree Physiology*, **20**, 23-32.
- Janssens I.A., Lankreijer, H., Matteucci, G., Kowalski, A.S., Buchmann, N., Epron, D., Pilegaard, K., Kutsch, W., Longdoz, B., Grünwald, T., Montagnani, L., Dore, S., Rebmann, C., Moors, E.J., Grelle, A., Rannik, Ü., Morgenstern, K., Oltchev, S., Clement, R., Gudmundsson, J., Minerbi, S., Berbigier, P., Ibrom,

- A., Moncrieff, J., Aubinet, M., Bernhofer, C., Jensen, N.O., Vesala, T., Granier, A., Schulze, E-D., Lindroth, A., Dolman, A.J., Jarvis, P.G., Ceulemans, R. and Valentini, R. (2001) Productivity overshadows temperature in determining soil and ecosystem respiration across European forests. *Global Change Biology*, **7**, 269-278.
- Janssens I.A., Meiresonne, L. and Ceulemans, R. (1999) Mean soil CO₂ efflux from a mixed forest: temporal and spatial integration. In: *Forest ecosystem modelling, upscaling and remote sensing* (ed R.J.M. Ceulemans, Veroustraete, F., Gond, V., Van Rensbergen, J.B.H.F.), pp. 19-32. SPB Academic Publishing, Netherlands.
- Jarvis P.G. (1975) Water transfer in plants. In: *Heat and Mass Transfer in the Biosphere. I. Transfer processes in the plant environment* (eds D.A.D. Vries & N.H. Afgan), pp. 69-394. Scripta Book Company, John Wiley and Sons, New York, London, Sydney and Toronto.
- Jarvis P.G. (1976) The interpretation of the variations in leaf water potential and stomatal conductance found in canopies in the field. *Phil. Trans. R. Soc. Lond. B.*, **273**, 593-610.
- Jarvis P.G. (1981) Production efficiency of coniferous forest in the UK. In: *Physiological Processes Limiting Plant Productivity* (ed C.B. Johnson), pp. 81-107. Butterworth Scientific Publications, London.
- Jarvis P.G. (1993) Water losses of crowns, canopies and communities. In: *Water Deficits - Plant Responses from Cell to Community* (ed J.A.C.S.a.H. Griffiths), pp. 285-315. Bios Scientific Publishers, Environmental Plant Biology Series.
- Jarvis P.G. (1994) Capture of carbon dioxide by coniferous forest. In: *Resource Capture by Crops* (ed J.L. Monteith, R.K. Scott and M.H. Unsworth), pp. 351-374. Nottingham University Press.
- Jarvis P.G. (1995) Scaling processes and problems. *Plant Cell and Environment*, **18**, 1079-1089.
- Jarvis P.G., James, B.G. and Landsberg, J.J. (1976b) Coniferous forest. In: *Vegetation and Atmosphere* (ed J.L. Monteith), pp. 171-204. Academic Press, London and New York.
- Jarvis P.G., Massheder J.M., Hale S.E., Moncrieff J.B., Rayment M. and Scott S.L. (1997) Seasonal variation of carbon dioxide, water vapor, and energy exchanges of a boreal black spruce forest. *Journal of Geophysical Research-Atmospheres*, **102**, 28953-28966.

-
- Jarvis P.G. and McNaughton K.G. (1986) Stomatal control of transpiration: scaling up from leaf to region. *Advances in Ecological Research*, **15**, 1-49.
- Jarvis P.G. and Moncrieff, J.B.M. (1992) Atmosphere-biosphere exchange of CO₂. In: *TERRA-1: Understanding the terrestrial environment* (ed P.M. Mather), pp. 85-99. Burgess Science Press, London.
- Jarvis P.G. and Morison, J.I.L. (1981) The control of transpiration and photosynthesis by the stomata. In: *Stomatal Physiology* (ed P.G. Jarvis, Mansfield, T.A.), pp. 247-279. Cambridge University Press.
- Jarvis P.G. and Stewart, J.B. (1979) Evaporation of water from plantation forest. In: *The Ecology of Even-Aged Plantations* (ed E.D. Ford, D.C. Malcolm and J. Atterson), pp. 327-349. ITE, Cambridge.
- Jeffree C.E., Johnson R.P.C. and Jarvis P.G. (1971) Epicuticular wax in the stomatal antechamber of Sitka spruce and its effects on the diffusion of water vapour and carbon dioxide. *Planta*, **98**, 1-10.
- Jensen L.S., Mueller, T., Tate, K.R., Ross, D.J., Magid, J. and Nielsen, N.E. (1996) Measuring soil surface CO₂ flux as an index of soil respiration in situ: A comparison of two chamber methods. *Soil Biol. Biochem.*, **28**, 1297-1306.
- Jordan D.B. and Ogren, W.L. (1984) The CO₂/O₂ specificity of ribulose-1,5-bisphosphate carboxylase/oxygenase: dependence on ribulose bisphosphate concentration, pH and temperature. *Planta*, **161**, 308-313.
- Kakubari Y. (1988) Diurnal and seasonal fluctuations in the bark respiration of standing *Fagus sylvatica* trees at Solling, West Germany. *J. Jpn. For. Soc.*, **70**, 64-70.
- Kaplan J.O. (2001) *Geophysical application of vegetation modelling*. PhD, Lund University.
- Katul G.G., Ellsworth, D.S. and Lai, C.T. (2000) Modelling assimilation and intercellular CO₂ from measured conductance: a synthesis of approaches. *Plant, Cell and Environment*, **23**, 1313-1328.
- Keeling C.D. (1958) The concentrations and isotopic abundances of atmospheric carbon dioxide in rural areas. *Geochimica et Cosmochimica Acta*, **13**, 322-334.
- Keeling C.D. (1961) The concentration and isotopic abundances of carbon dioxide in rural and marine air. *Geochimica et Cosmochimica Acta*, **24**, 277-298.
-

- Keeling C.D., Mook W.G. and Tans P.P. (1979) Recent Trends in the C-13-C-12 Ratio of Atmospheric Carbon- Dioxide. *Nature*, **277**, 121-123.
- Keeling C.D., Whorf T.P., Wahlen M. and van der Plicht J. (1995) Interannual extremes in the rate of rise of atmospheric carbon dioxide since 1980. *Nature*, **375**, 666-670.
- Kelliher F.M., Leuning R. and Schulze E.D. (1993) Evaporation and canopy characteristics of coniferous forests and grasslands. *Oecologia*, **95**, 153-163.
- Kelliher F.M., Lloyd, J., Arneth, A., Luhker, B., Byers, J.N., McSeveny, T.M., Milukova, I., Grigoriev, S., Panfyorov, M., Sogatchev, A., Varlargin, A., Ziegler, W., Bauer, G., Wong, S-C. and Schulze, E.D. (1999) Carbon dioxide efflux density from the floor of a central Siberian pine forest. *Agricultural and Forest Meteorology*, **94**, 217-232.
- Kellomaki S., Hari P., Kanninen M. and Ilonen P. (1980) Eco-physiological studies on young Scots pine stands: II Distribution of needle biomass and its application in approximating light conditions inside the canopy. *Silva Fennica*, **14**, 243-257.
- Kermack K.A. and Haldane, J.B.S. (1950) Organic correlation and allometry. *Biometrika*, **37**, 30-41.
- Kimball B.A. and Lemon, E.R. (1971) Air turbulence effects upon soil gas exchange. *Proceedings of the Soil Science Society of America*, **35**, 16-21.
- Kirschbaum M.U.F. and Farquhar, G.D. (1984) Temperature dependence of whole-leaf photosynthesis in *Eucalyptus pauciflora* Sieb. ex Spreng. *Plant physiology*, **11**, 519-538.
- Korner C.H. (1994) Leaf diffusive conductances in the major vegetation types of the globe. In: *Ecophysiology of Photosynthesis*. (ed E.D. Schulze, Caldwell, M.M.), pp. 463-490. Springer-Verlag, Heidelberg.
- Kroopnick P. and Craig, H. (1976) Oxygen isotope fractionation in dissolved oxygen in the deep sea. *Earth Planet Sci Lett*, **32**, 375-388.
- Kruijt B., Barton, C., Rey, A. and Jarvis, P.G. (1999) The sensitivity of stand-scale photosynthesis and transpiration to changes in atmospheric CO₂ concentration and climate. *Hydrology and Earth System Sciences*, **3**, 55-69.
-

- Lafleur P.M. (1992) Energy balance and evapotranspiration from a subarctic forest. *Agricultural and Forest Meteorology*, **58**, 163-175.
- Lagergren F. and Lindroth, A. (2002) Transpiration response to soil moisture in pine and spruce trees in Sweden. *Agricultural and Forest Meteorology*, **112**, 67-85.
- Laisk A.K. (1977) *Kinetics of Photosynthesis and Photorespiration in C₃ plants.*, Nauka, Moscow.
- Lancaster J. (1990) *Carbon-13 fractionation in carbon dioxide emitting diurnally from soils and vegetation at ten sites on the North American continent.* Dissertation, University of California.
- Landsberg J.J., Jarvis P.G. & Slater M.B., eds (1973) *The radiation regime of a spruce forest.* (Vol. 5). UNESCO, Paris.
- Lange O.L., Tenhunen, J.D. and Braun, M. (1982) Midday stomatal closure in mediterranean type sclerophylls under simulated habitat conditions in an environmental chamber. I. Comparison of the behaviour of various European mediterranean species. *Flora*, **172**, 563-579.
- Larcher W. (1995) *Physiological Plant Ecology: ecophysiology and stress physiology of functional groups.* Springer-verlag, New York Berlin Heidelberg.
- Lauteri M., Brugnoli, E. and Spaccino, L. (1993) Carbon isotope discrimination in leaf soluble sugars and in whole-plant dry matter in *Helianthus annuus* L. grown under different water conditions. In: *Stable Isotopes and PLant Carbon-Water Relations* (ed J. Ehleringer, Hall, A.E., Farquhar, G.D.), pp. 93-108. Academic Press, Inc., California.
- Lavigne M.B. (1987) Differences in stem respiration responses to temperature between balsam fir trees in thinned and unthinned stands. *Tree Physiology*, **3**, 225-233.
- Lavigne M.B., Ryan M.G., Anderson D.E., Baldocchi D.D., Crill P.M., Fitzjarrald D.R., Goulden M.L., Gower S.T., Massheder J.M., McCaughey J.H., Rayment M. and Striegl R.G. (1997) Comparing nocturnal eddy covariance measurements to estimates of ecosystem respiration made by scaling chamber measurements at six coniferous boreal sites. *Journal of Geophysical Research-Atmospheres*, **102**, 28977-28985.
- Law B.E., Ryan, M.G. and Anthoni, P.M. (1999) Seasonal and annual respiration of a Ponderosa pine ecosystem. *Global Change Biology*, **5**, 69-82.

- Law B.E., Falge E., Gu L., Baldocchi D.D., Bakwin P., Berbigier P., Davis K., Dolman A.J., Falk M., Fuentes J.D., Goldstein A., Granier A., Grelle A., Hollinger D.Y., Janssens I.A., Jarvis P.G., Jensen N.O., Katul G.G., Mahli Y., Matteucci G., Meyers T.P., Monson R.K., Munger W., Oechel W., Olson R., Pilegaard K., Paw K.T., Thorgeirsson H., Valentini R., Verma S., Vesala T., Wilson K. & Wofsy S.C. (2002) Environmental controls over carbon dioxide and water vapor exchange of terrestrial vegetation. *Agricultural and Forest Meteorology*, **113**, 97-102.
- Le Dantec V., Epron, D. and Dufrene, E. (1999) Soil CO₂ efflux in a beech forest: comparison of two closed dynamic systems. *Plant and Soil*, **214**, 125-132.
- Le Roux, X., Bariac, T., Sinoquet, H., Genty, B., Piel, C., Mariotti, A., Girardin, C., and Richard, P. (2001) Spatial distribution of leaf water-use efficiency and carbon isotope discrimination within an isolated tree crown. *Plant Cell and Environment* **24**, 1021-1032.
- Leuning R. (1995) A critical appraisal of a combined stomatal-photosynthesis model for C₃ plants. *Plant, Cell and Environment*, **18**, 339-355.
- Leverenz J., Deans, J.D., Ford, E.D., Jarvis, P.G., Milne, R. and Whitehead, D. (1982) Systematic spatial variation of stomatal conductance in a Sitka spruce plantation. *J. Appl. Ecol.*, **19**, 835-851.
- Leverenz J.W. (1981) Photosynthesis and transpiration in large forest-grown Douglas fir: diurnal variation. *Can. J. Bot.*, **59**, 349-356.
- Leverenz J.W. and Jarvis, P.G. (1979) Photosynthesis in Sitka spruce VIII. The effects of light flux density and direction on the rate of net photosynthesis and the stomatal conductance of needles. *J. Appl. Ecol.*, **16**, 919-932.
- Leverenz J.W. and P.G. (1980a) Photosynthesis in Sitka spruce (*Picea sitchensis* (Bong.) Carr.) IX. The relative contribution made by needles at various positions on the shoot. *J. Appl. Ecol.*, **17**, 59-68.
- Leverenz J.W.J. and P.G. (1980b) Photosynthesis in Sitka spruce (*Picea sitchensis* (Bong.) Carr.) X. Acclimation to quantum flux density within and between trees. *J. Appl. Ecol.*, **17**, 697-708.
- Levy P.E. (1995) *Carbon dioxide exchange of Sahelian vegetation*. PhD, University of Edinburgh.
-

- Levy P.E. and Jarvis P.G. (1998) Stem CO₂ fluxes in two Sahelian shrub species (*Guiera senegalensis* and *Combretum micranthum*). *Functional Ecology*, **12**, 107-116.
- Levy P.E., Meir, P., Allen, S.J. and Jarvis, P.G. (1999) The effect of aqueous transport of CO₂ in xylem sap on gas exchange in woody plants. *Tree Physiology*, **19**, 53-58.
- Lin G. and Ehleringer, J.R. (1997) Carbon isotopic fractionation does not occur during dark respiration in C₃ and C₄ plants. *Plant physiology*, **114**, 391-394.
- Lindroth A., Grelle, A. and Moren, A. (1998) Long-term measurements of boreal forest carbon balance reveal large temperature sensitivity. *Global Change Biology*, **4**, 443-450.
- Lloyd J. and Farquhar G.D. (1994) ¹³C discrimination during CO₂ assimilation by the terrestrial biosphere. *Oecologia*, **99**, 201-215.
- Lloyd J., Kruijt B., Hollinger D.Y., Grace J., Francey R.J., Wong S.C., Kelliher F.M., Miranda A.C., Farquhar G.D., Gash J.H.C., Vygodskaya N.N., Wright I.R., Miranda H.S. and Schulze E.D. (1996) Vegetation effects on the isotopic composition of atmospheric CO₂ at local and regional scales: Theoretical aspects and a comparison between rain forest in amazonia and a boreal forest in Siberia. *Australian Journal of Plant Physiology*, **23**, 371-399.
- Lloyd J., Syvertsen J.P., Kriedemann P.E. and Farquhar G.D. (1992) Low conductances for CO₂ diffusion from stomata to the sites of carboxylation in leaves of woody species. *Plant Cell and Environment*, **15**, 873-899.
- Lloyd J. and Taylor J.A. (1994) On the temperature dependence of soil respiration. *Functional Ecology*, **8**, 315-323.
- Loreto F., Harley, P.C., Di Marco, G. and Sharkey, T.D. (1992) Estimation of mesophyll conductance to CO₂ flux by three different methods. *Plant physiology*, **98**, 1437-1443.
- Ludlow M.M. and Jarvis P.G. (1971) Photosynthesis in Sitka Spruce (*Picea-Sitchensis* (Bong) Carr) .1. General Characteristics. *Journal of Applied Ecology*, **8**, 925-&.
- Malhi Y., Baldocchi, D.D. and Jarvis, P.G. (1999) The carbon balance of tropical, temperate and boreal forests. *Plant, Cell and Environment*, **22**, 715-740.

- Martin T.A., Teskey, R.O. and Dougherty, P.M. (1994) Movement of respiratory CO₂ in stems of loblolly pine (*Pinus taeda* L.) seedlings. *Tree Physiology*, **14**, 481-495.
- Massheder J.M., Jarvis, P.G., Moncrieff, J.B. and Kruijt, B. (1993) *Net carbon uptake of Scottish forests*. (Preliminary Report for the Scottish Forestry Trust No.). Scottish Forestry Trust.
- Massman W.J. and Lee, X. (2002) Eddy covariance flux corrections and uncertainties in ecosystem studies of carbon and energy exchanges. *Agricultural and Forest Meteorology*, **113**, 121-144.
- Matteucci G., Dore, S., Stivanello, S., Rebmann, C. and Buchmann, N. (2000) Soil respiration in Beech and Spruce forests in Europe: Trends, controlling factors, annual budgets and implications for the ecosystem carbon balance. In: *Carbon and Nitrogen cycling in European forest ecosystems*. (ed E.D. Schulze). Springer, Berlin.
- Matyssek R. and Schulze, E.-D. (1988) Carbon uptake and respiration in above-ground parts of *Larix decidua* x *leptolepis* tree. *Trees*, **2**, 223-241.
- McCracken P.J. (1993) *Turbulent exchange of momentum and carbon dioxide of a sitka spruce plantation.*, University of Edinburgh.
- McDermitt D.K. (1990) Sources of error in the estimation of stomatal conductance and transpiration from porometer data. *Hortscience*, **25**, 1538-1548.
- McIntosh R. (1984) *The effect of thinning and fertilizer application on the relationship between leaf area and production in established Sitka spruce (Picea sitchensis) stands*. PhD, University of Edinburgh.
- McNaughton K.G. and Jarvis P.G. (1983) Predicting effects of vegetation changes on transpiration and evaporation. In: *Water Deficits and Plant Growth* (ed T.T. Kozlowski), pp. 1-47. Academic Press.
- McNaughton K.G. and Jarvis P.G. (1991) Effects of spatial scale on stomatal control of transpiration. *Agricultural and Forest Meteorology*, **54**, 279-302.
- Meir P. (1996) *The exchange of carbon dioxide in tropical forest*. PhD, University of Edinburgh.
- Meir P., Kruijt B., Broadmeadow M., Barbosa, E., Kull, O., Nobre, A. and Jarvis, P.G. (2002) Acclimation of photosynthetic capacity to irradiance in tree canopies in relation to leaf nitrogen concentration and leaf mass per unit area. *Plant, Cell and Environment*, **25**, 343-357.

-
- Milne R. (1979) Water loss and canopy resistance of a young Sitka spruce plantation. *Boundary-Layer Meteorology*, **16**, 67-81.
- Milne R., Deans J.D. & Ford E.D., Jarvis, P.G., Leverenz, J. and Whitehead, D. (1985) A comparison of two methods of estimating transpiration rates from a Sitka spruce plantation. *Boundary-Layer Meteorology*, **32**, 155-175.
- Mitchell C.P., Proe M.F. & MacBrayne C.G. (1981) *Biomass tables for young conifer stands in Britain*. Paper presented at the Proceedings of XVII IUFRO World Congress, Kyoto, Japan, Subject Group 5.4.01.
- Moncrieff J.B., Malhi Y. and Leuning R. (1996) The propagation of errors in long-term measurements of land atmosphere fluxes of carbon and water. *Global Change Biology*, **2**, 231-240.
- Moncrieff J.B., Massheder J.M., De Bruin, H., Elbers, J., Friborg, T., Heusinkveld, B., Kabat, P., Scott, S., Soegaard, H. and Verhoef, A. (1997) A system to measure surface fluxes of energy, momentum and carbon dioxide. *Journal of Hydrology*, **189**, 589-611.
- Monin A.S. and Obukhov A.M. (1954) Basic laws of turbulent mixing in the ground layer of the atmosphere. *Trans, Geophys. Inst. Acad*, **151**, 163-187.
- Monserud R.A. and Marshall J.D. (2002) Time-series analysis of $\delta^{13}\text{C}$ from tree rings. I. Time trends and autocorrelation. *Tree Physiology*, **21**, 1087-1102.
- Moren A.-S. (1999) *Carbon dioxide and water exchange in a Boreal forest in relation to weather and season*. PhD, Swedish University of Agricultural Sciences.
- Moren A.-S. and Lindroth A. (2000) CO_2 exchange at the floor of a boreal forest. *Agricultural and Forest Meteorology*, **101**, 1-14.
- Morison J.I.L. and Gifford R.M. (1983) *Plant physiology*, **71**, 784-796.
- Negisi K. (1972) Diurnal fluctuation of CO_2 release from bark of a standing *Magnolia obovata* tree. *J. Jpn. For. Soc.*, **54**, 257-263.
- Negisi K. (1975) Diurnal fluctuation of CO_2 release from the stem bark of standing young *Pinus densiflora* trees. *J. Jpn. For. Soc.*, **57**, 375-383.
- Negisi K. (1981) Diurnal and seasonal fluctuations in the stem bark respiration of a standing *Quercus myrsinaefolia* tree. *J. Jpn. For. Soc.*, **63**, 235-241.
-

- Negisi K. (1982) Diurnal fluctuations of the stem bark respiration in relationship to the wood temperature in standing young *Pinus densiflora*, *Chamaecyparis obtusa* and *Quercus myrsinaefolia* trees. *J. Jpn. For. Soc.*, **64**, 315-319.
- Neilson R.E. & Jarvis P.G. (1975) Photosynthesis in Sitka spruce (*Picea sitchensis* (Bong.) Carr.) VI. Response of stomata to temperature. *J. Appl. Ecol.*, **12**, 879-891.
- Neilson R.E., Ludlow M.M. and Jarvis P.G. (1972) Photosynthesis in Sitka spruce (*Picea sitchensis* (Bong.) Carr.) II. Response to temperature. *J. Appl. Ecol.*, **9**, 721-745.
- Nier A.O. and Gulbransen E.A. (1939) Variations in the relative abundance of the carbon isotopes. *J. Am. Chem. Soc.*, **61**, 697-698.
- Nisbet T.R., Mullins, C.E. and MacLeod, D.A. (1989) The variation of soil water regime, oxygen status and rooting pattern with soil type under Sitka spruce. *Journal of Soil Science*, **40**, 183-197.
- Norman J.M., Garcia, R. and Verma, S.B. (1992) Soil surface CO₂ fluxes and the carbon budget of a grassland. *J. Geophys. Res.*, **97**, 18845-18853.
- Norman J.M. and Jarvis P.G. (1974) Photosynthesis in Sitka spruce (*Picea sitchensis* (Bong.) Carr.) III. Measurements of canopy structure and interception of radiation. *J. Appl. Ecol.*, **11**, 375-398.
- Ogren E. and Evans, J.R. (1993) Photosynthetic light-response curves. 1. The influence of CO₂ partial pressure and leaf inversion. *Planta*, **189**, 182-190.
- O'Leary M.H. (1981) Carbon isotope fractionation in plants. *Phytochemistry*, **20**, 553-567.
- Osman A.M. (1971) Root respiration of wheat plants as influenced by age, temperature and irradiation of shoots. *Photosynthetica*, **5**, 107-112.
- Park R. and Epstein, S. (1961) Metabolic fractionation of ¹³C and ¹²C in plants. *Plant Physiology*, **36**, 133-.
- Parkinson K.J. (1981) An improved method for measuring soil respiration in the field. *J. Appl. Ecol.*, **18**, 221-228.
- Parnik T., Gardestrom, P. Ivanova, H. and Keerberg, O. (1998) Photosynthetic and respiratory CO₂ fluxes in winter rye leaves at low temperature. In: *Plant mitochondria: from gene to function*. (ed I.M. Moller, Gardestrom, P.

- Gliminius, K. and Glaser, E.), pp. 585-589. Bluckhuys Publishers, Leiden, The Netherlands.
- Pattey E., Strachan, I.B., Desjardins, R.L. and Massheder, J. (2002) Measuring nighttime CO₂ flux over terrestrial ecosystems using eddy covariance and nocturnal boundary layer methods. *Agricultural and Forest Meteorology*, **113**, 145-158.
- Pearcy R.W., Schulze, E.D. and Zimmermann, R. (1989) Measurement of transpiration. In: *Plant Physiological Ecology: Field methods and instrumentation*. (ed R.W. Pearcy, Ehleringer, J.R., Mooney, H.A., Rundel, P.W.), pp. 137-160. Chapman and Hall, London.
- Penman H.L., Angus, D.E. and van Bavel, C.H. (1967) Microclimatic factors affecting evaporation and transpiration. *Agronomy*, **11**, 483-505.
- Pereira J.S., Tenhunen, J.D. and Lange, O.L. (1987) Stomatal control of photosynthesis of *Eucalyptus globulus* Labill. trees under field conditions in Portugal. *J. Exp. Bot.*, **38**, 1678-1688.
- Pyatt D.G. and Smith, K.A. (1983) Water and oxygen regimes of four soil types at Newcastleton Forest, south Scotland. *Journal of Soil Science*, **34**, 465-482.
- Raich J.W. and Schlesinger W.H. (1992) The global carbon dioxide flux in soil respiration and its relationship to vegetation and climate. *Tellus Series B-Chemical and Physical Meteorology*, **44**, 81-99.
- Rasulov B.K., Laisk, A.K. and Asrorov, K.A. (1984) Photosynthesis and photorespiration during ontogenesis of several species of cotton. *Sov. Plant Physiology*, **30**, 486-493.
- Rayment M. and Jarvis, P.G. (1997) An improved open chamber system for measuring soil CO₂ effluxes in the field. *Journal of Geophysical Research*, **102**, 28779-28784.
- Rayment M.B. (1998) *Carbon and water fluxes in a boreal forest ecosystem*. PhD, University of Edinburgh.
- Rayment M.B. and Jarvis P.G. (1999) Seasonal gas exchange of black spruce using an automatic branch bag system. *Canadian Journal of Forest Research*, **29L**, 1528-1538.
- Rayment M.B. and Jarvis, P.G. (2000a) Temporal and spatial variation of soil CO₂ efflux in a Canadian boreal forest. *Soil Biology and Biochemistry*, **32**, 35-45.

-
- Rayment M.B., (2000) Closed chamber systems underestimate soil CO₂ efflux. *European Journal of Soil Science*, **51**, 107-110
- Rayment M.B., Loustau, D. and Jarvis, P.G. (2002) Photosynthesis and respiration of black spruce at three organisational scales: shoot, branch and canopy. *Tree Physiology*, **22**, 219-229.
- Rayment M.B., Loustau, D., and Jarvis, P.G. (2000b) Measuring and modelling conductances of black spruce at three organisational scales: shoot, branch and canopy. *Tree Physiology*, **20**, 713-723.
- Ritchie J. (1971) *An investigation into the carbon dioxide production of Spruce litter*. Honours, University of Aberdeen.
- Roberts J. (1983) Forest transpiration: A conservative hydrological process? *Journal of Hydrology*, **66**, 133-141.
- Roeske C.A. and OLeary M.H. (1984) Carbon Isotope Effects On the Enzyme-Catalyzed Carboxylation of Ribulose Bisphosphate. *Biochemistry*, **23**, 6275-6284.
- Rooney M.A. (1988) *Short-term carbon isotope fractionation by plants*. PhD.
- Ruimy A., Jarvis, P.G., Baldocchi, D.D., Saugier, B. and Valentini, R. (1995) CO₂ fluxes over plant canopies: A review. In: *Advances in Ecological Research* (ed M.a.F. Begon, A.H.), pp. 2-68. Academic Press, London.
- Ryan M.G. (1990) Growth and maintenance respiration in stems of *Pinus contorta* and *Picea engelmannii*. *Can. J. For. Res.*, **20**, 48-57.
- Ryan M.G. (1991) A simple method for estimating gross carbon budgets for vegetation in forest ecosystems. *Tree Physiology*, **9**, 255-266.
- Ryan M.G., Gower S.T., Hubbard R.M., Waring R.H. and Gholz H.L., Cropper W.P., Jr. & Running S.W. (1995) Woody tissue maintenance respiration of four conifers in contrasting climates. *Oecologia*, **101**, 133-140.
- Ryan M.G., Lavigne M.B. and Gower S.T. (1997) Annual carbon cost of autotrophic respiration in boreal forest ecosystems in relation to species and climate. *Journal of Geophysical Research-Atmospheres*, **102**, 28871-28883.
- Sanderson P.L. and Armstrong, W. (1980) The responses of conifers to some of the adverse factors associated with waterlogged soils. *New Phytologist*, **85**, 351-362.
-

-
- Sandford A.P. and Jarvis P.G. (1986) Stomatal responses to humidity in selected conifers. *Tree Physiology*, **2**, 89-103.
- Santruckova H., Bird, M.I. and Lloyd, J. (2000) Microbial processes and carbon-isotope fractionation in tropical and temperate grassland soils. *Functional Ecology*, **14**, 108-114.
- Saugier B., Granier A., Pontailier J.Y., Dufrêne E. and Baldocchi D.D. (1997) Transpiration of a boreal pine forest measured by branch bag, sap flow and micrometeorological methods. *Tree Physiology*, **17**, 511-519.
- Schaedle M. (1975) Tree photosynthesis. *Annual Review of Plant Physiology*, **26**, 308-313.
- Schlesinger W.H. (1977) Carbon balance in terrestrial detritus. *Annual Review of Ecology and Systematics*, **8**, 51-81.
- Schulze E.D., Kelliher F.M., Körner C., Lloyd J. and Leuning R. (1994) Relationships among maximum stomatal conductance, ecosystem surface conductance, carbon assimilation rate, and plant nitrogen nutrition: a global ecology scaling exercise. *Annual Review of Ecology and Systematics*, **25**, 629.
- Seibt, U. (2003) *Processes controlling the isotopic composition of CO₂ and O₂ in canopy air: a theoretical analysis with some observations in a Sitka spruce plantation*. PhD thesis, University of Hamburg.
- Sellers P.J., Hall F.G., Kelly R.D., Black A., Baldocchi D., Berry J., Ryan M., Ranson K.J., Crill P.M., Lettenmaier D.P., Margolis H., Cihlar J., Newcomer J., Fitzjarrald D., Jarvis P.G., Gower S.T., Halliwell D., Williams D., Goodison B., Wickland D.E. and Guertin F.E. (1997) BOREAS in 1997: experiment overview, scientific results, and future directions. *Journal of Geophysical Research-Atmospheres*, **102**, 28731-28769.
- Sharp R.E., Matthews, M.A. and Boyer, J.S. (1984) Kok effect and the quantum yield of photosynthesis: light partially inhibits dark respiration. *Plant physiology*, **75**, 95-101.
- Silim S.N., Guy, R.D., Patterson, T.B. and Livingston, N.J. (2001) Plasticity in water-use efficiency of *Picea sitchensis*, *P. glauca* and their natural hybrids. *Oecologia*, **?**, **?**
- Sinclair F.L. (1995) *Light interception and growth in agroforestry systems*. PhD, University of Edinburgh.
-

- Smith B.N. (1971) Carbon isotope ratios of respired CO₂ from castor bean, corn, peanut, pea, radish, squash, sunflower and wheat seedlings. *Plant and Cell Physiology*, **12**, 451-455.
- Soulsby C. (1993) Contrasting hydrological regimes in two ploughed forest soils in upland Wales. *Forestry Commission Bulletin*, **66**, 153-170.
- Sprugel D.G. (1990) Components of woody-tissue respiration in *Abies amabilis* (Dougl.) Forbes trees. *Trees*, **4**, 88-98.
- Sternberg L. (1989) A model to estimate carbon dioxide recycling in forests using ¹³C/¹²C ratios and concentrations of ambient carbon dioxide. *Agricultural and Forest Meteorology*, **48**, 163-173.
- Stockfors J. and Linder S. (1998) Effect of nitrogen on the seasonal course of growth and maintenance respiration in stems of Norway spruce trees. *Tree Physiology*, **18**, 155-166.
- Stromgren M. (2001) *Soil-surface CO₂ flux and growth in a Boreal Norway spruce stand. Effects of soil warming and nutrition.*, Swedish University of Agricultural Sciences.
- Syvertsen J.P., Lloyd, J., McConchie, C. and Farquhar, G.D. (1995) On the relationship between leaf anatomy and CO₂ diffusion through the mesophyll of hypostomatous leaves. *Plant Cell and Environment* **18**: 149-157.
- Tajchman S.J., Hadrich, F. and Lee, R. (1979) Energy budget evaluation of the transpiration - PF relationship in a young pine forest. *Water Resource Research*, **15**, 159-163.
- Tans P.P., Berry J.A. and Keeling R.F. (1993) Oceanic ¹³C/¹²C observations: a new window on ocean CO₂ uptake. *Global Biogeochemical Cycles*, **7**, 353-368.
- Thom A.S. (1975) Momentum, mass and heat exchange of plant communities. In: *Vegetation and the Atmosphere*. (ed J.L. Monteith), pp. 57-109. Academic Press, London.
- Trolier M., White, J.W.C., Tans, P.P., Masarie, K.A. and Gemery, P.A. (1996) Monitoring the isotopic composition of atmospheric CO₂: measurements from the NOAA Global Air Sampling Network. *Journal of Geophysical Research-Atmospheres*, **101**, 25897-25916.
- Valentini R. (1999) Discussion on Part I. In: *Forest Ecosystem Modelling, Upscaling and Remote Sensing*. (ed R. Ceulemans, Veroustraete, F., Gond, V., Van Rensbergen, J.B.H.F.), pp. 87-91. SPB Academic Publishing, Netherlands.

- Valentini R., Matteucci G., Dolman A.J., Schulze E.D., Rebmann C., Moors E.J., Granier A., Gross P., Jensen N.O., Pilegaard K., Lindroth A., Grelle A., Bernhofer C., Grunwald T., Aubinet M., Ceulemans R., Kowalski A.S., Vesala T., Rannik U., Berbigier P., Loustau D., Guomundsson J., Thorgeirsson H., Ibrom A., Morgenstern K., Clement R., Moncrieff J., Montagnani L., Minerbi S. and Jarvis P.G. (2000) Respiration as the main determinant of carbon balance in European forests. *Nature*, **404**, 861-865.
- Van Wijk M. (2001) *Quantification of the mutual relationships between forest growth and water use: determining factors, feedbacks and strategies*. PhD, University of Amsterdam.
- Villar R., Held, A.A. and Merino, J. (1994) Comparison of methods to estimate dark respiration in the light in leaves of two woody species. *Plant physiology*, **105**, 167-172.
- Von Caemmerer S., Evan, J.R., Hudson, G.S. and Andrews, T.J. (1994) The kinetics of ribulose-1,5-bisphosphate carboxylase/oxygenase in vivo inferred from measurements of photosynthesis in leaves of transgenic tobacco. *Planta*, **195**, 88-97.
- Von Caemmerer S. and Evans J.R. (1991) Determination of the average partial pressure of carbon dioxide in chloroplasts from leaves of several C₃ plants. *Australian Journal of Plant Physiology*, **18**, 287-306.
- Wallin G., Linder, S., Lindroth, A., Rantfors, M., Flemberg, S. and Grelle, A. (2001) Carbon dioxide exchange in Norway spruce at the shoot, tree and ecosystem scale. *Tree Physiology*, **21**, 969-976.
- Wang Y.P. and Jarvis, P.G. (1990) Effect of incident beam and diffuse radiation on PAR absorption, photosynthesis and transpiration of Sitka spruce - a simulation study. In: *Understanding Tree Structure* (ed P.H. P. Pelkonen, A. Ma'kela and R. Luxmoore), pp. 167-180. Silva Carelica.
- Waring R.H. (1983) Estimating forest growth and efficiency in relation to canopy leaf area. *Advances in Ecological Research*, **13**, 327-354.
- Waring R.H., Landsberg J.J. and Williams M. (1998) Net primary production of forests: a constant fraction of gross primary production? *Tree Physiology*, **18**, 129-134.
- Watts W.R., Neilson, R.E. and Jarvis, P.G. (1976). Photosynthesis in Sitka spruce (*Picea sitchensis* (Bong.) Carr.) VII. Measurements of stomatal conductance and CO₂ uptake in a forest canopy. *J. Appl. Ecol.*, **13**, 622-638.

- Webb T., Howe S.E., Bradshaw R.H.W. and Heide K.M. (1981) Estimating plant abundances from pollen percentages: the use of regression analysis. *Review of Palaeobotany and Palynology*, **34**, 269-300.
- Werner R.A. and Brand W.A. (2001) Referencing strategies and techniques in stable isotope ratio analysis. *Rapid Communications in Mass Spectrometry*, **15**, 501-519.
- Werner R.A., Bruch, B.A. and Brand, W.A. (1999) ConFlo III - An interface for high precision $\delta^{13}\text{C}$ and $\delta^{14}\text{N}$ analysis with an extended dynamic range. *Rapid Communication in Mass Spectrometry*, **13**, 1237-1241.
- Werner R.A., Rothe M. and Brand W.A. (2001) Extraction of CO_2 from air samples for isotopic analysis and limits to ultra high precision delta O-18 determination in CO_2 gas. *Rapid Communications in Mass Spectrometry*, **15**, 2152-2167.
- Westbeek M.H.M., Pons, T.L., Cambridge, M.L. and Atkin, O.K. (1999) Analysis of differences in photosynthetic nitrogen-use efficiency of alpine and lowland *Poa* species. *Oecologia*, **120**, 19-26.
- Whelan T., Sackett, W.M. and Benedict, C.R. (1973) Enzymatic fractionation of carbon isotopes by phosphoenolpyruvate carboxylase from C_4 plants. *Plant physiology*, **51**, 1051-1054.
- Whitehead D.J. (1978) The estimation of foliage area from sapwood basal area in Scots pine. *Forestry*, **51**, 137-149
- Whitehead D. and Jarvis, P.G. (1981) Coniferous forests and plantations. In: *Water Deficits and Plant Growth* (ed T.T. Kozlowski), pp. 49-152. Academic Press, London and New York.
- Williams M., Rastetter E.B., Fernandes D.N., Goulden M.L., Wofsy S.C., Shaver G.R., Melillo J.M., Munger J.W., Fan S.M. and Nadelhoffer K.J. (1996) Modelling the soil-plant-atmosphere continuum in a *Quercus-Acer* stand at Harvard forest: the regulation of stomatal conductance by light, nitrogen and soil/plant hydraulic properties. *Plant Cell and Environment*, **19**, 911-927.
- Wingate L. (1998) *Calibration of the hemispherical photographic and beam transmittance techniques to measure leaf area index distribution in a Picea sitchensis (Bong.) Carr. plantation*. BSc, University of Edinburgh.
-

- Wofsy S.C., Goulden M.L., Munger J.W., Fan S.-M., Bakwin P.S., Daube B.C., Bassow S.L. and Bazzaz F.A. (1993) Net exchange of CO₂ in a mid-latitude forest. *Science*, **260**, 1314-1317.
- Wong S.C., Cowan I.R. and Farquhar G.D. (1979) Stomatal conductance correlates with photosynthetic capacity. *Nature*, **282**, 424-426.
- Wong W.W., Benedict, C.R. and Kohel, R.J. (1979) Enzymatic fractionation of the stable carbon isotopes of carbon dioxide by ribulose-1,5-bisphosphate carboxylase. *Plant physiology*, **63**, 852-856.
- Yakir D. and Wang X.F. (1996) Fluxes of CO₂ and water between terrestrial vegetation and the atmosphere estimated from isotope measurements. *Nature*, **380**, 515-517.

Appendix I

STABLE ISOTOPE MEASUREMENT AND UNITS

The first stable carbon isotope measurements of atmospheric carbon dioxide, were made by Nier & Gulbransen (1939). Atmospheric carbon dioxide was found to contain about 1.11% of the heavier isotope ^{13}C and 98.9% of the lighter isotope ^{12}C .

Expressing Isotope Composition

Isotopic compositions are measured by means of a specially designed mass spectrometer equipped with two collectors, two amplifiers and a bridging circuit. The output from the mass spectrometer is an isotope ratio compared to some standard. After minor corrections for instrumental effects and for the presence of ^{17}O in the sample, the ratio is converted to the molar abundance ratio, r (Craig, 1957).

$$r = {}^{13}\text{CO}_2 / {}^{12}\text{CO}_2 \quad (\text{Eq I.1})$$

In plant physiology and geochemistry applications this is more commonly expressed as a δ value, in units per mil (parts per thousand, ‰), as shown for carbon below:

$$\delta = \left(\frac{r_{\text{sample}}}{r_{\text{standard}}} - 1 \right) \times 1000 \quad (\text{Eq I.2})$$

Absolute isotope ratios are troublesome to obtain, and for most purposes it is adequate to give δ values relative to some standard. The standard for ^{13}C is a carbonate from the Pee Dee Belemnite Formation in South Carolina, USA (PDB)(Craig, 1953), which has an absolute ratio of 0.01118 (Allison *et al.*, 1995). The original carbonate deposit is now exhausted and new standards have been

chosen by the International Atomic Energy Agency (IAEA) in Vienna and the United States National Bureau of Standards (NBS) and calibrated against the original PDB.

Expressing Isotope Fractionation

Variations in r are a consequence of fractionations expressed during the formation and destruction of bonds involving atoms, like carbon and oxygen, or because of other processes that are mass dependent, such as gaseous diffusion. Fractionation events are often classified as being either kinetic or thermodynamic, the distinction really being between non-equilibrium and equilibrium situations. Kinetic isotope effects are non-equilibrium events and occur when the rates of chemical reactions or physical processes of isotopic species differ from one another. For example, during the diffusion of $^{13}\text{CO}_2$ and $^{12}\text{CO}_2$ through air, $^{12}\text{CO}_2$ moves faster as its binary diffusivity differs from that of $^{13}\text{CO}_2$, the fractionation factor for this process is 1.0044. Another example is the difference between the kinetic constants for the reaction of $^{13}\text{CO}_2$ and $^{12}\text{CO}_2$ with ribulose biphosphate carboxylase-oxygenase (RUBISCO). In both cases the kinetic effects in the process are “normal” and discriminate against the heavier isotope. Thermodynamic effects represent the balance of two kinetic effects at chemical equilibrium. For example, the unequal distribution of isotope species among phases in a system is a thermodynamic effect.

The degree of fractionation (α) is expressed as a ratio of the reactant (r_r) and the product (r_p) given by:

$$\alpha = \frac{r_r}{r_p} \quad (\text{Eq I.3})$$

Where α is greater than 1, there is a depletion of the heavy isotope in the product and where α is less than 1, there is an enrichment in the heavy isotope. For numerical convenience, instead of using α , Farquhar & Richards, (1984) proposed the use of Δ , the deviation of α from unity, as the measure of the carbon isotope discrimination by the plant:

$$\Delta = (\alpha - 1) \times 1000 \quad (\text{Eq I.4})$$

APPENDIX II

Derivation of C_i/C_a corrected for respiratory processes from net observed discrimination Δ_{obs} (Farquhar *et al.*, 1982).

An expression for C_i/C_a was derived from the extended formulation of ^{13}C discrimination (Eq 2.19, see Appendix 2 of Farquhar *et al.*, 1982):

$$\Delta = a \frac{C_a - C_i}{C_a} + a_m \frac{C_i - C_c}{C_a} + b \frac{C_c}{C_a} - f \frac{\Gamma^*}{C_a} - e \frac{R_d}{kC_a} \quad (\text{Eq II.1})$$

This equation is based on the assumption that isotopic signatures of respiratory substrates are the same as those of fresh plant assimilates (i.e. those from assimilation-weighted Δ). This is likely to be the case for photorespiration on average as well as instantaneously, as it recycles freshly assimilated carbon with an isotopic signature of (or close to) instantaneous Δ . For mass balance reasons, it must also be true for dark respiration on average, that $\delta_{\text{plant}} \approx \delta_a - \Delta$, but this is not always the case for instantaneous observations.

The substrate of dark respiration has an isotopic composition of integrated assimilation weighted Δ (denoted by $\int \Delta$), whereas instantaneous Δ follows a pronounced diurnal cycle with values different from this integrated value at most times. To take this into account, the above equation has to be modified. Thus, an apparent fractionation factor, e^* is defined, expressing the difference between the isotopic signal of dark respiration ($\delta^{13}\text{C}_R = \delta_a - \delta_{\text{plant}}$) and photosynthesis (Δ) at each time step according to:

$$e^* = \delta_e - \Delta = \delta_a - \delta_{\text{plant}} - \Delta \quad (\text{Eq II.2})$$

Because $\delta_{\text{plant}} = \delta_a - \int \Delta$, e^* is zero on average. With this, Eq I.1 is modified to:

$$\Delta = a + (a_m - a) \frac{C_i}{C_a} + (b - a_m) \frac{C_c}{C_a} - f \frac{\Gamma^*}{C_a} - (e + e^*) \frac{R_d}{k C_a} \quad (\text{Eq II.3})$$

using $k = (A + R_d) / (C_i (1 - \Gamma^*/C_i))$ (from Appendix 2 of Farquhar *et al.*, (1982)) gives:

$$\Delta = a + (a_m - a) \frac{C_i}{C_a} + (b - a_m) \frac{C_c}{C_a} - f \frac{\Gamma^*}{C_a} - (e + e^*) \frac{R_d}{A + R_d} \frac{C_i}{C_a} + (e + e^*) \frac{R_d}{A + R_d} \frac{\Gamma^*}{C_a} \quad (\text{Eq II.4})$$

and substituting C_c from Eq 2.21 ($A = g_w(C_i - C_c)$) yields:

$$\Delta = a + (b - a) \frac{C_i}{C_a} - (b - a_m) \frac{A}{g_w C_a} - f \frac{\Gamma^*}{C_a} - (e + e^*) \frac{R_d}{A + R_d} \frac{C_i}{C_a} + (e + e^*) \frac{R_d}{A + R_d} \frac{\Gamma^*}{C_a} \quad (\text{Eq II.5})$$

By collecting like terms and re-arranging, this can be solved for C_i/C_a :

$$\frac{C_i}{C_a} = \frac{\Delta - a + (b - a_m) \frac{A}{g_w C_a} + \left(f - (e + e^*) \frac{R_d}{A + R_d} \right) \frac{\Gamma^*}{C_a}}{b - a - (e + e^*) \frac{R_d}{A + R_d}} \quad (\text{Eq II.6})$$

[N.B.: Introduction of the term e^* would change equation B8 (and B9 etc) in Appendix 2 of Farquhar *et al.*, (1982) from

$$R_d'/R_d = (1 - e/1000)(A'/A) \text{ to}$$

$$R_d'/R_d = (1 - (e + e^*)/1000)(A'/A)$$

$$\text{With } R_d'/R_d = (1 - e/1000)(l'/l) \text{ and } l'/l = (1 - e^*/1000)(A'/A)$$

So that e^* , the difference between fresh assimilate (A'/A) and long term mean assimilate (l'/l), is an “apparent fractionation” but zero on average.]

APPENDIX III

Solution to the stable isotope partitioning equations as described in the Appendix of Bowling *et al.*, 2001 .

The formal combination of (5.1), (5.14), (3.16) and (5.19) can yield an equation for F_A .

$$\Delta = a + (b_R - a) \frac{C_i}{C_a} \quad (\text{Eq 3.16})$$

Firstly, re-arrangement of Eq 5.19 solving for C_i/C_a then substituting into (3.16) gives

$$\Delta = b_R + (b_R - a) \frac{F_A}{(G_c C_a)} \quad (\text{Eq III.1})$$

This Δ is then substituted into Eq (5.14), and collecting like terms

$$F_I = \delta_R F_R + (\delta_a - b_R) F_A - \left(\frac{b_R - a}{G_c C_a} \right) F_A^2 \quad (\text{Eq III.2})$$

Multiplying (Eq 5.1) by δ_R and subtracting from (Eq III.2) gives

$$F_I - \delta_R F_E = (\delta_a - b_R - \delta_R) F_A - \left(\frac{b_R - a}{G_c C_a} \right) F_A^2 \quad (\text{Eq III.3})$$

which upon re-arrangement yields the quadratic equation

$$-\left(\frac{b_R - a}{G_c C_a}\right) F_A^2 + (\delta_a - b_R - \delta_R) F_A + (\delta_R F_E - F_1) = 0 \quad (\text{Eq III.4})$$

The solution to this equation is

$$F_A = -(\delta_a - b_R - \delta_R) \pm \frac{\sqrt{(\delta_a - b_R - \delta_R)^2 - 4 \left[-\left(\frac{b_R - a}{G_c C_a}\right) (\delta_R F_E - F_1) \right]}}{2 \left[-\left(\frac{b_R - a}{G_c C_a}\right) \right]} \quad (\text{Eq III.5})$$

and only one of the two roots yields a realistic value for F_A .

The solution presented in (Eq III.5) differs from the solution presented by Bowling *et al*, (2001) (A5) as that contains a number of errors that render the equation incorrect and unable to resolve F_A .